

ICLIAD 65 (2), 131-263, 2024

p-ISSN 0535-5133
e-ISSN 2477-9393

Volumen 65
No. 2
Junio 2024

Investigación Clínica

Universidad del Zulia
Facultad de Medicina
Instituto de Investigaciones Clínicas
"Dr. Américo Negrette"
Maracaibo, Venezuela



Investigación Clínica

<https://sites.google.com/site/revistainvestigacionesclinicas>

Revista arbitrada dedicada a estudios humanos, animales y de laboratorio relacionados con la investigación clínica y asuntos conexos.

La Revista es de Acceso Abierto, publicada trimestralmente por el Instituto de Investigaciones Clínicas “Dr. Américo Negrette”, de la Facultad de Medicina, de la Universidad del Zulia, Maracaibo, Venezuela.

Investigación Clínica está indizada en Science Citation Index Expanded (USA), Excerpta Medica/EMBASE y Scopus (Holanda), Tropical Diseases Bulletin y Global Health (UK), Biblioteca Regional de Medicina/BIREME (Brasil), Ulrich’s Periodicals, Journal Citation Reports (USA), Index Copernicus (Polonia), SIIEC Data Bases, Sección Iberoamérica (Argentina) e Infobase Index (India), Redalyc y las bases de datos: SciELO (www.Scielo.org.ve), Reveneyt, LILACS, LIVECS, PERIODICA y web de LUZ: <http://www.produccioncientificaluz.org/revistas>

Américo Negrette †
Editor Fundador (1960-1971)

Editora
Elena Ryder

Slavia Ryder
Editora 1972-1990

Asistente al Editor
Lisbeny Valencia

Comité Editorial (2022-2024)

Deyseé Almarza	Jesús Mosquera
María Díez-Ewald	Jesús Quintero
Juan Pablo Hernández	Enrique Torres
Yraima Larreal	Nereida Valero
Humberto Martínez	Gilberto Vizcaíno

Asesores Científicos Nacionales (2022-2024)

Alberto Aché (Maracay)	Oscar Noya (Caracas)
Trino Baptista (Mérida)	José Núñez Troconis (Maracaibo)
Rafael Bonfante-Cabarcas (Barquisimeto)	Mariela Paoli (Mérida)
Javier Cebrian (Caracas)	Flor Pujol (Caracas)
Rodolfo Devera (Ciudad Bolívar)	Alexis Rodríguez-Acosta (Caracas)
Saul Dorfman (Maracaibo)	Martín Rodríguez (Caracas)
Jorge García Tamayo (Maracaibo)	Vanessa Romero (Maracaibo)
José Golaszewski (Valencia)	Liseti Solano (Valencia)
Liliana Gomez Gamboa (Maracaibo)	Lisbeth Soto (Valencia)
Maritza Landaeta de Jiménez (Caracas)	Marisol Soto Quintana (Maracaibo)
Jorymar Leal (Maracaibo)	Herbert Stegemann (Caracas)
Diego Martinucci (Maracaibo)	Ezequiel Trejo-Scorza (Caracas)
Edgardo Mengual (Maracaibo)	

Asesores Científicos Internacionales (2022-2024)

Carlos Aguilar Salinas (México)	Carlos Lorenzo (USA)
Francisco Alvarez-Nava (Ecuador)	Juan Ernesto Ludert (México)
Germán Añez (USA)	Valdair Muglia (Brasil)
César Cuadra Sánchez (Nicaragua)	Alejandro Oliva (Argentina)
Peter Chedraui (Ecuador)	José Antonio Páramo (España)
Marcos de Donato (México)	Isela Parra Rojas (México)
José Esparza (USA)	Joaquín Peña (USA)
Francisco Femenia (Argentina)	Mercede Pineda (España)
Hermes Flórez (USA)	Heberto Suárez-Roca (USA)
Elvira Garza-González (México)	Rodolfo Valdez (USA)
José María Gutiérrez (Costa Rica)	Gustavo Vallejo (Colombia)
Tzasna Hernández (México)	

*Para cualquier otra información dirigir
su correspondencia a:*

*Dra. Elena Ryder, Editora
Instituto de Investigaciones Clínicas
"Dr. Américo Negrette"
Facultad de Medicina, Universidad del Zulia
Maracaibo, Venezuela.*

Teléfono:

+58-0414-6305451

Correos electrónicos:

elenaryder@gmail.com

riclinicas@gmail.com

Páginas web:

*[https://sites.google.com/site/
revistainvestigacionesclinicas](https://sites.google.com/site/revistainvestigacionesclinicas)*

<http://www.produccioncientificalu.org/revistas>

*For any information please address
correspondence to:*

*Dr. Elena Ryder, Editor
Instituto de Investigaciones Clínicas
"Dr. Américo Negrette"
Facultad de Medicina, Universidad del Zulia
Maracaibo, Venezuela.*

Phone:

+58-0414-6305451

E-mails:

elenaryder@gmail.com

riclinicas@gmail.com

Web pages:

*[https://sites.google.com/site/
revistainvestigacionesclinicas](https://sites.google.com/site/revistainvestigacionesclinicas)*

<http://www.produccioncientificalu.org/revistas>



**Universidad del Zulia
Publicación auspiciada por el
Vicerrectorado Académico
Serbiluz-CONDES**

© 2024. INVESTIGACIÓN CLÍNICA

© 2024. Instituto de Investigaciones Clínicas

CODEN: ICLIAD

Versión impresa ISSN: 0535-5133

Depósito legal pp 196002ZU37

Versión electrónica ISSN: 2477-9393 Depósito
legal ppi 201502ZU4667

Artes finales:

Lisbeny Valencia

lisbenyvalencia@gmail.com

EDITORIAL

Impacto de las infecciones virales en la autoinmunidad.

Los trastornos autoinmunes tienen su origen en una respuesta inmunitaria aberrante, y dentro de los factores que contribuyen a esta respuesta anómala, se encuentran la genética, la edad y el medio ambiente. Los virus han sido implicados como los principales patógenos infecciosos ambientales, desencadenantes de la autoinmunidad ¹.

Entre los principales virus implicados como disparadores de fenómenos autoinmunes, se encuentran: Epstein-Barr (VEB), citomegalovirus (CMV), herpes virus-6, parvovirus B19, virus linfotrópico humano tipo 1, virus de hepatitis, rubéola, rotavirus, Coxsackie B, y más recientemente se han asociado también los virus de dengue, chikungunya, zika y SARS-CoV2 ²⁻⁴. No hay duda de que demostrar y explicar la etiopatogenia de esta asociación es extremadamente complejo; al parecer, todo podría depender de la naturaleza del virus, de la predisposición genética y del estado inmunitario del hospedero.

Los virus pueden desencadenar enfermedades autoinmunes al confluir con otros elementos como polimorfismos genéticos, factores ambientales, infecciones, estado hormonal, microbiota, sustancias químicas, drogas e incluso vacunas. De forma opuesta, podrían tener un efecto protector en el huésped, como sucede con el CMV, capaz de inducir la activación de células NK y linfocitos T específicos, que destruyen células autorreactivas específicas de GlialCAM, mediadoras de la patogénesis de la esclerosis múltiple, y que son inducidas por la infección del VEB ⁵.

Entre los mecanismos inmunopatológicos, el mimetismo molecular es el principal mecanismo de autoinmunidad mediada por

los virus. Este es causado por la pérdida de la tolerancia periférica y la reacción cruzada entre péptidos extraños y propios con la activación de células T y B autorreactivas; aunque estas células también podrían provocar tolerancia ⁶. En un ambiente proinflamatorio, que favorece segundas señales co-estimuladoras, los linfocitos T y B autorreactivos se pueden activar en ausencia del antígeno, por medio de ligandos de co-señalización e interacción con células vecinas. La acción de estos linfocitos provoca más daño tisular, liberando antígenos patógenos y neoantígenos, que en las cercanías del foco inflamatorio, son expuestos por las células presentadoras de antígenos y activan linfocitos autorreactivos (*activación del espectador*), promoviendo la liberación de más neoantígenos, que son reconocidos, exacerbándose el daño (*propagación del epítope*)^{1,7}. Si los autoantígenos que se liberan estaban “secuestrados” (proteínas intraoculares, espermatozoides, entre otros), se puede generar un reconocimiento antigénico pues no se había desarrollado tolerancia previamente. Tanto las infecciones virales agudas, como las crónicas y los superantígenos, están asociados a autoinmunidad. Hay que recordar que todos estos mecanismos descritos, se presentan en procesos infecciosos y que no pueden causar autoinmunidad por sí solos, debe existir una predisposición.

Bajo este enfoque, las infecciones virales, principalmente las crónicas, resaltan también como factores predisponentes en la inmunopatogenia de la autoinmunidad, formando parte de un enorme conglomerado de agentes ambientales que pueden

afectar en diferentes momentos y maneras, la homeostasia del individuo ⁸, y aunque se describan principalmente como desencadenantes de la enfermedad, los virus podrían representar solo la parte más visible de la tautología autoinmune y del mosaico de la autoinmunidad.

Aunque los trastornos autoinmunes son comparativamente raros, su incidencia y prevalencia en todo el mundo está aumentando, y tienen importantes implicaciones adversas en la morbimortalidad de la población. Su expresión clínica es diversa, y son muchas las enfermedades asociadas a autoinmunidad, entre las que resaltan: la diabetes Tipo 1, la artritis reumatoidea y las artritis seronegativas, el lupus eritematoso sistémico, la polimiositis, el síndrome de Sjögren, la uveítis, la tiroiditis, la enfermedad de Crohn, la colangitis biliar primaria, la hepatitis autoinmune, las miocardiopatías, la anemia hemolítica autoinmune, las púrpuras de origen inmunitario y la esclerosis múltiple, entre otras. Son muchos los reportes en la literatura, posteriores a COVID-19, sobre casos de enfermedades autoinmunes de nueva aparición, en pacientes sin antecedentes de autoinmunidad ⁹.

Este escenario complejo, se refleja también en el diagnóstico de laboratorio, pues son necesarias varias pruebas para validar esta asociación; por una parte, los polimorfismos genéticos que determinan la mayor susceptibilidad a una enfermedad, por otra parte, la confirmación del posible agente disparador y finalmente, la certificación de la enfermedad autoinmune. Una prueba diagnóstica puede carecer de especificidad y sensibilidad, aunque ayude a estimar la gravedad de la enfermedad y a evaluar su pronóstico y actividad. Tal es el caso de la detección de autoanticuerpos en individuos sin un diagnóstico concluyente de enfermedad autoinmune. Por otro lado, se han hecho esfuerzos en tratar de identificar factores de riesgo clave y posibles biomarcadores, que

permitan hacer un diagnóstico enfocado en la susceptibilidad de los individuos, tomando en cuenta la exposición al medio ambiente y basándose en estudios epidemiológicos y clínicos, que utilizan pruebas toxicológicas, microbiológicas, bioquímicas e inmunológicas. Al respecto, existen evidencias significativas que vinculan una enfermedad autoinmune particular, con agentes ambientales específicos ⁸, aunque se cree que este enfoque sería más útil en enfermedades autoinmunes con etapas subclínicas largas y estados frecuentes de remisión-recaída.

El período de tiempo entre una infección viral y el inicio de la autoinmunidad es variable; la aparición de un cuadro infeccioso, eventualmente crítico, puede ser extremadamente difícil de detectar. Una vez que se establece la enfermedad autoinmune, difícilmente se regresa al estado de equilibrio anterior, y es necesario en la mayoría de casos, algún tipo de tratamiento permanente. Han sido muchos los tratamientos propuestos para controlar esta respuesta inapropiada del sistema inmunitario, la mayoría de ellos con efectos adversos importantes; sin embargo, la inmunoterapia ha abierto nuevos caminos. Es necesario promover más investigación básica sobre los mecanismos moleculares de las enfermedades autoinmunes, para que avances como la vacuna inversa y las nanopartículas, sean plenamente efectivos. De igual manera, es imperioso un abordaje multidisciplinario, desde el conocimiento de la predisposición genética, el mayor control de disparadores ambientales (entre ellos los virus), hasta la mayor equidad en cuanto al acceso de las nuevas terapias biológicas para el tratamiento, que contribuya a mejorar la calidad de vida de estos pacientes.

Yraima Larreal

ORCID 0000-0003-0862-9842

Renata Vargas

ORCID 0009-0007-0598-6971

REFERENCIAS

1. **Sundaresan B, Shirafkan F, Ripperger K, Rattay K.** The role of viral infections in the onset of autoimmune diseases. *Viruses* 2023;15(3):782. <https://doi.org/10.3390/v15030782>.
2. **Monsalve DM, Pacheco Y, Acosta-Ampudia Y, Rodríguez Y, Ramírez-Santana C, Anaya JM.** Zika virus and autoimmunity. One-step forward. *Autoimmun Rev* 2017; 16(12):1237-1245. <https://doi.org/10.1016/j.autrev.2017.10.008>.
3. **Tanay A.** Chikungunya virus and autoimmunity. *Curr Opin Rheumatol* 2017; 29(4):389-393. <https://doi.org/10.1097/bor.0000000000000396>.
4. **Shih HI, Chi CY, Tsai PF, Wang YP, Chien YW.** Re-examination of the risk of autoimmune diseases after dengue virus infection: A population-based cohort study. *PLoS Negl Trop Dis* 2023; 17(3): e0011127. <https://doi.org/10.1371/journal.pntd.0011127>.
5. **Vietzen H, Berger SM, Kühner LM, Furlano PL, Bsteh G, Berger T, Rommer P, Puchhammer-Stöckl E.** Ineffective control of Epstein-Barr-virus-induced autoimmunity increases the risk for multiple sclerosis. *Cell* 2023; 186(26):5705-5718. <https://doi.org/10.1016/j.cell.2023.11.015>.
6. **Rojas M, Restrepo-Jiménez P, Monsalve DM, Pacheco Y, Acosta-Ampudia Y, Ramírez-Santana C, Leung PSC, Ansari AA, Gershwin ME, Anaya JM.** Molecular mimicry and autoimmunity. *J Autoimmun* 2018; 95:100-123. <https://doi.org/10.1016/j.jcaut.2018.10.012>.
7. **Pacheco Y, Acosta-Ampudia Y, Monsalve DM, Chang C, Gershwin ME, Anaya JM.** Bystander activation and autoimmunity. *J Autoimmun* 2019; 103:102301. <https://doi.org/10.1016/j.jcaut.2019.06.012>.
8. **Gonzalez-Quintal R, Mayeux JM, Kono DH, Theofilopoulos AN, Pollard KM, Baccala R.** Silica exposure and chronic virus infection synergistically promote lupus-like systemic autoimmunity in mice with low genetic predisposition. *Clin Immunol* 2019; 205:75-82. <https://doi.org/10.1016%2Fj.clim.2019.06.003>.
9. **Knight JS, Caricchio R, Casanova JL, Combes AJ, Diamond B, Fox SE, Hanauer DA, James JA, Kanthi Y, Ladd V, Mehta P, Ring AM, Sanz I, Selmi C, Tracy RP, Utz PJ, Wagner CA, Wang JY, McCune WJ.** The intersection of COVID-19 and autoimmunity. *J Clin Invest* 2021; 131(24):e154886. <https://doi.org/10.1172/jci154886>.

Impact of viral infections on autoimmunity

Autoimmune disorders arise from an abnormal immune response influenced by genetic factors, age, and the environment. Many viruses, such as the Epstein-Barr virus, cytomegalovirus, herpes virus-6, and more recently, the SARS-CoV-2 virus, have been identified as environmental triggers of autoimmunity. The complex association between viruses and autoimmunity depends on the nature of the virus, genetic predisposition, and the host's immune status. Additionally, viruses can trigger autoimmune diseases by interacting with factors such as genetic polymorphisms, infections, hormonal status, microbiota, chemicals, drugs, and even vaccines. Molecular mimicry is the primary mechanism of virus-mediated autoimmunity caused by the loss of peripheral tolerance and cross-reactivity between foreign and self-peptides. Therefore, viral infections, especially chronic ones, stand out as a predisposing factor in the immunopathogenesis of autoimmunity. The incidence and prevalence of autoimmune disorders are increasing globally, with significant implications for population morbidity and mortality, including cases of autoimmune diseases following COVID-19 in patients without a history of autoimmunity. Laboratory diagnosis of autoimmune diseases requires several tests to validate the association, including confirmation of the potential triggering agent and certification of the autoimmune disease. The period between viral infection and the onset of autoimmunity is variable, and once established, autoimmune diseases generally require some form of permanent treatment. The complex relationship between viruses and autoimmunity underlines the need for further research to understand the molecular mechanisms of autoimmune diseases and to develop more effective therapeutic approaches.

Surgical complications in children with IgA vasculitis: clinical analysis of 28 cases.

Jing Mu, Jing Hao, Xiaofang Zhen, Xin Mo, Yan Sheng

Department of Traditional Chinese Medicine, Beijing Children's Hospital, Capital Medical University, National Center for Children's Health, Beijing, China.

Keywords: intussusception; intestinal perforation; Henoch-Schönlein purpura; enterectomy; enterostomy; D-dimer; C-reactive protein.

Abstract. Intussusception and intestinal perforation are surgical severe complications in children with IgA vasculitis (IgAV). Early diagnosis and timely appropriate surgical intervention can reduce damage to the children. We analyzed retrospectively the clinical characteristics, auxiliary examinations, diagnosis, treatment, and prognosis of 28 children with IgAV accompanied by surgical complications (including intussusception in 21 patients and intestinal perforation in seven patients) who were admitted to the Beijing Children's Hospital of the Capital Medical University from May 2016 to December 2020. Within one year after the data was collected, the parents of the children were interviewed by telephone about their treatment. Increased peripheral leukocytes were observed in 60.7% of children. Serum C-reactive protein (CRP) and D-dimer were elevated in 53.3% and 75% of children, respectively. Gastrointestinal bleeding was identified in 39% of children. Of the children with intussusception, the symptoms subsided spontaneously in four children and after air enema in another four. Four children underwent laparotomy and manual reduction. Nine patients underwent enterectomy and anastomosis. Enterectomy and anastomosis were performed in the seven patients with intestinal perforation, two of whom underwent enterostomy concurrently. Increased inflammation indexes, elevated D-dimer, and persistent abdominal pain without relief may be risk factors for surgical complications in children with IgAV.

Complicaciones quirúrgicas en niños con vasculitis IgA: análisis clínico de 28 casos.

Invest Clin 2024; 65 (2): 134 – 142

Palabras clave: intususcepción; perforación intestinal; púrpura de Henoch-Schönlein; enterectomía; enterostomía; dímero D; proteína C-reactiva.

Resumen. La intususcepción y la perforación intestinal son complicaciones quirúrgicas graves en niños con vasculitis por IgA (IgAV). El diagnóstico temprano y la intervención quirúrgica adecuada y oportuna pueden reducir el daño de esta enfermedad a los niños. Analizamos retrospectivamente las características clínicas, exámenes auxiliares, diagnóstico, tratamiento y pronóstico de 28 niños con IgAV acompañada de complicaciones quirúrgicas (incluida intususcepción en 21 pacientes y perforación intestinal en siete pacientes) que ingresaron en el Hospital Infantil de Beijing de la Universidad Médica de la Capital, de mayo de 2016 a diciembre de 2020. Un año después de la recopilación de datos, los padres de los niños fueron entrevistados telefónicamente sobre su tratamiento. Se observó un aumento de leucocitos periféricos en el 60,7% de los niños. La proteína C reactiva (PCR) y el dímero D séricos estaban elevados en el 53,3% y el 75% de los niños, respectivamente. Se identificó hemorragia gastrointestinal en el 39% de los niños. De los niños con intususcepción, los síntomas desaparecieron espontáneamente en cuatro niños y después de un enema de aire en otros cuatro. Cuatro niños fueron sometidos a laparotomía y reducción manual. Nueve pacientes fueron sometidos a enterectomía y anastomosis. Se realizó enterectomía y anastomosis en los siete pacientes con perforación intestinal, dos de los cuales fueron sometidos a enterostomía al mismo tiempo. El aumento del índice de inflamación, el dímero D elevado y el dolor abdominal persistente sin alivio pueden ser factores de riesgo de complicaciones quirúrgicas en niños con IgAV.

Received: 20-01-2023 Accepted: 18-03-2024

INTRODUCTION

IgA Vasculitis (IgAV), formerly known as Henoch-Schönlein purpura (HSP), is a systemic small vasculitis syndrome that usually occurs in children. In 1802, Heberden first described this syndrome. He reported a child with joint pain and subcutaneous edema, abdominal pain, vomiting, blood in the stool and blood in the urine, as well as “blood spots” on the skin of the legs ¹. Initially,

Schönlein used the term “rheumatic purpura” to describe the association between joint pain and purpuric skin lesions in children. In 1874, Henoch described the syndrome of purpura, severe abdominal cramps, and melena. Later, Henoch referred to nephritis as a complication of the syndrome ².

The disease can cause purpuric skin lesions and is accompanied by various symptoms, including gastrointestinal symptoms, arthritis, and nephritis. Approximately 50%

to 75% of IgAV children present with gastrointestinal symptoms, such as abdominal pain³ with various degrees, from mild abdominal pain to severe intestinal colic. Some children may have serious surgical complications, including intussusception, intestinal perforation, intestinal necrosis, intestinal obstruction, significant gastrointestinal bleeding, severe pancreatitis, and testicular torsion. Delayed management and surgical intervention are associated with serious consequences and even death. We should carefully watch for surgical complications in children with severe abdominal pain and gastrointestinal bleeding. Complete examinations should be performed promptly to identify early complications, such as intussusception and intestinal perforation. Appropriate and timely treatment should be given accordingly. There are many reports on the use of corticosteroids and immunosuppressive drugs¹. These specific treatments are still controversial, and their efficacy remains to be evaluated. If the complications are severe, including severe gastrointestinal complications or proliferative glomerulonephritis, steroids or/and immunosuppressive drugs may be needed, including coledicine, dapson, montelukast, corticosteroids and azathioprine and other drugs⁴⁻⁶.

There have been relatively few clinical and epidemiological studies on childhood HSP in the past few years. To investigate this syndrome further, we retrospectively analyzed the clinical data of 28 children with intussusception or intestinal perforation among 7374 children with IgAV.

METHODS

From May 2016 to May 2020, 7374 children with IgAV were treated in the Department of Traditional Chinese Medicine, Beijing Children's Hospital, Capital Medical University. Surgical complications were reported in 28 children, including intussusception in 21 children and intestinal perforation in seven children. We retrospectively

analyzed the clinical characteristics, auxiliary examinations, diagnosis, treatment, and prognosis of all 28 children with IgAV. All data were collected from our Hospital's electronic medical record system.

Inclusion criteria

Patients with primary cutaneous vasculitis were classified as HSP or allergic vasculitis², according to the American College of Rheumatology (ACR) standards and the standards proposed by Michel *et al.* If the patient met the following three or more criteria, the patients were classified as HSP: 1) palpable purpura, 2) intestinal colic, 3) gastrointestinal bleeding, 4) hematuria (macroscopic or microscopic hematuria), 5) disease onset age ≤ 20 years, and 6) there was no history of drug treatment before the onset of vasculitis. Patients who met less than three criteria were classified as allergic vasculitis. In addition, if children were diagnosed with primary skin vasculitis or other diseases, such as connective tissue diseases and infections, especially meningitis⁷, they were excluded from the study. Because electronic medical records have only been used recently in our Hospital, only no more than three years of medical records were collected. The incidence of IgA vasculitis with surgical complications is not high, so only 28 cases were collected. A pre-existing anatomical factor as the starting point of the invagination, an accidental finding, and where the intussusception was spotted in such cases as to be taken as criteria for inclusion or exclusion.

Treatment methods

Surgical treatment: Of the 21 children with intussusception, the symptoms subsided spontaneously in four children and after air enema in four. Four children underwent laparotomy and manual reduction. Nine patients underwent enterectomy and anastomosis due to intestinal necrosis (one of them underwent enterostomy). Enterectomy and anastomosis were performed in the seven patients with intestinal perforation

(two of them underwent enterostomy concurrently).

Conservative treatment methods: According to the specific conditions of the children, the children were treated with fasting, gastrointestinal decompression, enteral or parenteral nutrition support, glucocorticoids, proton pump inhibitors, or gamma globulin, as needed.

Follow up

During the follow-up of all 28 children, three children had adhesive intestinal obstruction and underwent secondary surgery. Four children had multiple hospitalizations due to IgAV nephritis, and one child was readmitted due to abdominal pain.

Statistical analysis

The data are expressed as mean \pm standard deviation. The differences between the groups were analyzed using the chi-square test. $P < 0.05$ was considered statistically significant. All statistical analysis is performed using SPSS software (SPSS 19, IBM, USA).

RESULTS

General data

Twenty-eight of the 7,374 children with IgAV were accompanied by surgical complications, a rate of 0.38%. Twenty-one children had intussusception, and seven children had intestinal perforation. Of the 28 children, 10 were males and 18 were females. The age at onset ranged from 3 to 13 years (mean age: 7.2 years). The time from onset of purpura to occurrence of surgical complications ranged from 1 to 37 days (mean: 11 days), and the time from onset of abdominal pain to occurrence of surgical complications ranged from 1 to 40 days (mean: 9.8 days). Of these patients, 6 (6/28) children complained of abdominal pain before purpura appeared.

Clinical manifestations

All 28 children had symptoms of skin purpura. Seven children (7/28) had joint

swelling and pain, 11 (11/28) had gastrointestinal bleeding, and five (5/28) had IgAV nephritis (two cases with nephrotic syndrome and three cases with hematuria and proteinuria). All patients presented with apparent abdominal pain. Tenderness and rebound tenderness were noted on abdominal examination. An abdominal mass was palpated in four patients. The severity of the complications in patients was different, and four patients developed shock (hemorrhagic shock in one patient and septic shock in three patients). Convulsions occurred in two children (due to IgAV involving the cerebrovascular system). Three patients were complicated with pneumonia. After surgery, venous thrombosis occurred in three patients, renal dysfunction in one patient, pancreatic damage in one patient, thrombocytopenia in one patient, and coagulation disorders in one patient.

Auxiliary examination

A routine blood count showed increased leukocyte count in 17 children (17/28), with the highest value being $33.11 \times 10^9/L$ (normal range: $4-10 \times 10^9/L$). Elevated CRP was noted in 15 children (15/28), with the highest value being $> 160 \text{ mg/L}$ (average value $< 8 \text{ mg/L}$). Elevated D-dimer was noted in 21 children (21/28), with the highest value being 7.565 mg/L (normal limits: $0-0.243 \text{ mg/L}$). Four children tested positive in the ^{13}C -urea breath test. Serum influenza B virus IgM was positive in six children. Serum influenza A virus IgM was positive in two children. Serum mycoplasma pneumoniae IgM was positive in two children. According to abdominal B-mode ultrasonography or surgical exploration in some patients, 12 children were diagnosed with ileo-ileal intussusception, six children with ileo-colonic intussusception, two children with jejunal-jejunal intussusception, and one child with colon-colonic intussusception. Of the seven children with intestinal perforations, six were diagnosed with ileal perforation (including a child accompanied by colonic perforation) and a child with jejunal perforation.

DISCUSSION

IgAV is a common small-blood-vessel allergic disease occurring during childhood; it is most common in children aged three to eight years⁸, with a predominance in males. Skin purpura is most commonly accompanied by digestive tract, joint, or kidney lesions. Abdominal symptoms are reported in 50% to 75% of IgAV children, including gastrointestinal bleeding, gastric ulcers, pancreatitis, cystic effusion, and protein-losing enteropathy. Some rare surgical complications include intussusception, intestinal obstruction, intestinal fistula, and intestinal perforation^{3,9}.

Intussusception is the most common condition for surgery in IgAV children, with an incidence of 3% to 4%¹⁰. Intestinal perforation is the second-leading condition for surgery, with an incidence of approximately 0.38%¹¹. In the past three years, we have treated 7,374 patients with IgAV; surgical complications were reported in 28 patients. The incidence of intussusception was 0.28%, and the incidence of intestinal perforations was 0.09%. Due to our Hospital's late use of electronic medical records, no more than three years of case data have been counted. If the statistical years were longer, the data may be more meaningful. The pathogenesis of intussusception may be due to the aseptic inflammation of small blood vessels in the intestinal wall, which increases the permeability of the intestinal wall blood vessels^{10,12} to result in extravasation of blood components and segmental bleeding under the serosa and mucosa. These lead to uneven peristaltic movement, local slow peristalsis, spasms of the intestinal loop, or even intussusception¹³. As the disease progresses, tissue hypoxia and hypoperfusion may occur. Intestinal wall edema, ischemia, and hypoxia lead to intestinal necrosis and even intestinal perforation¹⁴. In the acute phase of IgAV, increased blood viscosity results in slow local blood flow and exacerbates intestinal ischemia and hypoxia. The circulating D-dimer level in children with IgAV is significant-

ly increased¹⁵. This reflects the presence of hypercoagulable states and the formation of thrombi. Another study¹⁶ found that IgAV caused a significant increase in serum CRP in children with abdominal surgical complications, suggesting that the occurrence of this complication may be closely related to infectious factors. Furthermore, serum CRP level has been positively correlated with the occurrence of these complications. This further indicates that infectious factors play an essential role in the occurrence of surgical complications. We summarized the clinical data of all 28 children in this study and found that the average time from the onset of abdominal pain to the first surgical complication was 9.8 days, and the longest time was 40 days. Increased peripheral leukocyte count was observed in 60.7% of children. Serum CRP and D-dimer levels were elevated in 53.3% and 75% of children, respectively. Gastrointestinal bleeding was identified in 39%. Increased inflammation index, elevated D-dimer, and persistent abdominal pain without relief may be risk factors for surgical complications in children with IgAV. For this child population, we should carefully watch for surgical complications. Early and precise diagnosis and timely, appropriate treatment can reduce the harm to these children.

Intussusception in IgAV patients usually originates from the ileum (90%) or jejunum (7%)¹⁷. The common sites of intussusception are ileo-ileal (51.4%), ileo-colonic (38.6%), and jejunal-jejunal (7.0%). In IgAV, colo-colonic intussusception is extremely rare, with only a few cases reported¹⁶. The most common site of intestinal perforation is the small intestine, especially the ileum, followed by the jejunum. This may be due to the intestinal wall swelling in the small intestine in IgAV patients. Children with IgAV also often have infection, which can enlarge the aggregated lymphoid nodules in the ileum. Therefore, the local intestinal wall thickens and even protrudes into the intestinal lumen to form a starting point of intussusception¹⁸. Among the children with

intussusception in this study, ileo-ileal intussusception, ileum-colonic intussusception, and jejunal-jejunal intussusception made up 57%, 28%, and 9.5% of all intussusceptions, respectively. Colo-colonic intussusception was seen in one patient. Of the seven children with intestinal perforation, six had ileal perforation, and one had jejunal perforation. The incidence of intestinal perforation is basically consistent with that in the literature.

Some researchers have suggested¹⁹ that air enema is the best reduction treatment for IgAV-related early intussusception. Air enema is minimally traumatic to children and can be done more than once. It is difficult to differentiate the abdominal pain caused by IgAV from the abdominal pain caused by complicated intussusception in IgAV because of certain similarities in the symptoms. Intussusception that occurs based on intestinal bleeding and edema is associated with rapid progression and intestinal necrosis. On the other hand, ileo-ileal intussusception is the most common kind, in which the failure rate and recurrence rate of air enema reduction is higher. This study relieved intussusception only in four children after air enema.

Children with IgAV-related surgical conditions may develop serious and even life-threatening complications. In this study, shock was reported in four children (hemorrhagic shock in one patient and septic shock in three patients), postoperative venous thrombosis in three patients, renal insufficiency in one patient, coagulation disorders in one patient, and adhesion intestinal obstruction in three patients, which required secondary surgery later. Therefore, we should improve our understanding of IgAV-related surgical complications to make early diagnoses and provide the appropriate surgical intervention.

The use of glucocorticoids for the treatment of IgAV has been controversial. Some researchers have suggested that early use of glucocorticoids can significantly relieve abdominal pain and reduce the risk of kidney disease²⁰. It can reduce the incidence²¹ or prevent intussusception²². Other research-

ers disagree^{10,23}. The use of glucocorticoids in patients with IgAV complicated with intussusception may mask the symptoms of intestinal perforation or aggravate the intussusception²⁴. Foreign studies have reported that IgAV-related intestinal perforation usually occurs two weeks after the application of glucocorticoids⁶. In this study, all 21 children with intussusception were treated with glucocorticoids, and some were treated with gamma globulin. The children's abdominal pain and purpura were alleviated. Of the seven children with intestinal perforation in this study, four had been taking glucocorticoids for more than 20 days, and three of them developed severe infections with septic shock. Therefore, the dosage and timing of glucocorticoids need to be further explored. However, it draws attention that from May 2016 to 2020, there is a registry of patients in the pediatric population that are diagnosed with IgA vasculitis (7,374 children), and none of the reports state that the diagnosis was confirmed through biopsies of white organs. There are a fair amount of cases (it is because the Hospital is a reference area, or the data collected is national or local); they may also have other pathologies that could be presented through a similar clinical picture, which would explain the large population reported. The risk-benefit of a steroid treatment prior to the appearance of surgical complications cannot be assessed in this work.

Due to the limited study funding and time, the deficiency of this study is the failure to collect the characteristics of each case (onset, relevant laboratory tests, treatment time before symptoms and signs, laparotomy results, air enema treatment, etc.). Moreover, a range of examinations evaluate the inflammatory response (CB, PCR, Dimer D), and the predictive value and prognostic value cannot be established with this work. Our team will conduct the study in the future. Meanwhile, a better collection of clinical, laboratory, and imaging data is needed to establish prognostic value in patients with said pathology.

Table 1
Clinical data of the 28 children with Henoch-Schönlein purpura accompanied by surgical complications.

Number	Joint swelling and pain	Gastrointestinal bleeding	Kidney damage	Surgical complications	Site	Surgical treatments	Other comorbidities	Reason for rehospitalization
1		+	+	Intussusception	Ileo-ileal	Air enema		IgAV nephritis
2	+	+		Intussusception	Ileo-ileal	Enterectomy and anastomosis		
3		+	+	Intussusception	Ileum-colon	Open laparotomy and manual reduction	Venous thrombosis	
4				Intussusception	Ileo-ileal	N/A	pneumonia	
5		+	+	Intussusception	Ileo-ileal	Enterectomy and anastomosis	Hemorrhagic shock, Pneumonia, Coagulation disorders	IgAV nephritis
6	+			Intussusception	Ileo-ileal	Open laparotomy and manual reduction		
7				Intussusception	Jejunum-jejunum	N/A		
8		+		Intussusception	Ileo-ileal	Enterectomy and anastomosis		Intestinal obstruction
9		+		Intussusception	Ileo-ileal	N/A		IgAV nephritis
10		+		Intussusception	Ileum-colon	Air enema		
11				Intussusception	Ileo-ileal	Enterectomy and anastomosis		
12				Intussusception	Ileo-ileal	Open laparotomy and manual reduction		
13	+			Intussusception	Ileum-colon	Enterectomy and anastomosis		
14				Intussusception	Ileum-colon	Open laparotomy and manual reduction		
15		+		Intussusception	Ileo-ileal	Enterectomy and anastomosis		
16	+			Intussusception	Ileum-colon	Air enema		IgAV
17				Intussusception	Jejunum-jejunal	Enterectomy and anastomosis		
18	+		+	Intussusception	Colonocolonic	Air enema	Pneumonia	
19		+		Intussusception	Ileo-ileal	Enterectomy and anastomosis	Pancreatic damage	Intestinal obstruction
20				Intussusception	Ileo-ileal	Enterectomy and anastomosis + enterostomy		
21				Intussusception	Ileum-colon	N/A		
22				Intestinal perforation	Ileum	Enterectomy and anastomosis		Intestinal obstruction
23				Intestinal perforation	Ileum, colon	Enterectomy and anastomosis + enterostomy	Septic shock, renal insufficiency, Convulsions	
24				Intestinal perforation	Ileum	Enterectomy and anastomosis	septic shock, Convulsions, Venous thrombosis	
25		+		Intestinal perforation	jejunum	Enterectomy and anastomosis	Septic shock, Venous thrombosis, Thrombocytopenia	
26			+	Intestinal perforation	Ileum	Enterectomy and anastomosis		
27				Intestinal perforation	Ileum	Enterectomy and anastomosis		
28			+	Intestinal perforation	Ileum	Enterectomy and anastomosis + enterostomy		IgAV nephritis

As a conclusion, intussusception and intestinal perforation are serious surgical complications of IgAV. Clinicians should make an effort to understand IgAV-related surgical complications. Once specific symptoms are present, including increased inflammation index, elevated D-dimer, persistent abdominal pain without relief, and digestive tract hemorrhage or previously existing intestinal malformations, we should observe for surgical complications and make a clear diagnosis as soon as possible. Appropriate and timely surgical intervention can avoid delayed treatment and reduce mortality.

Ethics approval and consent to participate

All procedures performed in studies involving human participants followed the ethical standards of the Independent Ethics Committee for Clinical Research and Animal Trials of the Beijing Children's Hospital, Capital Medical University, and the National Center for Children's Health. Informed consent was obtained from all individual participants included in the study.

Funding

This study was supported by Yan Huimin National Famous Traditional Chinese Medicine Experts Inheritance Studio Traditional Chinese Medicine Education [2016] No. 42.

Conflict of interest

The authors state that no financial, personal, or professional conflicts of interest may hinder this work.

Authors' ORCID

- Jing Mu (JM):
0000-0001-5542-8838
- Jing Hao (JH):
0000-0002-0260-1841
- Xiaofang Zhen (XZ):
0000-0001-8781-9999

- Xin Mo (XM):
0009-0004-5510-0508
- Yan Sheng (YS):
0009-0009-2075-6036

Authors' contributions

JM, JH, XFZ, and XM performed material preparation, data collection, and analysis. JM and YS wrote the first draft of the manuscript, and all authors commented on previous versions. All authors read and approved the final manuscript.

REFERENCES

1. **Audemard-Verger A, Pillebout E, Guillevin L, Thervet E, Terrier B.** IgA vasculitis (Henoch-Schonlein purpura) in adults: Diagnostic and therapeutic aspects. *Autoimmun Rev* 2015; 14(7):579-585.
2. **Calviño MC, Llorca J, Garcia-Porrúa C, Fernandez-Iglesias JL, Rodríguez-Ledo P, Gonzalez-Gay MA.** Henoch-Schönlein Purpura in Children from Northwestern Spain: A 20-Year Epidemiologic and Clinical Study. *Medicine* 2001; 80(5): 279-290.
3. **Fatima A, Gibson DP.** Pneumatosis intestinalis associated with Henoch-Schonlein purpura. *Pediatrics* 2014; 134(3):e880-883.
4. **Bar-Eli M, Wilson L, Peters RS, Schwabe AD, Territo MC.** Microtubules in PMNs from patients with familial Mediterranean fever. *Am J Med Sci* 1982; 284(2):2-7.
5. **Harper RM, Allen BS.** Use of colchicine in the treatment of Behcet's disease. *Int J Dermatol* 1982; 21(9):551-554.
6. **Saatei U, Ozen S, Ozdemir S, Bakkaloglu A, Besbas N, Topaloglu R, Arslan S.** Familial Mediterranean fever in children: report of a large series and discussion of the risk and prognostic factors of amyloidosis. *Eur J Pediatr* 1997; 156(8):619-623.
7. **Fiechtner J, Ito S, Nakano M, Gejyo F, Hanyu T, Murasawa A.** Thoughts on Japanese versus North American rheumatology. *J Clin Rheumatol* 2001; 7(3):208-209.

8. **Rostoker G.** Schonlein-Henoch purpura in children and adults: diagnosis, pathophysiology and management. *BioDrugs* 2001; 15(2):99-138.
9. **Yang X, Duan Y, Zhou C, Jin L, Zhang N, Huang S, Zhang M, Yang J, Zhang Y.** Primary central nervous system lymphoblastic B cell lymphoma located at cerebellum in a child: A case report and literature review. *Pediatr Investig.* 2021 Dec 13;5(4):318-322. doi: 10.1002/ped4.12303.
10. **Trnka P.** Henoch-Schonlein purpura in children. *J Paediatr Child Health* 2013; 49(12):995-1003.
11. **Brown PJ, Haught JM, English JC.** Periumbilical purpura prior to gastrointestinal involvement in Henoch-Schonlein purpura. *Am J Clin Dermatol* 2009; 10(2):127-130.
12. **Zhang R, Du G, Sun F.** Clinical analysis on Henoch-Schonlein purpura accompanied with intussusception. *J Clin Pediatr Surg* 2014; 13(6):540-542.
13. **Yavuz H, Arslan A.** Henoch-Schonlein purpura-related intestinal perforation: a steroid complication? *Pediatr Int* 2001; 43(4):423-425.
14. **Liu G, Dong K, Shen C.** Management of severe abdominal purpura with surgical complications. *Chin J Pediatr Surg* 2012; 33(12):905-908.
15. **Guo K, Ma S, Wang D.** Evaluation and comparison of thromboelastography and conventional coagulation tests for blood coagulation function in children with Henoch-Schonlein purpura. *China Journal of Leprosy and Skin Dis* 2019; 27(3):327-329.
16. **Li B, Yan B, Da Y, Shen Y, Li G, Li L.** The changes of serum procalcitonin, interleukin-6 and C reactive protein in children with Henoch-Schonlein purpura combined with surgical complications. *J Clin Pediatr* 2014; 32(7): 660. doi:10.3969/j.issn.1000-3606.2014.07.016.
17. **Seo MK, Hong J, Yim HE, Pai KS.** A patient with Henoch-Schonlein purpura with intussusception and intractable nephritis. *Child Kidney Dis* 2016; 20(2):92-96.
18. **Wang C, Di Z.** Analysis of diagnosis and treatment of Henoch-Schonlein purpura with intussusception in children. *China Journal of Leprosy and Skin Dis* 2018; 34(6):327-329.
19. **Matsui S, Kanemura T, Yokouchi Y, Kamiichi H, Kiriu N, Koike Y.** Successful treatment of ileocolic intussusception with air enema reduction in an adult patient. *Am J Emerg Med* 2014; 32(5):490 e491-493.
20. **Lerkvaleekul B, Treepongkaruna S, Saisawat P, Thanachatchairattana P, Angkathunyakul N, Ruangwattanapaisarn N, Vilaiyuk S.** Henoch-Schonlein purpura from vasculitis to intestinal perforation: A case report and literature review. *World J Gastroenterol* 2016; 22(26):6089-6094.
21. **Huber AM, King J, McLaine P, Klassen T, Pothos M.** A randomized, placebo-controlled trial of prednisone in early Henoch Schonlein purpura [ISRCTN85109383]. *BMC Med* 2004; 2:7.
22. **Shimoyama T, Matsuda N, Kurobe M, Hayakawa T, Nishioka M, Shimohira M, Takasawa K.** Colonoscopic diagnosis and reduction of recurrent intussusception owing to Henoch-Schonlein purpura without purpura. *Paediatr Int Child Health* 2019; 39(3):219-223.
23. **Blumen J, Goldman RD.** Henoch-Schonlein purpura in children: limited benefit of corticosteroids. *Can Fam Physician* 2014; 60(11):1007-1010.
24. **Krishnan M, Nahas J.** Adult onset Henoch-Schonlein purpura and intussusception: a rare presentation. *Case Rep Rheumatol* 2016; 2016:3957605.

Beneficial effects of gentiopiricin inhibiting experimental epilepsy in young rats through the P2X7R/NLRP3/Caspase-1 inflammatory pathway.

Jia Lin Li¹, Lin Hucang², Xing Jun Wu³, Min Ye³ and Chuan Yong Yu²

¹ Department of Medicine, Tongling Polytechnic, Tongling, China.

² Department of Neurology, Nanjing Brian Hospital affiliated to Nanjing Medical University, Nanjing, China.

³ Department of Neurology, the Affiliated BenQ Hospital of Nanjing Medical University, Nanjing, China.

Keywords: malondialdehyde; superoxide dismutase; apoptosis-associated speck-like protein; Tunel positive cells; gentiopicroside; hippocampal CA3 region.

Abstract. This study mainly examined the protective effect of gentiopiricin on experimental epileptic young rats. Seventy-two Sprague Dawley (SD) rats were used in this study. Twelve rats were randomly selected as the normal group, and the remaining 60 rats were injected with lithium chloride-pilocarpine intraperitoneally to establish an epileptic model, and were randomly divided into five groups of 12 rats each. The positive control group was given topiramate 5.9 mg/kg in normal saline, and the low, middle, and high dose groups were given gentiopiricin liquid, with the mass of gentiopicroside being 1.28 g/kg, 2.56 g/kg, and 5.12 g/kg respectively. The model and normal groups were given the same dose of normal saline daily for four weeks. Compared with the model group, the damage of neurons in the CA3 area of the hippocampus in the positive control group, low, medium, and high dose groups of gentiopiricin was reduced. The number of Tunel positive cells, malondialdehyde (MDA), P2X7R, NLRP3, ASC, Caspase-1 protein, and mRNA in the model group were significantly higher than those in the control group and superoxide dismutase (SOD) activity was significantly lower than that in the control group ($p < 0.05$). The number of Tunel positive cells, MDA content, P2X7R, NLRP3, ASC, Caspase-1 protein, and mRNA in the positive control group, low, medium, and high dosage groups of gentiopicroside were significantly lower than those in the model group, and the SOD activity was significantly higher than that in the model group ($p < 0.05$). Gentiopicroside may improve the behavior of young epileptic rats.

Efectos inhibitorios de la gentiopirina sobre la epilepsia experimental en ratas jóvenes mediante la vía inflamatoria P2X7R/NLRP3/Caspasa-1.

Invest Clin 2024; 65 (2): 143 – 154

Palabras clave: malondialdehído; superóxido dismutasa; proteína tipo punto asociada a la apoptosis; células Tunel positivas; gentiopirósido; región CA3 del hipocampo.

Resumen. Este estudio examinó principalmente el efecto protector del gentiopirina en ratas jóvenes epilépticas. En este estudio se utilizaron setenta y dos ratas Sprague Dawley (SD). Se seleccionaron al azar doce ratas como grupo normal y a las 60 ratas restantes se les inyectó cloruro de litio-pilocarpina por vía intraperitoneal para establecer un modelo epiléptico y se dividieron aleatoriamente en cinco grupos de 12 animales cada uno. El grupo de control positivo recibió 5,9 mg/kg de topiramato en solución salina normal, y los grupos de dosis baja, media y alta recibieron gentiopirina líquida, siendo la masa de gentiopirósido 1,28 g/kg, 2,56 g/kg y 5,12 g/kg. kg respectivamente. Los grupos modelo y normal recibieron la misma dosis de solución salina normal diariamente durante cuatro semanas. En comparación con el grupo modelo, se redujo el daño de las neuronas en el área CA3 del hipocampo en el grupo de control positivo y en los grupos de dosis baja, media y alta de gentiopirósido. El número de células Tunel positivas, malondialdehído (MDA), P2X7R, NLRP3, ASC, proteína caspasa-1 y ARNm en el grupo modelo fue significativamente mayor que en el grupo de control y la actividad de superóxido dismutasa (SOD) fue significativamente menor que esa. en el grupo control ($p < 0,05$). El número de células Tunel positivas, el contenido de MDA, P2X7R, NLRP3, ASC, proteína caspasa-1 y ARNm en el grupo de control positivo, los grupos de dosis baja, media y alta de gentiopirósido fueron significativamente menores que los del grupo modelo, y la actividad de SOD fue significativamente mayor que la del grupo modelo ($p < 0,05$). El gentiopirósido puede mejorar el comportamiento de ratas epilépticas jóvenes.

Received: 13-05-2023 Accepted: 18-02-2024

INTRODUCTION

Epilepsy is a neurological disorder characterized by sudden abnormal discharges of neurons in the brain, causing transient disruptions in brain function. It can lead to neuronal damage in regions such as the cerebral cortex and hippocampus, and it is one of the most common neurological disorders in children¹. Research shows that about 75% of

epilepsy patients develop the disease during childhood². The primary treatment method for epilepsy is oral antiepileptic drugs. However, despite advances in the diagnosis and treatment of epilepsy, long-term use of antiepileptic drugs can lead to numerous adverse reactions. Furthermore, about 30% of children with epilepsy do not respond well to treatment, and severe cases can result into intractable epilepsy, which significantly af-

ffects the physical and mental health of patients³. Therefore, exploring the pathogenesis of epilepsy and finding new therapeutic drugs and targets are crucial for the effective treatment of this disorder.

Research⁴ indicates that during epileptic seizures, the NLRP3 (nodlike receptor protein 3) inflammasome is involved in cellular pyroptosis through the classical Caspase-1-dependent pathway, regulating the expression of IL-1 β and IL-18. The P2X7R (purinergic ligand-gated ion channel 7 receptor), an ATP-gated cation non-selective channel receptor, is a crucial contributor to the formation and release of IL-1 β and has been widely considered an essential target in brain tissue inflammatory responses⁵. P2X7R is upregulated at different stages of seizure. In various models of epilepsy, including the hippocampus, amygdala, piriform cortex, and neocortex, and its activation can induce and worsen inflammatory reactions⁶. Multiple studies^{7,8} have demonstrated that in innate myeloid cells such as monocytes, macrophages, and dendritic cells, the P2X7R is the most effective activator of the NLRP3 inflammasome during the inflammatory process. Current research⁹ confirms that during epileptic seizures, the P2X7R/NLRP3/Caspase-1 pathway is significantly upregulated, and downstream-specific inflammatory factors such as IL-1 β and IL-18 significantly increase. These findings suggest that the P2X7R/NLRP3/Caspase-1 pathway plays a vital role in the development of epileptic seizures.

Gentiopterin, the primary active ingredient of *Gentiana macrophylla*, a plant belonging to the Gentianaceae family, has demonstrated pharmacological properties such as anti-inflammatory, anti-oxidative stress, and anti-apoptotic effects, making it an effective natural medicine. Additionally, it has been found to have low toxicity, high safety, and multi-target synergistic effects¹⁰. The study aims to induce status epilepticus (SE) in juvenile rats through intraperitoneal injection of lithium chloride-pilocarpine and

examine whether gentiopterin can impact the occurrence of epilepsy by regulating the P2X7R/NLRP3/Caspase-1 inflammatory pathway. The results of this study will provide a foundation for gentiopterin to be considered as a potential candidate for the effective treatment of childhood epilepsy.

MATERIALS AND METHODS

Experimental Animals

Seventy-two specified pathogen-free male Sprague Dawley (SD) rats, aged 21 days and weighing 50-80g, were procured from Beijing Vital River Laboratory Animal Technology Co., Ltd. The production license number is SCXK (JING) 2021-0011. The rats were kept at the Central Animal Laboratory of our institute under optimal conditions, with a relative humidity of 70%, a temperature of 25°C, and a 12-hour light/dark cycle. We strictly follow the 3R principle in the experiment. The Animal Experiment Center of Tongling Vocational and Technical College Ethics Committee approved this study.

Reagents and Instruments

Main reagents: Tropisetron was purchased from Xi'an Yangsen Pharmaceutical Co., Ltd. Lithium chloride and pyrrolidine carboxamide were purchased from Fluka, USA. Gentiopterin was purchased from Jingzhu Biotechnology Co., Ltd., and the Reverse transcription kit from Jiangsu Kangwei Century Biotechnology Co., Ltd. SYBR Premix Ex Taq II was purchased from Takara, Japan. BCA protein quantification kit and protein marker were purchased from Beijing Solarbio Science & Technology Co., Ltd. P2X7R, NLRP3, ASC, and Caspase-1 primary antibodies from Affinity, USA. Tunel staining solution was purchased from Shanghai Biyun Tian Biotechnology Co., Ltd.

Main instruments: A Micro 17R low-temperature high-speed centrifuge was purchased from Thermo, USA. CFX Connect real-time fluorescence quantitative PCR instrument was purchased from BIORAD, USA.

EPS300 electrophoresis apparatus, EPS300 electrophoresis tank, and VE186 transfer apparatus were purchased from Zhejiang Tianneng Corporation. 610020-9Q chemiluminescence analyzer was purchased from Shanghai Qinxiong Scientific Instrument Co., Ltd. RM2016 pathological slicer was purchased from Shanghai Leica Instrument Co., Ltd. Nikon Eclipse C1 upright fluorescence microscope and Nikon DS-U3 imaging system were purchased from Nikon, Japan.

Animal grouping and model establishment

A total of 72 SD rats were used in the study. Twelve rats were randomly assigned to the normal group, while the remaining 60 rats were used to establish an epilepsy model. The rats were first weighed and then injected with 127 mg/kg of lithium chloride into the abdominal cavity to induce epilepsy. After 20 hours, 1mg/kg of atropine sulfate was also injected to reduce the peripheral cholinergic reaction of pilocarpine. Thirty minutes later, the rats were injected with 50mg/kg of pilocarpine. The success of the epilepsy model was determined by using the Racine scoring standard, which required a seizure frequency of ≥ 4 and a duration of ≥ 30 minutes¹¹. The model construction is shown in Fig. 1.

The rats that were successfully modeled were divided into groups randomly. The positive control group received 5.9 mg/kg of topiramate dissolved in 2 mL of normal saline via gavage. The low-dose, medium-dose, and high-dose groups were administered

gentiopicrotin solution via gavage, dissolved in 2 mL of normal saline, at doses of 1.28g/kg, 2.56g/kg, and 5.12g/kg, respectively. The model and normal groups were given the same volume of saline via gavage once a day for four weeks.

Behavioral assessment

Within two hours of administering pilocarpine, the rats were observed for any behavioral changes, and the onset latency and duration of the first seizure were recorded. The severity of SE in each group was graded according to the Racine scoring system, as follows: Stage 0, no seizures; Stage I, facial twitching and mouth movements; Stage II, frequent nodding or wet dog shakes; Stage III, localized clonic seizures in the forelimbs; Stage IV, generalized tonic-clonic seizures with forelimb clonus and rigid posture in the hindlimbs; and Stage V, generalized tonic-clonic seizures with falling and rolling.

Tissue processing

After one, two, and seven days of modeling, rats from each group were intraperitoneally injected with a 5% chloral hydrate solution for anesthesia. Four rats from each group were then quickly decapitated to obtain brain tissue, rats were fixed on the operating table, and their chests were opened to expose the heart. The right auricle was incised, and 150 mL of saline was perfused to flush out the blood, followed by perfusion with 150 mL of 4% paraformaldehyde

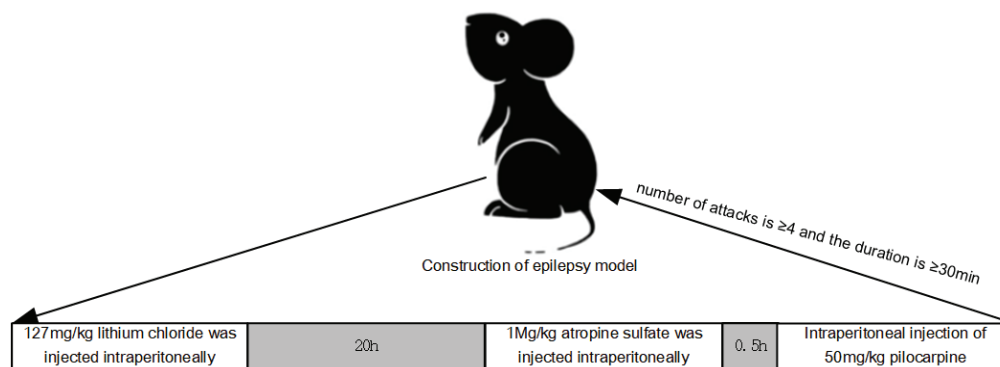


Fig. 1. Schematic diagram of epilepsy model construction.

for fixation. The brain was quickly removed after fixation and placed in a 4% paraformaldehyde solution for an additional 48 hours of fixation before being subjected to Tunel staining. The rest of the brain tissue was stored at -80°C for subsequent analysis using ELISA kits, Western blotting, and qRT-PCR.

Tunel staining to observe pathological changes in hippocampal tissue

Brain tissue was fixed in 4% paraformaldehyde, and coronal brain sections containing the hippocampus, from 3 mm anterior to 3 mm posterior to the optic chiasm, were obtained. The sections were routinely dehydrated, transparentized, and embedded in paraffin before being pre-cooled for sectioning (thickness of $4\ \mu\text{m}$). The sections were then deparaffinized with xylene, rehydrated with gradient ethanol, and stained with Tunel staining solution for 1-10 minutes. After rinsing with distilled water twice for 15 seconds each, the sections were dehydrated with 95% ethanol for 5 minutes, transparentized with xylene for 5 minutes, and mounted with neutral gum. Under a microscope, the number of Tunel-positive stained cells in each high-power field was counted, and the average value was obtained.

ELISA detection of superoxide dismutase (SOD) activity and malondialdehyde (MDA) content in hippocampal tissue

Hippocampal tissue from rats obtained on the 7th day after modeling was added to pre-cooled PBS buffer, ground into a homogeneous slurry on ice, and centrifuged at 10,000 rpm for 10 minutes. The supernatant was collected and divided into Eppendorf (EP) tubes, then stored at -80°C . ① SOD activity detection: $20\ \mu\text{L}$ of the test sample was taken and sequentially added to the SOD detection buffer, WST-8 working solution, and reaction start working solution. The mixture was incubated at 37°C for 30 minutes, and the absorbance (A) value was measured at 450 nm wavelength. Using the formula inhibition percentage = $(\Delta\text{A blank} - \Delta\text{A test}) /$

$\Delta\text{A blank} \times 100\%$, the inhibition percentage was calculated. The SOD enzyme activity (U/mg) of the test sample was determined from the standard curve. ② MDA content detection: $100\ \mu\text{L}$ of the test sample was taken and sequentially added to the working solution, distilled water, and test sample. The mixture was incubated at 100°C in a water bath for 60 minutes, cooled in an ice bath, and centrifuged at room temperature at $10,000\text{g}$ for 10 minutes. Next, $200\ \mu\text{L}$ of the supernatant was transferred to a glass cuvette, and the absorbance (A) values at 450 nm, 532 nm, and 600 nm were measured. The $\Delta\text{A}450 = \text{A}450\ \text{test} - \text{A}450\ \text{blank}$, $\Delta\text{A}532 = \text{A}532\ \text{test} - \text{A}532\ \text{blank}$, and $\Delta\text{A}600 = \text{A}600\ \text{test} - \text{A}600\ \text{blank}$ were calculated. The MDA content (nmol/g) was calculated as $\text{MDA content} = 5 \times [12.9 \times (\Delta\text{A}532 - \Delta\text{A}600) - 2.58 \times \Delta\text{A}450]$.

Western blot analysis of P2X7R, NLRP3, ASC, and Caspase-1 Protein expression in hippocampal tissue

Hippocampal tissue was collected and homogenized on ice on the seventh day after modeling. The supernatant was obtained after centrifugation, and protein concentration was measured using a BCA protein assay kit. Protein lysates were separated on a 15% SDS-PAGE gel with a 5% stacking gel, run at 80V for two hours, and transferred to a membrane at 60V for two hours. After blocking with 5% skim milk for two hours, the membrane was incubated overnight at 4°C with rabbit primary antibodies against P2X7R, NLRP3, ASC, and Caspase-1 (diluted 1:1000). The following day, the membrane was washed with TBST and incubated with a goat anti-rabbit secondary antibody (diluted 1:2000) for two hours at 37°C . After washing, the membrane was incubated with a chemiluminescence reagent, and the protein expression levels were quantified using ImageJ software with GAPDH as an internal reference protein. The relative protein expression levels were calculated as the protein gray value of the target protein divided by the protein gray value of the internal reference protein.

qRT-PCR detection of hippocampal P2X7R, NLRP3, ASC, and Caspase-1 mRNA expression

On the 7th day after modeling, hippocampal tissue was obtained and ground on ice. Total RNA was extracted using 1 mL of Trizol lysis buffer. The RevertAid™ First Strand cDNA Synthesis Kit synthesized cDNA as the fluorescent quantification template. Takara designed and synthesized Primers in Japan, and GAPDH was used as the internal reference for all samples. The reaction system included 0.5% μ L dNTPs, 5 μ L 5 \times Buffer, 0.3 μ L Taq enzyme, 21.5 μ L MgCl₂, 2 μ L cDNA template, and 1 μ L of upstream and downstream primers. Deionized water was added to a total volume of 25 μ L. The reaction conditions were as follows: pre-denaturation at 95°C for 5 minutes, denaturation at 95°C for 30 seconds, annealing at 62°C for 30 seconds, extension at 72°C for 30 seconds, repeated for 40 cycles, and final extension at 72°C for 10 minutes. The reaction was terminated at 4°C for 5 minutes, and the experiment was repeated three times. The relative expression level of the target gene mRNA was calculated using the $2^{-\Delta\Delta CT}$ method. Primer sequences are shown in Table 1.

Table 1
Primer Sequences.

Gene	Sequence
P2X7R	Forward GGACGAGCTACCCTTCGGT
	Reverse CTGTCTCACCCCCAGCATAG
NLRP3	Forward CACATCATGAAGGAGGAGG
	Reverse GCTATCACACAGCCTGGGTC
ASC	Forward ACCCTAATGCCTTGTTCCCA
	Reverse TGGGGAAGTCTTCAGCAAC
Caspase-1	Forward GGCAGACCTATTTTGCACGA
	Reverse TAGCTGTCGATGGATGCCTC
U6	Forward CTGATGAAATACGCCAGGT
	Reverse CTGTGGTTCTGGTTCGCTTT

Statistical Analysis

The experimental data were analyzed using SPSS 26.0 software, and GraphPad 8.0 was utilized for plotting. Data that followed a normal distribution, such as pathological changes and protein expression level in each sample group, were presented as mean \pm standard deviation ($\bar{x}\pm$ SD). One-way analysis of variance (ANOVA) was employed for comparisons among multiple groups, and t-tests were used for pairwise comparisons. A p of less than 0.05 was considered statistically significant.

RESULTS

Effects of Gentiopicroin on behavioral performance in juvenile rats with epilepsy

In the blank control group, the behavior of the rats was normal, and no epileptic seizures were observed, indicating a grade 0 level of epileptic seizures. In the positive control group and gentiopicroin low, medium, and high dose groups, the latency period was significantly increased compared to the model group. Moreover, the duration and severity of epileptic seizures were significantly reduced in the groups mentioned above compared to the model group ($p<0.05$) (Fig. 2).

Effects of Gentiopicroin on TUNEL staining positive cell numbers in hippocampal tissue

TUNEL staining revealed that in the normal group, neurons in the CA3 region of rat hippocampus were evenly distributed across multiple layers, with pyramidal and granular cells showing normal morphology, uniform staining, tight arrangement, and round or oval cell bodies with distinct nucleoli. The cytoplasm of these cells had abundant TUNEL bodies, and occasional nuclear condensation was observed. In contrast, compared to the normal group, the model group showed a reduction in the number and shape of neurons in the CA3 region, with decreased cell bodies, ruptures, nuclear condensation, and a significant decrease in TUNEL bodies in the

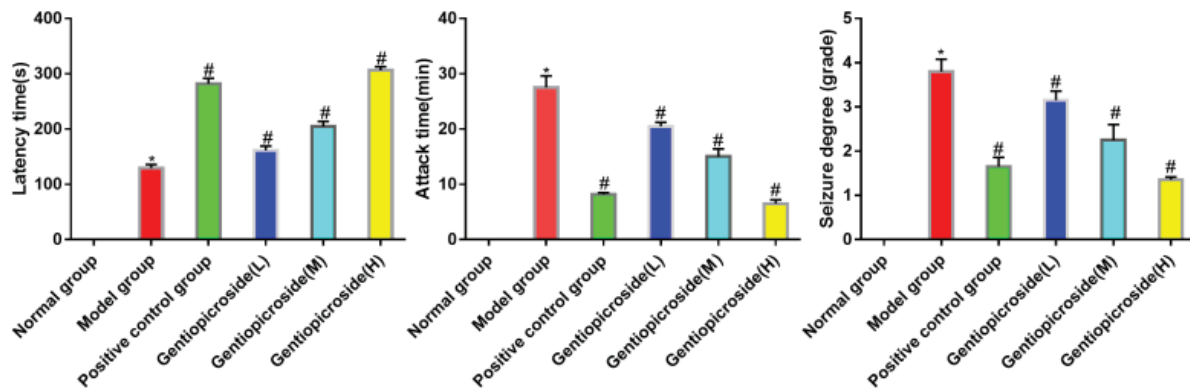


Fig. 2. Effect of gentiopicroside on epileptic behavior in young rats (*compared with Normal group, $p < 0.05$, # compared with Model group, $p < 0.05$).

cytoplasm. Compared to the model group, the positive control group and gentiopierin low, medium, and high dose groups showed a reduction in the degree of neuronal damage in the CA3 region of the rat hippocampus. The number of TUNEL-stained positive cells in the model group was significantly higher than in the control group ($p < 0.05$). However, the number of TUNEL-stained positive cells in the positive control group and gentiopierin low, medium, and high dose groups was significantly lower than that in the model group, and the differences were statistically significant ($p < 0.05$) (Fig. 3).

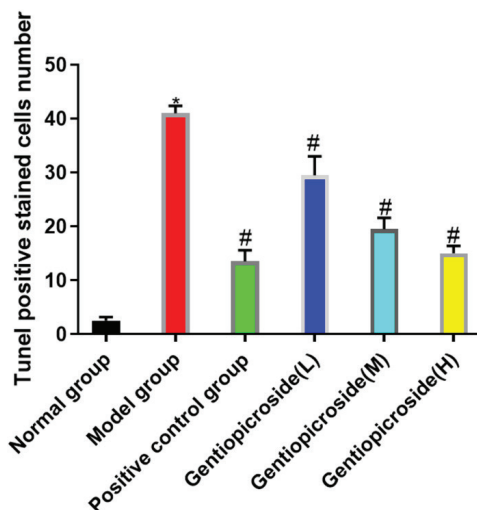


Fig. 3. Comparison of TUNEL staining results in each group (*compared with Normal group $p < 0.05$, # compared with Model group $p < 0.05$).

Effects of Gentiopierin on superoxide dismutase (SOD) activity and malonaldehyde (MDA) content in hippocampal tissue

In the model group, the SOD activity was significantly lower, and the MDA content was significantly higher than that in the control group, with statistical significance ($p < 0.05$). However, in the positive control group and gentiopierin low, medium, and high dose groups, the SOD activity was significantly higher, while the MDA content was significantly lower than that in the model group, with statistical significance ($p < 0.05$), (Fig. 4).

Effects of Gentiopierin on the expression of P2X7R, NLRP3, ASC, Caspase-1 proteins, and mRNA in hippocampal tissue

The expression levels of P2X7R, NLRP3, ASC, Caspase-1 proteins, and mRNA in the model group were significantly higher than those in the control group, with statistical significance ($p < 0.05$). However, in the positive control group and gentiopierin low, medium, and high dose groups, the expression levels of P2X7R, NLRP3, ASC, Caspase-1 proteins, and mRNA were significantly lower than those in the model group, with statistical significance ($p < 0.05$), (Fig. 5).

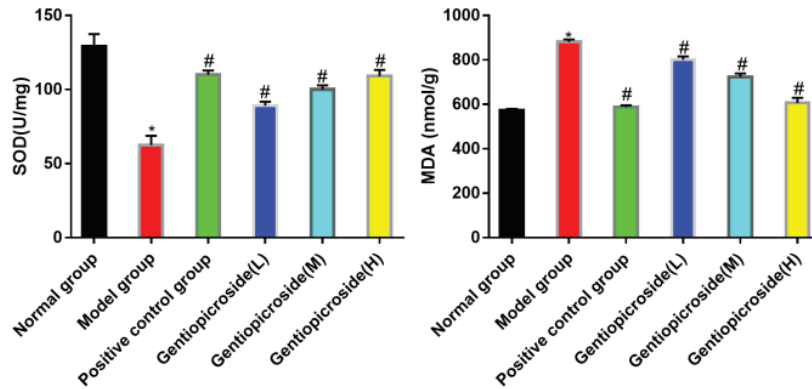


Fig. 4. Effect of gentiopicroside on SOD activity and MDA content in the hippocampus (*compared with Normal group, $p < 0.05$, # compared with Model group, $p < 0.05$). SOD: superoxide dismutase; MDA: malonilaldehyde.

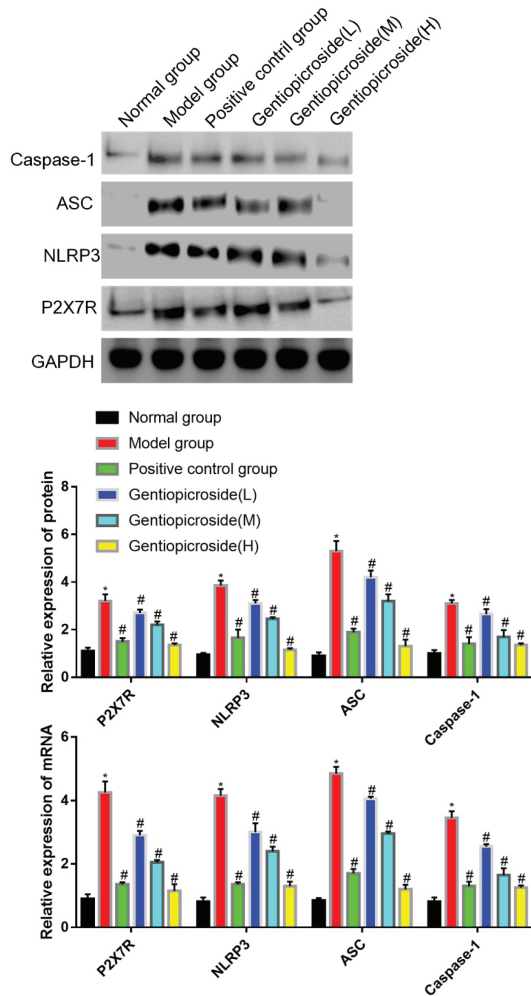


Fig. 5. Effects of gentiopicroside on P2X7R, NLRP3, ASC, Caspase-1 protein and mRNA in hippocampus (*compared with Normal group, $p < 0.05$, #compared with Model group, $p < 0.05$).

Gentiopicroside improves behavioral performance in juvenile rats with epilepsy by regulating the P2X7R/NLRP3/Caspase-1 pathway to inhibit inflammatory factor expression.

Gentiopicroside significantly prolonged the latency period of epileptic rats, reduced the duration and severity of seizures, improved hippocampal tissue pathology, increased hippocampal tissue SOD activity, and decreased MDA levels. Furthermore, it down-regulated critical proteins in the P2X7R/NLRP3/Caspase-1 pathway. Therefore, we speculate that gentiopicroside may improve behavioral performance in epileptic rats by regulating the P2X7R/NLRP3/Caspase-1 pathway to inhibit inflammatory factor expression. A schematic diagram of the mechanism is shown in Fig. 6.

DISCUSSION

Epilepsy is a common and severe neurological disorder that can cause recurrent, transient, and paroxysmal seizures, resulting in high mortality and disability rates, particularly among children. This condition significantly affects the quality of life of patients¹². At present, the primary clinical approach for treating epilepsy is through the use of antiepileptic drugs (AEDs). However, AEDs only provide partial and incomplete control

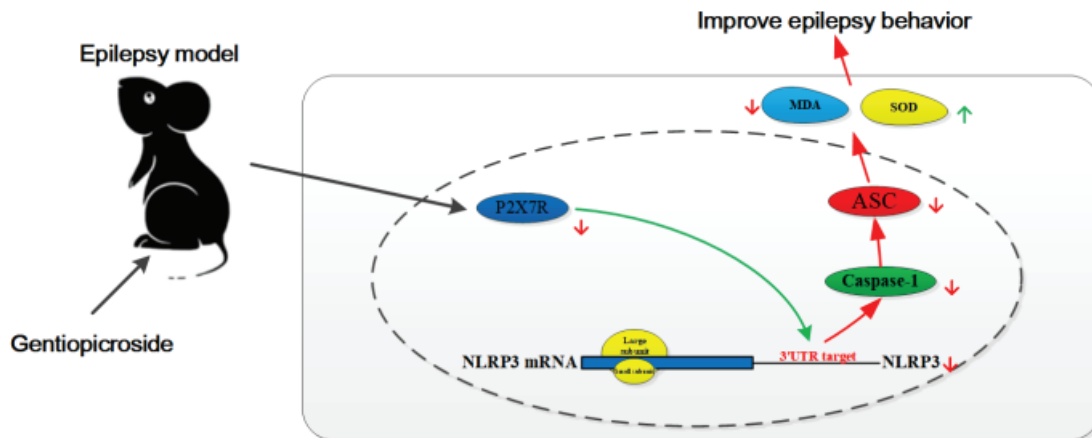


Fig. 6. Mechanism diagram of gentiopiroside improving the behavior of epileptic young rats by regulating P2X7R/NLRP3/Caspase-1 to inhibit the expression of inflammatory factors.

of seizures in approximately 30% of epilepsy patients¹³. Moreover, long-term use of AEDs can lead to significant adverse reactions, such as cognitive impairment, psychiatric side effects, teratogenic effects, and toxic effects on the liver. Therefore, it is of utmost importance to identify new drug targets and develop new antiepileptic drugs for children. Gentiopiricin is a natural bicyclic diterpenoid lactone compound with various biological activities, mainly extracted from *Gentiana macrophylla*, a characteristic medicinal plant in Ningxia, China¹⁴. Previous studies¹⁵ have shown that gentiopiricin can help alleviate anxiety and depression symptoms, memory impairment, and nerve damage.

The P2X7 receptor can affect the release of downstream inflammatory factors and the activation of immune cells by influencing various signaling pathways, such as the P-38MAPK, NF-KB, and NLRP3/Caspase-1 pathways¹⁶. Recent studies have confirmed that the P2X7R/NLRP3/Caspase-1 pathway is significantly upregulated during seizures, leading to increased expression of specific inflammatory factors like IL-1 β and IL-18¹⁷. This suggests that the P2X7R/NLRP3/Caspase-1 pathway is a critical mediator in seizure activity¹⁸. In this study, we focused on the protective effect of gentiopiricin on neurons in a rat model of epilepsy by targeting

the P2X7R/NLRP3/Caspase-1 pathway. We induced SE in rats using lithium chloride-pilocarpine and used topiramate as the positive control drug. The results showed that the gentiopiricin intervention significantly prolonged the SE latent period, shortened seizure duration, and reduced SE in a dose-dependent manner, indicating its antiepileptic effects in SE rats. Seizures can lead to decreased brain nerve cells, neuronal damage, and cell apoptosis, directly affecting the patient's prognosis and condition development¹⁹. In this study, the protective effect of gentiopiricin on hippocampal damage in epileptic rats was observed through Tunel staining. Pathological section staining revealed that hippocampal neurons in the model group exhibited significant damage, with disordered arrangement, small or ruptured cell bodies, condensed nuclei, reduced Tunel bodies in the cytoplasm, and an increased number of damaged cells over time. Compared with the model group, the number of damaged neurons in the CA3 region of the hippocampus in the positive control and gentiopiricin low, medium, and high dose groups decreased, the degree of damage was reduced, and the number of damaged cells did not increase over time. These results suggest that gentiopiricin has an inhibitory effect on hippocampal neuronal

damage caused by epilepsy. Oxidative stress-induced brain cell damage and weakened antioxidant capacity are essential mechanisms underlying the occurrence and persistence of epilepsy and other neurological diseases²⁰. SOD, an important antioxidant enzyme, reflects the body's ability to remove free radicals, while MDA is related to the degree of tissue cell damage and is a lipid peroxide produced after tissue cells are damaged by oxygen free radicals²¹. The findings of this study showed that epilepsy can increase the MDA content in hippocampal tissue and reduce SOD activity, whereas gentiopiricin can inhibit oxidative stress-induced damage caused by epilepsy, increase SOD activity, and reduce MDA production.

The NLRP3 inflammasome is a complex composed of three essential proteins: the NOD-like receptor NLRP3, the adapter protein ASC, and the effector protein Caspase-1²². Once activated, NLRP3 releases Caspase-1, which in turn cleaves precursor forms of IL-1 β and IL-18, generating mature and activated forms of these cytokines that promote the development of inflammation²³. The P2X7R receptor is a crucial factor in activating the NLRP3 inflammasome. When neural tissue is damaged, a large amount of ATP is released, which binds to the P2X7 receptor on microglia and promotes the formation of the NLRP3 inflammasome. This results in the acceleration of maturation and release of inflammatory factors such as IL-1 β and IL-18, initiating a cascade effect²⁴⁻²⁶. The study results show that both the protein and mRNA levels of P2X7R, NLRP3, ASC, and Caspase-1 were significantly higher in the model group than in the control group. However, in the positive control group and the low, medium, and high dose groups of gentiopiricin, the protein and mRNA levels of P2X7R, NLRP3, ASC, and Caspase-1 were significantly lower than those in the model group. Yang Wenwei and other scholars have also found that gentiopiricin inactivates NLRP3 inflammatory corpuscles by inhibiting P2X7R expression, thus reducing the

occurrence of epilepsy in young rats²⁷, which is similar to the results of this study.

In conclusion, the results of this study suggest that gentiopiricin may improve behavioral deficits in epileptic rats by regulating the expression of inflammatory factors through the P2X7R/NLRP3/Caspase-1 pathway.

Funding

None.

Conflicts of interest

The authors declare no conflicts of interest to report regarding the present study.

The authors declare that they have no competing interests.

ORCID numbers

- JiaLin Li (JLL):
0009-0008-7613-3439
- Lin Huang (LH):
0009-0000-3220-9157
- XingJun Wu (XJW):
0009-0001-3390-5493
- MinYe (MY):
0009-0002-9862-3427
- ChuanYong Yu (CYY):
0009-0005-0969-6547

REFERENCES

1. **Gong X, Liu L, Li X, Xiong J, Xu J, Mao D, Liu L.** Neuroprotection of cannabidiol in epileptic rats: Gut microbiome and metabolome sequencing. *Front Nutr.* 2022; 9:1028459.
2. **Desai D, Shende P.** β -Cyclodextrin-crosslinked synthetic neuropeptide Y-based nanosponges in epilepsy by contributing GABAergic signal. *Nanomedicine: NBM.* 2022; 45:102594.
3. **Colangeli R, Morena M, Werner A, Thompson R J, van der Stelt M, Pittman QJ, Hill MN, Teskey GC.** 2-AG-mediated

- control of GABAergic signaling is impaired in a model of epilepsy. *J Neurosci.*2023; 43:571-583.
4. Qin Z, Song J, Lin A, Yang W, Zhang W, Zhong F, Huang L, Lü Y, Yu W. GPR120 modulates epileptic seizure and neuroinflammation mediated by NLRP3 inflammasome. *J Neuroinflamm.* 2022; 19:121.
 5. Guerra Leal B, Barros-Barbosa A, Ferreirinha F, Chaves J, Rangel R, Santos A, Carvalho C, Martins-Ferreira R, Samões R, Freitas J, Lopes J, Ramalheira J, Lobo MG, Martins da Silva A, Costa PP, Correia-de-Sá P. Mesial Temporal Lobe Epilepsy (MTLE) Drug-refractoriness is associated with P2X7 receptors overexpression in the human hippocampus and temporal neocortex and may be predicted by low circulating levels of miR-22. *Front Cell Neurosci.* 2022; 16:910662.
 6. Engel T. The P2X7 Receptor as a mechanistic biomarker for epilepsy. *Int J Mol Sci.* 2023;24:5410.
 7. Wang Y, Shan Z, Zhang L, Fan S, Zhou Y, Hu L, Wang Y, Li W, Xiao Z. P2X7R/NLRP3 signaling pathway-mediated pyroptosis and neuroinflammation contributed to cognitive impairment in a mouse model of migraine. *J Headache Pain.*2022;23:75.
 8. Liu C, She Y, Huang J, Liu Y, Li W, Zhang C, Zhang T, Yu L. HMGB1-NLRP3-P2X7R pathway participates in PM(2.5)-induced hippocampal neuron impairment by regulating microglia activation. *Ecotoxicol Environ Saf.* 2022;239:113664.
 9. Pohlentz MS, Müller P, Cases-Cunillera S, Opitz T, Surges R, Hamed M, Vatter H, Schoch S, Becker AJ, Pitsch J. Characterisation of NLRP3 pathway-related neuroinflammation in temporal lobe epilepsy. *PLoS one.*2022;17:e0271995.
 10. Ren G, Zhang Q, Xia P, Wang J, Fang P, Jin X, Peng X, Xu Y, Zhang J, Zhao L. Synthesis and biological evaluation of gentiopicroside derivatives as novel cyclooxygenase-2 inhibitors with anti-inflammatory activity. *Drug Des Dev Ther.*2023;17:919-935.
 11. Wu L, Qin Y, Yuan H, Zhu Y, Hu A. Anti-inflammatory and neuroprotective effects of insulin-like growth factor-1 overexpression in pentylenetetrazole (PTZ)-induced mouse model of chronic epilepsy. *Brain Res.* 2023;15:1785.
 12. Piper RJ, Richardson RM, Worrell G, Carmichael DW, Baldeweg T, Litt B, Denison T, Tisdall MM. Towards network-guided neuromodulation for epilepsy. *Brain* 2022;145:3347-3362.
 13. Belete D, Jacobs BM, Simonet C, Bestwick JP, Waters S, Marshall CR, Dobson R, Noyce AJ. Association between antiepileptic drugs and incident Parkinson disease. *JAMA Neurol* 2023;80:216.
 14. Zhang L, Ulriksen ES, Hoel H, Sandvik L, Malterud KE, Inngjerdingen KT, Inngjerdingen M, Wangensteen H. Phytochemical characterization and anti-inflammatory activity of a water extract of *Gentiana purpurea* roots. *J Ethnopharmacol.* 2023;301:115818.
 15. Wang Y, Sheng Y, Ji N, Zhang H. Gentiopicroside enhances the protective effect of trimetazidine against myocardial ischemia-reperfusion injury via the AMPK/NLRP3 inflammasome signaling. *J Biochem Mol Toxic.*2023;37:e23366
 16. Sun S, Jiang W, Yan X, Zhang J, Gao L, Wu C, Zhu B, Wu L. Ligand-gated ion channel P2X7 regulates NLRP3/Caspase-1-mediated inflammatory pain caused by pulpitis in the trigeminal ganglion and medullary dorsal horn. *Brain Res Bull.*2023;192:1-10.
 17. Fu Z, Lin Q, Xu Z, Fu W, Shi D, Cheng Y, Yang T, Liu G, Shi H, Cheng D. Longitudinal positron emission tomography imaging with P2X7 receptor-specific radioligand 18F-FTTM in a kainic acid rat model of temporal lobe epilepsy. *ACS Chem Neurosci.* 2022;13:3512-3522.
 18. Tashakori-Miyanroudi M, Ramazi S, Hashemi P, Nazari-Serenjeh M, Baluchnejadmojarad T, Roghani M. Acetyl-L-carnitine exerts neuroprotective and anticonvulsant effect in kainate murine model of temporal lobe epilepsy. *J Mol Neurosci.*2023;72:1224-1233.
 19. Zhou Y, Su Y, Li S, Kennedy BC, Zhang DY, Bond AM, Sun Y, Jacob F, Lu L, Hu P, Viaene AN, Helbig I, Kessler SK, Lucas T,

- Salinas RD, Gu X, Chen HI, Wu H, Kleinman JE, Hyde TM, Nauen DW, Weinberger D R, Ming GL, Song H. Molecular landscapes of human hippocampal immature neurons across lifespan. *Nature* 2022;607:527-533.
20. Alyami NM, Abdi S, Alyami HM, Almeer R. Proanthocyanidins alleviate pentylene-tetrazole-induced epileptic seizures in mice via the antioxidant activity. *Neurochem Res* 2022;47:3012-3023.
 21. Wang Z, Na Z, Cui Y, Wei C, Wang S. LncRNA ZFAS1 regulates the hippocampal neurons injury in epilepsy through the miR-15a-5p/OXSR1/NF- κ B pathway. *Metab Brain Dis* 2022;37:2277-2290.
 22. Arab HH, Abd El Aal HA, Alsufyani SE, El-Sheikh AAK, Arafa EA, Ashour AM, Kabel AM, Eid AH. Topiramate reprofiling for the attenuation of cadmium-induced testicular impairment in rats: role of NLRP3 inflammasome and AMPK/mTOR-linked autophagy. *Pharma* 2023;15:1402.
 23. Pohlentz MS, Müller P, Cases-Cunillera S, Opitz T, Surges R, Hamed M, Vatter H, Schoch S, Becker AJ, Pitsch J. Characterisation of NLRP3 pathway-related neuroinflammation in temporal lobe epilepsy. *Plos One* 2023;17:e0271995.
 24. Luo L, Liu M, Fan Y, Zhang J, Liu L, Li Y, Zhang Q, Xie H, Jiang C, Wu J, Xiao X, Wu Y. Intermittent theta-burst stimulation improves motor function by inhibiting neuronal pyroptosis and regulating microglial polarization via TLR4/NF κ B/NLRP3 signaling pathway in cerebral ischemic mice. *J Neuroinflamm* 2022;19:141.
 25. Jung ES, Suh K, Han J, Kim H, Kang HS, Choi WS, Mook-Jung I. Amyloid- β activates NLRP3 inflammasomes by affecting microglial immunometabolism through the Syk-AMPK pathway. *Aging cell* 2023;21:e13623.
 26. Vezzani A, Friedman A, Dingledine RJ. The role of inflammation in epileptogenesis. *Neuropharmacology*. 2013;69:16-24.
 27. Yang W, Ma L, Xu S, Zheng P, Du J, Wu J, Yu J, Sun T. Gentiopicroside alleviated epileptogenesis in immature rats through inactivation of NLRP3 inflammasome by inhibiting P2X7R expression. *Int J Dev Neurosci* 2023;83(1):53-66.

Benefits of a modified local precision liver resection using intraoperative laparoscopic ultrasound in the treatment and prognosis of patients with liver cancer.

Yansong Xu¹ and Lin Shen²

¹Department of Hepatobiliary Surgery, Affiliated Hospital of Beihua University, Jilin, China.

²Department of Anesthesiology, Affiliated Hospital of Beihua University, Jilin, China.

Keywords: precision hepatectomy; liver function; hepatic venous injury; immune factors; immune response; cytokines; Karnofsky performance scale.

Abstract. The incidence and mortality rate of liver cancer has increased significantly. Recently, intraoperative laparoscopic ultrasound (LUS) has been used in hepatectomy, in addition to open liver resection, as the most common treatment method. The current research aims to address this issue. Seventy-six patients with liver cancer who were admitted to the Hospital of Beihua University from February 2018 to September 2021 were randomly divided into two groups of 38 patients, one group undergoing conventional laparoscopic surgery (control group) and the other group undergoing a precise laparoscopic liver resection after placing an intraoperative LUS instrument (study group). Blood loss and hepatic vein damage during surgery were less in the study group ($p < 0.05$). Seven days after surgery, liver function indices (albumin, total bilirubin, and alanine and aspartate aminotransferases) and indices related to immune function interleukin 6, tumor necrosis factor α , CD3+ and CD4+ T lymphocytes and NK cells level in the study group improved compared to the control group. The postoperative complications were less in the study group, and the nine-month follow-up showed that the recurrence rate was lower and the survival rate was higher in this group. This study shows that precise laparoscopic hepatectomy modified with the use of intraoperative laparoscopic ultrasound results in better intraoperative and postoperative outcomes for the prognosis and survival rate of patients with liver cancer, which makes this surgical technique worth generalizing in clinical practice.

Beneficios de la resección hepática de precisión local modificada, utilizando ecografía intraoperatoria laparoscópica en el tratamiento y pronóstico de pacientes con cáncer de hígado.

Invest Clin 2024; 65 (2): 155 – 168

Palabras clave: hepatectomía de precisión; función hepática; lesión venosa hepática; factores inmunológicos; respuesta inmune; citocinas; escala de desempeño de Karnofsky.

Resumen. La tasa de incidencia y mortalidad del cáncer de hígado ha aumentado drásticamente. Además de la resección hepática abierta como método de tratamiento más común, la ecografía laparoscópica intraoperatoria (LUS) se ha utilizado recientemente en la hepatectomía. El objetivo de la investigación actual es responder a esta pregunta. 76 pacientes con cáncer de hígado ingresados en el Hospital de la Universidad de Beihua entre febrero de 2018 y septiembre de 2021 fueron asignados aleatoriamente a dos grupos de 38 pacientes, un grupo sometido a cirugía laparoscópica convencional (grupo control) y el otro grupo sometido a resección hepática laparoscópica precisa, después de colocar un instrumento LUS intraoperatorio (grupo de estudio). La pérdida de sangre y el daño a las venas hepáticas durante la cirugía fueron menores en el grupo de estudio ($p < 0,05$). Siete días después de la cirugía, los índices de función hepática (albúmina, bilirrubina total y alanina y aspartato aminotransferasas) e índices relacionados con la función inmune, interleucina 6, factor de necrosis tumoral α , linfocitos T CD3+ y CD4+ y nivel de células NK en el grupo de estudio mejoraron en comparación con el grupo control. Las complicaciones postoperatorias fueron menores en el grupo de estudio, y el seguimiento a los 9 meses mostró que la tasa de recurrencia fue menor y la tasa de supervivencia fue mayor en este grupo. Este estudio demuestra que la hepatectomía laparoscópica precisa modificada con el uso de la ecografía laparoscópica intraoperatoria da como resultado mejores resultados intraoperatorios y postoperatorios para el pronóstico y la tasa de supervivencia de los pacientes con cáncer de hígado, y hace que valga la pena generalizar esta técnica quirúrgica en la práctica clínica.

Received: 20-07-2023

Accepted: 11-11-2023

INTRODUCTION

Liver cancer is a malignant tumor that seriously affects Chinese residents' health, and its incidence is relatively high^{1,2}. The early stage of hepatocellular carcinoma courses with insidious characteristics and rapid growth, but it is often diagnosed in

the middle and late stages. At the same time, liver cancer has high recurrence and mortality rates^{3,4}. At present, liver cancer is mainly treated through surgery. In clinical practice, different treatment measures are adopted according to the different liver function reserve abilities, the physical conditions of people with liver cancer, and the dif-

ferent stages of cancer the patients present. Liver resection is preferred for patients with localized liver cancer without accompanying cirrhosis⁵. Hepatectomy is the most common surgical method for radical liver cancer treatment, which can notoriously reduce the recurrence and spread of liver tumors and effectively prolong the survival time of sufferers^{6,7}. Conventional open liver resection is a standard clinical method. However, the patient's postoperative recovery and prognosis are unsatisfactory due to the extensive surgical trauma and the risk of acquiring a postoperative infection⁸. With the development of science and technology and the enhancement of medical standards, the application value of laparoscopy in various surgical operations has become increasingly apparent. In the 1990s, Reich performed the world's first laparoscopic liver resection. Since then, the door has been opened to minimally invasive surgery through laparoscopy⁹.

In contrast with conventional open liver resection, laparoscopic liver resection has the advantages of less trauma and quick postoperative recovery, which surgeons and patients favor. However, laparoscopic surgery also has limitations since the laparoscopic surgeon operates only through a few holes and cannot directly contact and manipulate the related visceral structure, and because of the reduced abdomen's display, the surgeon may not fully understand the abdominal situation, leading to a limited surgical field. At the same time, the lack of palpation increases the risk in laparoscopic surgery¹⁰. In addition, because the field is not comprehensive, it is easy to ignore some small lesions, and it can easily result in the presence of tumor residues, leading to a high recurrence rate in patients. Enhanced local precision resection was developed based on a conventional laparoscopic resection. Using laparoscopic ultrasound (laparoscopic ultrasonography, LUS) can help the operator detect complex lesions. It can synchronously guide the surgeon to operate, reduce damage to related organs and tissues, and make up for the deficiencies of conventional laparoscopic surgery.

Relevant studies have shown that laparoscopic surgery with LUS is more effective^{11,12}. In recent years, ultrasound examination has been gradually applied to laparoscopic surgery. The period of clinical use has not been very long, and since the related studies are few, the therapeutic effect of laparoscopic surgery on liver cancer still needs further analysis¹³. Therefore, this study aimed to evaluate the clinical benefits of modified precision hepatectomy using intraoperative LUS in patients with liver cancer so that this new treatment technique can be tested to find a better way to treat liver cancer.

PATIENTS AND METHODS

General Information

In this study, all eighty-seven patients with liver cancer admitted to the Hospital of Beihua University, China, from February 2018 to September 2021 were selected for this study. The inclusion criteria were as follows: met the diagnosis and implications of liver cancer, according to the Guidelines on the diagnosis and treatment of primary liver cancer (2011 edition)¹⁴. Relevant criteria in TNM stages I, II, and III; Child-Pugh grades A or B; no associated surgery or radiofrequency ablation for six months; and nine months of telephone follow-up after laparoscopic surgery. Exclusion criteria were tumor involvement of adjacent organs or metastases; severe abdominal adhesion; patients with cardiac or renal failure; abnormal mental status; diabetes; women during pregnancy or lactation; and patients with an allergic condition. All patients signed the informed consent form, and the medical ethics committee of our hospital approved this study. Of the eighty-seven patients who were accepted at the beginning of the study, after checking the study conditions and the inclusion and exclusion criteria, seventy-six patients were finally included. Seventy-six patients were randomly selected as control variables according to the random number table method and randomly divided into two groups of 38 patients.

METHODS

Surgical method: Our institution's chief surgeon has been the same physician for over eight years. We used a conventional laparoscopic liver resection for the control group: a preoperative-related imaging (MRI or CT) examination in the supine position was performed to determine the lesion site, size, and number. This examination was followed by the conventional implementation of an artificial pneumoperitoneum (pressure 12-14 mmHg), the construction of the conventional "five-port technique" according to the location and size of the tumor, abdominal exploration, to free the perihaptic ligament and to fully reveal the tumor focus, the first portal vascular implication, the left hepatic artery and portal branch, according to the liver ischemia line or the anatomy Cantilie-line mark as a resection line^{9,11,15-17}.

For the Study group, we used a modified laparoscopic precision liver resection. After a preoperative imaging (MRI or CT) examination to determine the lesion location, size, and number in the supine position, we established an arc incision approximately 10 mm below the umbilicus. This incision was followed by the conventional implementation of an artificial pneumoperitoneum (pressure 12-14 mmHg) and placed the LUS (HITACHI ALOKA Noblus; with an L44LA soft probe, probe frequency of 7.5 MHz). Different liver parts were scanned successively, and the tumor location, size, number, and the relationship between the tumor body and the peripheral vasculature and tissues were determined again. The proper liver blood flow blocking method and liver parenchyma disconnection method were selected. For severe liver parenchyma lesions, it was not appropriate to block the blood flow into the liver and use an ultrasonic knife to stop the liver parenchyma and the bipolar electrocoagulation wound. Selective blood flow into the liver was blocked for patients with mild liver parenchymal lesions, and the liver

parenchyma was severed along the ischemic line with an ultrasound knife. The vascular structure was fully exposed for the liver resection, then treated accordingly to the vascular diameter¹⁷⁻²¹.

Blood tests: In the early morning, 5 mL of cubital venous blood was extracted and centrifuged at 3500 rpm for 10 min, with a centrifugation radius of 10 cm, and the serum was collected for indicator determinations.

Observation Indicators and Evaluation Criteria

(1) Perioperative-related indicators: data and blood samples were collected by the same nurse working in our hospital for over three years. The operation time, intraoperative blood loss, hepatic vein injury rate, lesion resection edge distance, drainage tube extubation time, and anal exhaust time were recorded.

(2) Fasting venous blood was collected before and seven days after the intervention, and an analysis was performed using a fully automatic biochemical analyzer (Beckman Coulter AU5800). Liver function-related indicators were measured in both groups of patients: albumin (ALB), alanine aminotransferase (ALT), aspartate aminotransferase (AST), and total bilirubin (TBIL), as well as the immune factor-related indicators interleukin 6 (IL-6), tumor necrosis factor α (TNF- α). T lymphocyte subsets were analyzed by flow cytometry (Beckman Coulter EPICS XL) to detect T lymphocytes (CD3⁺), inducible T cells (CD4⁺), and human natural killer (NK) cells (NK cell standard). The same physician performed the specific operations according to the instructions.

(3) The incidence of related complications (infection, abdominal hemorrhage, bile leakage, pleural effusion, etc.) in the two groups of patients was reported by the same nurses working for over three years.

(4) We used the Karnofsky scoring method (Karnofsky Performance Status, KPS) 22 to assess the recovery of quality of

life in the two groups of patients. If the score increased by more than ten points after the procedure, the activities of daily living (ADL) were better; if it lessened by more than ten, it was worse; if it increased or lessened by ten, it was stable.

(5) The survival and recurrence rates of both groups were recorded by telephone follow-ups at three months (T1), six months (T2), and nine months (T3) after surgery by the same nurse.

Statistical analysis

The required data of this study were sorted and entered into a Microsoft® Excel® table. We used the SPSS26.0 software to analyze the data. If the data ($\bar{x} \pm SD$) were normally distributed, we compared the groups with the independent sample *t*-test for the group's data and paired sample *t*-test; count data was analyzed by percentages and Chi-square test (χ^2 test). The *Kaplan-Meier* survival curves were employed to determine sufferers' survival and recurrence rates in the two groups. When $p \leq 0.05$, the data's differences were considered statistically significant.

RESULTS

This study was conducted to investigate the benefits of modified precise hepatectomy using intraoperative LUS in patients with liver cancer.

The clinical and demographic characteristics of the two groups of patients under investigation are presented in Table 1. The sex distribution among the study group patients showed that 21 (55.3%) were male and 17 (44.7%) were female; whereas, in the control group, there were 20 (52.6%) male and 18 (47.4%) female patients. The mean age of the study group was 51.52 ± 6.95 years, while the mean age of the control group was 52.36 ± 8.32 years. The mean body mass index (BMI) in the study group patients was 22.36 ± 2.68 kg/m²; whereas, in the control

group, it was 22.63 ± 3.01 kg/m². The two groups had no significant differences regarding sex distribution, mean age, and mean BMI.

The staging of patients based on TNM revealed that in the study group, 14 (36.8%) patients were in stage I, 13 (34.2%) patients were in stage II, and 11 (29%) patients were in stage III. Similarly, in the control group, there were 14 (36.8%) patients in stage I, 15 (39.5%) patients in stage II, and 9 (23.7%) patients in stage III. There were no significant differences between the two groups regarding cancer staging based on TNM. The tumor diameter in the study group patients was 5.16 ± 1.49 cm, while in the control group, it was 5.09 ± 1.53 cm, and there was no significant difference in tumor diameter between the two groups. The results of the Child Grade in the two groups of examined patients showed that 29 (76.3%) patients in the study group and 27 (71%) patients in the control group were classified as Group A. Additionally, 9 (23.7%) patients in the study group and 11 (29%) patients in the control group were classified as Group B, with no significant difference observed between the two groups.

Comparison of perioperative indicators between the two groups of patients

The mean duration of surgery in the study group was 103.59 ± 19.12 minutes, while in the control group, it was 98.59 ± 20.16 minutes. There was no significant difference in the duration of surgery between the two groups. Hepatic venous injury was observed in two (5.26%) patients in the study group and ten (14.28%) patients in the control group, showing there was a significant difference ($p=0.013$). The blood loss volume in the study group was 183.38 ± 29.71 mL; whereas in the control group, it was 233.56 ± 24.28 ml, and the two groups did not differ significantly in blood loss volume. Other preoperative indicators are presented in Table 2.

Table 1
Comparison of the clinical and demographic characteristics between the two groups of liver cancer patients.

Group	Sex*		Age** (years)	BMI** (kg/m ²)	TNM& by stages (n)			Tumor diameter (cm)	Child Grade (n)	
	Men	Women			I designated time	II designated time	III designated time		A	B
Study group (n=38)	21 (55.3%)	17 (44.7%)	51.52±6.95	22.36±2.68	14 (36.8%)	13 (34.2%)	11 (29%)	5.16±1.49	29 (76.3%)	9 (23.7%)
Control group (n=38)	20 (52.6%)	18 (47.4%)	52.36±8.32	22.63±3.01	14 (36.8%)	15 (39.5%)	9 (23.7%)	5.09±1.53	27 (71%)	11 (29%)
<i>t/x²</i>	0.818		0.769	0.185		0.267		0.486		1.32
<i>p</i>	0.500		0.436	0.498		0.782		0.512		0.329

*Frequency: n (%), ** Mean± (SD). [†]TNM [classifies cancers by the size and extent of the primary tumor (T), involvement of regional lymph nodes (N), and the presence or absence of distant metastases (M)].

Table 2
Perioperative indicators of the two groups of liver cancer patients.

Group	Sample number	Time of surgery (min)**	The rate of hepatic venous injury (%)&	Intraoperative blood loss volume (mL)**	Margin distance (cm)**	Drainage tube extubation time (d)**	Anal exhaust time (d)**
Study group	38	103.59±19.12	2 (5.26)	183.38±29.71	2.97±1.15	5.93±1.28	3.74±1.03
Control group	38	98.59±20.16	10 (14.28)	233.56±24.28	3.21±0.84	6.13±1.65	4.06±1.38
<i>t/x²</i>		1.425	8.725	13.125	0.541	1.683	1.532
<i>p</i> *		0.163	0.013	<0.01	0.423	0.113	0.136

**p t-test*, ** Mean± (SD), [†]Frequency: n(%).

Indexes of liver function

The examination of liver function indicators before and after surgery in the two groups of liver cancer patients revealed that the mean blood albumin level in the study group before surgery was 39.38 ± 2.19 g/L, while in the control group was 39.44 ± 2.17 g/L, showing no significant difference. However, the mean blood albumin level in the study group after surgery was 64.41 ± 2.91 g/L, compared to 52.91 ± 2.69 g/L in the control group, indicating a significant difference in albumin levels between the two groups after surgery ($p=0.032$). The mean alanine transaminase level in the study group before surgery was 39.61 ± 5.42 U/L, and in the control group, it was 39.64 ± 5.49 U/L, with no significant difference observed. However, the mean alanine transaminase level in the study group after surgery was 10.85 ± 2.36 U/L, while in the control group, it was 15.16 ± 2.42 U/L, demonstrating a significant difference in the mean alanine transaminase levels after surgery between the two groups ($p=0.037$).

The mean preoperative aspartate aminotransferase (AST) levels in the study group of patients were 42.95 ± 3.51 U/L, while in the control group, it was 43.13 ± 3.57 U/L, showing there was no statistically significant difference observed in the preoperative AST levels between the two groups. On the other hand, the postoperative mean AST levels in the study group were 28.47 ± 2.92 U/L, whereas, in the control group, it was 34.94 ± 2.35 U/L. These results indicated a significant difference in the postoperative AST levels between the study and control groups ($p=0.041$). No significant difference was observed in the preoperative total bilirubin levels between the control group (20.44 ± 2.66 $\mu\text{mol/L}$) and the study group (20.43 ± 2.64 $\mu\text{mol/L}$). However, the mean total bilirubin level in the study group after surgery was 4.38 ± 1.43 $\mu\text{mol/L}$, while in the control group, it was 7.34 ± 2.17 $\mu\text{mol/L}$. These findings demonstrated a significant difference in the postoperative total bilirubin

levels between the two groups ($p=0.031$). The relevant data are presented in Table 3.

Comparison of immune factor indicators

The investigation of immune factor indices before and after surgery in the two groups of patients with liver cancer revealed that the mean concentration of interleukin-6 (IL-6) in the study group prior to surgery was 92.83 ± 12.59 pg/mL, while in the control group, it was 92.89 ± 12.68 pg/mL, showing no statistically significant difference. However, the mean IL-6 concentration in the study group after surgery was 101.28 ± 15.28 pg/mL, whereas, in the control group, it was 124.49 ± 14.68 pg/mL, demonstrating a significant difference in IL-6 levels between the two groups after surgery ($p=0.023$).

Regarding tumor necrosis factor-alpha (TNF α), the mean concentration in the study group before surgery was 12.06 ± 1.29 ng/mL, while in the control group was 15.68 ± 2.41 ng/mL, with no significant difference observed. However, the mean TNF α concentration in the study group after surgery was 12.09 ± 1.32 ng/mL, whereas, in the control group, it was 19.82 ± 2.39 ng/mL, indicating a significant difference in the mean TNF α levels between the two groups after surgery ($p=0.037$).

The preoperative levels of CD3⁺ (cluster of differentiation 3), CD4⁺ (cluster of differentiation 4), and NK (Natural killer cells) did not show a significant difference between the study group and the control group. However, the postoperative percentage of CD3⁺ in the study group was $56.28 \pm 7.79\%$, whereas, in the control group, it was $50.22 \pm 4.63\%$. The postoperative percentage of CD4⁺ in the study group was $27.13 \pm 5.38\%$, while in the control group was $20.51 \pm 4.29\%$. Additionally, the postoperative level of NK in the study group was 10.33 ± 1.19 pg/mL, and in the control group was 8.29 ± 1.12 pg/mL. These differences in CD3⁺, CD4⁺, and NK levels after surgery were statistically significant between the two groups ($p<0.05$). The relevant data are presented in Table 4.

Table 3
The preoperative and postoperative liver function indicators in the two groups of liver cancer patients.

set	ALB (g/L)**		ALT (U/L)**		AST (U/L)**		TBIL (μmol/L)**	
	Preoperative	Postoperative	Preoperative	Postoperative	Preoperative	Postoperative	Preoperative	Postoperative
Study Group	39.38±2.19	64.41±2.91	39.61±5.42	10.85±2.36	42.95±3.51	28.47±2.92	20.43±2.64	4.38±1.43
Control Group	39.44±2.17	52.91±2.69	39.64±5.49	15.16±2.42	43.13±3.57	34.94±2.35	20.44±2.66	7.34±2.17
<i>t</i>	0.956	2.239	0.853	2.204	0.933	2.228	0.821	2.245
<i>p</i> *	0.425	0.032	0.328	0.037	0.379	0.041	0.455	0.031

*P-value t-test, ** Mean±SD.

ALB: albumin, ALT: alanine amino transferase, AST: aspartate amino transferase, TBIL: total bilirubin.

Table 4
Preoperative and postoperative immune factor indicators in the two groups of liver cancer patients.

Group	IL-6 (pg/mL)**		TNF-α (ng/mL)**		CD3+ (%)**		CD4+ (%)**		NK (pg/mL)**	
	Preoperative	Postoperative	Preoperative	Postoperative	Preoperative	Postoperative	Preoperative	Postoperative	Preoperative	Postoperative
Study Group	92.83±12.59	101.28±15.28	12.06±1.29	12.09±1.32	61.19±5.81	56.28±7.79	35.19±3.32	27.13±5.38	13.31±1.49	10.33±1.19
Control Group	92.89±12.68	124.49±14.68	15.68±2.41	19.82±2.39	62.39±4.91	50.22±4.63	34.25±3.17	20.51±4.29	13.29±1.61	8.29±1.12
<i>t</i>	0.826	9.265	0.756	7.531	0.930	4.283	1.242	5.58	0.813	4.361
<i>p</i> *	0.425	0.023	0.328	0.046	0.375	<0.01	0.219	<0.01	0.465	0.019

*p-value t-test, ** Mean±SD.

Postoperative complications in both sets

The analysis of surgical complications among the two groups of patients revealed notable findings (Table 5). Only one patient (2.63%) experienced infection in the study group, while another patient (2.63%) developed pleural effusion following the operation. Conversely, within the control group, complications were comparatively higher. Specifically, three patients (7.89%) encountered postoperative infection, two patients (5.26%) suffered from postoperative hemorrhage, three patients (7.89%) experienced bile leak, and one patient (2.63%) developed pleural effusion. These contrasting complication rates indicate a statistically significant difference between the two groups ($p=0.022$).

Quality of life score

There were no significant differences when comparing the postoperative KPS standard scores between the two groups, $p > 0.05$ (Table 6).

Postoperative survival and recurrence rates

The comparison of survival and recurrence rates in the two groups of patients is shown in Table 7. The analysis of survival rates among the two patient groups yielded significant statistical differences ($p=0.033$). In the study group, the survival rate was remarkably high, with 37 patients (97.4%) surviving during the first and second follow-up periods. Only one patient died in the period. As the study progressed to the third follow-up, 35 patients (92.1%) remained alive, while three patients succumbed to their condition. In comparison, the control group exhibited slightly lower survival rates, with 36 patients (94.7%) surviving the initial follow-up and 35 patients (92.1%) in the second follow-up. However, by the third follow-up, the number of surviving patients decreased to 28 (73.68%).

The study group showcased favorable outcomes regarding disease recurrence, as no recurrences were observed during the

Table 5
Contrast of the incidence of postoperative complications in the two groups.

Group	Sample number	Infections	Postoperative hemorrhage	Bile leak	Pleural effusion
Study Group	38	1 (2.63%)	0	0	1 (2.63%)
Control Group	38	3 (7.89%)	2 (5.26%)	3(7.89%)	1(2.63%)
			χ^2	5.208	
			p^*	0.022	

*p-value Chi-square (χ^2 tests).

Table 6
Comparison of the quality of life in the two groups.

Group	Sample number	KPS grade	
		Preoperative**	Postoperative**
Study Group	38	60.52 ± 12.88	69.03 ± 14.02
Control Group	38	60.46 ± 12.78	68.92 ± 12.43
		t	1.563
		p^*	0.312

*p-value t-test, ** Mean ± SD.

Table 7
Comparison of survival and recurrence rates in the two groups of patients.

Group	Sample number	Survival rate n (%)			Recurrence rate n (%)		
		T1	T2	T3	T1	T2	T3
Study Group	38	37 (97.4)	37 (97.4)	35 (92.1)	0 (0.0)	1 (2.6)	2 (5.3)
Control Group	38	36 (94.7%)	35 (92.1)	28 (73.68)	1 (2.6)	2 (5.3)	7 (8.16)
	χ^2		4.57			5.029	
	p^*		0.033			0.025	

*p-value Chi-square (χ^2 tests).

first follow-up. However, during the second follow-up, a marginal recurrence rate of one patient (2.6%) was identified, which increased slightly to two patients (5.3%) during the third follow-up. In contrast, the control group exhibited higher recurrence rates, with one patient (2.6%) experiencing a recurrence during the first follow-up, followed by two patients (5.3%) during the second follow-up, and a more significant number of seven patients (8.16%) during the third follow-up. These contrasting patterns in recurrence rates between the study and control groups were statistically significant ($p=0.025$). Over time, the control group exhibited lower survival rates than the study group. Conversely, the disease recurrence rate in the control group was higher than in the study group. These disparities in survival rates and disease recurrence between the two groups were statistically significant ($p<0.05$).

DISCUSSION

Liver cancer is one of the most common malignant tumors in China. One of the main options for liver cancer treatment is surgery¹⁰. With the development of technology, laparoscopic hepatectomy has become widely used in clinical practice, and many studies have proved that this surgical technique proceeds with less significant trauma, shorter recovery time, and a better prognosis¹¹. However, the limited field of laparoscopy and

the complex vascular and bile duct systems in the liver have brought many difficulties to laparoscopic liver resection, such as how to reduce liver vascular damage, avoid tumor residues, and reduce the postoperative recurrence rate and mortality, which have always been significant in liver surgery¹². In order to preserve more normal liver tissue, the pursuit of the concept of an accurate liver resection has gradually become an objective to accomplish¹³. In surgery, the LUS probe can reach deeper lesions, allowing more comprehensive liver information to be presented to the operator. Because of the physical characteristics of ultrasound, it can effectively avoid the interference of irrelevant factors. Furthermore, it can show the tumor size and depth in the liver, reduce the number of tumor contacts and extrusion, allow for complete tumor removal, avoid residual tumors, and reduce the postoperative recurrence rate^{14,23,24}.

Fu *et al.*²¹ found that under the guidance of LUS, the hepatic vein can be located accurately, which could avoid damage and reduce the risk of postoperative bleeding. Following the results of that study, it was found that intraoperative blood loss and hepatic vein injury rates during peri-surgery were lower than those in the conventional surgery group. However, other perioperative indicators (operative time, drainage tube extubation time, anal exhaust time, etc.) were not significantly different, indicating that the addition of ultrasound assistance during the opera-

tion would not prolong the operation time, which was in contrast with Lubner *et al.*²⁵.

The Allaire *et al.*²³ study found that the resection of liver tumors retained sufficient residual liver volume to ensure the sufficient compensatory capacity of postoperative liver function, which is also the key to enhancing the clinical prognosis. However, in this study, the liver function standard in the study group was notoriously higher than in the control group. The reasons may be attributable to the guidance of ultrasound. The tumor and tumor liver vein branches were cut down, achieving the purpose of accurate resection, effective partition lesions of blood flow, and reducing the remaining liver affected by blood flow reperfusion, thus reducing the damage to liver function and retaining more liver tissue with normal function.

In evaluating immune function indicators in this study, the immune indicators of the study group were higher than that of the control group after seven days, indicating that the precise resection resulted in less loss of immune function for sufferers, and the postoperative recovery was faster. Joliat *et al.*²⁶ and Tayar *et al.*²⁷ confirmed in their study that laparoscopic hepatectomy under LUS caused less tissue damage than conventional laparoscopic hepatectomy, producing less intraoperative bleeding, less postoperative stress response and a relatively mild degree of immunosuppression in postoperative patients. The mechanism may be that after the damage to the body, immune cells will synthesize and secrete IL-6 and TNF- α factors to regulate the related stress conditions. Increasing IL-6 and TNF- α levels will aggravate the body's inflammatory response and reduce the human body's immune capacity. CD3⁺ and CD4⁺ are indicators of the reactive T cell levels; the lower the levels, the more severely compromised immune capacity. NK cells are also essential cells involved in the immune response, together with CD3⁺ and CD4⁺ T-lymphocytes, and similarly, the lower the levels, the worse

the decline in the immune function. By comparing the study and the control groups, the study group's IL-6 and TNF α concentrations were lower than in the control. CD3⁺, CD4⁺, and NK cells were higher than those in the control group, indicating that laparoscopic precision liver resection results in less immune damage^{28,29}.

Some studies have shown that the immune function has a particular relationship with postoperative complications, and the less the postoperative immune function damage, the lower the incidence of postoperative complications^{30,31}. In this study, the rate of postoperative complications in the study group was lower than that in the control, and this result also reflects this relationship, which is consistent with the results of Shazly's *et al.*³² studies. Comparing the postoperative morbidity and survival rate of both groups, they were higher in the control group, possibly because the precise liver resection accomplished a complete resection of liver tumors and avoided the occurrence of tumor residues³³. The higher indicators of postoperative liver function show that the study group can retain more normal liver tissue, which is more beneficial for the patient's postoperative rehabilitation³⁴, consistent with the above scholars' research results.

In conclusion, the modified laparoscopic precision liver resection can effectively reduce the amount of intraoperative bleeding, reduce the impairment of liver and immune functions, reduce the incidence of complications, and reduce the postoperative recurrence rate of liver cancer, which shows that it is worth generalizing the use of this technique in clinical practice. Although this study has obtained relatively important results, it still needs to be improved to use these research conclusions as the gold standard. For example, only 76 patients with liver cancer were included in this study, and the research results will inevitably be biased, so the sample size should be expanded for further demonstration.

ACKNOWLEDGMENTS

We appreciate Dr Humberto Martínez's editing of this research paper.

Conflict of competence

The authors declare no conflict of interest.

Funding

None.

ORCID of the authors

- Yansong Xu: 0000-0002-1915-8014
- Lin Shen: 0000-0003-4192-2493

Contribution of authors

In the present study, both authors made equal contributions and collaborated closely throughout the research process.

REFERENCES

1. Wei Q, Zhou H, Hou X, Liu X, Chen S, Huang X, Chen Y, Liu M, Duan Zh. Current status of and barriers to the treatment of advanced-stage liver cancer in China: a questionnaire-based study from the perspective of doctors. *BMC Gastroenterol* 2022; 351. <https://doi.org/10.1186/s12876-022-02425-4>.
2. Sun H C, Zhou J, Wang Z, Liu X, Xie Q, Jia W, Zhao M, Bi X, Li G, Bai X, Ji Y, Xu L, Zhu X D, Bai D, Chen Y, Chen Y, Dai Ch, Guo R, Guo W, Hao Ch, Huang T, Huang Zh, Li D, Li Gang, Li Tao, Li X, Li G, Liang X, Liu J, Liu F, Lu Sh, Lu Zh, Lv W, Mao Y, Shao G, Shi Y, Song T, Tan G, Tang Y, Tao K, Wan Ch, Wang G, Wang L, Wang Sh, Wen T, Xing B, Xiang B, Yan Sh, Yang D, Yin G, Yin T, Yin Zh, Yu Zh, Zhang B, Zhang J, Zhang Sh, Zhang T, Zhang Y, Zhang Y, Zhang A, Zhao H, Zhou L, Zhang W, Zhu Zh, Qin Sh, Shen F, Cai X, Teng G, Cai J, Chen M, Li Q, Liu L, Wang W, Liang T, Dong J, Chen X, Wang X, Zheng Sh, Fan J. Chinese expert consensus on conversion therapy for hepatocellular carcinoma. *Hepatobiliary Surg Nutr* 2021; 11(2): 227–252. <https://doi.org/10.21037/hbsn-21-328>.
3. Sasaki K, Ruffolo LI, Kim MH, Fujili M, Hashimoto K, Imaoka Y, Melcher M L, MD, Aucejo F N, Tomiyama K, Hernandez-Alejandro R. The current state of liver transplantation for colorectal liver metastases in the United States: A call for standardized reporting. *Ann Surg Oncol* 2023; 30: 2769–2777. <https://doi.org/10.1245/s10434-023-13147-6>.
4. Sena G, Paglione D, Gallo G, Goglia M, Osso M, Nardo B. Surgical resection of a recurrent hepatocellular carcinoma with portal vein thrombosis: is it a good treatment option? A case report and systematic review of the literature. *J Clin Med* 2022; 11(18):5287.
5. Shannon AH, Ruff SM, Pawlik TM. Expert insights on current treatments for hepatocellular carcinoma: clinical and molecular approaches and bottlenecks to progress. *J Hepatocell Carcinoma* 2022; 9:1247-1261. <https://doi.org/10.2147/JHC.S383922>.
6. Boudjema K, Locher C, Sabbagh C, Ortega-Deballon P, Heyd B, Bachelier P, Metairie S, Paye F, Bourlier P, Adam R, Merdrignac A, Tual Ch, Pabic E L, Sulpice L, Meunier B, Regimbeau J-M, Bellissant E. Simultaneous versus delayed resection for initially resectable synchronous colorectal cancer liver metastases: A prospective, open-label, randomized, controlled trial. *Ann Surg* 2021;273(1):49-56. <https://doi.org/10.1097/SLA.0000000000003848>.
7. Aliseda D, Martí-Cruchaga P, Zozaya G, Rodríguez-Fraile M, Bilbao JI, Benito-Boillos A, De La Cuesta AM, Lopez-Olaondo L, Hidalgo F, Ponz-Sarvisé M, Chopitea A, Rodríguez J, Iñarrairaegui M, Herrero J I, Pardo F, Sangro B, Rotellar F. Liver resection and transplantation following Yttrium-90 radioembolization for primary malignant liver tumors: A 15-year single-center experience. *Cancers* 2023;15(3):733. <https://doi.org/10.3390/cancers15030733>.
8. Naidu CS, Sarin A. Postoperative liver failure. *GI Surgery Annual* 2017;23:59-81.

9. Hou H, Zhou D, Cui X, Wang L, Wu C, Xiong Q, Geng X. Laparoscopic liver resection ameliorates the postoperative liver function impairment for hepatocellular carcinoma patients. *Surg Laparosc Endosc Percutan Tech*. 2020;30(1):69-73. <https://doi.org/10.1097/SLE.0000000000000749>.
10. Kuemmerli C, Fichtinger RS, Moekotte A, Aldrighetti LA, Aroori S, Besselink MGH, D'Hondt M, Díaz-Nieto R, Edwin B, Efanov M, M. Ettorre G, Menon K V, Sheen A J, Soonawalla Z, Sutcliffe R, Troisi R I, White SA, Brandts L, van Breukelen GJP, Sijberden J, Pugh SA, Eminton Z, Primrose JN, Dam RV. Laparoscopic versus open resections in the posterosuperior liver segments within an enhanced recovery programme (ORANGE Segments): study protocol for a multi-centre randomised controlled trial. *Trials* 2022;23(1):206. <https://doi.org/10.1186/s13063-022-06112-3>.
11. Zhang W, Zhu W, Yang J, Xiang N, Zeng N, Hu H, Jia F, Fang Ch. Augmented reality navigation for stereoscopic laparoscopic anatomical hepatectomy of primary liver cancer: Preliminary experience. *Front Oncol* 2021;11:663236. <https://doi.org/10.3389/fonc.2021.663236>.
12. Lam J, Tam MS, Retting RL, McLemore EC. Robotic versus laparoscopic surgery for rectal cancer: A comprehensive review of oncological outcomes. *Perm J* 2021;25. <https://doi.org/10.7812/TPP/21.050>.
13. Serednicki W, Hołowko W, Major P, Małczak P, Pędziwiatr M. Minimizing blood loss and transfusion rate in laparoscopic liver surgery: a review. *Videosurgery and other miniinvasive techniques* 2023;18(2):213-223. <https://doi.org/10.5114/wiitm.2022.124088>.
14. Qin S. Guidelines on the diagnosis and treatment of primary liver cancer (2011 edition). *Chin Clin Oncol* 2012;1(1):10. <https://doi.org/10.3978/j.issn.2304-3865.2012.07.01>.
15. Huang Q, Zou MH, Jiang Y, Chen ZP, Wang Q, Wei JC, Li WL, Cao J. Outcomes of laparoscopic surgery for mucinous colorectal adenocarcinoma. *J Laparoendosc Adv Surg Tech A* 2021;31(6):638-647. <https://doi.org/10.1089/lap.2020.0588>.
16. Zhou J, Sun H-C, Wang Z, Cong W-M, Wang J-H, Zeng M-S, Yang J-M, Bie P, Liu L-X, Wen T-F, Han G-H, Wang M-Q, Liu R-B, Lu L-G, Ren Zh-G, Chen M-S, Zeng Z-Ch, Liang P, Liang Ch-H, Chen M, Yan F-H, Wang W-P, Ji Y, Cheng W-W, Dai C-L, Jia W-D, Li Y-M, Li Y-X, Liang J, Liu T-Sh, Lv G-Y, Mao Y-L, Ren W-X, Shi H-Ch, Wang W-T, Wang X-Y, Xing B-C, Xu J-M, Yang J-Y, Yang Y-F, Ye Sh-L, Yin Z-Y, Zhang B-H, Zhang Sh-J, Zhou W-P, Zhu J-Y, Liu R, Shi Y-H, Xiao Y-Sh, Dai Z, Teng G-J, Cai J-Q, Wang W-L, Dong J-H, Li Q, Shen F, Qin S-K, Fanl J. Guidelines for diagnosis and treatment of primary liver cancer in China (2017 Edition). *Liver Cancer* 2018;7(3):235-260. <https://doi.org/10.1159/000488035>.
17. Liu Y, Wang Q, Du B, Wang XZ, Xue Q, Gao WF. Meta-analysis of indocyanine green fluorescence imaging-guided laparoscopic hepatectomy. *Photodiagnosis Photodyn Ther* 2021;35:102354. <https://doi.org/10.1016/j.pdpdt.2021.102354>.
18. Ibuki S, Hibi T, Tanabe M, Geller DA, Cherqui D, Wakabayashi G. Short-term outcomes of “difficult” laparoscopic liver resection at specialized centers: Report from INSTALL (International Survey on Technical Aspects of Laparoscopic Liver Resection)-2 on 4478 patients. *Ann Surg* 2022;275(5):940-946. <https://doi.org/10.1097/SLA.0000000000004434>.
19. Matsukuma S, Tokumitsu Y, Nakagami Y, Shindo Y, Matsui H, Nakajima M, Iida M, Suzuki N, Takeda Sh, Nagano H. Laparoscopic resection reduces superficial surgical site infection in liver surgery. *Surg Endosc* 2021;35(12):7131-7141. <https://doi.org/10.1007/s00464-020-08233-9>.
20. Huang Y, Chen F, Li H. Effect of rapid rehabilitation nursing on inflammation and liver function after laparoscopic radical resection of primary liver cancer. *Am J Transl Res* 2022;14(11):8156-8165.
21. Fu XT, Tang Z, Chen JF, Shi YH, Liu WR, Gao Q, Ding G-Y, Song K, Wang X-Y, Zhou J, Fan J, Ding Z-B. Laparoscopic hepatec-

- tomy enhances recovery for small hepatocellular carcinoma with liver cirrhosis by postoperative inflammatory response attenuation: a propensity score matching analysis with a conventional open approach. *Surg Endosc* 2021;35(2):910-920. <https://doi.org/10.1007/s00464-020-07710-5>.
22. Schag CC, Heinrich RL, Ganz PA. Karnofsky performance status revisited: reliability, validity, and guidelines. *J Clin Oncol* 1984;2(3):187-193. <https://doi.org/10.1200/JCO.1984.2.3.187>.
 23. Allaire M, Goumard C, Lim C, Le Cleach A, Wagnier M, Scatton O. New frontiers in liver resection for hepatocellular carcinoma. *JHEP Rep* 2020;2(4):100134. <https://doi.org/10.1016/j.jhepr.2020.100134>.
 24. Sugawara Y, Hibi T. Surgical treatment of hepatocellular carcinoma. *BioSci Trends* 2021;15(3):138-41. <https://doi.org/10.5582/bst.2021.01094>.
 25. Lubner MG, Mankowski Gettle L, Kim DH, Ziemlewicz TJ, Dahiya N, Pickhardt P. Diagnostic and procedural intraoperative ultrasound: technique, tips and tricks for optimizing results. *Br J Radiol* 2021;94(1121):20201406. <https://doi.org/10.1259/bjr.20201406>.
 26. Joliat G-R, Kobayashi K, Hasegawa K, Thomson J-E, Padbury R, Scott M, Brustia R, Scatton O, Cao HST, Vauthey J-N, Dincler S, Clavien P-A, Wigmore SJ, Demartines N, Melloul E. Guidelines for perioperative care for liver surgery: Enhanced Recovery After Surgery (ERAS) Society Recommendations 2022. *World J Sur* 2023;47(1):11-34. <https://doi.org/10.1259/bjr.20201406>.
 27. Tayar DO, Ribeiro U, Jr., Ceconello I, Magalhães TM, Simões CM, Auler JOC, Jr. Propensity score matching comparison of laparoscopic versus open surgery for rectal cancer in a middle-income country: short-term outcomes and cost analysis. *Clinicoecon Outcomes Res* 2018;10:521-527. <https://doi.org/10.2147/CEOR.S173718>.
 28. Morise Z, Katsuno H, Kikuchi K, Endo T, Matsuo K, Asano Y, Horiguchi A. Laparoscopic repeat liver resection-selecting the best approach for repeat liver resection. *Cancers* 2023;15(2):421. <https://doi.org/10.3390/cancers15020421>.
 29. Berardi G, Muttillio EM, Colasanti M, Mariano G, Meniconi RL, Ferretti S, Guglielmo N, Angrisani M, Lucarini A, Garofalo E, Chiappori D, Di Cesare L, Vallati D, Mercantini P, Ettore GM. Challenging scenarios and debated indications for laparoscopic liver Resections for hepatocellular carcinoma. *Cancers* 2023;15(5):1493. <https://doi.org/10.3390/cancers15051493>.
 30. Dąbrowska AM, Słotwiński R. The immune response to surgery and infection. *Cent Eur J Immunol* 2014;39(4):532-537. <https://doi.org/10.5114/ceji.2014.47741>.
 31. Amodeo G, Bugada D, Franchi S, Moschetti G, Grimaldi S, Panerai A, Allegri M, Sacerdote P. Immune function after major surgical interventions: the effect of postoperative pain treatment. *J Pain Res* 2018;11:1297-1305. <https://doi.org/10.2147/JPR.S158230>.
 32. Elshazly M, Khair T, Bassem M, Mansour M. The use of intraoperative bedside lung ultrasound in optimizing positive end expiratory pressure in obese patients undergoing laparoscopic bariatric surgeries. *Surg Obes Relat Dis* 2021;17(2):372-378. <https://doi.org/10.1016/j.socard.2020.09.023>.
 33. Kurilova I, Bendet A, Petre EN, Boas FE, Kaye E, Gonen M, Covey A, Brody LA, Brown KT, Kemeny NE, Yarmohammadi H, Ziv E, D'Angelica MI, Kingham TP, Cercek A, Solomon SB, Beets-Tan RGH, Sofocleous CT. Factors associated with local tumor control and complications after thermal ablation of colorectal cancer liver metastases: a 15-year retrospective cohort study. *Clinical Colorectal Cancer* 2021;20(2):e82-e95. <https://doi.org/10.1016/j.clcc.2020.09.005>.
 34. Skrzep-Poloczek B, Poloczek J, Chelmecka E, Kazura W, Dulaska A, Idzik M, Jochem J, Stygar D. General, 21-day postoperative rehabilitation program has beneficial effect on oxidative stress markers in patients after total hip or knee replacement. *Oxid Med Cell Longev* 2020; 2020:4598437. <https://doi.org/10.1155/2020/4598437>.

Genetic association study of the rs10774671 variant of the *OAS1* gene with the severity of COVID-19 in an Ecuadorian population.

Kathya Pilataxi¹, Thalía Balarez¹, Erik Chávez, Camila Acosta¹, Ivonne Z. Peña², Katherin Narváez² and Francisco Álvarez-Nava¹

¹Facultad de Ciencias Biológicas, Universidad Central del Ecuador, Quito, Ecuador.

²Hospital Quito Sur del Instituto Ecuatoriano de Seguridad Social, Quito, Ecuador.

Keywords: complex trait; COVID-19; genetic association study; genetic variant; Hardy-Weinberg equilibrium; innate immune processes.

Abstract. COVID-19 exhibits a wide range of phenotypic manifestations, from asymptomatic to severe phenotypes with fatal complications. The existence of risk factors cannot entirely explain the variance in the phenotypic variability of COVID-19. Genome-wide association analyses have identified target human genes related to virus transmission and the clinical phenotype observed in COVID-19 patients. Genetic variants on the *OAS1* gene have been associated with innate immune processes (entry phase and viral replication in host cells). The A or G alleles of rs10774671 in *OAS1* encode isoforms with different antiviral activities. One hundred COVID-19 patients were genotyped for the rs10774671 using RFLP-PCR (severe form, n = 43; asymptomatic-mild, n = 57). The susceptibility of the two groups to the severe phenotype of COVID-19 was compared. The allele frequency for A was 0.8. The genotypic frequencies for AA and GG homozygotes were 0.62 and 0.02, respectively. A Hardy-Weinberg equilibrium deviation was found in both groups. No statistically significant associations were found in genetic models adjusted for sex (for the additive model OR = 1.18, 95% CI = (0.53-2.61), p = 0.69). A relatively recent mix of different ethnic groups and sample size may influence these findings.

Estudio de asociación genética de la variante rs10774671 del gen *OAS1* con la severidad de COVID-19 en una población ecuatoriana.

Invest Clin 2024; 65 (2): 169 – 178

Palabras clave: estudio de asociación genética; equilibrio Hardy-Weinberg; rasgo complejo; variante genética; procesos inmunes innatos.

Resumen. La COVID-19 presenta una amplia gama de manifestaciones clínicas, desde asintomáticas hasta formas graves con complicaciones mortales. La variabilidad fenotípica de la COVID-19 no puede explicarse totalmente por la existencia de factores de riesgo. Se han identificado genes humanos diana relacionados con la transmisión del virus y el fenotipo clínico observado en pacientes con COVID-19 mediante análisis de asociación de genoma completo. Las variantes genéticas del gen *OAS1* se han asociado con procesos inmunitarios innatos (fase de entrada y replicación viral en las células hospedadoras). Los alelos A o G de rs10774671 en *OAS1* codifican isoformas con diferentes actividades antivirales. Cien pacientes con COVID-19 fueron genotipados para el rs10774671 mediante RFLP-PCR (forma grave, n = 43; asintomática-leve, n = 57). Se comparó la susceptibilidad de los dos grupos al fenotipo severo de COVID-19. La frecuencia alélica para A fue de 0,8. Las frecuencias genotípicas para los homocigotos AA y GG fueron 0,62 y 0,02, respectivamente. Se observó una desviación del equilibrio de Hardy-Weinberg en ambos grupos. No se encontraron asociaciones estadísticamente significativas en los modelos genéticos ajustados por sexo (para el modelo aditivo OR = 1,18, IC 95% = (0,53-2,61), $p = 0,69$). La mezcla relativamente reciente de diferentes grupos étnicos y el tamaño de la muestra pueden influir en estos resultados.

Received: 24-06-2023

Accepted: 13-02-2024

INTRODUCTION

COVID-19 is a human-to-human transmissible viral infectious disease¹. Until the beginning of 2023, it had been responsible for about 7 million deaths worldwide². Subjects infected with SARS-CoV-2, the etiological agent of COVID-19, have a wide range of phenotypic variability, from asymptomatic to severe forms of the disease³. This broad clinical variability is partially explained by risk factors that include age (> 65 years), male sex, and the presence of comorbidities such as obesity, cardiovascular diseases,

diabetes mellitus, and respiratory disorders, among others⁴. Therefore, the variance in the clinical phenotype of COVID-19 may be caused by additional host-specific factors⁵.

Genome-wide association studies have reported associations between the severe form of COVID-19 and chromosomal regions, including 12q24.13, which harbors a gene cluster encoding antiviral restriction enzyme activators (*OAS1*, *OAS2*, and *OAS3*). These activators are involved in viral RNA degradation and viral replication inhibition^{6,7}. The *OAS1* gene encodes the enzyme 2'-5' oligoadenylate synthetase 1

(2-5A), an activator of the ribonuclease L (RNaseL), which degrades viral RNA within the host cell, blocks viral replication and inhibits viral protein synthesis. The genetic variant rs10774671 is a G→A transition in the last nucleotide of intron 5 of the *OAS1* gene, which affects the nonsense-mediated decay and the splicing site and controls the differential expression of isoforms with lesser enzymatic activity^{7,8}. Different allele and genotype frequencies have been reported in studies, including those of European, African, and Latin American Afro-Caribbean populations, likely due to the influence of the ancestral factor^{9,10}. Despite being a multiethnic society composed of different communities with South American, West Eurasian, and Sub-Saharan ancestries, the Ecuadorian population has a strong Native South American ancestral influence, which is considered the second highest for this region's population¹¹.

The percentage of severe cases and deaths among individuals of Hispanic ancestry was higher than that reported for the general population. For instance, in New York City, one of the communities hardest hit by the SARS-CoV-2 virus globally, more Hispanics per capita have died from COVID-19 than any other ethnic group. Infection rates on the Navajo Nation Indian Reservation have also been reported to be particularly high¹². Native Americans represent more than a third of the COVID-19 cases in the state of New Mexico, despite making up only 9% of the population¹³. These ethnic differences do not appear to be caused by socioeconomic conditions or access to health services since Latin American non-Sub-Saharan ancestry was reported as a factor associated with morbidity and mortality from COVID-19 in a study that included health professionals with similar economic and educational status¹⁴.

Latin America is one of the regions where the impact of COVID-19 has been most severe. Poor sanitary conditions of infrastructure, health personnel, and an immunologically vulnerable population are two

factors that influenced this impact. Ecuador was one of the countries that was dramatically impacted at the beginning of the pandemic. However, sustained vaccination campaigns were able to mitigate this impact partially. Fifteen million people, or 86% of the population, have received at least one dose¹⁵, with 14 million (or 79%) receiving two or more doses¹⁶. Few genetic association studies between COVID-19 and susceptibility genes have been reported for the Latin American populations. For this reason, we examined the association between the rs10774671 variant of the *OAS1* gene and the severe form of COVID-19 among Ecuadorian individuals.

METHODS

Design and Study Subjects

In this observational, analytical, and case-control study, a total of 100 Ecuadorian individuals with COVID-19 were analyzed. The individuals were divided into two groups: 43 patients with the severe clinical picture (group A) enrolled from October 2021 to March 2022 and 57 subjects with the asymptomatic-mild form (group B) enrolled in January 2021 at the Quito Sur Hospital of the Ecuadorian Institute of Social Security, Quito, Ecuador. Group A consisted of individuals without regard to sex who had a diagnosis of COVID-19 severe form confirmed by a positive RT-PCR test specific for SARS-CoV-2; a chest computed tomography image showing a pattern of viral pneumonia due to diffuse infiltration of both lungs greater than 50% (CORADS 6); and the presence of respiratory failure and the need for mechanical ventilation ($\text{PaO}_2/\text{FiO}_2 \leq 100\text{mmHg}$ (with PEEP $\geq 5\text{cm H}_2\text{O}$) and $\text{SpO}_2/\text{FiO}_2$ ratio <315). This group had received at least two doses of SARS-CoV-2 vaccines. Group B subjects presented the disease's asymptomatic or mild clinical form, validated by a positive RT-PCR test for SARS-CoV-2. Group B was made up of health workers from the same hospital who provided care for patients with the severe

form of COVID-19 admitted to the intensive care unit. When the subjects from Group B were diagnosed with COVID-19, they had not received any vaccination against COVID-19. This method of subject selection was carried out to identify COVID-19 protective alleles. The exclusion criteria for both groups included consanguineous individuals, minors, pregnant or nursing women, and refugees or displaced with little or no knowledge of the Spanish language.

Molecular Analysis

Ten milliliters of peripheral blood were drawn from each subject in an EDTA tube. In order to reduce bias in the laboratory phase, each tube was assigned a unique code without discriminating to which clinical group it belonged. The Column-Pure Blood Genomic DNA (ABM, Vancouver, Canada) kit was used to extract DNA according to the manufacturer's instructions. The Qubit dsDNA BR ASSAY Kit (21000 ng 100RX (Invitrogen, Massachusetts, USA) was then used to quantify the DNA using the Qubit fluorometer (Invitrogen, Massachusetts, USA). The DNA quality was determined by electrophoresis in 1.5% agarose gels at 80V for an hour, with the bands visualized using the Microtek Bio-1000F program scanner (Microtek International Inc., Hsinchu City, Taiwan). The forward primer 5'-TCC-AGA-TGG-CAT-GTC-ACA-GT-3' and the reverse primer 5'-TAG-AAG-GCC-AGG-AGT-CAG-GA-3' were used to carry out the PCR, based on earlier research¹⁷. The master mix and thermocycler settings (Applied Biosystems MiniAmp, Thermo Fisher Scientific Inc., Massachusetts, USA) for PCR were performed based on a previously published¹⁸ method with modifications. PCR products were examined by electrophoresis on 1.5% agarose gels in the blueGel™ system (48V, 45 minutes) (MiniPCR Bio, Massachusetts, USA). Subsequently, these products were digested with 10 U of *AfuI* at 37°C for 16 hours, in a total volume of 20 μ l, following the manufacturer's instructions. They were electrophoresed

in 3% agarose gels in the Thermo Scientific™ equipment (120V, 2 hours) (Thermo Fisher Scientific Inc., Massachusetts, USA). Ten percent of all samples were randomly sequenced to control the reproducibility and quality of genotyping of PCR-RFLP, which showed complete matching of results.

Statistical Analysis

Used software included InfoStat, Microsoft Excel 2019, SNPStats¹⁹ (<https://www.snpstats.net/>), and the Hardy-Weinberg statistical package for R Studio²⁰. Allelic and genotypic frequencies were calculated by direct counting and expressed in proportions and percentages. The exact test examined genotypic and allelic frequencies to determine whether the groups were in Hardy-Weinberg equilibrium (HWE)²¹. The Fisher's exact test was then used to compare allele frequencies between group A (severe COVID-19 phenotype) and group B (mild and moderate COVID-19 phenotype). The association between the rs10774671 alleles and the severe phenotype of COVID-19 was estimated considering different inheritance models (codominant, dominant, recessive, overdominant, and additive)²², expressed in frequencies and percentages. For each analysis, the odds ratios (OR), 95% confidence intervals (95% CI), and corresponding *p* values were calculated. An association was considered significant when the *p*-value was < 0.05 in all two-tailed statistical tests.

Ethical Considerations

Participants gave their written consent to sample extraction, the use of clinical histories, and the processing of biological samples. Hospital staff members collected the samples and data; they had no interaction with the researchers who conducted the molecular tests. The data were collected according to the WHO "COVID-19 Case Registration Form", and the information was handled confidentially. This study had the ethical, legal, and methodological endorse-

ment of the Ethics Committee for the Expedited Review of COVID-19 Investigations of the Ministry of Public Health of Ecuador (MSP-CGDES-2020-0244-O1).

RESULTS

Table 1 shows the allelic and genotypic frequencies discriminated by groups (whole group, groups A and B). Alleles and genotypes were not found in HWE in the analyzed groups. Likewise, no allele or genotype was significantly associated with the severe phenotype of COVID-19 enough to be considered an associated factor (risk or protective) (OR (95% CI) = 1.17 (0.43-1.72), 1.04 (0.46-2.35), respectively). Although it was not statistically significant, this estimation revealed that the additive model had the best fit (OR (95% CI) = 1.18 (0.53-2.61); *p* = 0.69; Table 2).

DISCUSSION

In the current study, a higher frequency of the A allele was found in the three groups analyzed, with a value around 0.8 for the rs10774671 variant of the *OAS1* gene in a mestizo population with a high Native South American influence. The contrast between

these values and those observed in other research conducted in various ethnic settings is striking. In a sample of 301,842 individuals from all continents, a higher frequency of the A allele of 0.6346 was reported¹⁰. In this same database, for Latin American individuals of Afro-Caribbean ancestry (*n* = 1,394) and subjects with primarily European and Native American ancestry (*n* = 6,656), the frequencies of the A allele were reported at 0.5703 and 0.7763, respectively¹⁰. A frequency similar to that of the present study for the A allele (0.796) was reported by a Mexican study with similar methodological features²³. The allele A determines the differential expression of isoforms depending on the virus type. This allele has been the subject of study for other viral diseases, finding significant associations as a risk factor for initial infection with West Nile virus (WNV)²⁴ as well as hepatitis C virus (HCV)²⁵.

Conversely, the worldwide genotype frequencies for AA and GG homozygotes and heterozygotes were 41%, 18.1%, and 40.9%, respectively²⁶. These genotype frequencies are very different from those found in the present study and in the data from the Mexican population, whose respective genotype frequencies were 61.2%, 2%, and 36.7%²³. Both studies analyzed populations (Mexican

Table 1
Allele and genotypic frequencies for the rs10774671 genetic variant in the *OAS1* gene in the groups analyzed.

Variable	General sample n=100	Group A n=43	Group B n=57	P	OR (CI 95%)
Allele§					
A	0.8	0.81	0.79	0.723	1.17 (0.43-1.72)
G	0.2	0.19	0.21		
Genotype§§					
A/A	62 (62)	27 (62.8)	35 (61.4)	1	-
A/G	36 (36)	16 (37.2)	20 (35.1)	0.347	1.04 (0.46-2.35)
G/G	2 (2)	0 (0)	2 (3.5)	0.312	0

Group A: individuals with a diagnosis of COVID-19 severe form. Group B: individuals with a diagnosis of COVID-19 asymptomatic or mild clinical severe form. Allelic frequencies are expressed in proportions. Genotypic frequencies are expressed in number of cases and percentages. § *p*-value of Fisher's exact test (2x2 contingency table). §§ *p*-value of the Exact test (R Studio).

Table 2
Genetic Models for the Estimation of the Association of the rs10774671 genetic variant of the *OAS1* gene and the severe phenotype of COVID-19.

Genetic Models [†]		Group A (n=43)	Group B (n=57)	p [§]	OR (CI 95%)
Co	A/A	27 (62.8)	35 (61.4)	0.34	NC [‡]
	G/G	0 (0)	2 (3.5)		
	A/G	16 (37.2)	20 (35.1)		
Do	A/A+A/G	43 (100)	55 (96.5)	0.14	NC
	G G/G	0 (0)	2 (3.5)		
Re	A/A+G/G	27 (62.8)	37 (64.9)	0.94	1.04 (0.44-2.42)
	G A/G	16 (37.2)	20 (35.1)		
Overdo	A/G+G/G	16 (37.2)	22 (38.6)	0.79	1.12 (0.48-2.60)
	G A/A	27 (62.8)	35 (61.4)		
Ad	-	-	-	0.69	1.18 (0.53-2.61)

Group A refers to individuals with a diagnosis of COVID-19 severe form and Group B refers to subjects who presented the asymptomatic or mild clinical form of the disease, § p-value of Fisher's exact test (2x2 contingency table).
[†] Genetic Models: codominant (Co), dominant (Do), recessive (Re), overdominant (Over-do) and additive (Ad).
[‡] NC: Not calculated.

and Ecuadorian) composed of several ethnic groups that underwent a complex process of biological mixing but with a solid Native South American component in their population structure^{27,28}. However, despite their close geographic and evolutionary proximity, the genotype frequencies reported for a Peruvian population (78.8%, 1.2%, and 20%, respectively) were very different from those of the present study. This difference could be explained by the fact that the data collected for the Peruvian population belongs to the results published by the 1000 Genomes Project (1 KGP) with a study design different from the one used in our study²⁶. Similarly, the effect of the study's sample size cannot be ignored. Despite this, the results for the Mexican and Peruvian populations and the current study show a similar frequency of homozygotes for the minor allele (GG). The high Native South American component of these mixed populations could explain this observation.

No statistically significant differences were found for allele and genotypic frequencies between groups A and B. Genetic models developed from the sex-adjusted frequencies did not support a possible association with

the severe form of COVID-19 in Ecuadorian patients. Significant associations were reported between the rs10774671 allele of the *OAS1* gene and the severe phenotype of COVID-19 for European populations (OR = 1.33 (1.13-1.56), $p = 6.45 \times 10^{-4}$)⁹. By contrast, for individuals with Sub-Saharan ancestry, no significant association was found (OR = 1.23 (0.98-1.55), $p = 0.079$) for the allele A. These findings suggest the possibility that ethnic differences in genotype and allele frequencies may account for the inconsistent results when examining the association between genotype and phenotype for this locus and COVID-19.

The evolutionary history of South American ethnic groups may help clarify the epidemiological findings that suggest these populations are more susceptible to developing the severe form of COVID-19. In this context, the G allele of rs10774671 of the *OAS1* gene has been associated with a protective effect against the severe form of COVID-19 for this haplotype in patients of European ancestry⁹. The G allele probably has a Neanderthal origin, whereas the A allele (which confers risk in the European population) is predominantly of Denisovan ancestry⁹.

It is proposed that Sapiens, Neanderthals, and Denisovans cohabited 100,000 years ago based on evolutionary history and gene flow²⁹. Data from genetic analyses of human fossils indicate that hybridization events occurred between modern humans and Neanderthals between 37,000 and 86,000 years ago³⁰. This hybridization led to the recombination of adaptive alleles that provided resistance against viruses. However, these genomic segments of Neanderthal origin were rapidly eliminated by selective environmental pressure among modern humans³¹. These haplotypes of Neanderthal ancestry in the *Homo sapiens* genomes of European and Asian populations dropped considerably from 10% to 4% and 2%, respectively²⁹. Hence, the decline in the frequency of the GG homozygotes with a protective effect for the severe form of COVID-19 reported in Latin American populations could be attributable to the selective environmental pressure when modern humans migrated to the Americas from Asia. However, the fixation of alleles in populations with recent admixture, such as the Ecuadorian population, may be influenced by other factors, such as genetic drift, including bottle-neck and founder effects. Our investigation's design study and statistical power were inadequate to assess this hypothesis.

The present study has several limitations. None of the analyzed groups presented HWE for the alleles and genotypes evaluated. Precautions were taken to avoid genotyping errors, as different researchers tested molecular analyses to confirm the results separately. In addition, we have randomly sequenced 10% of the samples to verify the results of the PCR-RFLP analysis, which showed complete matching of results. Sample size and stratification might be two more potential sources of this HWE deviation. We wanted to take advantage of the outbreak produced by the *Omicron* variant of SARS-CoV-2, which increased the number of patients hospitalized in our intensive care unit, selecting those who had received at least two doses of

the COVID-19 vaccine and contrasting them with subjects who presented COVID-19 in the asymptomatic and mild forms. This would make it possible to find protective alleles. However, this selection method introduces a selection bias that may distort the genetic composition of the groups studied. Such selection bias could explain the lack of homozygous genotypes for the minor allele (GG). The sample size was small, resulting in even smaller sample sizes when broken down into two groups for analysis. Thus, the main limitations of our study were the small sample size and the lack of a replication-independent cohort to verify our findings. The statistical interpretation of the associations is limited by the reduced sample size in our study. We know our results may have a type II error (false negative). Thus, although we did not find a significant association between the rs10774671 variant of the *OAS1* and the severe phenotype of COVID-19 in the Ecuadorian population, we cannot rule out such an association. Therefore, we suggest these associations be further investigated and replicated in other Latin American cohorts with a more significant number of individuals.

To the best of our knowledge, this study is the first effort to identify an association between the rs10774671 of the *OAS1* gene and COVID-19 in mestizo Latin American groups, as previous studies that involved the genotyping of this genetic variant did not assess this relationship. Due to the existing ethnic heterogeneity, new strategies will be needed to assess the genetic components implicated in emerging viral infections in the Latin American population.

ACKNOWLEDGEMENTS

This study was supported by the Bureau Direction of Central University of Ecuador, Quito, Ecuador (Grant No. DI-COVID19-26).

Statement of ethics

The Ethics Committee reviewed and approved the study protocol for the Expe-

dated Review of COVID-19 Investigations of the Ministry of Public Health of Ecuador (MSP-CGDES-2020-0244-O1). The ethical principles of the 1964 Declaration of Helsinki for medical research were adhered to throughout this research. Before beginning the study, the procedures and possible discomfort/risks were fully explained to all participating subjects. Each then voluntarily decided to participate in the study, approved their participation, and signed an informed written consent form in front of a witness. Subjects were allowed to withdraw their participation in the study at any time without consequence.

ORCID numbers

- Kathya Pilataxi:
0009-0002-3701-5284
- Thalía Balarezo:
0000-0002-5985-8525
- Erik Chávez:
0000-0001-5571-2441
- Camila Acosta:
0000-0001-6555-4627
- Francisco Álvarez-Nava:
0000-0002-4673-3643

Author Contributions

The authors' contributions to the paper are as follows: KP: study concepts and design, data analysis and interpretation, statistical analysis, critical revision of the manuscript for important intellectual content and manuscript preparation; TB: molecular studies and data analysis; CA: biochemical studies and data analysis; IZP: acquisition of data and data analysis; KN: acquisition of data and data analysis; and FAN: study concepts and design, data analysis and interpretation, statistical analysis, obtaining funding, critical revision of the manuscript for important intellectual content and manuscript preparation. All authors read and approved the final manuscript.

Conflict of interest

The authors declare that the research was conducted without any commercial or financial relationships that could be construed as a potential conflict of interest.

Data Availability Statement

The data supporting this study's findings are openly available in DOI: 10.5281/zenodo.7672228 at <https://zenodo.org>. The data are publicly available privacy and ethical restrictions, as stipulated by the Central University of Ecuador Institutional Review Board.

REFERENCES

1. Yuki K, Fujiogi M, Koutsogiannaki S. COVID-19 pathophysiology: A review. *Clin Immunol* 2020; 215: 108427. <https://doi:10.1016/j.clim.2020.108427>.
2. WHO. <https://covid19.who.int>. 2023. The WHO Coronavirus (COVID-19) Dashboard.
3. World Health Organization. <https://www.who.int/publications/i/item/clinical-care-of-severe-acute-respiratory-infections-tool-kit>. 2023. Clinical Care for Severe Acute Respiratory Infection.
4. Shahid Z, Kalayanamitra R, McClafferty B, Kepko D, Ramgobin D, Patel R, Aggarwal CS, Vunnam R, Sahu N, Bhatt D, Jones K, Golamari R, Jain R. COVID-19 and older adults: what we know. *J Am Geriatr Soc* 2020; 68(5): 926–929. <https://doi:10.1111/jgs.16472>
5. Godri Pollitt KJ, Peccia J, Ko AI, Kaminski N, Dela Cruz CS, Nebert DW, Reichardt JKV, Thompson DC, Vasiliou V. COVID-19 vulnerability: the potential impact of genetic susceptibility and airborne transmission. *Hum Genomics* 2020; 14(1): 17. <https://doi:10.1186/s40246-020-00267-3>.
6. Pairo-Castineira E, Clohisey S, Klaric L, Bretherick AD, Rawlik K, Pasko D, Walker S, Parkinson N, Fourman MH, Russell CD, Furniss J, Richmond A, Gountouna E, Wrobel N, Harrison D, Wang B,

- Wu Y, Meynert A, Griffiths F, Oosthuyzen W, Kousathanas A, Moutsianas L, Yang Z, Zhai R, Zheng C, Grimes G, Beale R, Millar J, Shih B, Keating S, Zechner M, Haley C, Porteous DJ, Hayward C, Yang J, Knight J, Summers C, Shankar-Hari M, Klenerman P, Turtle L, Ho A, Moore SC, Hinds C, Horby P, Nichol A, Maslove D, Ling L, McAuley D, Montgomery H, Walsh T, Pereira AC, Renieri A; GenOMICC Investigators; ISARIC4C Investigators; COVID-19 Human Genetics Initiative; 23andMe Investigators; BRACOVID Investigators; Gen-COVID Investigators; Shen X, Ponting CP, Fawkes A, Tenesa A, Caulfield M, Scott R, Rowan K, Murphy L, Openshaw PJM, Semple MG, Law A, Vitart V, Wilson JF, Baillie JK. Genetic mechanisms of critical illness in COVID-19. *Nature* 2021; 591(7848): 92–98. <https://doi:10.1038/s41586-020-03065-y>
7. Bonnevie-Nielsen V, Field LL, Lu S, Zheng DJ, Li M, Martensen PM, Nielsen TB, Beck-Nielsen H, Lau YL, Pociot F. Variation in antiviral 2',5'-oligoadenylate synthetase (2'5'AS) enzyme activity is controlled by a single-nucleotide polymorphism at a splice-acceptor site in the *OAS1* Gene. *Am J Hum Genet* 2005; 76(4): 623–633. <https://doi:10.1086/429391>.
 8. Kjær KH, Pahus J, Hansen MF, Poulsen JB, Christensen EI, Justesen J, Martensen PM. Mitochondrial localization of the *OAS1* p46 isoform associated with a common single nucleotide polymorphism. *BMC Cell Biol* 2014; 15(1): 33. <https://doi:10.1186/1471-2121-15-33>.
 9. Banday AR, Stanifer ML, Florez-Vargas O, Onabajo OO, Papenberg BW, Zahoor MA, Mirabello L, Ring TJ, Lee CH, Albert PS, Andreacos E, Arons E, Barsh G, Biesecker LG, Boyle DL, Brahier MS, Burnett-Hartman A, Carrington M, Chang E, Choe PG, Chisholm RL, Colli LM, Dalgard CL, Dude CM, Edberg J, Erdmann N, Feigelson HS, Fonseca BA, Firestein GS, Gehring AJ, Guo C, Ho M, Holland S, Hutchinson AA, Im H, Irby L, Ison MG, Joseph NT, Kim HB, Kreitman RJ, Korf BR, Lipkin SM, Mahgoub SM, Mohammed I, Paschoalini GL, Pacheco JA, Peluso MJ, Rader DJ, Redden DT, Ritchie MD, Rosenblum B, Ross ME, Anna HPS, Savage SA, Sharma S, Siouti E, Smith AK, Triantafyllia V, Vargas JM, Vargas JD, Verma A, Vij V, Wesemann DR, Yeager M, Yu X, Zhang Y, Boulant S, Chanock SJ, Feld JJ, Prokunina-Olsson L. Genetic regulation of *OAS1* nonsense-mediated decay underlies association with COVID-19 hospitalization in patients of European and African ancestries. *Nat Genet* 2022; 54(8): 1103–1116. <https://doi:10.1038/s41588-022-01113-z>
 10. National Center for Biotechnology Information. <https://www.ncbi.nlm.nih.gov/snp/rs10774671>. 2021. Reference SNP (rs) Report.
 11. Nagar SD, Conley AB, Chande AT, Rishishwar L, Sharma S, Mariño-Ramírez L, Aguinaga-Romero G, González-Andrade F, Jordan IK. Genetic ancestry and ethnic identity in Ecuador. *HGG Adv* 2021; 2(4): 100050. <https://doi:10.1016/j.xhgg.2021.100050>.
 12. Kovich H. Rural Matters — Coronavirus and the Navajo Nation. *N Engl J Med* 2020; 383(2): 105–107. <https://doi:10.1056/NEJMp2012114>.
 13. Huyser KR, Yang TC, Yellow Horse AJ. Indigenous Peoples, concentrated disadvantage, and income inequality in New Mexico: a ZIP code-level investigation of spatially varying associations between socioeconomic disadvantages and confirmed COVID-19 cases. *J Epidemiol Community Health* 2021; 75(11): 1044–1049. <https://doi:10.1136/jech-2020-215055>.
 14. Oda G, Sharma A, Lucero-Obusan C, Schirmer P, Sohoni P, Holodniy M. COVID-19 infections among healthcare personnel in the United States Veterans Health Administration, March to August, 2020. *J Occup Environ Med* 2021; 63(4): 291–295. <https://doi:10.1097/JOM.0000000000002109>.
 15. Coronavirus Resource Center from Johns Hopkins University. <https://coronavirus.jhu.edu/map.html>. 2023. COVID-19 Dashboard by the Center for Systems Science and Engineering (CSSE).

16. **Proyecto Rodillo.** <https://rodillo.org/estadisticas-coronavirus/ecuador/>. 2022. Ecuador - Estadísticas del Coronavirus.
17. **Fedetz M, Matesanz F, Caro-Maldonado A, Fernandez O, Tamayo JA, Guerrero M, Delgado C, López-Guerrero JA, Alcina A.** *OAS1* gene haplotype confers susceptibility to multiple sclerosis. *Tissue Antigens* 2006; 68(5): 446-9. <https://doi:10.1111/j.1399-0039.2006.00694.x>.
18. **Imran M, Manzoor S, Khattak NM, Tariq M, Khalid M, Javed F, Bhatti S.** Correlation of *OAS1* gene polymorphism at exon 7 splice acceptor site with interferon-based therapy of HCV infection in Pakistan. *Viral Immunol* 2014; 27(3): 105-111. <https://doi:10.1089/vim.2013.0107>.
19. **Solé X, Guinó E, Valls J, Iniesta R, Moreno V.** SNPStats: a web tool for the analysis of association studies. *Bioinformatics* 2006; 22(15): 1928-1929. <https://doi:10.1093/bioinformatics/btl268>.
20. **Graffelman J.** Exploring Diallelic Genetic Markers: The HardyWeinberg Package. *J Stat Softw* 2015; 64(3) 1-23. <https://doi.org/10.18637/jss.v064.i03>.
21. **Graffelman J, Weir BS.** Testing for Hardy–Weinberg equilibrium at biallelic genetic markers on the X chromosome. *Heredity (Edinb)* 2016; 116(6): 558-568. <https://doi:10.1038/hdy.2016.20>.
22. **Horita N, Kaneko T.** Genetic model selection for a case–control study and a meta-analysis. *Meta Gene* 2015; 5: 1-8. <https://doi:10.1016/j.mgene.2015.04.003>.
23. **Sánchez-González MT, Cienfuegos-Jiménez O, Álvarez-Cuevas S, Pérez-Maya AA, Borrego-Soto G, Marino-Martínez IA.** Prevalence of the SNP rs10774671 of the *OAS1* gene in Mexico as a possible predisposing factor for RNA virus disease. *Int J Mol Epidemiol Genet* 2021;12(3): 52–60.
24. **Lim JK, Lisco A, McDermott DH, Huynh L, Ward JM, Johnson B, Johnson H, Pape J, Foster GA, Krysztof D, Follmann D, Stramer SL, Margolis LB, Murphy PM.** Genetic variation in *OAS1* is a risk factor for initial infection with West Nile Virus in man. *PLoS Pathog* 2009; 5(2):e1000321. <https://doi:10.1371/journal.ppat.1000321>.
25. **Zhao Y, Kang H, Ji Y, Chen X.** Evaluate the relationship between polymorphisms of *OAS1* gene and susceptibility to chronic hepatitis C with high resolution melting analysis. *Clin Exp Med* 2013; 13(3): 171-176. <https://doi:10.1007/s10238-012-0193-6>.
26. **European Molecular Biology Laboratory -European Bioinformatics Institute [EMBL-EBI].** rs10774671 (SNP) - Population genetics - Homo_sapiens. 2022.
27. **Guardado-Estrada M, Juarez-Torres E, Medina-Martinez I, Wegier A, Macías A, Gomez G, Cruz-Talonia F, Roman-Bassauré E, Piñero D, Kofman-Alfaro S, Berumen J.** A great diversity of Amerindian mitochondrial DNA ancestry is present in the Mexican mestizo population. *J Hum Genet* 2009; 54(12): 695-705. <https://doi:10.1038/jhg.2009.98>.
28. **Zambrano AK, Gaviria A, Cobos-Navarrete S, Gruezo C, Rodríguez-Pollit C, Armendáriz-Castillo I, García-Cárdenas JM, Guerrero S, López-Cortés A, Leone PE, Pérez-Villa A, Guevara-Ramírez P, Yumiceba V, Fiallos G, Vela M, Paz-Y-Miño C.** The three-hybrid genetic composition of an Ecuadorian population using AIMS-Indels compared with autosomes, mitochondrial DNA and Y chromosome data. *Sci Rep* 2019; 9(1): 9247. <https://doi:10.1038/s41598-019-45723-w>.
29. **Harris K, Nielsen R.** The Genetic Cost of Neanderthal Introgression. *Genetics* 2016; 203(2): 881-891. <https://doi:10.1534/genetics.116.186890>.
30. **Fu Q, Hajdinjak M, Moldovan OT, Constantin S, Mallick S, Skoglund P, Patterson N, Rohland N, Lazaridis I, Nickel B, Viola B, Prüfer K, Meyer M, Kelso J, Reich D, Pääbo S.** An early modern human from Romania with a recent Neanderthal ancestor. *Nature* 2015; 524(7564): 216-219. <https://doi:10.1038/nature14558>.
31. **Enard D, Petrov DA.** Evidence that RNA viruses drove adaptive introgression between Neanderthals and Modern Humans. *Cell* 2018; 175(2): 360-371.e13. <https://doi:10.1016/j.cell.2018.08.034>.

Insulin-like growth factor-1 promotes the proliferation and odontogenic differentiation of human dental pulp cells *in vitro* and *in vivo*.

Yan Wang, Nan Du, Cong-na Liu and Wen-jing Li

Department of Oral Medicine, The Second Hospital of Hebei Medical University, Shijiazhuang, China.

Keywords: dental tissue regeneration; odontoblasts; osteogenic differentiation.

Abstract. Human dental pulp cells (hDPCs) have emerged as a potential alternative for the regeneration of dental tissues. Insulin-like growth factor-1 (IGF-1) is involved in the proliferation and osteogenic differentiation of hDPCs *in vitro*. However, the effect of IGF-1 on the proliferation and odontogenic differentiation of hDPCs *in vivo* remains unknown. This study collected hDPCs from healthy premolars and third molars by collagenase type I and dispase. Immunocytochemical staining showed positive vimentin staining and negative cytokeratin staining in hDPCs. Treatment with IGF-1 (50, 75, and 100 ng/mL) significantly increased the proliferation ability of hDPCs in a concentration-dependent manner. *In vivo* experiments, hDPCs were seeded into an acellular dermal matrix and transplanted subcutaneously into nude mice. After two and four weeks of transplantation, the hematoxylin and eosin staining revealed more cells and extracellular matrix in implants from the IGF-1 treatment group, and Alizarin Red staining revealed more mineralized tissue compared to the control group. Transmission electron microscopy (TEM) analysis of hDPCs showed an abundance of mitochondria, rough endoplasmic reticulum, and Golgi complexes. In conclusion, IGF-1 promotes the proliferation of hDPCs *in vitro* and odontogenic differentiation of hDPCs *in vivo*, indicating that modifying IGF-1 signaling may provide potential strategies for the regeneration of dental tissues.

El factor de crecimiento similar a la insulina-1 promueve la proliferación y diferenciación odontogénica de células de pulpa dental humana *in vitro* e *in vivo*.

Invest Clin 2024; 65 (2): 179 – 191

Palabras clave: regeneración del tejido dental; odontoblastos; diferenciación osteogénica.

Resumen. Las células de la pulpa dental humana (hDPCs) han emergido como una alternativa prometedora para la regeneración de tejidos dentales. El factor de crecimiento insulínico tipo 1 (IGF-1) juega un rol crucial en la proliferación y diferenciación osteogénica de las hDPCs en condiciones *in vitro*. No obstante, el impacto del IGF-1 sobre la proliferación y diferenciación odontogénica de las hDPCs en un contexto *in vivo* aún no ha sido completamente elucidado. En el presente estudio, se extrajeron hDPCs de premolares y terceros molares sanos mediante el uso de colagenasa tipo I y dispasa. La tinción inmunocitoquímica de las hDPCs reveló una reactividad positiva para vimentina y negativa para citoqueratina. El tratamiento con IGF-1 en concentraciones de 50, 75 y 100 ng/mL incrementó de manera significativa y dependiente de la dosis la capacidad proliferativa de las hDPCs. En experimentos *in vivo*, las hDPCs fueron implantadas en una matriz dérmica acelular y posteriormente trasplantadas de manera subcutánea en ratones desnudos. Tras 2 y 4 semanas de trasplante, la coloración con hematoxilina y eosina evidenció un aumento en la cantidad de células y matriz extracelular en los implantes tratados con IGF-1, mientras que la coloración con Rojo de Alizarina indicó una mayor formación de tejido mineralizado en comparación con el grupo control. El análisis mediante microscopía electrónica de transmisión (TEM) de las hDPCs mostró una abundante presencia de mitocondrias, retículo endoplásmico rugoso y complejos de Golgi. En conclusión, nuestros hallazgos sugieren que el IGF-1 favorece la proliferación de las hDPCs *in vitro* así como su diferenciación odontogénica *in vivo*, lo cual señala que la modificación de la señalización del IGF-1 podría ofrecer estrategias potenciales para la regeneración de tejidos dentales.

Received: 24-10-2023

Accepted: 02-03-2024

INTRODUCTION

Dental pulp, situated at the innermost tissue within teeth, primarily comprises loose connective tissue and plays an essential role in the repair and regeneration of dental tissues. Traumatic incidents or the impact of infectious agents and other pathogenic stimuli can readily give rise to pulpitis¹. Human dental pulp cells (hDPCs) are

present within dental pulp tissue, constituting a mixture of fibroblasts, inflammatory, immune cells, odontoblasts, and undifferentiated mesenchymal cells^{2,3}. Among these components, the undifferentiated mesenchymal cells possess a multipotent cellular phenotype with the potential to differentiate into various cell lineages, such as osteoblasts, adipocytes, neural progenitors, and chondrocytes⁴⁻⁶. When dental pulp tissue is

exposed to external stimuli, dental pulp cells can differentiate into odontoblasts under the regulation of various factors, which is a significant factor in the regeneration and repair capacity of dental tissue damage^{7,8}. Therefore, exploring the mechanisms of hDPCs proliferation and odontoblastic differentiation is essential.

Cell-based tissue engineering has become an irreplaceable method for regenerating dental tissues⁹. Its fundamental mechanism involves inducing stem cells to differentiate into odontoblast-like or osteoblast-like cells, ultimately achieving the regeneration of the dental pulp-dentin complex^{10,11}. Furthermore, hDPCs exhibit some advantages, characterized by no ethical controversy, low immunogenicity, and easy obtainment from impacted or orthodontic extraction^{12,13}. Therefore, hDPCs have emerged as a potential alternative for future use in regeneration therapy. In addition to stem cells and biomimetic materials, suitable growth factors are imperative in tissue regeneration by promoting cell proliferation, differentiation, and locomotion^{14,15}.

Insulin-like growth factor-1 (IGF-1), a member of the insulin-like peptide family, exerts essential roles in the bone formation and periodontal regeneration of teeth^{14,16,17}. Local controlled delivery of IGF-I from dextran-co-gelatin hydrogel microspheres enhances new bone formation and alveolar bone reconstruction in the periodontal defects¹⁷. Moreover, IGF-1 is also involved in the odontoblastic differentiation of hDPCs or human dental pulp stem cells (hDPSCs). In vitro experiments showed 100 ng/mL IGF-1 promotes proliferation and increases the osteogenic differentiation-related expression of DPSCs via mammalian target of rapamycin (mTOR) signaling pathway¹⁸, as well as the enhancement of proliferation and osteo/odontogenic differentiation was found in the human periodontal ligament stem cells via activating MAPK pathways¹⁹. Similarly, other in vitro research indicates that combined use of 100 ng/ml VEGF and 100 ng/mL IGF-

1 also improve the proliferation, migration, osteogenesis, and angiogenesis of hDPSCs via activation of the phosphoinositide 3-kinase (PI3K)/Akt signaling pathway²⁰.

This study aimed to investigate the effect of IGF-1 on the proliferation and odontogenic differentiation of hDPCs *in vitro* and *in vivo*. These findings may offer valuable insights into the potential utility of hDPCs in treating dental pulp diseases.

MATERIALS AND METHODS

Isolation of human DPCs

Healthy premolars for orthodontic needs or third molars were collected from patients without dental caries or periodontal tissue diseases at the dental clinic of The Second Hospital of Hebei Medical University. All study protocols were approved by the Ethics Committee of The Second Hospital of Hebei Medical University, and written informed consent was obtained from all patients. The hDPCs were obtained as described previously. To completely collect the dental pulp, the tooth surface attachments were scraped off, and the teeth were split in a sterile environment. After washing three times with phosphate buffer solution (PBS), dental pulp tissues were cut into pieces of 1 mm×1 mm in size, then digested in a solution of 3mg/mL collagenase type I (Sigma-Aldrich) and 4mg/mL dispase (Sigma-Aldrich) at 37°C on a shaker for one hour. Following filtration and centrifuging, cell suspensions of dental pulp were cultured in Dulbecco's modified Eagle's medium (DMEM, Gibco, Grand Island, NY, USA) supplemented with 20% fetal bovine serum and 1% penicillin-streptomycin (Gibco, Grand Island, NY, USA) at 37°C in a 5% CO₂ incubator. Observe whether dental pulp cells crawl out of the tissue blocks and cell morphology and growth. Once cells adhere to the culture surface, the medium was refreshed every three days. When cell fusion reached over 80%, the adherent cells were digested with 0.25% trypsin (Sigma-Aldrich), and passage culture was performed at a 1:3

ratio. The hDPCs from the mixed population at passages 3 to 6 were used for subsequent experiments.

Immunohistochemical staining

Passage 4 hDPCs were digested with 0.25% trypsin and prepared as cell suspension, then seeded into 6-well cell culture plates at a concentration of 1×10^4 cells per well. Immunohistochemical staining for vimentin and cytokeratin was carried out on the day following cell adherence. Briefly, cell slides were fixed with 4% formaldehyde for 10 minutes, then treated with 0.5% Triton X-100 (diluted in PBS) for 10 minutes at room temperature. Following PBS washing, cells were blocked with 10% FBS for 20 minutes and subsequently incubated overnight at 4°C with primary antibodies anti-vimentin and anti-cytokeratin (1:200, Abcam). After washing three times with PBS, cells were incubated with biotin-conjugated secondary antibodies (1:1000, Abcam) at room temperature for 20 minutes. DAB staining was performed, and counterstaining with hematoxylin was carried out to visualize the cell nuclei. After mounting coverslips with neutral balsam, photography was conducted under an optical microscope (Olympus, Tokyo, Japan).

Flow cytometry analysis

The purity of isolated hDPCs was assessed using flow cytometry analysis with specific antibodies for CD44 and CD45²¹. The cells were trypsinized and fixed in 4% paraformaldehyde in PBS. Subsequently, hDPCs were permeabilized with 0.1% Triton X-100 (Sigma-Aldrich) in PBS and then incubated with conjugated antibodies against CD44 (1:100, Biotech, Minneapolis, USA) and anti-CD45 (1:100, Biotech, Minneapolis, USA). After washing three times with PBS, flow cytometric analysis was conducted using a FACS (Becton, Dickinson, San Jose, CA) with Quest CELL software (Becton, Dickinson).

Cell proliferation assay

The proliferation ability of hDPCs was assessed using the MTT (3-(4, 5-dimethylthiazol-2-yl)-2, 5-diphenyl nyltetrazolium bromide, Sigma) assays. Passage 4 hDPCs were prepared as a cell suspension with 0.25% trypsin and seeded into 96-well cell culture plates at a concentration of 2×10^3 cells per well. After 24 hours of cultivation, cells were randomly divided into four groups. In the experimental groups, DMEM culture medium containing different concentrations of IGF-1 (50 ng/mL, 75 ng/mL, 100 ng/mL, Peprotech, USA) was added, while in the control group, DMEM without IGF-1 was added. Each group had five replicates. The cells were then cultured at 37°C for 1, 3, 5, and 7 days, respectively. Subsequently, 20 μ L of MTT (2 mg/mL in PBS) was added to each well. After 4 hours of incubation, the supernatant was removed, and 150 μ L DMSO were added. The absorbance values at A450 for each well were determined using a microplate reader (Bio-Rad).

Odontoblastic differentiation *in vivo*

The acellular dermal matrix (ADM, Beijing Qingyuan Weiye Company, China) underwent aseptic cutting into pieces measuring 5mm \times 5mm \times 1mm. These pieces were subjected to three washings with PBS and a 2-hour soak in 10% FBS within a sterile environment. The 2×10^5 hDPCs were prepared as a cell suspension. After removing the FBS, cells were gently seeded onto the scaffold using a pipette, ensuring even distribution within the scaffold interstices through gentle shaking. The composite was co-cultured at 37°C for 24 hours. The culture medium was replaced with 100 ng/mL IGF-1 culture medium supplemented with mineralization induction solution, consisting of 10% FBS, DMEM, 10 mmol/L β -glycerophosphate, 100 mg/mL vitamin C, and 10 nmol/L dexamethasone. The culture medium in the control group was replaced with a mineralization induction solution without IGF-1. The

induction culture was maintained for three days. For the *in vivo* phase, eight 4-week-old immunodeficient mice were selected. Under sterile conditions, incisions were made in the skin along their dorsal midlines. The hDPCs-scaffold complexes were transplanted subcutaneously into the left dorsal region, while control scaffolds were transplanted as controls into the right dorsal region. The odontoblastic differentiation in the hDPCs-scaffold complexes within the mice was observed at two and four weeks post-transplantation.

Histological staining

Hematoxylin and Eosin (HE) staining was used for the histological observation, and Alizarin red staining was performed to identify calcium-containing osteocytes or odontoblasts. The mice were euthanized at two and four weeks post-transplantation. The scaffold and surrounding tissues were immediately harvested and fixed in 4% paraformaldehyde. Subsequently, 4- μ m-thick sections were prepared using a freezing microtome. The sections were stained with hematoxylin for 3 minutes for HE staining, followed by differentiation and a 20-second rinse in alkaline water. Next, sections were stained with eosin for 20 seconds. For the alizarin red staining, sections were fixed in 95% anhydrous ethanol for 10 minutes. After rinsing in double-distilled water thrice, sections were stained in 0.1% alizarin red-Tris-HCl at 37°C for 30 minutes. All sections were observed and counted under a light microscope (Olympus, Tokyo, Japan).

Transmission electron microscopy (TEM)

TEM was used to assess the morphologies of hDPCs-scaffold complexes. After two and four weeks post-transplantation, the scaffold was immediately harvested and washed three times with PBS, then fixed in 4% (v/v) glutaraldehyde for 2 hours at room temperature. The complexes were dehydrated with varying ethanol concentrations and embedded with epoxy resin. Subse-

quently, 4- μ m-thick sections were prepared and stained with the toluidine blue staining. Ultimately, all the samples were air-dried overnight and viewed with a Hitachi Model H-7500 TEM (Hitachi, Japan).

Statistical analysis

Data were shown as mean \pm SD, and statistical analysis was performed using SPSS 17.0 software (IBM SPSS, Armonk, NY, USA). Group comparisons were performed using one-way ANOVA followed by a least significant difference (LSD) post-hoc comparisons. $P < 0.05$ was considered to indicate a statistically significant difference.

RESULTS

Identification of human dental pulp cells (hDPCs)

The inverted microscopy showed that hDPCs displayed clustered growth after seven days of adherent culture, primarily with a spindle-shaped morphology, while a smaller fraction of polygonal shapes (Fig. 1A). After passaging, the hDPCs adopted a vortex-like growth pattern, characterized by a more uniform, short spindle-shaped morphology with extending cytoplasmic processes (Fig. 1B). Immunocytochemical analysis was performed using passage 4 hDPCs, and showed positive staining for vimentin (Fig. 1C) and negative staining for cytokeratin (Fig. 1D), indicating their mesenchymal origin. Additionally, the flow cytometry analysis showed that the purity of hDPCs reached more than 95% (Fig. 1E). These morphological features were aligned with the typical biological characteristics of hDPCs.

IGF-1 promoted proliferation of hDPCs *in vitro*

MMT assay was performed to assess the effect of different IGF-1 concentrations (50, 75, and 100ng/mL) on the proliferation ability of hDPCs. As shown in Fig. 2, there was no significant difference among groups ($p > 0.05$), and 100ng/mL IGF-1 sig-

nificantly increased the proliferation of hDPCs three days after treatment compared to the control group ($p < 0.01$). At day five and day seven, treatment with IGF-1 significantly increased the proliferation of hDPCs compared with the control group ($p < 0.05$

and $p < 0.01$), 100 ng/mL IGF-1 displayed a more substantial enhancement compared to 50 ng/mL and 75 ng/mL ($p < 0.05$ and $p < 0.01$). These results indicated that IGF-1 promoted the proliferation of hDPCs in a concentration-dependent manner.

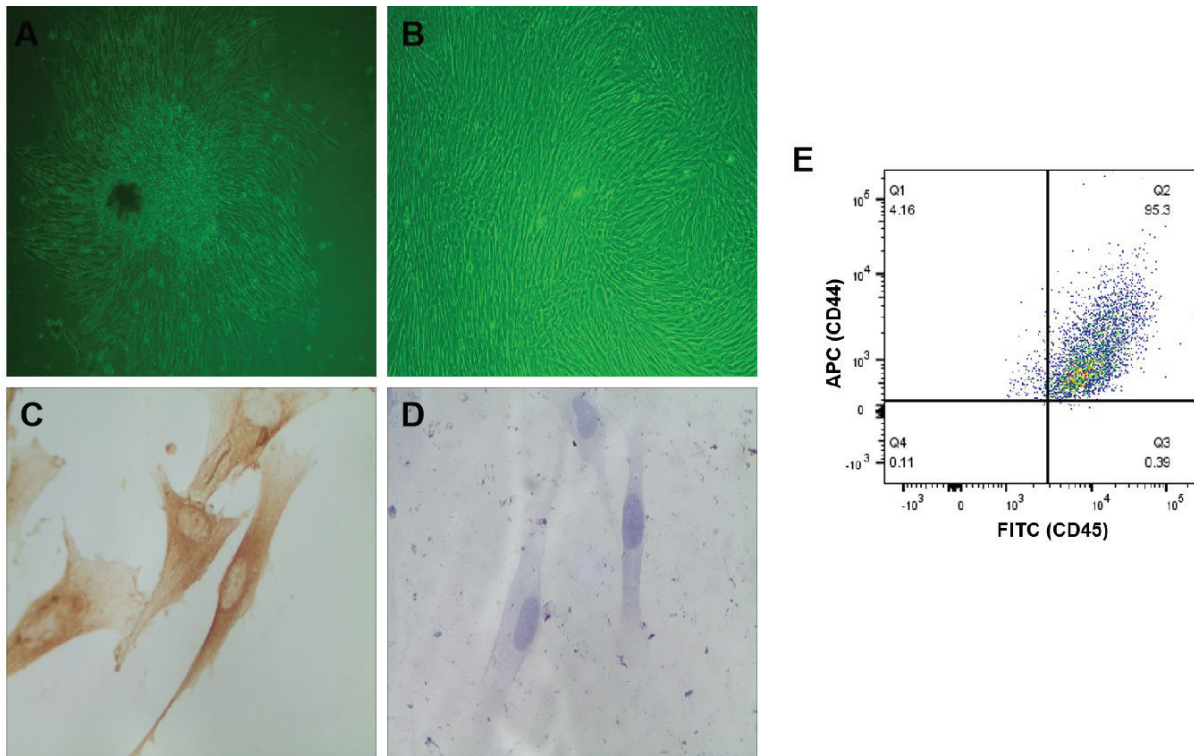


Fig. 1. Identification of hDPCs. A: Morphology after seven days of primary culture. B: Morphology of hDPCs in passage 3. C: Immunocytochemical staining for vimentin. D: Immunocytochemical staining for cytokeratin. E: Flow cytometric analysis for CD44 and CD45.

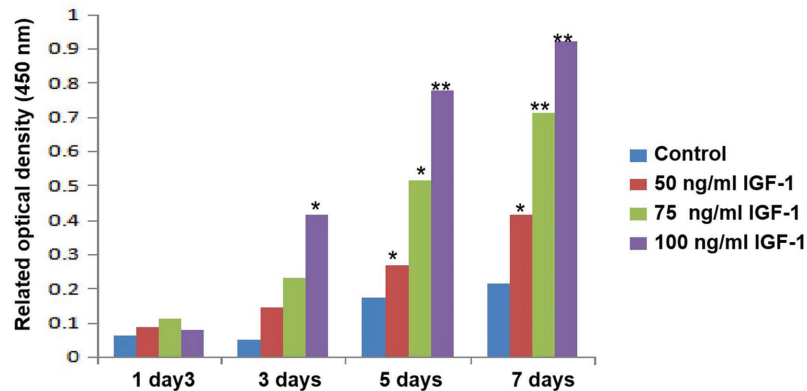


Fig. 2. IGF-1 promoted the proliferation of hDPCs in vitro. MMT assay showed treatment with 100 ng/mL IGF-1 significantly increased the proliferation of hDPCs from day 3, as well as 50 ng/mL and 75 ng/mL IGF-1 in day 5 and day 7 cultures. * $p < 0.01$ and ** $p < 0.01$ vs control (DMEM without IGF-1).

IGF-1 promoted odontogenic differentiation of hDPCs *in vivo*

In order to investigate the effect of IGF-1 on osteogenic differentiation *in vivo*, hDPCs were seeded into an ADM scaffold for the induction of odontogenic differentiation, and the hDPCs-scaffold complexes were transplanted subcutaneously into immunodeficient mice for two or four weeks. HE staining conducted at 2 and 4 weeks post-transplantation revealed more cells and extracellular matrix in implants from IGF-1 treatment group compared to the control group (Fig. 3). Alizarin red staining demonstrated that mineralized nodules in the IGF-1 group exhibited time-dependent enhancement, including the differentiation of odontoblast-like cells (Fig. 4). TEM analysis of hDPCs at 2 and 4 weeks post-transplantation showed an abundance of mitochondria, rough endoplasmic reticulum and Golgi complexes (Fig. 5). These findings indicated that IGF-1 progressively promoted the odontogenic differentiation of hDPCs *in vivo*.

DISCUSSION

Cell-based tissue engineering has become an irreplaceable method for regenerating dental tissues⁹, and the potential value of hDPCs has been widely accepted in bone tissue engineering due to their high self-renewal capacity and stemness^{22,23}. The process of dentinal regeneration involves the proliferation and differentiation of hDPCs into odontoblasts, dental pulp healing, and reparative dentin formation²⁴. Increasing studies have implicated IGF-1 in the maintenance of proliferation and differentiation of various stem cells, such as embryonic stem cells, bone marrow mesenchymal stem cells (BMSC), periodontal ligament stem cells, and hDPSCs²⁵. However, the effect of IGF-1 on the proliferation and differentiation of hDPCs *in vitro* and *in vivo* warrants further investigation. In this study, we found that exogenous IGF-1 promoted the proliferation of hDPCs in a concentration-dependent manner.

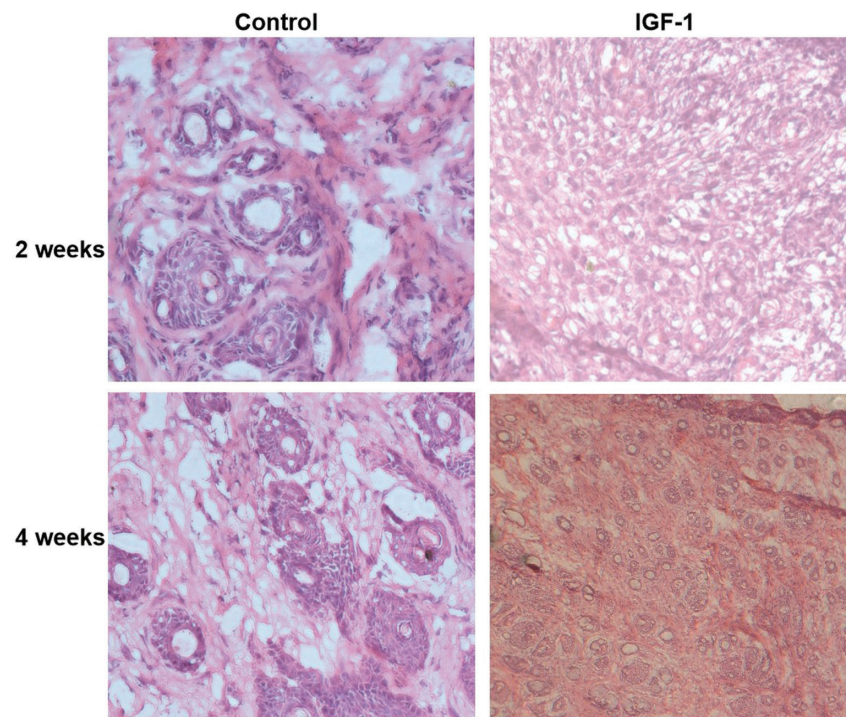


Fig. 3. HE staining revealed more cells and extracellular matrix in implants from the IGF-1 group compared to the control group (without IGF-1) at 2 and 4 weeks post-transplantation.

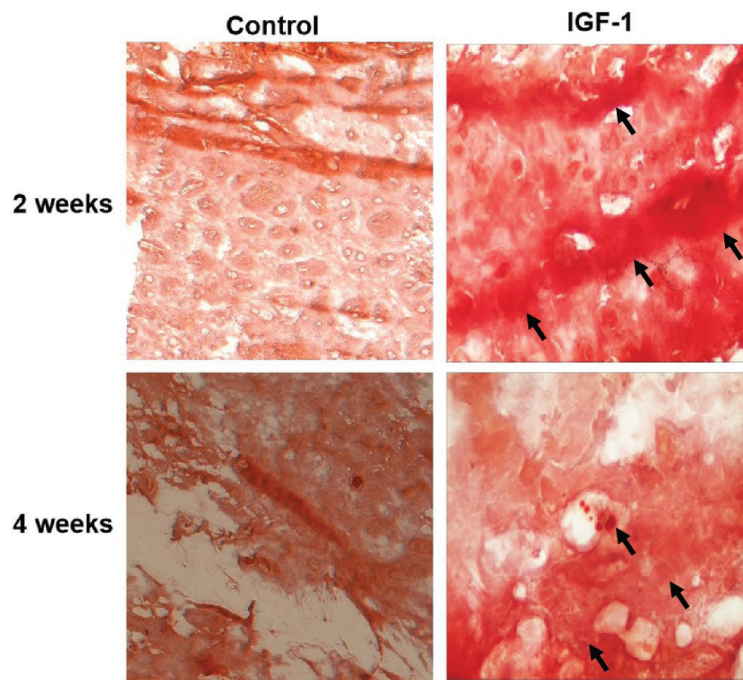


Fig. 4. IGF-1 promoted odontogenic differentiation of hDPCs *in vivo*. Alizarin red staining was performed to identify calcium-containing odontoblast, showing more mineralized tissues (arrows) in IGF-1 group compared to the control group (without IGF-1) at 2 and 4 weeks post-transplantation.

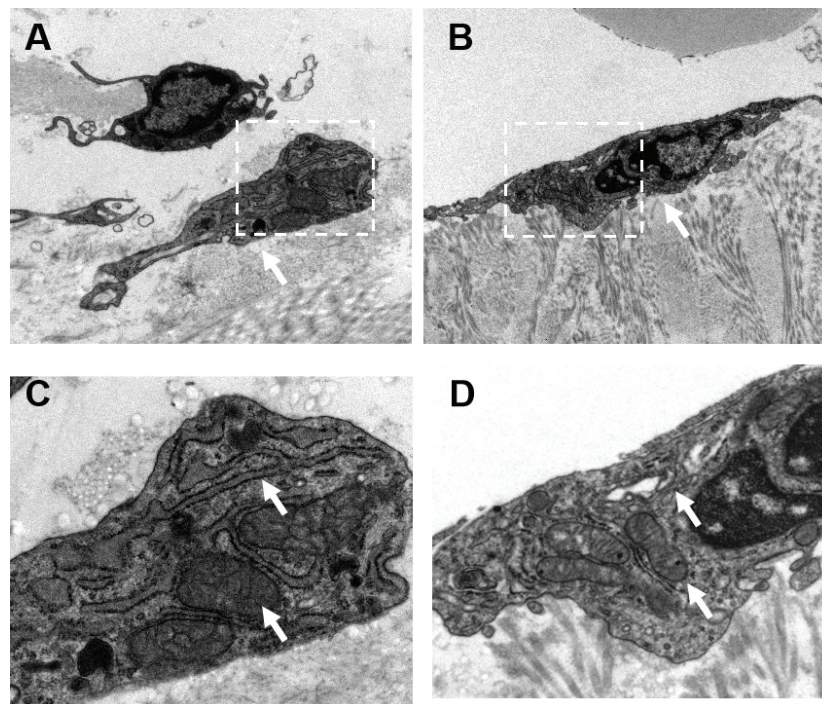


Fig 5. TEM analysis. A-B: The subcellular structure of hDPCs in scaffold 2 weeks (A) and 4 weeks (B) post-transplantation in IGF-1 group (magnification $\times 6K$). C-D: The subcellular structure of hDPCs in scaffold 2 weeks (C) and 4 weeks (D) post-transplantation in IGF-1 group (magnification $\times 15K$). Mitochondria and rough endoplasmic reticulum were highlighted using arrows.

Additionally, IGF-1 progressively promoted odontogenic differentiation of hDPCs *in vivo* by subcutaneous transplantation into nude mice.

As a unique type of dental stem cell, hDPCs are derived from the pulp in deep carious teeth and display stronger proliferation and osteogenic differentiation capability due to distinctive environmental stimulus^{26,27}. This distinctive trait provides valuable insights into the cellular mechanisms underlying tooth development and regenerative repair, offering the potential for dental pulp regeneration. The proliferation ability of colony-forming cultures of hDPCs and BMSCs was assessed by bromodeoxyuridine, showing that the number of proliferating cells in hDPC cultures was significantly higher than that in BMSC cultures. This result proves the more substantial proliferation capability of hDPCs compared to BMSCs²⁸. Moreover, under specific induction conditions, hDPCs can be induced to differentiate into various cell types, including odontoblast-like and osteoblast-like cells. Almushayt *et al.*²⁹ experimentally verified the capacity of hDPCs to differentiate into odontoblast-like cells *in vitro*. This study also found the odontoblast differentiation potential of hDPCs *in vivo* by subcutaneous transplantation into nude mice. Zhang *et al.*³⁰ isolated dental pulp cells from healthy third molars through enzymatic digestion, confirming their identity as hDPSCs. Subsequent induction assays revealed their multilineage differentiation potential, including differentiation potential toward adipogenic, osteogenic, fibrogenic, chondrogenic, and neurogenic lineages. Yang *et al.*³¹ demonstrated the capacity of dental pulp stem cells to differentiate into chondrocytes and myocytes under specific induction conditions.

Growth factors are critical in tooth tissue regeneration, as they have essential roles in regulating cell functions, such as platelet-derived growth factor, fibroblast growth factor, and epidermal growth factor^{32,33}. IGF-1, one of the ubiquitous peptide hormones, has

been identified to facilitate various cellular processes, including cell proliferation, differentiation, migration, apoptosis, and survival²⁵. Previous studies have reported that IGF-1 can affect hDPCs proliferation, promote osteogenesis, and help reconstruct tooth-supporting tissues³⁴⁻³⁶. A report by Onishi *et al.*³⁷ reveals multiple biological effects of IGF-1 on hDPCs. IGF-1 can stimulate hDPCs proliferation, increase mucin and extracellular matrix protein synthesis, enhance DNA synthesis, and increase alkaline phosphatase (ALPase) activity when hDPCs were cultured in a serum-free medium supplemented with IGF-1. Increasing investigations have illustrated the capacity of IGF-1 to induce the differentiation of ameloblasts and odontoblasts, facilitating dentin regeneration and the development of structures resembling enamel-dentin complexes^{34,35}. IGF-1 also influences the proliferation and differentiation of other odontogenic cell types, specifically periodontal ligament stem cells and stem cells from apical papilla^{19,38}. In this study, we also found that exogenous IGF-1 promoted the proliferation of hDPCs *in vivo* in a concentration-dependent manner and progressively promoted odontogenic differentiation of hDPCs *in vivo*.

IGF-1 receptor (IGF-1R) is a cell-surface receptor tyrosine kinase with its specific ligands IGF-1³⁹. It activates downstream signaling pathways, namely the phosphoinositide 3-kinase (PI3K)/AKT and the RAS/mitogen-activated protein kinase (MAPK) pathways. These pathways are widely involved in stem cell growth, proliferation, and differentiation^{40,41}. Previous studies have reported that the activation of IGF-1R signaling contributes to maintaining the self-renewal and differentiation of hDPCs²⁵. It has been demonstrated that treatment with IGF-1 can up-regulate the expression of phospho-ERK and phospho-p38 of hDPCs, suggesting MAPK signaling pathway during differentiation of hDPSCs and human periodontal ligament stem cells¹⁹. The interactions between IGF-1R and the p38 MAPK signaling pathway

control the quiescence and activation of hDPSCs. In addition, the downstream effectors between the MAPK signaling pathway and the PI3K/Akt signaling pathway partly overlap, resulting in the interaction effect of two signaling pathways. Some studies show that IGF-1 can promote the differentiation of adipose-derived stem cells and endothelial cells by the PI3K/AKT signaling pathway⁴². Meanwhile, the IGF-1-induced activation of the AKT signaling pathway also involved the proliferation, migration, osteogenesis, and angiogenesis of hDPSCs²¹. However, the underlying molecular mechanism of proliferation and odontogenic differentiation for hDPSCs needs further research.

In conclusion, we found that exogenous IGF-1 promoted the proliferation of hDPSCs in a concentration-dependent manner in vitro and progressively promoted odontogenic differentiation of hDPSCs in vivo. This suggests that modifying IGF-1 signaling may offer potential strategies for hDPSCs-based tissue engineering to regenerate dental tissues.

Declarations Ethics approval and consent to participate

This study was conducted following the Helsinki Declaration. This study was conducted with approval from the Ethics Committee of the Second Hospital of Hebei Medical University. Written informed consent was obtained from all participants. This study was conducted under the principles of ethical animal research outlined in the Basel Declaration and the ethical guidelines by the International Council for Laboratory Animal Science (ICLAS). This study was conducted following NC3Rs ARRIVE guidelines.

Competing interest

The authors had no separate personal, financial, commercial, or academic conflicts of interest.

Funding

Not applicable.

Authors ORCID'number

- Yan Wang (YW):
0009-0004-4323-0268
- Nan Du (ND):
0009-0009-3942-3872
- Cong-na Liu (CNL):
0009-0002-2022-0329
- Wen-jing Li (WJL):
0009-0007-4067-5845

Author contributions

Conception and design: Wang W; administrative support: YW and ND; provision of study materials or patients: ND and CNL; collection and assembly of data: CNL and WJL; data analysis and interpretation: YW and WJL; manuscript writing: all authors and final approval of manuscript: all authors.

REFERENCES

1. Liu S, Wang S, Dong Y. Evaluation of a bioceramic as a pulp capping agent in vitro and in vivo. *J Endod.* 2015;41(5):652-657. <https://doi.org/10.1016/j.joen.2014.12.009>.
2. Cooper PR, Takahashi Y, Graham LW, Simon S, Imazato S, Smith AJ. Inflammation-regeneration interplay in the dentine-pulp complex. *J Dent* 2010;38(9):687-697. <https://doi.org/10.1016/j.jdent.2010.05.016>.
3. Wang YL, Hu YJ, Zhang FH. Effects of GP-NMB on proliferation and odontoblastic differentiation of human dental pulp cells. *Int J Clin Exp Pathol* 2015;8(6):6498-6504.
4. Miura M, Gronthos S, Zhao M, Lu B, Fisher LW, Robey PG, Shi S. SHED: stem cells from human exfoliated deciduous teeth. *Proc Natl Acad Sci USA.* 2003;100(10):5807-5812. <https://doi.org/10.1073/pnas.0937635100>.
5. Jo YY, Lee HJ, Kook SY, Choung HW, Park JY, Choung JH, Choung YH, Kim ES, Yang HC, Choung PH. Isolation and

- characterization of postnatal stem cells from human dental tissues. *Tissue Eng.* 2007;13(4):767-773. <https://doi.org/10.1089/ten.2006.0192>.
6. **Paino F, Ricci G, De Rosa A, D'Aquino R, Laino L, Pirozzi G, Tirino V, Papaccio G.** Ecto-mesenchymal stem cells from dental pulp are committed to differentiate into active melanocytes. *Eur Cell Mater.* 2010;20:295-305. <https://doi.org/10.22203/ecm.v020a24>.
 7. **Kim BC, Bae H, Kwon IK, Lee EJ, Park JH, Khademhosseini A, Hwang YS.** Osteoblastic/cementoblastic and neural differentiation of dental stem cells and their applications to tissue engineering and regenerative medicine. *Tissue Eng Part B Rev.* 2012;18(3):235-244. <https://doi.org/10.1089/ten.TEB.2011.0642>.
 8. **Smith JG, Smith AJ, Shelton RM, Cooper PR.** Dental pulp cell behavior in biomimetic environments. *J Dent Res.* 2015;94(11):1552-1559. <https://doi.org/10.1177/0022034515599767>.
 9. **Chen FM, Zhang J, Zhang M, An Y, Chen F, Wu ZF.** A review on endogenous regenerative technology in periodontal regenerative medicine. *Biomaterials.* 2010;31(31):7892-7927. <https://doi.org/10.1016/j.biomaterials.2010.07.019>.
 10. **Liang C, Liao L, Tian W.** Stem cell-based dental pulp regeneration: insights from signaling pathways. *Stem Cell Rev Rep.* 2021;17(4):1251-1263. <https://doi.org/10.1007/s12015-020-10117-3>.
 11. **Suzuki T, Lee CH, Chen M, Zhao W, Fu SY, Qi JJ, Chotkowski G, Eising SB, Wong A, Mao JJ.** Induced migration of dental pulp stem cells for in vivo pulp regeneration. *J Dent Res.* 2011;90(8):1013-1018. <https://doi.org/10.1177/0022034511408426>.
 12. **Huang GT, Gronthos S, Shi S.** Mesenchymal stem cells derived from dental tissues vs. those from other sources: their biology and role in regenerative medicine. *J Dent Res.* 2009;88(9):792-806. <https://doi.org/10.1177/0022034509340867>.
 13. **Pierdomenico L, Bonsi L, Calvitti M, Rondelli D, Arpinati M, Chirumbolo G, Becchetti E, Marchionni C, Alviano F, Fossati V, Staffolani N, Franchina M, Grossi A, Bagnara GP.** Multipotent mesenchymal stem cells with immunosuppressive activity can be easily isolated from dental pulp. *Transplantation.* 2005;80(6):836-842. <https://doi.org/10.1097/01.tp.0000173794.72151.88>.
 14. **Chen FM, Zhang M, Wu ZF.** Toward delivery of multiple growth factors in tissue engineering. *Biomaterials.* 2010;31(24):6279-6308. <https://doi.org/10.1016/j.biomaterials.2010.04.053>.
 15. **Kim SG, Zhou J, Solomon C, Zheng Y, Suzuki T, Chen M, Song S, Jiang N, Cho S, Mao JJ.** Effects of growth factors on dental stem/progenitor cells. *Dent Clin North Am.* 2012;56(3):563-575. <https://doi.org/10.1016/j.cden.2012.05.001>.
 16. **Fang Y, Wang LP, Du FL, Liu WJ, Ren GL.** Effects of insulin-like growth factor I on alveolar bone remodeling in diabetic rats. *J Periodontal Res.* 2013;48(2):144-150. <https://doi.org/10.1111/j.1600-0765.2012.01512.x>.
 17. **Chen FM, Zhao YM, Wu H, Deng ZH, Wang QT, Zhou W, Liu Q, Dong GY, Li K, Wu ZF, Jin Y.** Enhancement of periodontal tissue regeneration by locally controlled delivery of insulin-like growth factor-I from dextran-co-gelatin microspheres. *J Control Release.* 2006;114(2):209-222. <https://doi.org/10.1016/j.jconrel.2006.05.014>.
 18. **Feng X, Huang D, Lu X, Feng G, Xing J, Lu J, Xu K, Xia W, Meng Y, Tao T, Li L, Gu Z.** Insulin-like growth factor 1 can promote proliferation and osteogenic differentiation of human dental pulp stem cells via mTOR pathway. *Dev Growth Differ.* 2014;56(9):615-624. <https://doi.org/10.1111/dgd.12179>.
 19. **Yu Y, Mu J, Fan Z, Lei G, Yan M, Wang S, Tang C, Wang Z, Yu J, Zhang G.** Insulin-like growth factor 1 enhances the proliferation and osteogenic differentiation of human periodontal ligament stem cells via ERK and JNK MAPK pathways. *Histochem Cell Biol.* 2012;137(4):513-525. <https://doi.org/10.1007/s00418-011-0908-x>.
 20. **Lu W, Xu W, Li J, Chen Y, Pan Y, Wu B.** Effects of vascular endothelial growth

- factor and insulin growth factor1 on proliferation, migration, osteogenesis and vascularization of human carious dental pulp stem cells. *Mol Med Rep.* 2019;20(4):3924-3932. <https://doi.org/10.3892/mmr.2019.10606>.
21. Lins-Candeiro CL, Paranhos LR, de Oliveira Neto NF, Ribeiro RAO, de-Souza-Costa CA, Guedes FR, da Silva WHT, Turrioni AP, Santos Filho PCF. Viability and oxidative stress of dental pulp cells after indirect application of chemomechanical agents: An in vitro study. *Int Endod J.* 2023; 57(3):315-327. doi: 10.1111/iej.14013.
 22. Schreier C, Rothmiller S, Scherer MA, Rummel C, Steinritz D, Thiermann H, Schmidt A. Mobilization of human mesenchymal stem cells through different cytokines and growth factors after their immobilization by sulfur mustard. *Toxicol Lett.* 2018;293:105-111. <https://doi.org/10.1016/j.toxlet.2018.02.011>.
 23. Martin-Del-Campo M, Rosales-Ibañez R, Alvarado K, Sampedro JG, Garcia-Sepulveda CA, Deb S, San Román J, Rojo L. Strontium folate loaded biohybrid scaffolds seeded with dental pulp stem cells induce in vivo bone regeneration in critical sized defects. *Biomater Sci.* 2016;4(11):1596-1604. <https://doi.org/10.1039/c6bm00459h>.
 24. Woo SM, Lim HS, Jeong KY, Kim SM, Kim WJ, Jung JY. Vitamin D promotes odontogenic differentiation of human dental pulp cells via ERK activation. *Mol Cells.* 2015;38(7):604-609. <https://doi.org/10.14348/molcells.2015.2318>.
 25. Teng CF, Jeng LB, Shyu WC. Role of insulin-like growth factor 1 receptor signaling in stem cell stemness and therapeutic efficacy. *Cell Transplant.* 2018;27(9):1313-1319. <https://doi.org/10.1177/0963689718779777>.
 26. Werle SB, Lindemann D, Steffens D, Demarco FF, de Araujo FB, Pranke P, Casagrande L. Carious deciduous teeth are a potential source for dental pulp stem cells. *Clin Oral Investig.* 2016;20(1):75-81. <https://doi.org/10.1007/s00784-015-1477-5>.
 27. Gnanasegaran N, Govindasamy V, Abu Kasim NH. Differentiation of stem cells derived from carious teeth into dopaminergic-like cells. *Int Endod J.* 2016;49(10):937-949. <https://doi.org/10.1111/iej.12545>. Epub 2015 Oct 3.
 28. Gronthos S, Mankani M, Brahimi J, Robey PG, Shi S. Postnatal human dental pulp stem cells (DPSCs) in vitro and in vivo. *Proc Natl Acad Sci U S A.* 2000;97(25):13625-13630. <https://doi.org/10.1073/pnas.240309797>.
 29. Almushayt A, Narayanan K, Zaki AE, George A. Dentin matrix protein 1 induces cytodifferentiation of dental pulp stem cells into odontoblasts. *Gene Ther.* 2006;13(7):611-620. <https://doi.org/10.1038/sj.gt.3302687>.
 30. Zhang W, Walboomers XF, Shi S, Fan M, Jansen JA. Multilineage differentiation potential of stem cells derived from human dental pulp after cryopreservation. *Tissue Eng.* 2006;12(10):2813-2823. <https://doi.org/10.1089/ten.2006.12.2813>.
 31. Yang X, Zhang W, van den Dolder J, Walboomers XF, Bian Z, Fan M, Jansen JA. Multilineage potential of STRO-1+ rat dental pulp cells in vitro. *J Tissue Eng Regen Med.* 2007;1(2):128-135. <https://doi.org/10.1002/term.13>.
 32. Moeller M, Pink C, Endlich N, Endlich K, Grabe HJ, Völzke H, Dörr M, Nauck M, Lerch MM, Köhling R, Holtfreter B, Kocher T, Fuellen G. Mortality is associated with inflammation, anemia, specific diseases and treatments, and molecular markers. *PLoS One.* 2017;12(4):e0175909. <https://doi.org/10.1371/journal.pone.0175909>.
 33. Alarçin E, Lee TY, Karuthedom S, Mohammadi M, Brennan MA, Lee DH, Marrella A, Zhang J, Syla D, Zhang YS, Khademhosseini A, Jang HL. Injectable shear-thinning hydrogels for delivering osteogenic and angiogenic cells and growth factors. *Biomater Sci.* 2018;6(6):1604-1615. <https://doi.org/10.1039/c8bm00293b>.
 34. Shinohara Y, Tsuchiya S, Hatae K, Honda MJ. Effect of vitronectin bound to insulin-like growth factor-I and insulin-like growth factor binding protein-3 on porcine ena-

- mel organ-derived epithelial cells. *Int J Dent*. 2012;2012:386282. <https://doi.org/10.1155/2012/386282>.
35. **Catón J, Bringas P Jr, Zeichner-David M.** Establishment and characterization of an immortalized mouse-derived odontoblast-like cell line to evaluate the effect of insulin-like growth factors on odontoblast differentiation. *J Cell Biochem*. 2007;100(2):450-463. <https://doi.org/10.1002/jcb.21053>.
 36. **Schminke B, Vom Orde F, Gruber R, Schliephake H, Bürgers R, Miosge N.** The pathology of bone tissue during peri-implantitis. *J Dent Res*. 2015;94(2):354-361. <https://doi.org/10.1177/0022034514559128>.
 37. **Onishi T, Kinoshita S, Shintani S, Sobue S, Ooshima T.** Stimulation of proliferation and differentiation of dog dental pulp cells in serum-free culture medium by insulin-like growth factor. *Arch Oral Biol*. 1999;44(4):361-371. [https://doi.org/10.1016/s0003-9969\(99\)00007-2](https://doi.org/10.1016/s0003-9969(99)00007-2).
 38. **Wang S, Mu J, Fan Z, Yu Y, Yan M, Lei G, Tang C, Wang Z, Zheng Y, Yu J, Zhang G.** Insulin-like growth factor 1 can promote the osteogenic differentiation and osteogenesis of stem cells from apical papilla. *Stem Cell Res*. 2012;8(3):346-356. <https://doi.org/10.1016/j.scr.2011.12.005>.
 39. **Chen C, Xu Y, Song Y.** IGF-1 gene-modified muscle-derived stem cells are resistant to oxidative stress via enhanced activation of IGF-1R/PI3K/AKT signaling and secretion of VEGF. *Mol Cell Biochem*. 2014;386(1-2):167-175. <https://doi.org/10.1007/s111010-013-1855-8>.
 40. **Liu C, Zhang Z, Tang H, Jiang Z, You L, Liao Y.** Crosstalk between IGF-1R and other tumor promoting pathways. *Curr Pharm Des*. 2014;20(17):2912-2921. <https://doi.org/10.2174/13816128113199990596>.
 41. **Girnit L, Worrall C, Takahashi S, Se-regard S, Girnit A.** Something old, something new and something borrowed: emerging paradigm of insulin-like growth factor type 1 receptor (IGF-1R) signaling regulation. *Cell Mol Life Sci*. 2014;71(13):2403-2427. <https://doi.org/10.1007/s00018-013-1514-y>.
 42. **Wan Y, Zhuo N, Li Y, Zhao W, Jiang D.** Autophagy promotes osteogenic differentiation of human bone marrow mesenchymal stem cell derived from osteoporotic vertebrae. *Biochem Biophys Res Commun*. 2017;488(1):46-52. <https://doi.org/10.1016/j.bbrc.2017.05.004>.

Gender-based comparative analysis of knee injury risk during cutting maneuvers in non-professional athletes: a kinetic and kinematic perspective.

Adrián Feria-Madueño¹, Timothy E. Hewett^{2,3} and Borja Sañudo¹

¹ Department of Physical Education and Sport, University of Seville. Pirotecnia Street, Seville, Spain.

² Department of Orthopedics, Marshall University Biomechanics Laboratories and Sports Medicine Research, Marshall University, Huntington, West Virginia, USA.

³ Hewett Global Consulting, Newport, KY.

Keywords: anterior cruciate ligament; Q angle; accelerometry; force platform.

Abstract. This study aimed to compare the risk of knee injury between men and women by integrating kinetic and kinematic parameters in a non-professional athlete population. Two hundred non-professional athletes were recruited for the present study. Three change of direction tests were conducted, consisting of two open cuts at 30 (SC₃₀) and 45 degrees (SC₄₅) and one closed cut at 45 degrees (SC_{45cl}). Kinetic variables, including three-dimensional force and accelerations in the three axes of movement and ground contact time, were assessed using force platform and accelerometers. The initial and maximum angles of the ankle, knee, hip, and trunk were analyzed by photogrammetry. The data was compared between males and females to examine gender differences. Gender analysis demonstrated significant differences in force values, with women displaying higher medial-lateral (ML) force in SC₃₀ and men exhibiting higher vertical ground reaction force (VGRF) and anterior-posterior (AP) force in SC₄₅. Gender-specific analysis indicated higher partial knee accelerations in women during SC₃₀ and SC₄₅, with significant differences observed in acceleration in the vertical axis. Gender differences were observed in certain kinematic variables, with women displaying higher ankle flexion at initial contact in SC₃₀ and higher ankle flexion at maximum flexion and ankle dorsiflexion range in SC₄₅. Men showed lower knee flexion angles in both SC_{45cl} and SC₄₅. These findings provide valuable insights into the kinetics and kinematics of change of direction movements and highlight gender-specific differences that may have implications for training and injury prevention strategies. Further research is needed to understand the underlying factors contributing to these differences and their impact on performance and injury risk.

Análisis comparativo, basado en el género, del riesgo de lesión de rodilla durante cambios de dirección en atletas no profesionales: una perspectiva cinética y cinemática.

Invest Clin 2024; 65 (2): 192 – 205

Palabras clave: ligamento cruzado anterior; ángulo Q; acelerómetro; plataforma de fuerza.

Resumen. El objetivo de este estudio fue comparar el riesgo de lesión de rodilla entre hombres y mujeres mediante la integración de parámetros cinéticos y cinemáticos en una población de atletas no profesionales. Doscientos atletas no profesionales fueron reclutados para el presente estudio. Se realizaron tres pruebas de cambio de dirección, consistentes en dos cortes abiertos a 30 (SC₃₀) y 45 grados (SC₄₅), y un corte cerrado a 45 grados (SC_{45cl}). Se evaluaron las variables cinéticas, incluida la fuerza tridimensional, así como las aceleraciones en los tres ejes de movimiento y el tiempo de contacto con el suelo mediante plataforma de fuerza y acelerometría. Se analizaron los ángulos iniciales y máximos del tobillo, la rodilla, la cadera y el tronco a través de fotogrametría. Se realizó una comparación de los datos entre hombres y mujeres para examinar las diferencias de género. El análisis de género demostró diferencias significativas en los valores de fuerza, mostrando las mujeres una mayor fuerza medial-lateral (ML) en SC₃₀, y los hombres una mayor fuerza de reacción vertical al suelo (VGRF) y fuerza anteroposterior (AP) en SC₄₅. Los análisis específicos de género indicaron mayores aceleraciones parciales de rodilla en las mujeres durante SC₃₀ y SC₄₅, observándose diferencias significativas en la aceleración en el eje vertical. Se observaron diferencias de género en determinadas variables cinemáticas, mostrando las mujeres mayor flexión del tobillo en el contacto inicial en SC₃₀ y mayor flexión del tobillo en flexión máxima y rango de dorsiflexión del tobillo en SC₄₅. Los hombres mostraron ángulos de flexión de rodilla más bajos tanto en SC_{45cl} como en SC₄₅. Estos resultados proporcionan información valiosa sobre la cinética y la cinemática de los movimientos de cambio de dirección y ponen de relieve las diferencias específicas de género que pueden tener implicaciones para las estrategias de entrenamiento y prevención de lesiones. Se necesita más investigación para comprender mejor los factores subyacentes que contribuyen a estas diferencias y su impacto en el rendimiento y el riesgo de lesiones.

Received: 12-10-2023

Accepted: 08-02-2024

INTRODUCTION

Gender is a significant factor to consider in the incidence and prevention of knee injuries during changes of direction^{1,2}. One of the structures with a higher incidence of injury is the anterior cruciate ligament

(ACL), and research has demonstrated that women have an increased risk compared to men in sports involving frequent changes of direction and deceleration³.

From a kinetic standpoint, the mechanism of injury during knee changes of directions involves a combination of torsional and

axial loading forces applied to the ACL³. The knee is vulnerable during direction changes due to the combination of rotational and axial loading movements on the ligament⁴. The assessment of the ACL using force platforms is well-established⁵⁻⁷. However, there is limited evidence on its analysis using other parameters such as accelerometry in each axis and ground contact time during changes of directions.

In women, hip anatomy and knee biomechanics during changes of directions may contribute to a higher incidence of ACL injuries⁸. Women have wider hips and a larger Q angle, which can increase internal knee rotation during direction changes and thus increase the risk of ACL injuries⁴. Consequently, women exhibit a smaller flexion angle and greater dynamic valgus during knee changes, associated with lower knee stability and an increased risk of injury³.

These kinetic and kinematic factors related to the risk of knee injuries include not only the direction and magnitude of forces applied to the knee during changes of direction⁹, but also depend on the knee angle maintained and ground contact time during changes of direction¹⁰. However, there is limited research integrating both factors. Despite knowledge of the risk factors most associated with an increased risk of knee injuries, there is a lack of evidence in evaluating these risk factors in a non-professional

athlete population, necessitating studies that assess kinetic and kinematic parameters, integrating them into a comprehensive analysis with innovative parameters such as acceleration or contact time.

Therefore, this study aimed to compare the risk of knee injury between men and women by integrating kinetic and kinematic parameters in a non-professional athlete population.

MATERIALS AND METHODS

Subjects

Two hundred non-professional athletes were recruited for the present study. After the initial meeting, the inclusion criteria were explained. These criteria consisted of engaging in physical activity for at least 30 minutes per day, three days per week, and having no history of knee or ankle injury in the past 12 months. Following this meeting, 38 athletes withdrew from the study, resulting in one hundred sixty-two participants (75% males, 25% females). All participants completed surveys to assess their weekly and daily levels of physical activity, as well as their height and body mass (Table 1). The potential risks of the tests were verbally communicated to the participants, and they provided signed informed consent. The Ethics Committee of the University of Seville approved the study.

Table 1
Characteristics of the participants.

Variables	Mean	Men (n=122)	Women (n=40)	<i>p</i>
Age (years)	24 ± 3	25 ± 2	22 ± 1	0.110
Body mass (Kg)	72.84 ± 12.76	76.92 ± 8.12	65.36 ± 4.52	0.103
Height (m)	1.74 ± 0.07	1.80 ± 0.09	1.63 ± 0.06	0.071
BMI (kg/m ²)	23.78 ± 2.86	24.75 ± 1.12	21.34 ± 2.12	0.096
PA (hours/week)	8.38 ± 4.01	8.79 ± 3.96	7.91 ± 2.34	0.101
PA _{day} (hours/day)	1.97 ± 1.66	2.03 ± .098	1.86 ± 1.10	0.510

**p* ≤ 0.05 Men vs Women. Statistical analysis was done using a repeated-measures two-way ANOVA. Results expressed as mean ± standard error of the mean. BMI: body mass index. PA: physical activity.

Procedures

The participants completed a Maximum Voluntary Contraction (MVC) test using the Biodex Multi-joint System (Shirley, New York). The exercise was knee flexion at 45° to assess the strength of the posterior thigh musculature and knee extension at 45° to assess the anterior thigh musculature. Following this, they underwent a directional change test with the dominant foot, which included two open cuts at 45° (SC₄₅) and 30° (SC₃₀), as well as a closed cut (SC_{45cl}) on a force platform (Kistler 9260 AA6, Winterthur, Switzerland). Prior to the test, all participants underwent a standardized warm-up, which involved a 5-minute cycling session on a cycloergometer (Ergoline 900, Ergometrics, Bitz, Germany) at an intensity of 60 W (60 rpm). Additionally, they familiarized themselves with sports-specific side-cutting maneuvers through five to eight practice attempts. The velocity of the movements was regulated using a metronome set at 4-5.5 m/s, and the designated direction for the movements was indicated on the floor using tape.

Kinetics

A force plate (Kistler 9260 AA6, Winterthur, Switzerland) assessed the Ground Reaction Forces (GRF) in the vertical, mediolateral, and anteroposterior axes. Additionally, triaxial accelerometers (xyz-PLUX, PLUX-Wireless Biosignals, S.A., Lisbon, Portugal) were employed to measure accelerations at the knee and ankle joints. The knee accelerometer was positioned on the lateral condyle. In contrast, the ankle accelerometer was placed on the malleolus (Fig. 1). Antero-posterior (AP), Medial-Lateral (ML), and Longitudinal (Z) axes were calculated, and all signals were recorded at a sampling rate of 1000 Hz. Contact Time was determined during side-cutting by measuring the duration from the initial ground contact until the foot entered the flight phase.



Fig. 1. Location of accelerometers.

Kinematics

An analysis of knee, ankle, hip, and trunk angles was conducted. Reflective markers were positioned on the lateral malleolus, lateral condyle, greater trochanter, and acromion to capture the movements precisely. The angles were calculated at two specific time points: first, during the initial contact between the foot and the ground, and second, when the Vertical Ground Reaction Force (VGRF) was recorded. Three video cameras (240 Fps) were positioned perpendicularly, one for each type of change of direction, at a distance of two meters from the central point of the force platform. Subsequently, the Kinovea software was employed for digitization and angle extraction by 2D analysis.

Statistical analysis

Statistical analysis was performed using the SPSS 22.0 software package (SPSS Inc., Chicago, IL, USA). The Kolmogorov-Smirnov

test assessed the data distribution, and parametric variables were identified. Baseline data were compared using an independent-sample t-test. Potential statistical differences were evaluated using a repeated-measures two-way ANOVA (time x group). Mean values are reported with standard deviation (SD), and statistical significance was set at $p \leq 0.05$.

The effect size (Cohen's d) was calculated by dividing the difference between the means of the groups by the combined standard deviation of both groups, considering the sample size. Effect sizes of 0.2 were considered small, 0.5 moderate, and 0.8 large.

RESULTS

Kinetic

During the SC₃₀, subjects exhibited a higher value of VGRF of 2135.49 ± 633.14 N, which corresponds to approximately three times their body weight, while ML Force (625.44 ± 170.99 N) and AP Force (945.62 ± 421.53 N) were lower. For the SC₄₅, VGRF was lower compared to SC₃₀, with a value of $2015.83 (\pm 687.27)$ N, while ML Force was $566.87 (\pm 189.22)$ N and AP Force was $765.75 (\pm 417.06)$ N. In SC_{45cl}, VGRF was

$1790.60 (\pm 517.55)$ N, and ML Force exhibited the smallest force value among all measured changes of directions (515.41 ± 181.53 N), as well as in AP Force (670.37 ± 368.42 N). For more specific results, the force was normalized to each subject's body weight for each directional change, as shown in Table 2.

Regarding the SC₃₀, the results showed the highest applied force in all axes, including VGRF, AP Force, and ML Force. The gender analysis in Table 2 revealed that during the SC₃₀ directional change, women exhibited significantly higher force values than men in ML Force ($p = 0.045$). On the other hand, in the SC₄₅, men demonstrated higher values than women in both VGRF ($p = 0.025$) and AP Force ($p = 0.020$). Finally, in SC_{45cl}, significant differences were only observed in the force exerted in AP Force, where women displayed a higher force value than males ($p = 0.020$).

The analysis of partial knee and ankle accelerations during changes of directions is presented in Table 3. The SC₃₀ exhibited the lowest ACC_{KNEE}AP (1.72 ± 1.48 g). Similarly, ACC_{ANKLE}Z had the lowest values compared to the other changes of directions ($4.11 \pm$

Table 2
Descriptive analysis of force during direction change.

	Variables	Mean	Men	Women	p	d-Cohen
SC ₃₀	VGRF (N/Kg)	29.49±7.75	29.54±7.42	29.33±8.81	0.465	0.02
	ForceAP (N/Kg)	12.99±5.32	13.54±5.45	11.26±4.53	0.159	0.43
	ForceML (N/Kg)	8.64±2.08	8.60±1.83	8.75±2.76	0.045*	-0.07
SC ₄₅	VGRF (N/Kg)	27.70±7.81	28.20±8.32	26.14±5.76	0.025*	0.26
	ForceAP (N/Kg)	10.54±5.39	11.14±5.68	8.68±3.90	0.020*	0.46
	ForceML (N/Kg)	7.78±2.09	7.96±2.15	7.23±1.77	0.568	0.35
SC _{45cl}	VGRF (N/Kg)	25.13±7.59	24.02±6.92	28.60±8.61	0.159	-0.62
	ForceAP (N/Kg)	9.35±5.09	9.02±4.54	10.39±6.48	0.020*	-0.26
	ForceML (N/Kg)	7.17±2.40	7.13±2.40	7.32±2.45	0.612	-0.07

* $p \leq 0.05$ Men vs Women. Statistical analysis was done using a repeated-measures two-way ANOVA. Results expressed as mean±standard error of the mean. d-Cohen = the effect size. VGRF (N) = Ground reaction force. ForceML (N) = Force in medio-lateral axe. ForceAP (N) = Force in antero-posterior axe.

Table 3
Descriptive analysis of the acceleration in the three axes during direction changes.

	SC ₃₀	SC ₄₅	SC _{45cl}
ACC _{KNEE_ML}	2.46±1.50	2.39±1.58	2.49±1.49
ACC _{KNEE_AP}	1.72±1.48	2.03±1.55	2.08±1.55
ACC _{KNEE_Z}	1.63±1.37	1.53±1.30	1.69±1.40
ACC _{ANKLE_ML}	4.19±0.78	4.23±0.75	4.14±0.88
ACC _{ANKLE_AP}	4.04±0.98	4.05±0.92	3.98±0.99
ACC _{ANKLE_Z}	4.11±0.81	4.13±0.68	4.20±0.79

Results expressed as mean ± standard error of the mean. ACC_{KNEE_ML} (g) = Acceleration in medio-lateral axis in knee. ACC_{KNEE_AP} (g) = Acceleration in antero-posterior axis in knee. ACC_{KNEE_Z} (g) = Acceleration in vertical axis in knee. ACC_{ANKLE_ML} (g) = Acceleration in medio-lateral axis in ankle. ACC_{ANKLE_AP} (g) = Acceleration in antero-posterior axis in ankle. ACC_{ANKLE_Z} (g) = Acceleration in vertical axis in ankle.

0.81). For the SC₄₅, both ACC_{KNEE_ML} (2.39 ± 1.58 g) and ACC_{KNEE_Z} (1.53 ± 1.30 g) showed the lowest values. However, both ACC_{ANKLE_ML} and ACC_{ANKLE_AP} were higher than in the other changes of directions (4.23 ± 0.75 g and 4.05 ± 0.92 g, respectively). During the SC_{45cl}, the highest ACC_{KNEE_ML} (2.49 ± 1.49 g), ACC_{KNEE_Z} (1.69 ± 1.40 g), and ACC_{ANKLE_Z} (4.20 ± 0.79 g) were found. Conversely, ACC_{ANKLE_ML} and ACC_{ANKLE_AP} were lower during this directional change (4.14 ± 0.88 g and 3.98 ± 0.99 g, respectively).

On the other hand, gender-specific acceleration was also evaluated (Table 4). During the SC₃₀, although no significant differences were observed, partial knee accelerations were higher in women than men. In the ankle, only ACC_{ANKLE_Z} showed higher values in women than men (4.20 ± 0.76 g). In the case of SC₄₅, there was a trend towards higher acceleration in women compared to men, both in the knee and ankle. Regarding ACC_{KNEE_Z}, the difference between women and men was significant (p=0.002), with women displaying an acceleration of 1.82 ± 1.54 g compared to 1.44 ± 1.21 g exhibited by men.

During the SC_{45cl}, no significant gender differences were found, except for ACC_{KNEE_ML} where men exhibited higher values (2.49 ± 1.48 g). In the remaining partial knee accelerations, women showed higher

values for this parameter, although they were not statistically significant. Regarding the ankle, only a trend towards higher values in men than women was observed for ACC_{ANKLE_Z} (4.22 ± 0.81 g), although statistical significance was not reached.

Kinematics

Kinematic factors were also studied during changes of direction. Knee flexion angles at initial contact (KneeFlexInit) and maximum knee flexion angle (KneeFlexMax) were analyzed. The range of ankle dorsiflexion (AnkleDorsiRange), initial hip flexion angle (HipFlexInit), maximum hip flexion angle (HipFlexMax), initial trunk flexion angle (TrunkFlexInit), and maximum trunk flexion angle (TrunkFlexMax) were also analyzed.

Regarding the changes of directions (Table 5), the highest value of KneeFlexInit was observed in SC₃₀ (144.6° ± 7.6°), while the lowest value of KneeFlexMax was found during SC₄₅ (125.2° ± 8.9°). For the hip, the maximum value of HipFlexMax was 60.6° during SC₃₀, while the trunk flexed 92.9°. Finally, a range of ankle dorsiflexion of 39.4° was found between the initial contact of the directional change and the maximum plantar flexion during the change.

In SC₄₅, KneeFlexMax was 125.2° (extension), similar to the value of 123.3° in

Table 4
Differences between men and women in acceleration during direction changes.

	Variables	Men	Women	<i>p</i>	d-Cohen
SC ₃₀	ACC _{KNEE_ML}	2.33±1.47	2.86±1.56	0.558	-0.35
	ACC _{KNEE_AP}	1.66±1.50	1.91±1.44	0.573	-0.16
	ACC _{KNEE_Z}	1.57±1.30	1.84±1.55	0.080	-0.19
	ACC _{ANKLE_ML}	4.20±0.73	4.14±0.94	0.215	0.07
	ACC _{ANKLE_AP}	4.04±0.96	4.02±1.06	0.433	0.02
	ACC _{ANKLE_Z}	4.08±0.83	4.20±0.76	0.413	-0.14
SC ₄₅	ACC _{KNEE_ML}	2.25±1.54	2.81±1.66	0.516	-0.35
	ACC _{KNEE_AP}	1.92±1.57	2.35±1.49	0.563	-0.27
	ACC _{KNEE_Z}	1.44±1.21	1.82±1.54	0.002*	-0.29
	ACC _{ANKLE_ML}	4.20±0.71	4.32±0.86	0.890	-0.16
	ACC _{ANKLE_AP}	4.04±0.92	4.09±0.95	0.483	-0.05
	ACC _{ANKLE_Z}	4.09±0.70	4.27±0.60	0.344	-0.26
SC _{45ml}	ACC _{KNEE_ML}	2.49±1.48	2.48±1.55	0.866	0.01
	ACC _{KNEE_AP}	1.96±1.53	2.46±1.58	0.795	-0.32
	ACC _{KNEE_Z}	1.64±1.37	1.85±1.51	0.200	-0.14
	ACC _{ANKLE_ML}	4.11±0.87	4.22±0.90	0.937	-0.12
	ACC _{ANKLE_AP}	3.97±1.01	4.01±0.96	0.965	-0.04
	ACC _{ANKLE_Z}	4.22±0.81	4.15±0.71	0.900	0.08

**p* ≤ 0.05 Men vs Women. Statistical analysis was done using a repeated-measures two-way ANOVA. Results expressed as mean±standard error of the mean. d-Cohen = the effect size. ACC_{KNEE_ML} (g) = Acceleration in medio-lateral axe in knee. ACC_{ANKLE_AP} (g) = Acceleration in antero-posterior axe in knee. ACC_{ANKLE_Z} (g) = Acceleration in vertical axe in knee. ACC_{ANKLE_ML} (g) = Acceleration in medio-lateral axe in ankle. ACC_{ANKLE_AP} (g) = Acceleration in antero-posterior axe in ankle. ACC_{ANKLE_Z} (g) = Acceleration in vertical axe in ankle.

Table 5
Description of the kinematics in the experimental phase in direction change.

	SC ₃₀	SC ₄₅	SC _{45cl}
Variable	Mean	Mean	Mean
Angle _{in} Knee (degrees °)	144.63±7.65	143.45±17.86	141.43±9.87
Angle _{max} Knee (degrees °)	123.33±10.00	125.16±8.91	119.97±14.18
Angle _{in} Hip (degrees °)	42.50±2.94	41.54±5.63	40.92±4.56
Angle _{max} Hip (degrees °)	60.57±5.50	51.21±6.36	54.37±5.37
Angle _{in} Trunk (degrees °)	104.54±6.35	105.15±5.15	98.98±4.76
Angle _{max} Trunk (degrees °)	92.99±5.36	95.02±5.73	77.77±6.54
Angle _{in} Ankle (degrees °)	99.12±6.87	98.92±5.30	98.82±5.25
Angle _{max} Ankle (degrees °)	59.70±7.45	57.19±5.40	56.97±4.28
Ankle_Dorsi_Angle (degrees °)	39.42±3.32	41.72±5.38	41.84±4.92

Results expressed as mean±standard error of the mean. Angle_{in} Knee = Angle of knee in the first contact. Angle_{max} Knee = Angle of knee in the maximum flexion. Angle_{in} Hip = Angle of hip in the first contact. Angle_{max} Hip = Angle of hip in the maximum flexion. Angle_{in} Trunk = Angle of trunk in the first contact. Angle_{max} Trunk = Angle of trunk in the maximum flexion. Angle_{in} Ankle = Angle of ankle in the first contact. Angle_{max} Ankle = Angle of ankle in the maximum flexion. Ankle_Dorsi_Angle = Range of ankle dorsiflexion.

SC₃₀. At that moment, HipFlexMax was 51.21°, while TrunkFlexMax showed a flexion of 95.1°. Additionally, the AnkleDorsiRange was 41.7°, defined as the amount of flexion from the first contact until maximum flexion occurred.

In SC_{45cl}, KneeFlexMax was 119.9°, representing the most significant flexion of the three change types. From initiating contact to maximum knee flexion, the hip flexed by 13.5°. As for the trunk, it exhibited a flexion of 77.8° at that moment. Finally, the AnkleDorsiRange was 41.8°.

Finally, a gender analysis of kinematics during direction changes was performed (Table 6). It was observed that during SC₃₀, women exhibited a significantly higher AnkleFlexInit than men ($p=0.040$). However, gender differences during SC₄₅ were found in AnkleFlexMax ($p=0.004$) and AnkleDorsiRange ($p=0.007$). Lastly, during SC_{45cl}, gender differences were found in KneeFlexInit ($p<0.001$) and KneeFlexMax ($p=0.006$), where men displayed a lower angle compared to women.

DISCUSSION

The main objective of this study was to compare the risk of knee injury between men and women through the analysis of kinetic and kinematic parameters in a population of non-professional athletes. Both kinetic aspects, such as GRF and accelerations, as well as kinematic elements, such as angles at the moment of directional change, have proven to be crucial, with women likely presenting a higher risk of injury.

Kinetics

During changes of directions, the VGRF relative to body weight was significantly higher in SC₃₀ (29.49 N/kg \pm 7.75) compared to SC₄₅ (27.70 N/kg \pm 7.81; $p=0.004$) and SC_{45cl} (25.13 N/kg \pm 7.59; $p<0.001$). One possible explanation for these differences is that greater force needs to be exerted in the medial-lateral (ML) axis to perform

more forceful or larger amplitude changes (remember that 30° is measured above the horizontal plane). According to Nigg's paradigm¹¹, which compiled studies spanning over 25 years, it became evident that VGRF plays a particularly important role in injuries among individuals engaged in physical activities such as running, especially in situations where pronation is accentuated, such as during changes of directions. This possibility is also supported by the values of ML force found in our study, as the analyzed subjects displayed significantly higher values during SC₃₀ (8.64 N/kg \pm 2.08) compared to SC₄₅ (7.78 N/kg \pm 2.08, $p<0.001$) and SC_{45cl} (7.17 N/kg \pm 2.40, $p<0.001$). Therefore, higher levels of force, especially in the ML axis, which need to be attenuated by the lower extremities, suggest the need for increased preventive strategies in these types of actions common in various sports. It is essential to highlight that these 30°-changes of directions do not only increase the ML force but also the AP force (12.9 N/kg \pm 5.32) when compared to SC₄₅ (10.54 N/kg \pm 5.39, $p<0.001$) or SC_{45cl} (9.35 N/kg \pm 5.09, $p<0.001$), suggesting that biomechanical modifications in the different involved joints occur in response to these increments, as will be discussed later.

Despite numerous studies regarding the biomechanical and kinetic factors manifested during direction changes, the results are contradictory¹². The aspect that seems most relevant in explaining this disparity of results may be the variety of procedures carried out in different studies. Brughelli *et al.*¹³ differentiate between anticipated and unanticipated changes of directions, changes towards the dominant or non-dominant foot, as elements that influence the final results. Regardless of the methodological variety, it is evident that both VGRF, ML-force, and AP-force are variables closely related to the onset of injury processes² and should be controlled and attenuated as much as possible.

While it is evident that higher forces in both axes are associated with a greater risk

Table 6
Kinematics during direction changes and differences between men and women.

Variables	SC ₃₀		p	d-Cohen	SC ₄₅		p	d-Cohen	SC _{45cl}		p	d-Cohen
	Men	Women			Men	Women			Men	Women		
Angle _{in} Knee (degrees °)	144.04±7.48	146.56±8.06	0.080	-0.33	145.33±7.53	145.13±6.43	0.891	-0.23	139.88±9.39	146.32±10.01	0.000*	-0.67
Angle _{max} Knee (degrees °)	122.86±9.28	125.13±11.97	0.229	-0.23	124.74±8.80	126.75±9.22	0.239	-0.09	118.20±14.34	125.56±12.40	0.006*	-0.53
Angle _{in} Hip (degrees °)	42.63±3.00	42.13±2.77	0.366	0.17	41.42±5.66	41.94±5.68	0.623	-0.15	40.93±4.74	41.00±4.01	0.938	-0.02
Angle _{max} Hip (degrees °)	60.97±5.28	59.37±6.12	0.125	0.29	51.01±6.67	51.97±5.29	0.427	-0.05	54.29±5.42	54.43±5.22	0.891	-0.03
Angle _{in} Trunk (degrees °)	104.45±6.53	104.72±5.87	0.819	-0.04	105.07±5.39	105.32±4.39	0.799	-0.12	98.91±4.87	99.08±4.44	0.855	-0.04
Angle _{max} Trunk (degrees °)	93.09±5.56	92.59±4.76	0.624	0.09	94.82±5.92	95.51±5.10	0.524	0.04	78.00±6.61	76.72±6.18	0.299	0.20
Angle _{in} Ankle (degrees °)	98.47±6.58	101.13±7.55	0.040*	-0.39	99.01±5.51	98.81±4.56	0.837	0.56	98.59±4.98	99.51±6.12	0.357	-0.17
Angle _{max} Ankle (degrees °)	59.10±7.22	61.48±8.05	0.091	-0.32	57.91±5.29	54.97±5.25	0.004*	-0.52	57.13±4.31	56.37±4.24	0.351	0.18
Ankle_Dorsi_Angle (degrees °)	39.36±3.26	39.64±3.56	0.658	-0.08	41.10±5.10	43.83±5.81	0.007*	-0.23	41.46±4.81	43.13±5.18	0.072	-0.34

*p ≤ 0.05 Men vs Women. Statistical analysis was done using a repeated-measures two-way ANOVA. Results expressed as mean ± standard error of the mean. d-Cohen = the effect size. Angle_{in} Knee = Angle of knee in the first contact. Angle_{max} Knee = Angle of knee in the maximum flexion. Angle_{in} Hip = Angle of hip in the first contact. Angle_{max} Hip = Angle of hip in the maximum flexion. Angle_{in} Trunk = Angle of trunk in the first contact. Angle_{max} Trunk = Angle of trunk in the maximum flexion. Angle_{in} Ankle = Angle of ankle in the first contact. Angle_{max} Ankle = Angle of ankle in the maximum flexion. Ankle_Dorsi_Angle = Range of ankle dorsiflexion.

of injury in this population group, it is essential to mention the differences observed in the different variables according to gender. Sigward and Powers¹⁴ suggested that an increased risk of knee injury through increased valgus can occur due to greater forces in either axis in both men and women. In fact, their work reflected values that were very similar to those found in the present study regarding VGRF during changes of directions. Our results show that during SC₃₀, where women sustained higher relative loads than men ($p=0.045$), there were significant differences in the force exerted in the ML axis. This finding has been widely observed in studies with athletes, where women have shown significantly greater valgus than men¹⁵. Differences in the ML axis between men and women could be related to an increased risk of injury in females due to the biomechanical position of the knee in abduction or adduction during ground contact^{1,16}.

On the other hand, during SC₄₅, the differences were found in VGRF ($p=0.025$) and AP force ($p=0.020$), where men significantly exceeded women. Our results are consistent with those of Liu *et al.*¹⁷, who related a reduction of VGRF and Force_{AP} with a reduction of the load supported by the knee during open direction changes. However, authors such as James *et al.*¹⁸ found the opposite during maximum speed changes of directions. One possible explanation for these differences could be the openness of the directional change at a non-maximal speed. SC₄₅ may involve less demand than SC₃₀, so being a more vertical change and closer to straight-line running, it is possible that AP force is increased, as well as VGRF in men.

Another important finding was that women exhibited a significantly higher AP force during SC_{45cl} ($p=0.020$) than men. Our results align with those presented by McLean *et al.*², who found higher AP force in women compared to men during a directional change with an angle of exit between 35° and 55° (women = 1.80BW [± 0.54]; men 1.54BW [± 0.76]). Moreover, although

not statistically significant, women in our study also showed higher VGRF during SC_{45cl}. Recently, de Hoyo *et al.*¹⁹ reported very similar data in male athletes who performed a closed change with a 60° opening (24.1 N/kg ± 8.4). Unfortunately, these authors only conducted their intervention with male subjects, making a comparison impossible. Nevertheless, there is limited research on the role of gender in VGRF during closed changes of directions. This is the first study to assess vertical force in men and women during closed changes.

What seems evident is the increased risk of knee injury through ML force values during changes of directions based on gender¹. Authors like Sigward and Powers¹⁴ indicated that women who exerted greater ML force also exhibited a greater valgus moment, which increased the risk of a knee injury. Although our results do not provide data on impulse outcomes, a possible contribution can be inferred from the partial knee and ankle acceleration. As described previously, women reported significantly higher ML force during SC₃₀ than men and a slightly higher trend was observed in this variable during SC_{45cl}. In this regard, it can also be observed that women experience 18.53% more ML knee acceleration than men during SC₃₀ and 19.93% during SC₄₅, with almost no difference (0.4%) during SC_{45cl}. This ML knee acceleration could represent valgus moments, although this fact should be corroborated in future studies through a kinematic analysis in the frontal plane.

There were significant differences between the different changes of direction. ACC_{KNEE}AP was significantly higher in SC_{45cl} compared to SC₃₀ ($p=0.006$). This finding suggests an increased risk in closed changes compared to open changes, as the load is mobilized more rapidly in the sagittal axis, potentially leading to an increase in tibial translation. However, ForceAP was significantly lower in SC_{45cl} than SC₃₀ ($p<0.001$). These differences also existed between open changes, as ACC_{KNEE}AP was significantly

higher in SC₄₅ than SC₃₀ ($p=0.023$). One possible explanation for these differences could be the biomechanical demand, with SC₄₅ being less demanding than SC₃₀, resulting in a faster strategy during less open changes. Analyzing ACC_{KNEE}ML between changes of directions, SC₃₀ showed a significantly higher acceleration than SC₄₅ ($p<0.001$) and SC_{45cl} ($p<0.001$). Sigward and Powers¹⁴ suggest that frontal plane control is necessary to reduce the relative risk of knee injury. Our data indicate that SC₃₀ poses an increased risk compared to the other changes of directions, characterized by higher ForceML and ACC_{KNEE}ML, which are associated with an increase in knee valgus.

Regarding gender differences during changes of directions, significant differences were found only in SC₄₅ ($p\leq 0.05$), with women exhibiting higher ACC_{KNEE}Z than men. One possible explanation could be that Chapell *et al.*²⁰ suggested that women experience greater shear force in the tibia during ground contact. This negative strategy indicates that energy absorption by women is less efficient than in men, or at least faster, which may be related to an increased risk of knee injury. Surprisingly, this trend is not observed in SC₃₀, which would be expected to be more demanding at this level. However, the trend still favored women, who presented 14.67% more ACC_{KNEE}Z during SC₃₀ and 11.35% more during SC_{45cl}.

Kinematics

It is evident that a knee angle close to the extension increases the risk of injury²⁰⁻²². Our results indicate a higher KneeAnglein during SC₃₀ compared to the other changes of directions ($144.63^\circ \pm 7.65$). However, the maximum KneeAngle reached is highest during SC₄₅ ($125.16^\circ \pm 8.91$). Concerning the 180° representing full knee extension, the KneeAngle during SC₃₀ averaged 35.37° . Markolf *et al.*²³ mentioned that knee flexion of 40° or less increases tibial translation supported by the ACL and, consequently, the

tension sustained by the joint complex, leading to an increased risk of injury. A preventive strategy should involve increasing knee flexion to absorb impact. Cochrane *et al.*²⁴ went further by identifying angles below 30° of flexion during initial contact as a critical factor in ACL injuries during changes of directions. Consistent with Markolf *et al.*²³, our results showed that for all changes of directions, the KneeAnglein exceeded 30° (SC₃₀ = 35.37° ; SC₄₅ = 36.55° ; SC_{45cl} = 38.57°) but remained below 40°, suggesting that participants subjected the joint to excessive stress, which could partially explain the previously reported increases in force.

Despite the relationship between knee flexion angle and the relative risk of joint injury, it is evident that the biomechanical strategy during direction changes is not exclusive to the knee. Several studies have attributed a determining role to other joints reflecting greater or lesser knee flexion. Imwalle *et al.*²⁵ confirmed a direct influence of the hip on the knee during direction changes. Potter *et al.*²⁶ stated that open and closed changes of directions influence the biomechanical strategies manifested by subjects, with significantly greater hip flexion in open changes than in closed changes. However, our results do not align with those reported by these authors, as hip flexion was practically the same regardless of the type of directional change. One possible explanation could be that kinematic aspects were evaluated in an agility circuit with open and closed changes of direction, where athletes performed different direction changes depending on their own technique.

Moreover, gender-based differentiation in knee kinematics has been observed, showing different biomechanical strategies related to an increased risk of knee injury between men and women²⁷. In our study, during SC₃₀, women exhibited a KneeAnglemax (in extension) of 33.4° , although without significant differences compared to men ($p = .080$), who exhibited an angle close to 36° . Significant differences were found during SC_{45cl},

where women had a KneeAnglein close to 146° and men to 140°. Additionally, significant gender differences were found in KneeAnglemax ($p = 0.006$), with women exhibiting more significant knee extension than men, indicating a higher injury risk. These results are consistent with those reported by James *et al.*¹⁸, who conducted a comparative study by gender during closed direction changes to 60° and found a KneeAnglein in women 5.8° lower than in men. In our study, during SC_{45cl}, women flexed 6.4° less than men, with significant differences compared to men. This indicates that the directional change technique employed by women may be associated with an increased risk of knee injury during closed direction changes. Furthermore, in the study mentioned above, the researchers found that women significantly exceeded men in KneeAnglemax, with greater extension (64.1° and 61.4°, respectively). Our results are very similar, with men exhibiting an average of 61.8° and women 54.4°.

Regarding open changes of directions, a slightly higher, but not significant, trend in extension can be observed in women compared to men during SC₃₀. Additionally, during SC₄₅, the KneeAnglein values are practically the same in men and women, with an increase in knee extension in women at the moment of VGRF. Dai *et al.*²⁸ evaluated knee kinematics in men and women during SC₄₅ and also found greater extension in women compared to men at the moment of VGRF. A greater range of knee flexion during the first contact could serve as a biomechanical strategy to absorb impact and reduce the load. In this sense, women have a higher relative risk of knee injury than men, as they exhibit more significant knee extension during changes of direction²⁹.

In conclusion, the study highlights the importance of controlling GRF and biomechanical strategies during changes in direction to reduce the risk of knee injuries. Significant gender differences in forces and accelerations during changes of directions were observed, underscoring the need to

consider specific gender factors in injury prevention. Variables such as VGRF, Force_{ML}, and ForceAP, as well as acceleration in the vertical axis, appear to be deterministic kinetic variables that explain these gender differences and knee flexion angles. The results can be helpful in informing the design of preventive strategies in the sports field and improving the understanding of the underlying mechanisms of knee injuries during changes of direction.

Funding

None.

Conflict of interests

The authors declared that they have no competing interests.

Authors' ORCID

- Adrián Feria-Madueño (AFM):
0000-0001-7425-8694
- Timothy E. Hewett (TH):
0000-0001-9729-7573
- Borja Sañudo (BS):
0000-0002-9969-9573

Contributions of authors

Conception (AFM), design and acquisition of data (AFM), formal analysis (BS), interpretation of data (AFM and BS), investigation (AFM and BS), writing the original draft preparation (AFM), writing the review and editing (TH), supervision (TH and BS).

REFERENCES

1. Hewett TE, Myer GD, Ford KR, Heidt RS, Colosimo AJ, McLean SG, van den Bogert J, Paterno MV, Succop P. Biomechanical measures of neuromuscular control and valgus loading of the knee predict anterior cruciate ligament injury risk in female athletes: a prospective study. *Am J Sports Med* 2005;33(4):492-501. doi:10.1177/0363546504269591

2. **McLean SG, Walker KB, Van Den Bogert AJ.** Effect of gender on lower extremity kinematics during rapid direction changes: An integrated analysis of three sports movements. *J Sci Med Sport* 2005;8(4):411-422. doi:10.1016/S1440-2440(05)80056-8
3. **Hewett TE, Ford KR, Myer GD.** Anterior cruciate ligament injuries in female athletes: Part 2, A meta-analysis of neuromuscular interventions aimed at injury prevention. *Am J Sports Med* 2006;34(3):490-498. doi:10.1177/0363546505282619
4. **Myer GD, Ford KR, Paterno MV, Nick TG, Hewett TE.** The effects of generalized joint laxity on risk of anterior cruciate ligament injury in young female athletes. *Am J Sports Med* 2008;36(6):1073-1080. doi:10.1177/0363546507313572
5. **Chen CH, Condello G, Chen WH, Liu TH, Tessitore A, Shiang TY, Liu C.** Effects of a novel inclined-adaptive footwear on change-of-direction performance in male athletes. *Gait Posture* 2022;94:189-194. doi:10.1016/j.gaitpost.2022.03.010
6. **Condello G, Kernozek TW, Tessitore A, Foster C.** Biomechanical analysis of a change-of-direction task in college soccer players. *Int J Sports Physiol Perform* 2016;11(1):96-101. doi:10.1123/ij-spp.2014-0458
7. **McFadden C, Daniels KAJ, Strike S.** Six methods for classifying lower-limb dominance are not associated with asymmetries during a change of direction task. *Scand J Med Sci Sports* 2022;32(1):106-115. doi:10.1111/sms.14054
8. **Olmsted LC, Carcia CR, Hertel J, Shultz SJ.** Efficacy of the star excursion balance tests in detecting reach deficits in subjects with chronic ankle instability. *J Athl Train* 2002;37(4):501-506.
9. **Maniar N, Schache AG, Pizzolato C, Opar DA.** Muscle contributions to tibiofemoral shear forces and valgus and rotational joint moments during single leg drop landing. *Scand J Med Sci Sports* 2020;30(9):1664-1674. doi:10.1111/sms.13711
10. **McBurnie AJ, Dos'Santos T, Jones PA.** Biomechanical associates of performance and knee joint loads during A 70–90° cutting maneuver in subelite soccer players. *J Strength Cond Res* 2021;35(11):3190-3198. doi:10.1519/JSC.0000000000003252
11. **Nigg BM.** The role of impact forces and foot pronation: A new paradigm. *Clin J Sport Med* 2001;11(1):2-9. doi:10.1097/00042752-200101000-00002
12. **Griffin LY, Albohm MJ, Arendt EA, Bahr R, Beynonn BD, Demaio M, Dick RW, Engbretsen L, Garrett WE Jr, Hannafin JA, Hewett TE, Huston LJ, Ireland ML, Johnson RJ, Lephart S, Mandelbaum BR, Mann BJ, Marks PH, Marshall SW, Myklebust G, Noyes FR, Powers C, Shields C Jr, Shultz SJ, Silvers H, Slauterbeck J, Taylor DC, Teitz CC, Wojtys EM, Yu B.** Understanding and preventing noncontact anterior cruciate ligament Injuries: A review of the Hunt Valley II Meeting, January 2005. *Am J Sports Med* 2006;34(9):1512-1532. doi:10.1177/0363546506286866
13. **Brughelli M, Cronin J, Levin G, Chaouachi A.** Understanding change of direction ability in sport: A review of resistance training studies. *Sports Med* 2008;38(12):1045-1063. doi:10.2165/00007256-200838120-00007
14. **Sigward SM, Powers CM.** Loading characteristics of females exhibiting excessive valgus moments during cutting. *Clin Biomech* 2007;22(7):827-833. doi:10.1016/j.clinbiomech.2007.04.003
15. **Stoffel KK, Nicholls RL, Winata AR, Dempsey AR, Boyle JJW, Lloyd DG.** Effect of ankle taping on knee and ankle joint biomechanics in sporting tasks. *Ed Sci Sports Exerc* 2010;42(11):2089-2097. doi:10.1249/MSS.0b013e3181de2e4f
16. **Wikstrom EA, Tillman MD, Chmielewski TL, Borsa PA.** Measurement and evaluation of dynamic joint stability of the knee and ankle after injury. *Sports Med* 2006;36(5):393-410. doi:10.2165/00007256-200636050-00003
17. **Liu H, Wu W, Yao W, Spang JT, Creighton RA, Garrett WE, Yu B.** Effects of knee extension constraint training on knee flexion angle and peak impact ground-reaction force. *Am J Sports Med* 2014;42(4):979-986. doi:10.1177/0363546513519323

18. James CR, Sizer PS, Starch DW, Lockhart TE, Slauterbeck J. Gender differences among sagittal plane knee kinematic and ground reaction force characteristics during a rapid sprint and cut maneuver. *Res Q Exerc Sport* 2004;75(1):31-38. doi:10.1080/02701367.2004.10609131
19. de Hoyo M, de la Torre A, Pradas F, Sañudo B, Carrasco L, Mateo-Cortes J, Domínguez-Cobo S, Fernandes O, Gonzalo-Skok O. Effects of eccentric overload bout on change of direction and performance in soccer players. *Int J Sports Med* 2014;36(04):308-314. doi:10.1055/s-0034-1395521
20. Chappell JD, Herman DC, Knight BS, Kirkendall DT, Garrett WE, Yu B. Effect of fatigue on knee kinetics and kinematics in stop-jump tasks. *Am J Sports Med* 2005;33(7):1022-1029. doi:10.1177/0363546504273047
21. Tillman MD, Hass CJ, Brunt D, Bennett GR. Jumping and landing techniques in elite women's volleyball. *J Sports Sci Med* 2004;3(1):30-36.
22. Pappas E, Nightingale EJ, Simic M, Ford KR, Hewett TE, Myer GD. Do exercises used in injury prevention programmes modify cutting task biomechanics? A systematic review with meta-analysis. *Br J Sports Med* 2015;49(10):673-680. doi:10.1136/bjsports-2014-093796
23. Markolf KL, O'Neill G, Jackson SR, McAllister DR. Effects of Applied quadriceps and hamstrings muscle loads on forces in the anterior and posterior cruciate ligaments. *Am J Sports Med* 2004;32(5):1144-1149. doi:10.1177/0363546503262198
24. Cochrane JL, Lloyd DG, Buttfield A, Seward H, McGivern J. Characteristics of anterior cruciate ligament injuries in Australian football. *J Sci Med Sport* 2007;10(2):96-104. doi:10.1016/j.jsams.2006.05.015
25. Imwalle LE, Myer GD, Ford KR, Hewett TE. Relationship between hip and knee kinematics in athletic women during cutting maneuvers: A possible link to noncontact anterior cruciate ligament injury and prevention. *J Strength Cond Res* 2009;23(8):2223-2230. doi:10.1519/JSC.0b013e3181bc1a02
26. Potter D, Reidinger K, Szymialowicz R, Martin T, Dione D, Feinn R, Wallace D, Garbalosa JC. Sidestep and crossover lower limb kinematics during a prolonged sport-like agility test. Sidestep and crossover lower limb kinematics during a prolonged sport-like agility test. *Int J Sports Phys Ther* 2014;9(5):617-627.
27. Galloway RT, Xu Y, Hewett TE, Barber Foss K, Kiefer AW, DiCesare CA, Magnussen RA, Khoury J, Ford KR, Diekfuss JA, Grooms D, Myer GD, Montalvo AM. Age-dependent patellofemoral pain: hip and knee risk landing profiles in prepubescent and postpubescent female athletes. *Am J Sports Med* 2018;46(11):2761-2771. doi:10.1177/0363546518788343
28. Dai B, Garrett WE, Gross MT, Padua DA, Queen RM, Yu B. The Effects of 2 landing techniques on knee kinematics, kinetics, and performance during stop-jump and side-cutting tasks. *Am J Sports Med* 2015;43(2):466-474. doi:10.1177/0363546514555322
29. Mallinos A, Jones K, Davis BL. Comparison of side-cutting maneuvers versus low impact baseball swing on knee ligament loading in adolescent populations. *Clin Biomech* 2023;106:106004. doi:10.1016/j.clinbiomech.2023.106004

The effectiveness of personalized medication based on drug-related genes, for schizophrenia patients with resistance to traditional drugs.

Shujun Zhou^{1#}, Guangqin Zhang^{2#}, Zhe Wang³, Long Wei¹, Min Zhu⁴, Jinquan He⁵

¹Department of Pharmacy, Nanjing Gaochun People's Hospital, Nanjing, Jiangsu, China.

²Department of Pharmacy, Ezhou Central Hospital, Ezhou, Hubei, China.

³Department of Pharmacy, Medical Supplies Center of PLA General Hospital, Beijing, China.

⁴Department of Pharmacy, The Affiliated Taizhou People's Hospital of Nanjing Medical University, Taizhou Jiangsu, China.

⁵Department of Psychosomatic Medicine, Chenzhou First People's Hospital, Chenzhou, Hunan, China.

They contributed equally to this work.

Keywords: inflammatory cytokines; neurotrophic factors; PANSS; BPRS; social skills; ADL; CYP2D6.

Abstract. We aimed to study the impact of personalized medication based on drug-related genes for schizophrenia patients with resistance to traditional drugs. One hundred and ten schizophrenia patients who sought treatment at our medical facility between June 2021 and February 2023 were chosen and divided at random into two groups: one group (n=55) received conventional medication, while the other group (n=55) received personalized medication based on their genetic profile. The study compared the levels of inflammatory cytokines and neurotrophic factors, as well as the scores on the Positive and Negative Symptoms Scale (PANSS), Brief Psychiatry Rating Scale (BPRS), Social Skills Psychometric Instruments (SSPI), and Ability of Daily Living Scale (ADL) between the two groups. Following the treatment, both groups exhibited reduced levels of TNF- α and IL-1 β compared to pre-treatment levels, with the gene-guided group showing even lower levels ($p < 0.05$). Conversely, the levels of NGF and BDNF increased in both groups post-treatment, with the gene-guided group demonstrating even higher levels ($p < 0.05$). Additionally, the PANSS and BPRS scores decreased in both groups after treatment, with the gene-guided group showing even lower scores ($p < 0.05$). On the other hand, both groups'

SSPI and ADL scores increased post-treatment, with the gene-guided group exhibiting higher scores ($p < 0.05$). The overall efficacy of the treatment in the gene-guided group was superior to that in the conventionally treated group ($p < 0.05$). Personalized medication guided by pharmacogenetics has the potential to enhance cognitive function, facilitate neurological recovery, improve social functioning, and enhance the daily living skills of individuals with schizophrenia, thereby facilitating their successful reintegration into society.

La eficacia de la medicación personalizada basada en genes relacionados con fármacos, para pacientes con esquizofrenia resistente a los fármacos tradicionales.

Invest Clin 2024; 65 (2): 206 – 219

Palabras clave: citoquinas inflamatorias; factores neurotróficos; PANSS; BPRS; habilidades sociales; ADL; CYP2D6.

Resumen. Nuestro objetivo fue estudiar el impacto de la medicación personalizada basada en genes relacionados con medicamentos para pacientes con esquizofrenia resistentes a los medicamentos tradicionales. Se seleccionaron 110 pacientes con esquizofrenia que buscaron tratamiento en nuestra instalación médica entre junio de 2021 y febrero de 2023, y se dividieron al azar en dos grupos: un grupo ($n=55$) recibió medicación convencional, mientras que el otro grupo ($n=55$) recibió medicación personalizada basada en su perfil genético. El estudio comparó los niveles de citocinas inflamatorias y factores neurotróficos, así como las puntuaciones en la Escala de Síntomas Positivos y Negativos (PANSS), la Escala Breve de Evaluación Psiquiátrica (BPRS), los Instrumentos Psicométricos de Habilidades Sociales (SSPI) y la Escala de Habilidades de Vida Diaria (ADL) entre los dos grupos. Después del tratamiento, ambos grupos mostraron niveles reducidos de TNF- α y IL-1 β en comparación con los niveles previos al tratamiento, con el grupo guiado por genes mostrando aún niveles más bajos ($p < 0,05$). Por el contrario, los niveles de NGF y BDNF aumentaron en ambos grupos después del tratamiento, con el grupo guiado por genes demostrando incluso niveles más altos ($p < 0,05$). Además, las puntuaciones de PANSS y BPRS disminuyeron en ambos grupos después del tratamiento, con el grupo guiado por genes mostrando incluso puntuaciones más bajas ($p < 0,05$). Mientras que las puntuaciones de SSPI y ADL aumentaron en ambos grupos después del tratamiento, con el grupo guiado por genes mostrando puntuaciones más altas ($p < 0,05$). La eficacia general del tratamiento en el grupo guiado por genes fue superior a la del grupo tratado convencionalmente ($p < 0,05$). La medicación personalizada guiada por farmacogenética tiene el potencial de mejorar la función cognitiva, facilitar la recuperación neurológica, mejorar el funcionamiento social y mejorar las habilidades de vida diaria de las personas con esquizofrenia, facilitando así su reintegración exitosa en la sociedad.

Received: 01-11-2023

Accepted: 16-11-2023

INTRODUCTION

Schizophrenia stands as one of the most prevalent mental disorders globally, often afflicting young adults and characterized by prolonged duration, frequent relapses, and abrupt onset¹. Individuals with schizophrenia typically exhibit disturbances in thought, consciousness, behavior, and emotion, along with inappropriate psychological and physical activities. Concurrently, they experience negative emotions encompassing fear, anger, and depression. In severe cases, some patients may even demonstrate self-destructive tendencies or resort to suicide². Integration into society proves challenging for schizophrenia patients due to their limited sense of affiliation and prominent negative emotional states. These significantly hamper their subjective well-being and self-esteem^{3,4}. While antipsychotic medications can effectively manage the condition for the majority of schizophrenia patients, approximately 30% exhibit poor or partial responses to these treatments, categorizing them as drug-resistant individuals⁵. Thus, improving the efficacy of antipsychotics on mental diseases has become an attractive issue in the psychiatry department. At the same time, individualized medication can be made based on genetic evidence derived from the analysis of drug-related genes and gene polymorphisms to select the drugs and doses more precisely⁶. Gene detection has been widely applied to develop antipsychotic drugs, but fewer studies report the efficacy of drugs on drug-resistant patients with schizophrenia. Consequently, we carried out this study to investigate the efficacy of drug-related-gene-guided individualized medication on drug-resistant patients with schizophrenia and its effect on patients.

PATIENTS AND METHODS

Subjects

One hundred and ten individuals diagnosed with schizophrenia admitted to the

Department of Psychosomatic Medicine at The First People's Hospital of Chenzhou, Luojiaying, Chenzhou, Hunan, People's Republic of China, during the period spanning June 2021 to February 2023, were enrolled in this study. They were subsequently categorized into the regular medication group (Group A) and the gene-guided medication group (Group B), each comprising 55 patients.

Comprehensive information about the study was provided to all patients and their families, and written informed consent was obtained. The Ethical Committee of the Hospital approved the study.

Criteria for inclusion: 1. Patients with manifestations conforming to the diagnostic criteria of schizophrenia of *The Diagnostic and Statistical Manual of Mental Disorders (4th edition)*. 2. Patients aged between 18 and 60 years, with no response to the high-dose treatment of three kinds of antipsychotics. 3. Patients with a disease course not shorter than five years.

Criteria for exclusion: 1. Patients with other diseases. 2. Patients who had received appropriate treatment prior to this study. 3. Patients with communication difficulties. 4. Patients who were uncooperative with the staff. 5. Patients with severe adverse responses to the drugs used in this study. 6. Patients with a history of drug use that might affect the result of this study.

Methods

In the current study, two distinct approaches to medication were compared: Group A received antipsychotics selected by physicians based on their expertise, whereas Group B received personalized medication determined through drug-related gene tests and the evaluation of physicians and clinical pharmacists.

Group A

The specific antipsychotic medications used in Group A included Haloperidol at doses of 2-10 mg per day, chosen for pa-

tients with positive symptoms like hallucinations and delusions based on its efficacy for these symptoms; Risperidone at 2-6 mg per day, selected for patients with both positive and negative symptoms given its broader efficacy profile; Olanzapine at 5-20 mg per day, used for patients with predominant negative symptoms like social withdrawal due to its efficacy for these symptoms; Quetiapine at 150-750 mg per day, chosen for patients with mood or sleep issues given its sedating and mood-stabilizing effects; and Aripiprazole at 10-30 mg per day, used for patients susceptible to side effects like tardive dyskinesia due to its lower risk of these effects.

Group B

In the Group B, medication was personalized based on drug-related gene tests and the collaborative analysis of physicians and clinical pharmacists. The gene tests identified genetic variations that could influence an individual's response to specific antipsychotic medications. For example, the CYP2D6 gene was of particular interest, as it encodes an enzyme responsible for the metabolism of many antipsychotic drugs. Variations in this gene can lead to differences in how quickly medications are metabolized, potentially affecting their efficacy and side-effect profiles^{7,8}.

Patients with the 'poor metabolizer' phenotype, characterized by certain SNP combinations, were prescribed lower doses or given antipsychotics not primarily metabolized by the CYP2D6 enzyme to avoid drug accumulation and subsequent side effects. In contrast, 'rapid metabolizers' may have required higher doses or more potent medications to achieve therapeutic drug levels.

The treatment protocol was adjusted within two weeks after the gene test, including maintaining, increasing, or reducing the initial drug dose or its combination with other antipsychotics or switching to other antipsychotics. The specific medications and doses used were determined based on a

comprehensive analysis of the recommended drugs by the DSM4, the patient's gene test results, and the individual's symptomatology and treatment history.

The distribution of crucial CYP2D6 genotypes in Group B were as follows:

- Poor metabolizers: 7 patients (12.7%).
- Intermediate metabolizers: 18 patients (32.7%).
- Normal metabolizers: 25 patients (45.5%).
- Ultra-rapid metabolizers: 5 patients (9.1%).

Medications were adjusted based on this genotype data. For example, poor metabolizers were prescribed lower doses of risperidone, switched from Haloperidol to Quetiapine, or changed from Olanzapine to Aripiprazole. Ultra-rapid metabolizers were given higher doses of Haloperidol or switched from Quetiapine to Olanzapine. Table 1 shows examples of specific medication changes made.

Gene test

A customized tube obtained from Shanghai Conlight Medical Laboratory Co., Ltd was utilized to gather detached cells from the oral epithelium. This was achieved by gently swabbing the buccal region of the mouth with a cotton swab. The collected cells were then securely sealed within the tube, ensuring no contact with external materials. Two sets of samples were procured from both the left and right sides of the mouth for subsequent DNA extraction. These samples were subsequently stored at room temperature.

The genotypes and allele frequencies of three single nucleotide polymorphisms (SNPs) within the CYP2D6 gene (rs16947, rs1065852, and rs5030865) were examined. The analysis used the general sequencing kit (NovaSeq 6000 Reagent Kits) and the fluorescence in situ hybridization (FISH Tag™ DNA Multicolor Kit by Invitrogen).

Table 1
Medication adjustments based on CYP2D6 genotypes in Group B.

Genotype	Patients n (%)	Initial Medication and Dose	Adjusted Medication and Dose	Rationale for Adjustment
Poor metabolizer	7 (12.7%)	Haloperidol 5mg daily	Quetiapine 100mg twice daily	Haloperidol is primarily metabolized by CYP2D6 ³¹ . Due to poor metabolism, it was switched to quetiapine, which has alternate metabolic pathways to avoid drug accumulation.
		Risperidone 3mg daily	Risperidone 1mg daily	Risperidone dosage was reduced by 50% to avoid side effects due to poor CYP2D6 metabolism ³² .
Intermediate metabolizer	18 (32.7%)	Olanzapine 10mg daily	Olanzapine 5mg daily	The dose was reduced as metabolism was expected to be slower in intermediate metabolizers.
		Risperidone 4mg daily	Risperidone 2mg daily	
Normal metabolizer	25 (45.5%)	Haloperidol 5mg twice daily	No change	Normal metabolizer phenotype indicates haloperidol metabolism is expected to be typical. No dose adjustment was needed.
		Quetiapine 400mg daily	Quetiapine 400mg twice daily	As a normal metabolizer, can tolerate higher doses of quetiapine. The dose was increased for improved efficacy.
Ultra rapid metabolizer	5 (9.1%)	Risperidone 4mg daily	Risperidone 6mg daily	More rapid CYP2D6 metabolism is expected in ultra-rapid metabolizers. The risperidone dose was increased by 50% to ensure therapeutic levels were achieved.
		Quetiapine 400mg daily	Olanzapine 20mg daily	Switched from quetiapine to olanzapine due to concerns that quetiapine might be metabolized too rapidly in ultra-rapid metabolizers, affecting its effectiveness.

Genomic analysis and protocol adjustment

Genomic analysis was conducted on patients belonging to Group B, encompassing the identification of metabolic, responsive, and toxic gene phenotypes, along with their distribution frequencies. Within two weeks after the gene testing, the treatment regimen was modified based on a comprehensive analysis that considered the recommendations provided by the DSM4 and the outcomes of the gene tests.

These adjustments entailed the maintenance, augmentation, or reduction of the initial drug dosage, either in isolation or in combination with other antipsychotic medi-

cations. In some cases, a transition to alternative antipsychotic drugs was also considered. The recommended medications were categorized into primary, secondary, and tertiary options. Furthermore, medications were selected sequentially, following the gene test outcomes, and were tagged as suitable for direct use, utilization with caution, or utilization with caution accompanied by frequent monitoring.

Observation of indicators

Before and after treatment, a fasting 6 mL elbow venous blood sample was collected from each patient and subsequently centri-

fused at 3000 rpm to facilitate the separation of the supernatant. This supernatant was then carefully preserved at a temperature of -70°C .

The quantification of TNF- α , IL-1 β , NGF, BDNF, PI3K, and mTOR levels was done utilizing a double sandwich enzyme-linked immunosorbent assay (ELISA). The procedure encompassed the following steps: an ELISA plate was appropriately labeled at room temperature, and a standard curve was meticulously prepared using the appropriate standard reagents. The patient samples and the standard reagents were appropriately diluted and introduced into individual wells (100 μL per well). Subsequently, incubation was carried out at 37°C within a humid environment.

Following the incubation period, the plate underwent repeated rinsing steps, after which an antibody-working solution was meticulously added to each well at a dilution of 1:100 (100 μL per well). This was followed by an additional incubation at 37°C for 45 minutes. The plate was then rinsed again, and solutions of TNF- α , IL-1 β , NGF, BDNF, PI3K, and mTOR were introduced to the respective wells (100 μL per well), followed by another incubation under humid conditions for 45 minutes.

The enzymatic reaction was eventually halted by introducing a termination solution (100 μL per well). Subsequently, a microplate reader obtained an optical density reading at a wavelength of 450 nm. This reading was then utilized to calculate the alterations in the concentrations of the factors mentioned above.

The assessment of clinical responses in patients involved the utilization of the Positive and Negative Syndrome Scale (PANSS) and the Brief Psychiatric Rating Scale (BPRS) ^{9,10}. The PANSS comprises 30 items, each scored on a scale of 1 to 7. Similarly, the BPRS encompasses five items, specifically targeting anxiety, depression, thought disturbance, and excitability, with a pivotal score of 35 points. It should be noted that both PANSS and BPRS scores exhibit a nega-

tive correlation with the observed clinical response. In other words, as the scores on these scales increase, the corresponding clinical response tends to decrease, indicating a greater severity of symptoms.

Social skills psychometric instruments (SSPI) and activities of daily living (ADL) scale were used to evaluate patients' social and living abilities ^{11,12}. The SSPI scale includes ten dimensions, such as familial activity, social activity, responsibility, and planning, and scores according to the following criteria: 1 point for no anomaly or only slight functional defect; 2 points for a definite functional defect; 3 points for severe functional defect. Patients who scored not fewer than 2 points should be considered as having social dysfunction. The ADL scale includes 14 items, such as diet, medication, and housekeeping, and patients are scored as per the following criteria: 1. Patients can take care of themselves independently; 2. Patients have difficulties in taking care of themselves independently; 3. Patients need help in taking care of themselves; 4. Patients fail to take care of themselves independently.

Evaluation of clinical response

Clinical responses were classified into three grades: remarkable response, response, and failure. Remarkable response: no psychotic symptoms, with a decrease in PANSS scores between 50% and 74%. Response: no significant psychotic symptoms, with a decrease in PANSS score between 25% and 49%. Failure: no significant improvement in psychotic symptoms, with a decrease in PANSS score lower than 25%. Total effectiveness rate = Rate of remarkable response + rate of response.

Statistical methods

The SPSS 20.0 software was applied for data analysis. Measurement data were described as means \pm standard deviations ($\bar{x} \pm \text{SD}$), and the difference between the two groups was validated by an independent sample *t*-test. Enumeration data were expressed

as ratios, and the chi-square test validated the difference. $P < 0.05$ indicated that the difference had statistical significance.

RESULTS

Demographic characteristics

In Group A, there were 32 males and 23 females, aged 25 to 67 years (mean \pm SD: 44.5 ± 20.1 years). Education varied: 21 had diplomas below high school, 18 had high school diplomas, and 16 had diplomas beyond high school. Illness duration ranged from 2 to 24 years (mean \pm SD: 13 ± 9 years), with onset age from 18 to 37 years (mean \pm SD: 24 ± 9 years); three patients reported familial cases. In Group B, 30 males and 25 females were aged 26 to 67 years (mean \pm SD: 45.5 ± 20.1 years). Education-wise, 25 had diplomas below high school, 16 had high school diplomas, and 14 had diplomas beyond high school. Illness duration ranged from 2 to 25 years (mean \pm SD: 12 ± 9 years), with onset age from 18 to 35 years (mean \pm SD: 25 ± 9 years); four patients reported familial cases (Table 2).

Comparison of the inflammatory cytokines

As depicted in Fig. 1, a comparison of TNF- α and IL-1 β levels between the two

groups before treatment revealed no statistically significant differences ($p > 0.05$). However, substantial reductions were observed following treatment in both TNF- α and IL-1 β levels. Notably, the declines in Group B were more pronounced than Group A's ($p < 0.05$).

Comparison of nerve growth factors between the two groups

Before treatment, we found no significant differences in the levels of NGF and BDNF between the two groups ($p > 0.05$); after treatment, significant increases were found in the levels of NGF and BDNF of the two groups, while the increases in Group B were more evident ($p < 0.05$), (Fig. 2).

Comparison of the PANSS and BPRS scores between two groups

As shown in Fig. 3, comparing the scores of PANSS and BPRS between the two groups before treatment showed no significant differences ($p > 0.05$). However, after treatment, significant decreases were noted in scores of PANSS and BPRS, and decreases in Group B were more pronounced than those in Group A ($p < 0.05$).

Social function and daily living activities

Before treatment, we found no significant differences when comparing the scores

Table 2
Demographic characteristics.

		Group A	Group B
	Participants	55	55
Sex	Male	32	30
	Female	23	25
Age (Mean \pm SD)		44.5 ± 20.1	45.5 ± 20.1
Education Level	Lower Secondary	21	25
	Diploma	18	16
	Post-High School	16	14
Disease Duration (Mean \pm SD)		13 ± 9	12 ± 9
Age of Onset (Mean \pm SD)		24 ± 9	25 ± 9
Familial Positivity		3	4

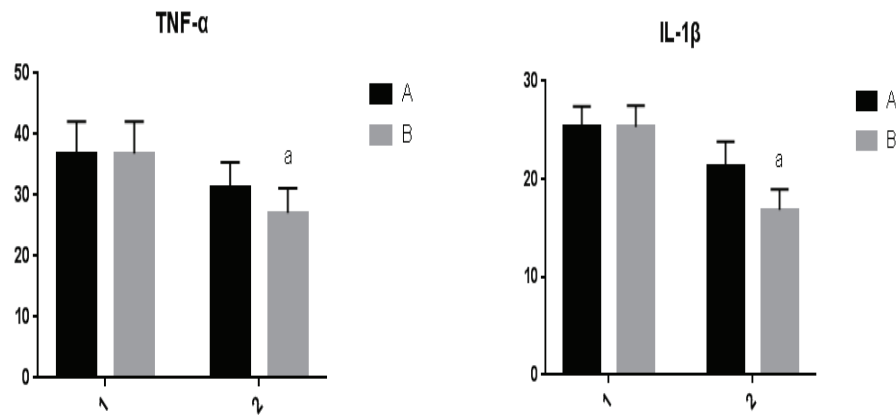


Fig. 1. Comparison of the levels of TNF- α and IL-1 β between two groups (ng/mL).

Note: Group A for the regular medication group, Group B for the gene-guided medication group, 1 for before treatment, 2 for after treatment; a for $p < 0.05$.

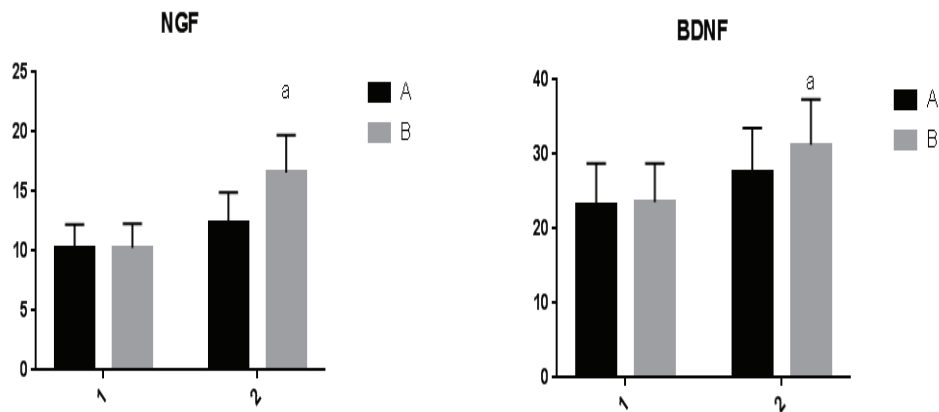


Fig. 2. Comparison of the levels of NGF and BDNF between two groups (ng/mL)

Note: Group A for the regular medication group, Group B for the gene-guided medication group, 1 for before treatment, 2 for after treatment; a for $p < 0.05$.

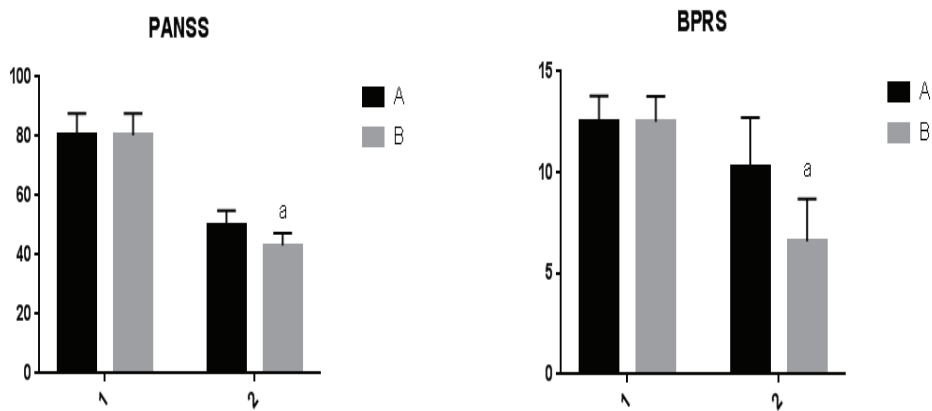


Fig. 3. Comparison of the Positive and Negative Syndrome Scale (PANSS) and the Brief Psychiatric Rating Scale (BPRS) scores between two groups (Points).

Note: Group A for the regular medication group, Group B for the gene-guided medication group, 1 for before treatment, 2 for after treatment; a for $p < 0.05$.

of SSPI and ADL between the two groups ($p > 0.05$); after treatment, significant increases were found in the scores of SSPI and ADL of both groups, while the increases in Group B were more noticeable ($p < 0.05$, Fig. 4).

Comparison of the effectiveness rate between two groups

The total effectiveness rate in Group B was much higher than that in Group A ($p < 0.05$; Table 3).

Comparison of the rate of adverse events between two groups

As shown in Table 4, the rate of adverse events in patients of Group B was lower than that in Group A, although this difference had no statistical significance ($p > 0.05$).

DISCUSSION

Schizophrenia represents a severe mental disease, and antipsychotics remain the predominant treatment for managing schizophrenia. However, about one-third of patients with schizophrenia respond poorly to these drugs¹³. Clinically, diagnosis or even treatment for schizophrenia mainly depends on the expertise of clinicians or the evalua-

tion by scales¹⁴. Currently, the prevalence of schizophrenia remains high, and an available but simple medication that can perfect the precise treatment is an ideal strategy for schizophrenia treatment¹⁵. Continuous progress in pharmaceuticals and pharmacogenomics enables the detection of drug-related genes to guide the clinical use of psychotropic drugs¹⁶. Gene tests before medication can clarify the patients' genotype, thus promoting rational, precise, and individualized medication¹⁷.

The essential gene examined was CYP2D6, which encodes a critical enzyme involved in metabolizing many commonly used antipsychotics¹⁸. Patients received drug changes according to their CYP2D6 genotype to maximize efficacy and reduce adverse effects, as shown in Table 1. Poor metabolizers, possessing alleles leading to nonfunctional CYP2D6, were switched from Haloperidol and risperidone to alternative antipsychotics not extensively metabolized by this enzyme, like quetiapine¹⁹. This avoids drug accumulation and toxicity in these patients from impaired metabolism. In contrast, doses were increased for normal or ultra-rapid metabolizers to achieve adequate plasma concentrations.

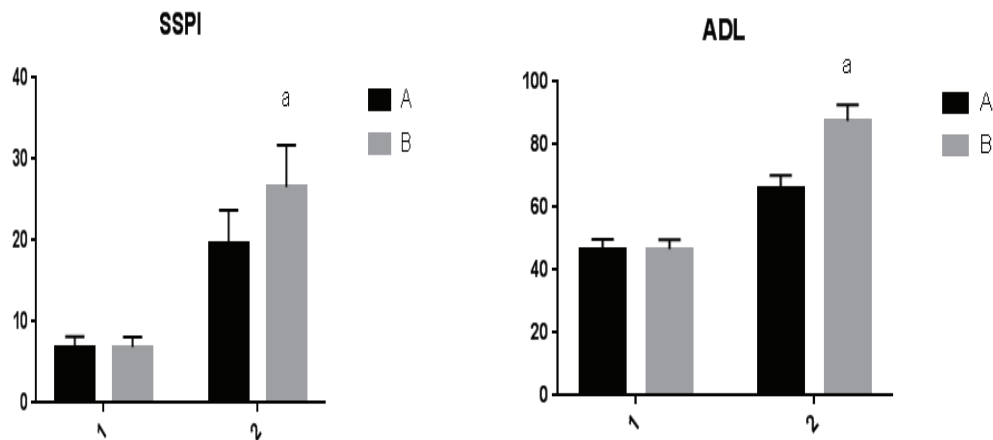


Fig. 4. Comparison of social function and activity of daily living between two groups (Points)
 Note: Group A for the regular medication group, Group B for the gene-guided medication group, 1 for before treatment, 2 for after treatment; a for $p < 0.05$.
 -Social skills psychometric instruments (SSPI) and activities of daily living (ADL) scores.

Table 3
Comparison of the effectiveness rate between two groups

Group	Case (n)	Remarkable response	Response	Failure	Effectiveness rate*
Group A	55	25	20	10	47 (85.45)
Group B	55	28	25	2	53 (96.36)
c^2					5.986
P					0.014

*Values are expressed as n (%).

Table 4
Comparison of the rate of adverse events between two groups.

Group	Case (n)	Leukopenia	Constipation	Insomnia	Anomaly in blood glucose/lipid	Rate of adverse event*
Group A	55	1	1	2	1	5 (9.09)
Group B	55	0	2	0	1	3 (5.45)
c^2						0.539
P						0.462

*Values are expressed as n (%).

The improved outcomes with gene-guided treatment are biologically plausible based on the pharmacokinetics of antipsychotics. Variations in CYP2D6 polymorphisms can profoundly impact drug exposure by causing variations in metabolic capacity across different genotypes. CYP2D6 is an essential drug-metabolizing enzyme that contributes to the metabolism of 15-25% of all clinically used drugs. Genetic variations in the CYP2D6 gene can lead to considerable phenotypical interindividual differences in CYP2D6-dependent drug metabolism²⁰. A study by Novalbos *et al* (2010), examining the relationship between the CYP2D6 genotype and the effects of risperidone found that individuals with different metabolizer phenotypes (ultrarapid metabolizers (UMs), extensive metabolizers (EMs), intermediate metabolizers (IMs), and poor metabolizers (PMs)) displayed distinct pharmacokinetic patterns. PMs and IMs exhibited higher levels and longer half-life of risperidone, while UMs and EMs had higher levels of 9-hydroxy risperidone²¹. Elmokadem *et al.*²² conducted

another study on aripiprazole, an antipsychotic, revealing significant time-to-effect differences between CYP2D6 EMs and PMs. This suggests a necessity for customized dosing strategies for PMs²² and that tailoring medication and dosage based on CYP2D6 activity can optimize plasma levels, potentially reducing side effects in PMs and improving efficacy in rapid metabolizers

According to a current clinical study, schizophrenia is somehow related to the levels of inflammatory cytokines. For instance, TNF- α and IL-1 β are clinically common inflammatory cytokines that can be used to evaluate the patients' inflammation state more accurately²³. This study uncovered abnormal elevations in inflammatory cytokine levels among individuals with schizophrenia. With the aid of gene tests to inform individualized medication, the levels of TNF- α and IL-1 β were reduced in patients. These results imply a direct association between inflammatory cytokines and schizophrenia, indicating that tailored medication can effectively mitigate inflammatory cytokine levels and enhance drug efficacy.

As a nerve growth factor, NGF can regulate the growth and development of neurons in the peripheral and central nervous system, maintain neurons' survival, promote synaptic growth, and restore nerve function^{24,25}. BDNF, as a member of the family of neurotrophic factors, mainly distributes in the central nervous system and the endocrine system, restores the survival of damaged neurons and improves the functions in memory and learning^{26,27}. In the present study, a decline in levels of NGF and BDNF was observed following the onset of schizophrenia. However, with the application of gene tests to guide individualized medication, it was observed that the levels of NGF and BDNF could be elevated in patients with schizophrenia. This finding indicates that personalized medication has the potential to facilitate the restoration of patients' learning and memory capacities, as well as promote the recovery of nerve function.

Since physicians may not provide the optimal choice in the efficacy and safety of antipsychotics according to their expertise or evaluation results, precise individualized medication is necessary for improving social function and activities of daily living^{28,29}. The PANSS scale is a clinically established tool for assessing mental functioning, encompassing positive and negative symptom dimensions. The SSPI scale is applicable for gauging the social functionality of individuals with epilepsy-related mental disorders, whereas the ADL scale serves to evaluate the daily living activities of patients grappling with mental illnesses³⁰. In the present study, we discovered that personalized medication, guided by genetic tests, has the potential to decrease PANSS scores while simultaneously elevating SSPI and ADL scores. These findings imply that this approach may effectively address mental symptoms and enhance the social functioning and daily activities of individuals dealing with schizophrenia.

In conclusion, the utilization of personalized medication guided by genetic testing has the potential to enhance the effective-

ness of drugs. This improvement can enhance learning and memory capabilities in individuals with schizophrenia, facilitating the restoration of neural function and bolstering social engagement and daily activities. Ultimately, this approach aids patients in transitioning back to their daily lives. Furthermore, this strategy holds the promise of refining drug selection and dosages and providing guidance for developing treatment protocols. As a result, it enables the realization of precise treatment using psychotropic medications.

Conflict of competence

The authors declare no conflict of interest.

Authors' ORCID number

- Shujun Zhou (SZ):
0000-0002-3836-2803
- Guangqin Zhang (GZ):
0009-0007-6999-9130
- Zhe Wang (ZW):
0000-0002-8887-7979
- Long Wei (LW):
0000-0001-5962-3235
- Min Zhu (MZ):
0000-0001-7219-6944
- Jinquan He (JH):
0000-0003-0381-6884

Authors' contribution

The present study involved a collaborative effort where S.Z. provided expertise in gene-based medication, conducted data analysis, and contributed to result interpretation; GZ coordinated the study, collected and organized data, and drafted the manuscript; ZW contributed expertise in gene-based medication, assisted in data interpretation, and critically reviewed the manuscript; LW contributed to the litera-

ture review, performed statistical analysis, and assisted in manuscript revisions; M.Z assisted in data collection and participated in data analysis and J.H supervised the study, contributed to data analysis and interpretation, and provided overall guidance in manuscript preparation.

REFERENCES

1. Yan Y, Qifeng D, Daiwei Z, Haiping Z. A random control trial of group psychological crisis intervention on defensive style and anxiety for the first-degree relatives of patients with schizophrenia. *Chinese Ment Heal J.* 2021;35(6):466-471.
2. Xiong H, Zhang H, Chen X, Cheng Y, Huang C. Clinical characteristics and related factors of pneumonia in patients with aplastic anemia. *Chinese J Infect Chemother.* 2019;19(1):27-31. <https://doi.org/10.16718/j.1009-7708.2019.01.006>
3. Green MF, Horan WP, Lee J, McCleery, Reddy L F, Wynn JK. Social disconnection in schizophrenia and the general community. *Schizophrenia bulletin.* 2018;44(2):242-249. <https://doi.org/10.1093/schbul/sbx082>
4. Barut JK, Dietrich MS, Zanoni PA, Ridner SH. Sense of belonging and hope in the lives of persons with schizophrenia. *Arch Psych Nursing.* 2016;30(2):178-184. <https://doi.org/10.1016/j.apnu.2015.08.009>
5. Ying J, Jue L, Minghuan Z, Zuo H, Dianhong S, Jia L. Comparison of efficacy and safety between sodium valproate and modified electroconvulsive therapy in clozapine-resistant refractory schizophrenia. *J Tongji Univ Medical Sci.* 2022;43(2):388-393.
6. Xu QW, Liu X, Yao QK, Zheng ZJ. CYP correlation study of refractory schizophrenia drug gene detection. *J Hainan Med Coll.* 2019;25(5).
7. Kane M. CYP2D6 overview: allele and phenotype frequencies. *Medical Genetics Summaries [Internet]: National Center for Biotechnology Information (US);* 2021.
8. Pouget JG, Shams TA, Tiwari AK, Müller DJ. Pharmacogenetics and outcome with antipsychotic drugs. *Dialogues Clin Neurosci.* 2014;16(4):555-566. <https://doi.org/10.31887/DCNS.2014.16.4/jpouget>
9. Zanello A, Berthoud L, Ventura J, Merlo MC. The Brief Psychiatric Rating Scale (version 4.0) factorial structure and its sensitivity in the treatment of outpatients with unipolar depression. *Psychiatry Res.* 2013;210(2):626-633. <https://doi.org/10.1016/j.psychres.2013.07.001>
10. Depp CA, Loughran C, Vahia I, Molinari V. Chapter 5 - Assessing Psychosis in Acute and Chronic Mentally Ill Older Adults. In: Lichtenberg PA, editor. *Handbook of Assessment in Clinical Gerontology (Second Edition)*. San Diego: Academic Press; 2010. p. 123-54. <https://doi.org/10.1016/B978-0-12-374961-1.10005-3>
11. Edemekong PF, Bomgaars DL, Sukumaran S, Schoo C. Activities of Daily Living. *StatPearls [Internet]*. Treasure Island (FL): StatPearls Publishing; 2023 Jan. 2023 Jun 26. [PubMed ID: 29261878].
12. Yu W, Tong J, Sun X, Chen F, Zhang J, Pei Y, Zhang T, Zhang J, Zhu B. Analysis of medication adherence and its influencing factors in patients with schizophrenia in the Chinese Institutional Environment. *Int J Environ Res and public health.* 2021;18(9). <https://doi.org/10.3390/ijerph18094746>
13. Yun F, Yanfang Z, Xuehao W, Jinghui T, Mengzhuang G, Fude Y, Baopeng T, Yunlong T. Allostatic load and its relationship with cognitive deficits in patients with first-episode schizophrenia. *Chinese Ment Heal J.* 2021;35(10):814-819.
14. Patel KR, Cherian J, Gohil K, Atkinson D. Schizophrenia: overview and treatment options. *P & T: a peer-reviewed journal for formulary management.* 2014;39(9):638-645.
15. Zhi L, Qinfang B, Ning L, Fangbin C, Ying C, Xiaoyan W, Falin Q. Pharmaceutical care in 3 Patients with schizophrenia treated with clozapine. *Her Med.* 2021;40(5):674-677. <https://doi.org/10.3870/j.issn.1004-0781.2021.05.019>
16. Guo-qin H, Qin-yu L, Jing Z, Ming-huan Z, Shun-ying Y, Zheng-hui Y, Jian C. Association study of non-coding variant

- of NOS1AP gene with schizophrenia. *Journal of Shanghai Jiaotong University (Medical Science)* 2021;41(1):29-34. <https://doi.org/10.3969/j.issn.1674-8115.2021.01.005>
17. **Omelchenko MA, Atadzhikova YA, Migalina VV, Nikiforova IY, Kaleda VG.** Clinical and pathopsychological characteristics of juvenile depression with attenuated schizophrenic spectrum symptoms. *Neurosci Behav Physiol* 2022;52(3):330-335. <https://doi.org/10.1007/s11055-022-01244-0>
 18. **Wannasuphprasit Y, Andersen SE, Arranz MJ, Catalan R, Jürgens G, Kloosterboer SM.** CYP2D6 genetic variation and antipsychotic-induced weight gain: a systematic review and meta-analysis. *Front Psychol* 2021;12:768748. <https://doi.org/10.3389/fpsyg.2021.768748>
 19. **Dean L.** Risperidone therapy and CYP2D6 genotype. In: Pratt VM, Scott SA, Pirmohamed M, Esquivel B, Kattman BL, Malheiro AJ, editors. *Medical Genetics Summaries*. Bethesda (MD): National Center for Biotechnology Information (US); 2012. [PubMed ID: 28520384].
 20. **Rüdesheim S, Wojtyniak JG, Selzer D, Hanke N, Mahfoud F, Schwab M.** Physiologically based pharmacokinetic modeling of metoprolol enantiomers and α -hydroxymetoprolol to describe CYP2D6 drug-gene interactions. *Pharmaceutics* 2020;12(12). <https://doi.org/10.3390/pharmaceutics12121200>
 21. **Novalbos J, López-Rodríguez R, Román M, Gallego-Sandín S, Ochoa D, Abad-Santos F.** Effects of CYP2D6 genotype on the pharmacokinetics, pharmacodynamics, and safety of risperidone in healthy volunteers. *J Clin Psychopharmacol* 2010;30(5):504-511. <https://doi.org/10.1097/JCP.0b013e3181ee84c7>
 22. **Elmokadem A, Bruno CD, Housand C, Jordie EB, Chow CR, Lesko LJ.** Brexpiprazole pharmacokinetics in CYP2D6 poor metabolizers: using physiologically based pharmacokinetic modeling to optimize time to effective concentrations. *J Clin Pharmacol* 2022;62(1):66-75. <https://doi.org/10.1002/jcph.1946>
 23. **Zhu F JM, Ma Q.** Correlation of serum inflammatory factors with clinical symptoms and cognitive functions in schizophrenia. *J Xi'an Jiaotong Univ Medical Sci* 2021;42(2):301-305. <https://doi.org/10.7652/jdyxb202102023>
 24. **Ding X-W, Li R, Geetha T, Tao Y-X, Babu JR.** Nerve growth factor in metabolic complications and Alzheimer's disease: Physiology and therapeutic potential. *Biochim Biophys Acta - (BBA) Molecular Basis of Disease*. 2020;1866(10):165858. <https://doi.org/10.1016/j.bbadis.2020.165858>
 25. **Aloe L, Rocco ML, Bianchi P, Manni L.** Nerve growth factor: from the early discoveries to the potential clinical use. *J Translat Med*. 2012;10(1):239. <https://doi.org/10.1186/1479-5876-10-239>
 26. **Gao L, Zhang Y, Sterling K, Song W.** Brain-derived neurotrophic factor in Alzheimer's disease and its pharmaceutical potential. *Translational Neurodegeneration*. 2022;11(1):4. <https://doi.org/10.1186/s40035-022-00279-0>
 27. **Li Y, Li F, Qin D, Chen H, Wang J, Wang J.** The role of brain derived neurotrophic factor in central nervous system. *Front Aging Neurosc*. 2022;14:986443. <https://doi.org/10.3389/fnagi.2022.986443>
 28. **Fuentes-Claramonte P, Ramiro N, Torres L, Argila-Plaza I, Salgado-Pineda P, Soler-Vidal J.** Negative schizophrenic symptoms as prefrontal cortex dysfunction: Examination using a task measuring goal neglect. *NeuroImage: Clinical*. 2022;35:103119. <https://doi.org/10.1016/j.nicl.2022.103119>
 29. **Yali W, Xiaoping Z** To study the efficacy and safety of phenobarbital and phenytoin combined with valproate sodium in the treatment of epileptic mental disorders. *Cardiovasc Dis J Integr Tradit Chinese West Med*. 2020;8(34):5-9.
 30. **Fleischhacker W, Galderisi S, Laszlovszky I, Szatmári B, Barabássy Á, Acsai K, Szalai E, Harsányi J, Earley W, Patel M, Németh G.** The efficacy of cariprazine in negative symptoms of schizophrenia: Post hoc analyses of PANSS individual items and PANSS-derived factors. *Euro-*

- pean Psychiatry.2019;58:1-9. <https://doi.org/10.1016/j.eurpsy.2019.01.015>
- 31. Šimić I, Potočnjak I, Kraljičković I, Stanić Benić M, Čegec I, Juričić Nahal D.** CYP2D6 *6/*6 genotype and drug interactions as cause of haloperidol-induced extrapyramidal symptoms. *Pharmacogenomics*. 2016;17(13):1385-0389. <https://doi.org/10.2217/pgs-2016-0069>
- 32. Cui Y, Yan H, Su Y, Wang L, Lu T, Zhang D.** CYP2D6 genotype-based dose recommendations for risperidone in Asian people. *Front Pharmacol* 2020;11:936. <https://doi.org/10.3389/fphar.2020.00936>

Effect of thiamine pyrophosphate on oxidative damage in the brain and heart of rats with experimentally induced occlusion of the common carotid artery.

İzzet Emir¹, Zeynep Suleyman² and Halis Suleyman³

¹Department of Cardiovascular Surgery, Faculty of Medicine, Erzincan Binali Yildirim University, Erzincan/Türkiye.

²Department of Nursing, Faculty of Health Sciences, Erzincan Binali Yildirim University, Erzincan/Türkiye.

³Department of Pharmacology, Faculty of Medicine, Erzincan Binali Yildirim University, Erzincan/Türkiye.

Keywords: carotid artery; ischemia; occlusion; rat; reperfusion; thiamine pyrophosphate.

Abstract. It is known that a sudden increase in cerebral blood flow (hyperperfusion) with carotid revascularisation may disrupt and damage the blood-brain barrier. This study aimed to explore thiamine pyrophosphate's (TPP) protective effects against potential brain and heart damage resulting from carotid cross-clamping and unclamping in rats. The animals were divided into common carotid cross-clamping and unclamping (CCU), TPP+common carotid cross-clamping and unclamping (TCCU), and sham operation (SG) groups. The TCCU group received an intraperitoneal injection (IP) of 20 mg/kg TPP one hour before anesthesia. The CCU and SG groups received distilled water as a solvent. Ischemia was induced by maintaining the clips closed for 10 min. For the SG group, only a subcutaneous incision was made. Afterward, the clips were removed, the incisions were stitched, and reperfusion was continued for six hours. Subsequently, the rats were euthanized with high-dosage general anesthesia, and heart and brain tissues were removed. TPP significantly suppressed the I/R-induced malondialdehyde (MDA) increase and decreased total glutathione (tGSH) levels in brain and heart tissues. TPP prevented the increase of tumor necrosis factor-alpha (TNF- α), interleukin-1 β (IL-1 β), and interleukin-6 (IL-6) levels in both brain and heart tissues. In blood serum, TPP suppressed I/R-induced increase in troponin I (TP I) and creatine kinase-MB (CK-MB) in the blood. TPP was shown to protect the brain and distant cardiac tissues against oxidative and inflammatory damage induced by cerebral I/R.

Efecto del pirofosfato de tiamina sobre el daño oxidativo en el cerebro y el corazón de ratas con oclusión inducida experimentalmente de la arteria carótida común.

Invest Clin 2024; 65 (2): 220 – 229

Palabras clave: arteria carótida; ischemia; oclusión; rata; reperfusión; pirofosfato de tiamina.

Resumen. Se sabe que un aumento repentino del flujo sanguíneo cerebral (hiperperfusión) con la revascularización carotídea puede causar la alteración y daños de la barrera hematoencefálica. El objetivo de este estudio fue explorar los efectos protectores del pirofosfato de tiamina (TPP) contra los posibles daños cerebrales y cardíacos resultantes del pinzamiento y despinzamiento de la carótida en ratas. Los animales se dividieron en grupos de pinzamiento y despinzamiento de la carótida común (CCU), TPP + pinzamiento y despinzamiento de la carótida común (TCCU) y operación simulada (SG). El grupo TCCU recibió una inyección intraperitoneal (IP) de TPP a una dosis de 20 mg/kg una hora antes de la anestesia. Los grupos CCU y SG recibieron agua destilada como disolvente. La isquemia se indujo manteniendo los clips en posición cerrada durante 10 min. En el grupo SG solo se realizó una incisión subcutánea. Luego se retiraron los clips, se suturaron las incisiones y se mantuvo la reperfusión durante 6 horas. Posteriormente, los animales fueron sacrificados con altas dosis de anestesia y se extrajeron tejidos del corazón y del cerebro. El TPP suprimió significativamente el aumento de malondialdehído (MDA) inducido por I/R y la disminución de los niveles de glutatión total (tGSH) tanto en el tejido cerebral como en el cardíaco. El TPP impidió el aumento de los niveles de factor de necrosis tumoral alfa (TNF- α), interleucina 1 β (IL-1 β) e interleucina-6 (IL-6) en los tejidos del cerebro y del corazón. En el suero sanguíneo, el TPP suprimió el aumento de la troponina I (TP I) y la creatina quinasa-MB (CK-MB) inducido por I/R en la sangre. Se demostró que el TPP protege el cerebro y los tejidos cardíacos distantes contra el daño oxidativo e inflamatorio inducido por la I/R cerebral.

Received: 20-11-2023 Accepted: 13-02-2024

INTRODUCTION

In instances of acute occlusion of the extracranial internal carotid artery, 40%-60% of patients experience severe disability, while 16%-55% experience stroke-related complications that lead to death¹. As known, atherosclerotic carotid artery disease is a significant cause of stroke worldwide². Patients

with severe carotid artery stenosis ($\geq 70\%$) have an increased risk of myocardial infarction and cardiovascular death (22%)³. Total occlusion of the common carotid artery is rare. However, endarterectomy and endovascular revascularization are recommended in cases where inadequate cerebral perfusion leads to various neurological symptoms⁴. During carotid endarterectomy, cross-clamp-

ing of the carotid artery may induce local cerebral ischemia, and unclamping may induce ischemia/reperfusion (I/R) injury⁵. A sudden cerebral blood flow (hyper-perfusion) increase following carotid revascularization may disrupt and damage the blood-brain barrier⁶. It is argued that this damage is due to an increased production of reactive oxygen species (ROS)⁷. I/R may cause damage not only in the primary tissue but also in distant organs⁸. ROS, pro-inflammatory cytokines, and polymorphonuclear leukocytes are implicated in I/R-related distant organ injury^{9,10}. The neutrophil-to-lymphocyte ratio is recognized as a marker for systemic inflammation and is significantly associated with postoperative complications¹¹. Myocardial ischemia has been reported to occur with ST-segment depression during carotid cross-clamping¹². These data suggest that severe cardiac and systemic complications develop during carotid endarterectomy and endovascular revascularization and that antioxidant and anti-inflammatory medicines are beneficial in curing cardiac and systemic organ injury that may develop due to reperfusion. Myocardial ischemia and hypoxia have been associated with abnormal increases in TPI and CK-MB levels¹³. It is known that elevated levels of TPI and CK-MB are also positively correlated with elevated levels of oxidants and pro-inflammatory cytokines¹⁴.

The current study investigated thiamine pyrophosphate (TPP) for its potential protective effects against cardiac and other organ damage arising from carotid artery cross-clamping and unclamping. TPP, the active metabolite of thiamine¹⁵, is synthesized in the liver through the phosphorylation of thiamine by thiamine pyrophosphokinase¹⁶. Existing literature suggests that TPP exerts a protective effect by inhibiting the increase in oxidant and pro-inflammatory parameters¹⁷. Furthermore, TPP protects cardiac tissue from oxidative damage¹⁸. All these data suggest that TPP is beneficial against possible cardiac and other organ damage resulting from carotid cross-clamping and unclamp-

ing. There is a lack of literature investigating the potential impact of TPP on cardiac damage caused by carotid cross-clamping and unclamping procedures. Hence, our study aimed to biochemically explore TPP's protective effects against potential brain and heart damage from animal carotid cross-clamping and unclamping.

MATERIALS AND METHODS

Animals

This experimental study, employed 18 male albino Wistar rats weighing 285-298 g. All experimental rats were sourced from the Erzincan Binali Yıldırım University Experimental Animals Application and Research Center. The rats were housed and fed in groups for one week under standard conditions, including a regular room temperature (22°C) and a 12-h light/12-h dark cycle to facilitate environmental adaptation. All protocols and procedures were confirmed by the Ethics Committee of the Center for Animal Experiments (October 27, 2022, Meeting No. 10/53, Approval No. E-85748827-050.01.04-212799).

Chemicals

The chemicals used in the experiment and ketamine were sourced from Pfizer Pharmaceuticals Inc., Sti (Türkiye), while TPP was sourced from Biofarma (Russia).

Experimental animals

All experimental rats were divided into right and left common carotid cross-clamping and unclamping (CCU), TPP + common carotid cross-clamping and unclamping (TCCU), and sham operation (SG) groups.

Experimental Procedures

Surgical operations were done under sterile conditions in a suitable laboratory environment. The TCCU (n = 6) group received 20 mg/kg TPP intraperitoneally (IP) one hour before anesthesia. The CCU (n = 6) and SG (n = 6) groups received an equiv-

alent volume of distilled water as a solvent via the IP route. General anesthesia was induced with 60 mg/kg of ketamine hydrochloride via the IP route. The period during which the animals remain immobile in the supine position is considered a suitable anesthesia period for surgical intervention¹⁹. During this period, rats in all groups were secured in the supine position on the operating table, and the midline of the neck was shaved. After disinfecting this shaved area, a midline incision was made. After a superficial microdissection, a deep microdissection was done on the right common carotid artery. The trachea was exposed, paratracheal muscles were dissected to access the common carotid artery, and a clip was placed on the common carotid artery. Ischemia was induced by maintaining the clips closed for 10 min. In the SG group, only a subcutaneous incision was made. At the end of this period, the clips were removed, the incisions were sutured, and reperfusion was sustained for six hours. Subsequently, the rats were euthanized with high-dose anesthesia. The levels of oxidant/antioxidant markers, including malondialdehyde (MDA) and total glutathione (tGSH), as well as pro-inflammatory cytokines tumor necrosis factor-alpha (TNF- α), interleukin-6 (IL-6), and interleukin 1 β (IL-1 β), were measured in the extracted brain and heart tissue samples. Troponin I (TP I) and creatine kinase-MB (CK-MB) levels were also investigated in the blood serum. All biochemical results were compared between the groups.

Biochemical analyses

Preparation of Samples

After rinsing the tissue samples with physiological saline, they were ground into powder using liquid nitrogen. Tissue samples were homogenized to determine GSH, thiobarbituric acid reactive substances (TBARS), and protein levels. Clear filtrates were used to analyze MDA, GSH, and protein levels.

Quantification of MDA and GSH, and Protein Levels

MDA and GSH levels in the brain and heart tissues were quantified following the (ELISA) kit instructions of the respective assays (Cayman Chemical Company). Protein was detected according to the Bradford method²⁰.

TNF- α , IL-1 β , and IL-6 Analyses

The tissues were disrupted and homogenized by adding liquid nitrogen. We then added phosphate-buffered saline (pH 7.4) in a 1/10 (w/v) ratio and vortexed, followed by centrifugation for 15 min at 15000 \times g to collect the supernatant. The samples were maintained at 2-8°C after melting. The TNF- α , IL-1 β , and IL-6 levels were determined using a commercial ELISA kit supplied by Eastbiopharm Co. Ltd. ELISA kit, China.

Troponin I (TP I) and Creatine Kinase-MB (CK-MB) Determination

Blood serum TPI levels were measured using the enzyme-linked fluorescent assay technique with the VIDAS TPI Ultra kit and the ELFA (Enzyme-Linked Fluorescent Assay) technique. The test was performed automatically on the VIDAS device using the ready-to-use test reagents provided in the kit. The Roche/Hitachi Cobas C 701 system determined blood serum CK-MB levels. According to the procedure, the test was performed using the immune-UV assay. And ready-to-use test reagents.

Statistical Analyses

The experiment results were presented as "mean value \pm standard deviation" ($\bar{x} \pm$ SD). The normality test in the groups was determined by the Shapiro-Wilk test, and the Levene test determined the homogeneity of variances. Since the data were normally distributed, one-way ANOVA was used for all analyses, and then the Tukey HSD test was used post-hoc for pairwise. "GraphPad Prism

8 Software” was used. Biochemical results were analyzed using “IBM SPSS 25.00 (Armonk, NY: IBM Corp)”. $P < 0.05$ was accepted to be significant.

RESULTS

Biochemical Findings

Oxidant/Antioxidant levels in brain tissue

As seen in Table 1, MDA levels in the brain tissue of animals were significantly higher in the CCU group than in the sham operation (SG) group ($p < 0.001$). TPP significantly inhibited the increase in MDA levels in the CCU group ($p < 0.001$), and there was a statistically significant difference in MDA levels between the TCCU and SG ($p = 0.014$).

The tGSH, an antioxidant parameter, significantly decreased in the CCU group compared to the SG group ($p < 0.001$). The tGSH level in the TCCU group significantly increased compared to the CCU group ($p < 0.001$). A statistically significant difference in tGSH levels was found between the TCCU and SG groups ($p = 0.006$).

Pro-inflammatory cytokines levels in brain tissue

According to Table 1, TNF- α , IL-1 β , and IL-6 levels in the brain tissues of animals were significantly higher in the CCU group than in the sham group ($p < 0.001$). TPP administration significantly inhibited the increase in pro-inflammatory cytokines levels in the TCCU group compared to the CCU group ($p < 0.001$). TNF- α , IL-1 β , and IL-6 levels showed statistically significant differences between the TCCU and SG groups ($p = 0.021$; $p = 0.001$; $p = 0.034$).

Oxidant/Antioxidant levels in heart tissue

MDA levels in the heart tissues of animals were significantly higher in the CCU group than in the SG group ($p < 0.001$). TPP inhibited the increase in MDA levels in the CCU group ($p < 0.001$). MDA levels differed significantly between the TCCU and SG groups ($p = 0.009$).

Compared to the SG, the tGSH level significantly decreased in the CCU group ($p < 0.001$). Compared to the CCU group, the tGSH level significantly increased in

Table 1
Biochemical analysis results in the brain and heart tissues and blood serum.

Biochemical parameters	Mean \pm Standard Deviation			p values			
	SG	CCU	TCCU	SG vs. CCU	SG vs. TCCU	CCU vs. TCCU	
Brain tissue	MDA ($\mu\text{mol/g protein}$)	3.46 \pm 0.22	5.87 \pm 0.68	3.96 \pm 0.39	<0.001	<0.05	<0.001
	tGSH (nmol/g protein)	4.57 \pm 0.12	2.13 \pm 0.40	3.95 \pm 0.26	<0.001	<0.05	<0.001
	TNF- α (ng/L)	2.13 \pm 0.08	4.51 \pm 0.13	2.30 \pm 0.06	<0.001	<0.05	<0.001
	IL-1 β (pg/L)	1.80 \pm 0.12	4.26 \pm 0.07	2.13 \pm 0.08	<0.001	<0.001	<0.001
	IL-6 (pg/L)	2.55 \pm 0.05	4.70 \pm 0.23	2.79 \pm 0.07	<0.001	<0.05	<0.001
Heart tissue	MDA ($\mu\text{mol/g protein}$)	1.60 \pm 0.16	3.05 \pm 0.14	1.90 \pm 0.16	<0.001	<0.05	<0.001
	tGSH (nmol/g protein)	7.23 \pm 0.13	3.65 \pm 0.20	6.48 \pm 0.23	<0.001	<0.001	<0.001
	TNF- α (ng/L)	3.30 \pm 0.09	6.05 \pm 0.34	4.37 \pm 0.28	<0.001	<0.001	<0.001
	IL-1 β (pg/L)	2.41 \pm 0.19	4.50 \pm 0.22	2.70 \pm 0.08	<0.001	<0.05	<0.001
	IL-6 (pg/L)	2.19 \pm 0.41	4.77 \pm 0.16	2.48 \pm 0.16	<0.001	>0.05	<0.001
Blood serum	TP I ($\mu\text{g/L}$)	0.02 \pm 0.002	0.04 \pm 0.004	0.02 \pm 0.003	<0.001	>0.05	<0.001
	CK-MB (U/L)	40 \pm 6.31	82 \pm 6.31	44 \pm 6.09	<0.001	>0.05	<0.001

MDA; malondialdehyde, tGSH; total glutathione, TNF- α ; tumor necrosis factor alpha, IL-1 β ; interleukin 1 beta, IL-6; interleukin 6, TP I; Troponin I, CK-MB; Creatine kinase-MB. SG: Sham operation group, CCU: Common karotis cross-clamping and unclamping, TCCU: TPP + common karotis cross-clamping and unclamping. All analysis was done by one-way ANOVA and then Tukey HSD test was used as post-hoc for pairwise comparisons (N=6) “ $p < 0.05$ was considered significant”.

the TCCU group ($p = 0.001$). A statistically significant difference was observed in tGSH levels between the TCCU and SG groups ($p < 0.001$) (Table 1).

Pro-inflammatory levels in heart tissue

As seen in Table 1, TNF- α , IL-1 β , and IL-6 levels in the heart tissues of animals were significantly higher in the CCU than in the sham group ($p < 0.001$). Pro-inflammatory cytokine levels were significantly lower in the TCCU than in the CCU group ($p < 0.001$). TNF- α and IL-1 β levels between the TCCU and SG groups were significantly different ($p < 0.001$, $p = 0.025$, respectively), whereas IL-6 levels showed similar values ($p = 0.184$).

TP I and CK-MB levels in blood serum

TPI and CK-MB levels in blood serum were significantly higher in the CCU group than in the sham group ($p < 0.001$). TPI and CK-MB levels in the TCCU group significantly decreased compared to those in the CCU group ($p < 0.001$). There was no significant difference in TPI and CK-MB levels between the SG and TCCU groups ($p = 0.238$; $p = 0.550$) (Table 1).

DISCUSSION

This study investigated the effect of TPP against oxidative brain and heart damage resulting from experimentally induced common carotid artery occlusion in rats using biochemical methods. The literature indicates that reversing cerebral blood flow during reperfusion after ischemia increases ROS levels²¹. Numerous studies have reported that brain damage resulting from I/R can impact distant tissues, including the heart^{22,23}. Although many different mechanisms are responsible for the pathogenesis of distant tissue damage, it has been well established that ROS generation is one of the most frequently observed mechanisms²⁴. ROS react with unsaturated fats in biological membranes to form MDA, the end product

of lipid peroxidation (LPO)²⁵. MDA is a biological sign of tissue damage and one of the most significant markers of oxidative damage²¹. Therefore, our study assessed MDA levels in brain and cardiac tissues using our I/R model induced by the common carotid artery occlusion method in rats. Our experimental findings demonstrated a significant increase in MDA levels in the brain and heart tissues of rats in the cerebral I/R group compared to the sham group. The literature suggests that increased MDA levels in the brain due to cerebral I/R are associated with neuronal damage^{21,26}. Ojo *et al.* demonstrated that brain tissue damage impacted heart tissue in an I/R model created by bilateral carotid artery occlusion/reperfusion in rats²⁴. They reported cerebral ischemia induces LPO through increased ROS production in cardiac tissue, leading to oxidative damage. Our findings and existing data indicate that cerebral I/R injury increases ROS, affecting cardiac tissue.

Conversely, in our study, the administration of TPP to rats significantly suppressed the I/R-induced increase in MDA levels in both brain and heart tissues. To our knowledge, our study is the first to examine the protective effect of TPP against cardiac damage caused by common carotid artery occlusion. Yasar *et al.* reported that brain damage caused by focal I/R²⁷, and Polat *et al.* reported that doxorubicin-induced cardiac toxicity¹⁸, TPP has a protective effect against significantly decreasing the increased MDA level. Our experimental results and existing literature data suggest that TPP protects the heart from oxidative damage by significantly reducing LPO during cerebral I/R, owing to its antioxidant properties.

Excessive ROS production during cerebral I/R causes cell damage by surpassing the capacity of endogenous antioxidants^{21,28}. Endogenous antioxidants, such as GSH, are responsible for defense against ROS and are crucial in protecting brain and heart tissues against I/R injury^{29,30}. GSH is an important antioxidant enzyme that protects cells from

superoxide and hydroxyl radicals^{29,31}. Studies have associated decreased GSH levels resulting from cerebral I/R with increased LPO³². Sharipov *et al.* reported oxidative damage in the heart mitochondria of rats in the brain focal I/R model due to an increase in superoxide and hydroxyl radicals³³. However, it was emphasized that decreased GSH levels in cardiac tissue were associated with increased MDA levels following cerebral I/R in rats²⁴. Our findings demonstrate reduced tGSH levels in both brain and heart tissue, consistent with the literature. This suggests that tGSH cannot counteract the elevated ROS levels of I/R. However, TPP significantly suppressed the I/R injury-related decrease in tGSH levels in the brain and heart tissues of rats, which is consistent with previous findings^{18,30} demonstrating that TPP prevents the reduction in GSH levels, exerts antioxidant effects, and thereby protects heart and brain tissues against oxidative damage. Our findings suggest that TPP protects against distant cardiac tissue damage due to cerebral I/R by inhibiting LPO and preserving the antioxidant system.

Ischemia, followed by reperfusion, disrupts the redox balance in favor of pro-oxidants and prompts the release of pro-inflammatory cytokines such as TNF- α , IL- β , and IL-6³⁴. Existing studies indicate that TNF- α is the primary cytokine responsible for stimulating the synthesis of cytokines, such as IL- β and IL-6, during cerebral I/R.^{35,36} TNF- α and interleukins released due to microglia and astrocyte activation exacerbate neuroinflammation, causing secondary I/R damage in distant tissues, such as the heart, ultimately leading to cell death²⁴. Consistent with the literature, cerebral I/R significantly increased TNF- α , IL-1 β , and IL-6 levels in both brain and distant cardiac tissues in our study. Our findings suggest that I/R injury begins with oxidative stress and persists due to inflammation. We examined the impact of TPP on inflammation and observed that

TPP significantly prevented the increase of TNF- α , IL-1 β , and IL-6 levels in both brain and heart tissues. While the study by Yasar *et al.*²⁷ showed that TPP significantly suppressed increased TNF- α and IL-1 β levels due to focal I/R injury, there is no study showing the protective effect of TPP against distant cardiac tissue damage induced by I/R injury resulting from bilateral common carotid artery occlusion.

The bilateral common carotid artery occlusion procedure led to an increase in serum TPI and CK-MB levels. The significant increase in TPI and CK-MB levels explains heart tissue damage and reflects the impact of the brain I/R event on the heart tissue. In the literature, abnormal elevation of TPI and CK-MB levels has been associated with myocardial ischemia and hypoxia¹³. Furthermore, increased TPI and CK-MB levels correlate positively with increased oxidants and pro-inflammatory cytokines¹⁴. The results of the current experimental study align with another study³⁷, showing that TPI and CK-MB are associated with increased oxidative and pro-inflammatory cytokines.

In our study, bilateral common carotid artery occlusion increased pro-inflammatory cytokine levels in cardiac and brain tissue, accompanied by increased oxidants and decreased antioxidants. Furthermore, TPP protects the brain and distant cardiac tissues against oxidative and inflammatory damage induced by cerebral I/R. This is the first study to demonstrate the effect of TPP against distant tissue heart damage caused by cerebral I/R injury. However, the current study suggests that TPP administration reduces cardiac damage. The most significant limitations of this study include the absence of common carotid occlusion monitoring and the lack of histopathological examinations. Further studies are necessary to clarify the role of TPP in preventing cerebral I/R injury and its protective effects on distant tissue damage.

ACKNOWLEDGMENTS

Thanks to Taha Abdulkadir Coban for the biochemical analysis of data.

Conflict of interest

None.

ORCID number of authors

- Izzet Emir (IE):
0000-0002-1098-4889
- Zeynep Suleyman (ZS):
0000-0003-0128-7990
- Halis Suleyman (HS):
0000-0002-9239-4099

Participation of authors

Conception and design: IE, HS; Acquisition of data: TAC; Analysis and interpretation of data: ZS; Drafting of the manuscript: IE, HS; Critical revision of the manuscript for important intellectual content: HS; Statistical analysis: ZS; Final approval of the submitted manuscript: IE, ZS, HS, TAC.

REFERENCES

1. **Benes V3rd, Bradac O, Horvath D, Suchomel P, Benes VJr.** Surgery of acute occlusion of the extracranial internal carotid artery - a meta-analysis. *Vasa*. 2020;49(1): 6-16. doi: 10.1024/0301-1526/a000801
2. **Dossabhoy S, Arya S.** Epidemiology of atherosclerotic carotid artery disease. *Semin Vasc Surg*. 2021;34(1):3-9. doi: 10.1053/j.semvascsurg.2021.02.013
3. **Sirimarco G, Amarenco P, Labreuche J, Touboul PJ, Alberts M, Goto S, Rother J, Mas JL, Bhatt DL, Steg PG; REACH Registry Investigators.** Carotid atherosclerosis and risk of subsequent coronary event in outpatients with atherothrombosis. *Stroke*. 2013;44(2): 373-379. doi: 10.1161/STROKEAHA.112.673129
4. **Hsu JC, Tsai HL.** Endovascular recanalization of common carotid artery Total occlusion: two case reports and literature review. *CVIR Endovasc*. 2020;3(1): 6. doi: 10.1186/s42155-020-0097-6.
5. **Kragsterman B, Bergqvist D, Siegbahn A, Parsson H.** Carotid endarterectomy induces the release of inflammatory markers and the activation of coagulation as measured in the jugular bulb. *J Stroke Cerebrovasc*. 2017;26(10): 2320-2328. doi: 10.1016/j.jstrokecerebrovasdis.2017.05.020.
6. **Cho HJ, Kim YJ, Lee JH, Choi JW, Moon WJ, Roh HG, Chun YI, Kim HY.** Post-carotid stenting reperfusion injury with blood-brain barrier disruption on gadolinium-enhanced FLAIR MRI. *BMC Neurol*. 2014;14: 178. doi: 10.1186/s12883-014-0178-8
7. **Kalimeris K, Kouni S, Kostopanagiotou G, Nomikos T, Fragopoulou E, Kakisis J, Vasdekis S, Matsota P, Pandazi A.** Cognitive function and oxidative stress after carotid endarterectomy: comparison of propofol to sevoflurane anesthesia. *J Cardiothor Vasc An*. 2013;27(6): 1246-1252. doi: 10.1053/j.jvca.2012.12.009
8. **Blaisdell FW.** The pathophysiology of skeletal muscle ischemia and the reperfusion syndrome: a review. *Cardiovasc Surg*. 2002;10(6): 620-630. doi:10.1016/s0967-2109(02)00070-4.
9. **Katzen BT, MacLean AA.** Complications of endovascular repair of abdominal aortic aneurysms: a review. *Cardiovasc Intervent Radiol*. 2006;29(6): 935-946. doi: 10.1007/s00270-005-0191-0
10. **Onk D, Coskun R, Onk OA, Cimen FK, Kurt N, Suleyman B, Mammadov R, Altuner D, Gul V, Malkoc I, Bilgin AO, Suleyman H.** The effect of esomeprazole on postoperative pain and lung and heart complications in rats. *Lat Am J Pharm*. 2018;37(6):1182-1191.
11. **Yu Y, Cui WH, Cheng C, Lu Y, Zhang Q, Han RQ.** Association between neutrophil-to-lymphocyte ratio and major postoperative complications after carotid endarterectomy: A retrospective cohort study. *World J Clin Cases*. 2021;9(35):10816-10827. doi: 10.12998/wjcc.v9.i35.10816
12. **Godet G, Bernard JM, Bertrand M, Fusciardi J, Kieffer E, Coriat P, Petitjean C,**

- Viars P. Hemodynamic effect of the clamping of the carotid in the surgically treated coronary patient. *Ann Fr Anesth Reanim.* 1986;5(5): 473-478. doi: 10.1016/s0750-7658(86)80031-4.
13. Cordwell SJ, Edwards AVG, Liddy KA, Moshkanbaryans L, Solis N, Parker BL, Yong ASC, Wong C, Kritharides L, Hambly BD, White MY. Release of tissue-specific proteins into coronary perfusate as a model for biomarker discovery in myocardial ischemia/reperfusion injury. *J Proteome Res.* 2012;11(4): 2114-2126. doi: 10.1021/pr2006928.
 14. Mahmoud KM, Ammar AS. Effect of N-acetylcysteine on cardiac injury and oxidative stress after abdominal aortic aneurysm repair: A randomized controlled trial. *Acta Anaesth Scand.* 2011;55(8): 1015-1021. doi: 10.1111/j.1399-6576.2011.02492.x.
 15. Sica DA. Loop diuretic therapy, thiamine balance, and heart failure. *Congest Heart Fail.* 2007;13(4): 244-247. doi: 10.1111/j.1527-5299.2007.06260.x.
 16. Rindi G, Patrini C, Laforenza U, Mandel H, Berant M, Viana MB, Poggi V, Zarra AN. Further studies on erythrocyte thiamin transport and phosphorylation in seven patients with thiamin-responsive megaloblastic anaemia. *J Inherited Metab Dis;*17(6):667-677. doi: 10.1007/BF00712009.
 17. Ozer M, Ince S, Gundogdu B, Aktas M, Uzel K, Gursul C, Suleyman H, Suleyman Z. Effect of thiamine pyrophosphate on cyclophosphamide-induced oxidative ovarian damage and reproductive dysfunction in female rats. *Adv Clin Exp Med.* 2022;31(2): 129-137. doi: 10.17219/acem/142535.
 18. Polat B, Suleyman H, Sener E, Akeay F. Examination of the effects of thiamine and thiamine pyrophosphate on doxorubicin-induced experimental cardiotoxicity. *J Cardiovasc Pharmacol Ther.* 2015;20(2):221-229. doi: 10.1177/1074248414552901.
 19. Kurt A, Isaoglu U, Yilmaz M, Calik M, Polat B, Hakan H, Ingec M, Suleyman H. Biochemical and histological investigation of famotidine effect on postischemic reperfusion injury in the rat ovary. *J Pediatr Surg.* 2011;46(9): 1817-1823. doi: 10.1016/j.jpedsurg.2011.04.092.
 20. Bradford MM. A rapid and sensitive method for the quantitation of microgram quantities of protein utilizing the principle of protein-dye binding. *Anal Biochem.* 1976;72:248-254.
 21. Ozoner B, Yuceli S, Aydin S, Yazici GN, Sunar M, Arslan YK, Coban TA, Suleyman H. Effects of pycnogenol on ischemia/reperfusion-induced inflammatory and oxidative brain injury in rats. *Neurosci Lett.* 2019;704:169-175. doi: 10.1016/j.neulet.2019.04.010.
 22. Frick T, Springe D, Grandgirard D, Leib SL, Haenggi M. An improved simple rat model for global cerebral ischemia by induced cardiac arrest. *Neurol Res.* 2016;38(4): 373-380. doi: 10.1179/1743132815Y.0000000090.
 23. Wang R, Liu YY, Liu XY, Jia SW, Zhao J, Cui D, Wang L. Resveratrol protects neurons and the myocardium by reducing oxidative stress and ameliorating mitochondria damage in a cerebral ischemia rat model. *Cell Physiol Biochem.* 2014;34(3): 854-864. doi: 10.1159/000366304.
 24. Ojo OB, Grace Boluwatife Olagunju, Olajide AO, Jegede ME, Fakorede AS, Crown OO, Olaleye MT, Akinmoladun AC. Spondias mombin leaf extract ameliorates cerebral ischemia/reperfusion-induced cardiohepatorenal oxidative stress in rats. *Phytomedicine Plus.* 2022;2(1): 100196. doi: 10.1016/j.phyplu.2021.100196.
 25. Chen CH, Hsieh CL. Effect of acupuncture on oxidative stress induced by cerebral ischemia-reperfusion injury. *Antioxidants-Basel.* 2020;9(3)248. doi: 10.3390/antiox9030248.
 26. Su D, Li P, Wang X, Zhang W, Zhang YD, Wu CC, Zhang W, Li Y, Tai WJ, Tang B. Observing malondialdehyde-mediated signaling pathway in cerebral ischemia reperfusion injury with a specific nanolight. *Anal Chem.* 2020;92(3): 2748-2755. doi: 10.1021/acs.analchem.9b05008
 27. Yasar H, Demirdogun F, Suleyman B, Mammadov R, Altuner D, Coban TA, Bu-

- lut S, Gursul C, Suleyman H. Effect of thiamine pyrophosphate upon oxidative brain injury induced by ischemia-reperfusion in rats. *Int J Pharmacol.* 2023;19(2): 277-285. doi: 10.3923/ijp.2023.277.285
28. Jurcau A, Ardelean AI. Oxidative stress in ischemia/reperfusion injuries following acute ischemic stroke. *Biomedicines.* 2022;10(3):574. doi: 10.3390/biomedicines10030574
29. Higashi Y, Aratake T, Shimizu T, Shimizu S, Saito M. Protective role of glutathione in the hippocampus after brain ischemia. *Int J Mol Sci.* 2021;22(15): 7765. doi: 10.3390/ijms22157765.
30. Goshovska YV, Fedichkina RA, Balatskyi VV, Piven OO, Dobrzyn P, Sagach VF. Induction of glutathione synthesis provides cardioprotection regulating no, ampk and ppara signaling in ischemic rat hearts. *Life (Basel).* 2021;11(7): 631 doi: 10.3390/life11070631.
31. He L, He T, Farrar S, Ji LB, Liu TY, Ma X. Antioxidants maintain cellular redox homeostasis by elimination of reactive oxygen species. *Cell Physiol Biochem* 2017;44(2): 532-553. doi: 10.1159/000485089
32. Wang T, Chen HB, Xia SY, Chen XF, Sun H, Xu ZX. Ameliorative effect of parishin c against cerebral ischemia-induced brain tissue injury by reducing oxidative stress and inflammatory responses in rat model. *Neuropsych Dis Treat.* 2021;17:1811-1823. doi: 10.2147/NDT.S309065.
33. Sharipov RR, Kotsiuruba AV, Kop'riak BS, Sahach VF. Induction of oxidative stress in heart mitochondria in brain focal ischemia-reperfusion and protective effect of ecdysterone. *Fiziol Zh* 1994. 2014;60(3): 11-17.
34. Turan MI, Cayir A, Cetin N, Suleyman H, Siltelioglu Turan I, Tan H. An investigation of the effect of thiamine pyrophosphate on cisplatin-induced oxidative stress and DNA damage in rat brain tissue compared with thiamine: thiamine and thiamine pyrophosphate effects on cisplatin neurotoxicity. *Hum Exp Toxicol.* 2014;33(1): 14-21. doi: 10.1177/0960327113485251.
35. Jurcau A, Simion A. Neuroinflammation in cerebral ischemia and ischemia/reperfusion injuries: from pathophysiology to therapeutic strategies. *Int J Mol Sci.* 2021;23(1): 14. doi 10.3390/ijms23010014.
36. Zhu H, Hu S, Li Y, Sun Y, Xiong X, Hu X, Chen J, Qiu S. Interleukins and ischemic stroke. *Front Immunol.* 2022;13:828447. doi: 10.3389/fimmu.2022.828447.
37. Liu SZ, He Y, Shi J, Liu LL, Ma H, He L, Guo YQ. Allicin attenuates myocardial ischemia reperfusion injury in rats by inhibition of inflammation and oxidative stress. *Transpl P.* 2019;51(6): 2060-2065. doi: 10.1016/j.transproceed.2019.04.039.

Mechanisms of programmed cell death: structural and functional pathways. A narrative review.

Diego Fernández-Lázaro^{1,2,3}, Begoña Sanz^{4,5} and Jesús Seco-Calvo^{3,4,6}

¹Department of Cellular Biology, Genetics, Histology and Pharmacology, Faculty of Health Sciences, University of Valladolid, Campus of Soria, Soria, Spain.

²Neurobiology Research Group, Faculty of Medicine, University of Valladolid, Valladolid, Spain.

³SARCELLOMICS® Research Group, León, Spain.

⁴Department of Physiology, University of the Basque Country, Leioa, Spain.

⁵Biocruces Bizkaia Health Research Institute, Barakaldo Spain.

⁶Institute of Biomedicine, University of León, León, Spain.

Keywords: apoptosis; caspases; mitochondrial/intrinsic pathway; extrinsic pathway; necroptosis; autophagy.

Abstract. Apoptosis, necroptosis, and autophagy are cellular mechanisms by which cells are programmed to die under various physiological and developmental stimuli. A multitude of protein mediators of programmed cell death have been identified, and apoptosis, necroptosis, and autophagy signals have been found to utilize common pathways that elucidate the proteins involved. This narrative review focuses on caspase-dependent and caspase-independent programmed cell death systems. Including studies of caspase-dependent programmed cell death, extrinsic pathway apoptotic mechanisms, phosphatidylserine (PS), FAS (APO-1/CD95), tumor necrosis factor (TNF) receptor type 1 (TNF-R1) and TNF-related apoptosis-inducing ligand (TRAIL), and intrinsic or mitochondrial pathway such as cytochrome C, the Bcl-2 family of proteins and Smac/Diablo. The Bcl-2 family has apoptotic mediators Bcl-2-associated X protein (Bax) and Bcl-2 homologous antagonist/killer (Bak), Bcl-2-interacting protein BIM (Bim), Bcl-2 agonist of cell death (Bad), Bid, Bcl-2 adenovirus E1B 19kDa-interacting protein 1 NIP3 (Bnip3), BMF, HRK, Noxa and PUMA and antiapoptotic proteins such as Bcl-2 itself, Mcl-1, Bcl-w, A1, and Bcl-XL. Moreover, caspase-independent programmed cell death pathways include the mitochondrial pathway with the protein mediators apoptosis inducing factor (AIF) and endonuclease G, and the pathways necroptosis, and autophagy. Understanding programmed cell death from those reported in this review could shed substan-

tial light on the processes of biological homeostasis. In addition, identifying specific proteins involved in these processes is mandatory to identify molecular biomarkers and therapeutic targets. Furthermore, it could provide the ability to modulate the programmed cell death response and could lead to new therapeutic interventions in a disease.

Mecanismos de muerte celular programada: vías estructurales y funcionales. Una revisión narrativa.

Invest Clin 2024; 65 (2): 230 – 252

Palabras clave: apoptosis; caspasas; vía mitocondrial/intrínseca; vía extrínseca; necroptosis; autofagia.

Resumen. La apoptosis, la necroptosis y la autofagia son mecanismos celulares mediante los cuales las células se programan para morir bajo una amplia gama de estímulos fisiológicos. Esta revisión describe en los sistemas de muerte celular programada dependientes e independientes de la caspasa. Los estudios incluidos sobre la muerte celular programada dependiente de la caspasa incluyen mecanismos apoptóticos de la vía extrínseca que incluyen fosfatidilserina (PS), FAS (APO-1/CD95), receptor del factor de necrosis tumoral (FNT) tipo 1 (FNT-R1) e inductor de la apoptosis relacionada con ligando FNT (TRAIL) y vía intrínseca o mitocondrial como el citocromo C, la familia de proteínas Bcl-2 y Smac/Diablo. La familia Bcl-2 tiene mediadores apoptóticos, proteína X asociada a Bcl-2 (Bax) y antagonista/asesino homólogo de Bcl-2 (Bak), proteína BIM que interactúa con Bcl-2 (Bim), agonista de la muerte celular de Bcl-2 (Bad), Bid, proteína 1 que interactúa con el adenovirus E1B 19kDa de Bcl-2, NIP3 (Bnip3), BMF, HRK, Noxa y PUMA y proteínas antiapoptóticas como la propia Bcl-2, Mcl-1, Bcl-w, A1 y Bcl-XL. Además, las vías de muerte celular programada independientes de la caspasa incluyen la vía mitocondrial con los mediadores proteicos factor inductor de apoptosis (FIA) y endonucleasa G, las vías necroptosis y autofagia. Comprender la muerte celular programada a partir de los contenidos descritos en esta revisión podría arrojar luz sustancial sobre los procesos de la homeostasis biológica y podría proporcionar la capacidad de modular la respuesta de muerte celular programada y conducir a nuevas intervenciones terapéuticas en una amplia gama de enfermedades.

Received: 19-10-2023

Accepted: 18-11-2023

INTRODUCTION

Every hour, billions of cells die in us, and our tissues do not shrink because of a natural regulation whereby cell death is balanced by cell division. It is necessary to

control both death and cell division in differentiated cells to balance the different cell populations, avoiding affecting the adjacent cells¹.

The process in which cells eliminate themselves in a controlled manner is called

programmed cell death. Programmed cell death plays an important role during embryonic development, maintaining tissue homeostasis in the body and eliminating damaged cells ². In contrast, excessive or defective cell death contributes to a broad spectrum of human pathologies. Low-rate cell death can result in the formation of cancer and autoimmune diseases ³, whereas high-rate cell death can result in neurodegenerative disease, immunodeficiency, or muscle atrophy ⁴.

Knowledge of specific/differential proteomic expression in each cell death is essential for the early detection, diagnosis, and prognosis of cell-death-related diseases. This knowledge is also crucial for the use of more precise and personalized pharmacological treatments ⁵. Cell death can be divided into three groups: programmed, regulated, and accidental ⁶. Programmed cell death is present in embryonic development and tissue homeostasis, such as apoptosis and necroptosis. Regulated cell death is that which, programmed or not, can be induced or inhibited by a specific molecular mechanism through pharmacology or genetic interventions, for example, the release of neutrophil extracellular traps (NETs), a regulated form of neutrophil cell death known as NETosis, modulates neutrophil toxic effects. Accidental cell death is triggered by external physical conditions, such as ischemia, freeze-thaw cycles, or high concentrations of pro-oxidants, an example of this type of death are oncosis and necrosis ⁶. Two mechanisms of programmed cell death are distinguished: apoptotic cell death, dependent on caspases such as extrinsic and intrinsic apoptosis, and non-apoptotic cell death, independent of caspases, such as autophagy and necroptosis ⁷.

MATERIALS AND METHODS

Search strategy

The present study is a narrative literature review comprising scientific studies conducted between May and July 2023

that sought to group and describe caspase-dependent and caspase-independent programmed cell death, describing the molecular mechanisms of apoptosis, necroptosis, and autophagy. The bibliographic search was carried out in the following electronic databases: Medline (PubMed), Sci-ELO, Scopus, Science Direct, Cinahl, EMBASE - Excerpta Medica Data Base, LILACS, Google Scholar, Dialnet, and Cochrane Library Plus. The keywords used for the search were: programmed cell death, apoptosis, caspases, caspase inhibitory proteins, mitochondrial / intrinsic pathway, extrinsic pathway, necroptosis, autophagy, phosphatidylserine, FAS (APO-1/CD95), tumor necrosis factor (TNF) receptor type 1 (TNF-R1) and TNF-related apoptosis-inducing ligand (TRAIL) and cytochrome C, linked by the Boolean operators “AND” and “OR”. Additional records were gleaned by conducting a ‘snowball’ search, checking the reference lists of publications eligible for full-text review, and using ResearchGate to identify potential articles not included in the databases used in the study.

Inclusion and exclusion criteria

The following inclusion criteria were applied to select the articles: (1) Access to the full text; (2) be a review, clinical trial, observational study, or case report/study; (3) identify caspase-dependent and caspase-independent programmed cell death; (4) describe the molecular mechanisms of apoptosis, necroptosis, and autophagy; (5) studies whose publication date is from the beginning of the databases until July 2023; (6) languages were restricted to English, German, French, Italian, Spanish, and Portuguese. The exclusion criteria applied were: (1) Publications not related to programmed cell death and/or describe its molecular mechanisms; (2) duplicate documents.

Data extraction

After searching the databases for studies, the search titles were checked to identify duplicates and possible publications to

add. After reading the abstract, a full-text review of the selected studies was performed. Two reviewers (D.F.-L. and J.S.-C.) scrutinized and synthesized data from all selected studies into a comprehensive table using a standardized data extraction. A third reviewer (B.S.) resolved all disagreements between them.

RESULTS AND DISCUSSION

Programmed Cell death

Apoptotic cell death functions individually and selectively and is executed through a highly stereotyped series of biochemical events that ensure rapid non-inflammatory cell elimination. For this reason, the apoptotic physiological process is produced and characterized by decreased cell size, vesicle formation, and condensation of the nucleus. This series of transformations regulates the control of morphogenesis and organogenesis during embryonic development, in addition to tissue homeostasis in adult organisms⁸.

Non-apoptotic cell death is usually described as a secondary mechanism for deficient apoptotic conditions. However, it is also possible that non-apoptotic programmed cell death mechanisms may function in first-order lines; for example, autophagic cell death is carried out during metamorphosis in insects. This autophagic cell death eliminates a tissue in its entirety⁹.

In 1972, Kerr *et al.*⁸ coined the term apoptosis to differentiate it from the death of natural origin, necrosis. The word comes from Greek, which refers to the leaves that fall from the trees or the petals that fall from the flowers. The prefix apo means “distance, outside or part” and ptosis “fall,” which literally means “fall from”. Apoptosis is associated with caspases, a family of cysteine proteases that control not only apoptosis but also proliferation, differentiation, cell shape, and cell migration.

Apoptosis is a form of programmed cell death¹⁰, which occurs because of tissue and cell aging or in response to different external

agents such as ionizing radiation and chemotherapeutic agents¹⁰. It can be considered a process that facilitates the elimination of defective cells, so the alteration in the regulation of genes involved in cell death by apoptosis can cause and be associated with the development of different neoplasms, autoimmune diseases, viral infections, and neurodegenerative diseases¹¹. Apoptosis is an active process where the cells react and execute their death, programmed, by themselves¹⁰. Apoptotic death is considered when a cell has lost its individuality or reached a “point of no return” at which the cell definitively loses its function. Apoptotic cell death triggers two stages. In the first stage, biochemical mediators attempt to repair a damaged cell. If they fail, the cell enters the second stage or execution phase, where structural changes occur that lead the cell to death¹². These structural changes affect the cell membrane, intracytosolic organelles, and the nucleus⁸. The cytoskeleton collapses, the nuclear envelope disassembles, redistributing the nuclear pores, the nuclear protein is altered, and the nuclear chromatin condenses and fragments, becoming dense clumps, with an electrophoretic “ladder” pattern, which migrate towards the nuclear membrane that shapes. DNA and RNA cleavage, due to the activation of Ca^{2+} and Mg^{2+} dependent endonucleases that cleave genomic DNA through the internucleosomal spaces¹³. Also in the mitochondria, DNA degrades, and the endoplasmic reticulum loses its envelope; its cisterns widen and fuse¹⁰. The phospholipids of the cell membrane change orientation and the phosphatidylserine residues are exposed to the external environment; the fragmentation of the phospholipids is induced because of these disruptions, the integrity of the plasma membrane is lost, and the mitochondrial membrane potential decreases. On the surface of the plasma membrane, fragments of membrane-enclosed cytoplasm called apoptotic bodies protrude and are shed, which are cytoplasmic remnants surrounded by a membrane

such that they are rapidly engulfed by an adjacent cell or macrophage when released into the external environment, without causing an inflammatory response^{12,14,15}.

Caspases

Cysteine aspartate-specific proteases (Caspases, EC 3.4.22.-) are synthesized as inactive 30-50 kDa precursors (zymogens) that have three domains: an amino-terminal domain (prodomain), a domain that will result in a large subunit (p20) containing the active site, and another domain that will end in a smaller subunit catalyst (p10) C-terminus¹⁶ (Fig. 1). In the presence of appropriate stimuli, a proteolysis process occurs between the domains, generating the active fragments. There are two types of caspases: initiator caspases (Caspase-2, 8, 9, and 10) that are activated in response to signs of stress or cell damage and that protect and activate effector caspases (Caspase-3, 6, and 7), these will oversee the direct proteolysis of different substrates that will lead to the death of the cell. One of their first identified substrates was Poly ADP-ribose polymerase (PARP)^{17,18}.

Initiator caspases present in their N-terminal region one or two essential adapter domains for their function. In contrast, effector caspases do not have these domains. There are two fundamental ways caspases can

be activated (intrinsic and extrinsic pathways of caspase-dependent apoptosis), but although both pathways converge on effector caspases, they require different caspases to initiate the process. Thus, the activation of the extrinsic pathway mainly causes the recruitment of Caspase-8, and the intrinsic pathway principally causes the recruitment of Caspase-9^{18,19}.

During the process of apoptosis, there is a massive activation of caspases, which specifically cut proteins in cysteine residues located near aspartic acid. Caspases initiate a cascade of events that converge into a common effector caspase pathway that leads to the execution of apoptosis^{12,20}. The apoptotic machinery of the cytoskeleton has inactive precursors or initiating procaspases⁸⁻¹⁰ that are activated by proteolytic cleavage and are catalyzed by other already active caspases; here, the process remains reversible. When activated, the initiator procaspases and cell-specific target proteins cleave and activate the executor procaspases (3, 6, and 7). From Caspase-3, the process is irreversible^{17,19}.

Apoptosis constitutes a complex series of positive and negative events with multiple positive and negative regulators and is integrated into other critical intracellular pathways such as cell cycle progression, phosphorylation-mediated signals, and DNA

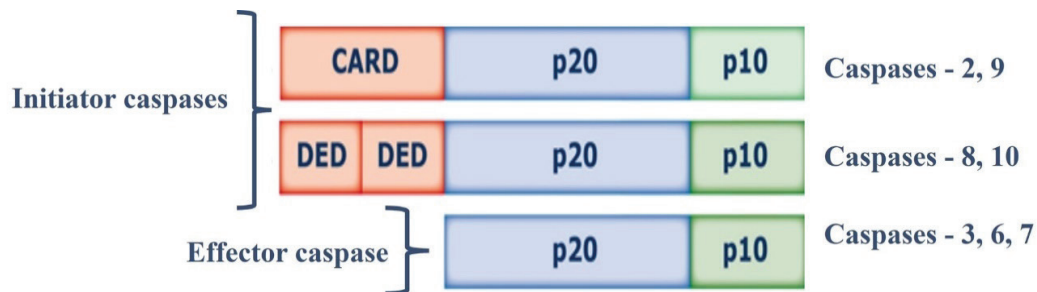


Fig. 1. Structure of Caspases.

CARD: caspase recruitment and activation domain; DED: Death Effector Domain; p20: large subunit (p20); p10: small subunit (p10).

Caspases contain three domains: an N-terminal prodomain, a large subunit (p20) containing the active center with cysteine within a conserved QACXG motif, and a small subunit (p10) at the C-terminus.

damage repair⁶. Apoptosis is carried out mainly by two alternative pathways of apoptosis induction divided into i) apoptosis mediated by death receptors expressed on the cell surface or extrinsic pathway; ii) apoptosis mediated by the mitochondrial or intrinsic pathway¹⁸. Signaling by both pathways induces the activation of caspases, and each pathway uses its own initiator caspases and activation complex^{12,20}.

Inhibitors of Apoptosis Proteins (IAPs)

Inhibitors of apoptosis proteins (IAPs) could inhibit apoptosis by selectively binding and inhibiting Caspase-3 and Caspase-7, but not Caspase-8. IAPs block the caspase cascade and inhibit cell death in response to proapoptotic stimuli²¹. There are currently eight protein members of this family, but two of them, survivin and X-linked inhibitor of protein apoptosis (XIAP), are particularly interesting. In this sense, survivin is the only IAP associated with the mitotic spindle²². Its expression depends on the cell cycle²³. It has a double function since it inhibits apoptosis through direct and indirect interaction with caspases and regulates the cell cycle²⁴. Survivin is expressed in embryonic tissue and is overexpressed in tumor cells, associated with resistance to chemotherapy, but not in normal adult tissues^{24,25}. XIAP is possibly the best-studied IAP both at the structural level and at the level of its mechanism of action²⁶.

Furthermore, XIAP is the only member of this family that can inhibit both effector and initiator caspases. XIAP is frequently elevated in tumor cells, leading to resistance to chemotherapy²⁵. Therefore, XIAP is an optimal therapeutic target based on its functions; moreover, the inhibition of XIAP restores cellular chemosensitivity^{27,28}.

Caspase-dependent pathways of apoptosis

Extrinsic pathway: recipients of death

The extrinsic pathway is activated by ligands of the family of Tumor necrosis factor (TNF) proteins. Some ligands can induce

apoptosis; when they bind to their receptors, they trigger caspase activation and initiate apoptosis²⁹. Death receptors are characterized by having cysteine-rich extracellular domains. They all have in common a death domain (DD) domain in the cytoplasmic region. In general, the binding of ligands to death receptors induces their trimerization, and subsequently, the DD domains recruit adapter molecules that will activate Caspase-8 and, when activated, activate Caspase-3³⁰. Extrinsic apoptosis is related to death receptors on the plasma membrane, such as phosphatidylserine (PS), FAS (APO-1/CD95), TNF receptor type 1 (TNF-R1), and TNF-related apoptosis-inducing ligand (TRAIL)³¹.

Phosphatidylserine (PS)

In cells, the negatively charged PS is only localized to the cytosolic side of the lipid bilayer of the plasma membrane, but when it is translocated to the outer monolayer of the cell, it acts as an “eat me” signal, so it is considered as a marker of extrinsic apoptosis. In addition to expressing signals on the cell surface that stimulate apoptosis, PS also blocks inflammation in the phagocytic cell by inhibiting the production of cytokines proinflammatory signaling proteins³². It must be considered that apoptotic cells must not only activate the signals that induce cell death but also inactivate or lose the death signals¹².

Fas (APO-1/CD95)

Fas (APO-1 / CD95) is ubiquitously expressed on the cell's surface as a membrane protein of 40 kDa, which is highly expressed in T lymphocytes and activated natural killer (NK) cells³³. The activation of Fas at the cell surface is done by binding the Fas ligand (FasL) to the surface of a cytotoxic lymphocyte. The death domains of the cytosolic tails of Fas death receptors recruit adapter proteins, which in turn recruit procaspase initiators such as procaspase-8, procaspase-10, or both, forming the death-inducing signal-

ing complex (DISC)³⁴. In practice, once activated in the DISC, the initiator caspases activate the next executor procaspases in the cascade, inducing apoptosis. This pathway begins with the formation of the DISC in which an adapter molecule called Fas associated death domain (FADD) and procaspase-8 intervene. FADD binds to Fas through their respective DD domains and to procaspase-8 through a death effector domain (DED). The oligomerization of procaspase-8 in the DISC complex results in the activation of Caspase-8 and subsequent activation of other caspases. Depending on the cell type, Caspase-8 can directly activate Caspase-3 or proteolyze the carboxy-terminus of BH3 interacting domain death agonist (Bid), a proapoptotic protein from the Bcl-2 family. Translocation of the truncated form of Bid into the mitochondria will activate the mitochondrial pathway^{35,36} (Fig. 2).

The Fas / Fas ligand (FasL) system participates in the elimination of T and B lymphocytes, viruses-infected cells, and cancer cells. Doxorubicin and methotrexate (cytotoxic agents) or immunomodulatory drugs (IMiDs) activate this pathway to achieve cell death in malignant cells in cancer disease³⁷.

Furthermore, FasL can also interact with the DcR receptor, a soluble secreted receptor of the TNF superfamily. Some cells produce “decoy” receptors on the cell surface with a ligand-binding domain but no death domain; therefore, they can bind to a death ligand but do not trigger apoptosis. When FasL binds to DcR3, it inhibits FasL/Fas apoptotic activity, thus acting as a “decoy.” Cells can also produce intracellular blocking proteins such as FADD-like IL-1 β -converting enzyme (FLICE)-inhibitory protein (FLIP), which resembles procaspase but lacks a proteolytic domain; FLIP competes

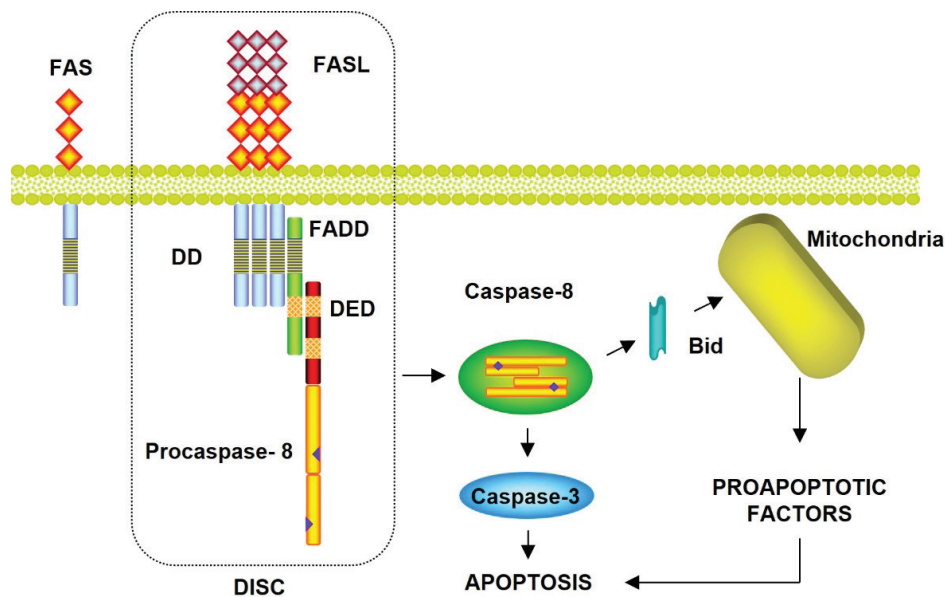


Fig. 2. Extrinsic apoptotic pathway by FAS cell death receptors.

FAS is a cell surface receptor that, when binding to its ligand, causes apoptosis. (APO-1/CD95); FASL: Fas ligand; FADD: Fas Associated Death Domain; DD: Death Domain; DED: Death Effector Domain; DISC: Death-Inducing Signaling Complex; Bid: BH3 Interacting Domain Death Agonist Protein.

Diagram of apoptotic signals of the extrinsic pathway: mediated by FAS receptors of cell death. Caspase-8 can directly activate Caspase-3 or proteolyze the carboxy-terminal end of Bid, a proapoptotic protein of the Bcl-2 family. The translocation of the truncated form of Bid to the mitochondria will activate the mitochondrial pathway.

with procaspases-8 and 10 for binding sites on DISC and thus inhibits the activation of these initiating procaspases^{38,39}.

Tumor necrosis factor (TNF) receptor type 1

Tumor necrosis factor- α (TNF- α) is a type II transmembrane protein that mediates the inflammatory response, regulation of immune cells, and cytotoxicity. TNF- α binds to tumor necrosis factor receptor 1 (TNF-R1), also known as death receptor 1 (DR1), and tumor necrosis factor receptor 2 (TNF-R2). TNFR1 and TNFR2 are involved in pro-survival signaling and proliferation by activating the nuclear factor kappa B (NF- κ B) pathway^{31,40}.

TNF-R1 can be found in all cell types, and TNF-R2 is mainly expressed in immune and endothelial cells⁴⁰. TNF-R1 is ubiquitously expressed, like Fas, whereas its ligand TNF- α is only expressed on activated macro-

phages and lymphocytes in response to infections³⁵. TNF-R1 has a death domain that can trigger apoptosis by activating the caspase cascade. Upon activation, TNF binds to its receptor via trimerization of TNFR1. Subsequently, a TNFR-associated death domain protein (TRADD) adapter molecule is added that induces association with FADD and activation of Caspase-8. In addition to the apoptotic pathway, TNF induces other signal transduction pathways from TRADD that trigger the activation of NF- κ B and c-Jun Kinase (JNK)/Ap-1^{41,42} (Fig. 3).

TNF-Related Apoptosis-Inducing Ligand (TRAIL)

TRAIL is a type II homotrimeric transmembrane protein expressed on the surface of T cells, macrophages, and NK cells, modulating the immune response³¹. Zinc binding is essential for recognizing the receptor and the subsequent induction of apoptosis

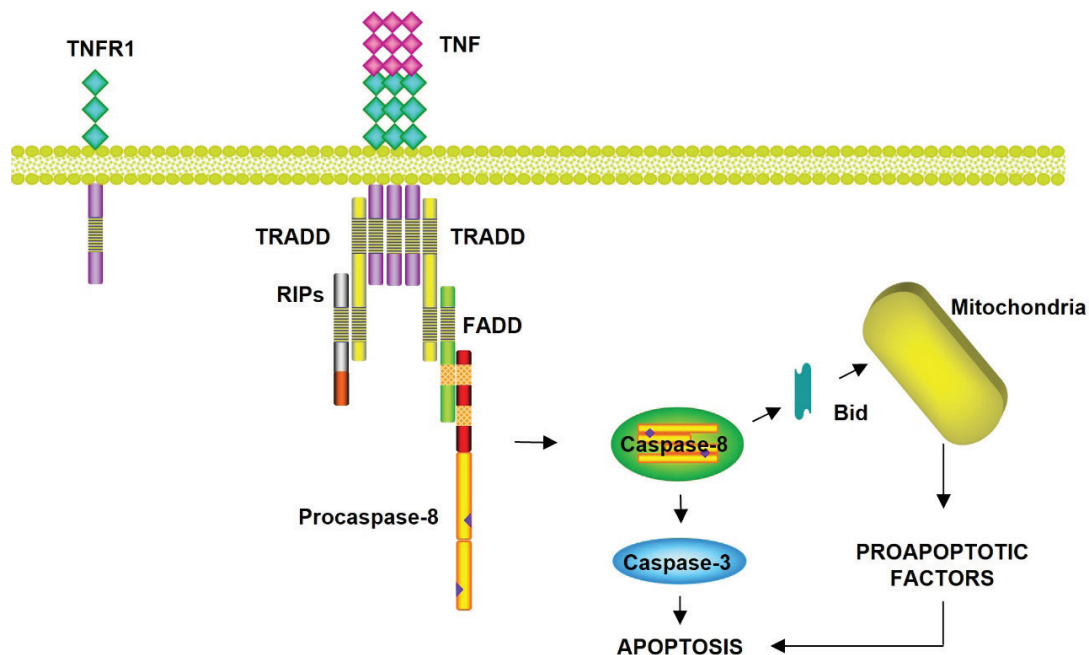


Fig. 3. Extrinsic apoptotic pathway by Tumor Necrosis Factor Receptor type 1 cell death receptors. TNF: tumor necrosis factor; TNFR1: Tumor Necrosis Factor Receptor; TRADD: Tumor Necrosis Factor Receptor (TNFR)-Associated Death Domain protein; RIPs: Receptor Interacting Proteins; FADD: Fas Associated Death Domain; Bid: BH3 Interacting Domain Death Agonist Protein. Signaling pathway of the TNF receptor 1. TRADD adapter molecule is added, which induces the association with FADD and the activation of Caspase-8.

by stabilizing the trimeric conformation in TRAIL residue Cys230, which is essential⁴³. When TRAIL binds to DRs, it induces receptor trimerization, which triggers the extrinsic apoptotic pathway in transformed cells without affecting non-transformed cells⁴⁴.

TRAIL binds to two death receptors (DR), DR 4 and DR5, and “three decoys receptors” (DcR) (DcR1, DcR2, and osteoprotegerin (OPG)). TRAIL-R1 or DR4 and TRAIL-R2 or DR5, with 60% homology, can trigger apoptosis and determine whether a cell is resistant or sensitive to TRAIL³¹. DcR1, or TRAIL-R3, is a GPI-anchored protein lacking the intracellular and transmembrane domains, while DcR2 or TRAIL-R4 has an intracellular portion containing a truncated DD; both receptors are unable to induce apoptosis after binding of TRAIL^{45,46}. OPG is a soluble receptor that can be re-

leased from the cardiovascular system, gastrointestinal tract, lung, kidney, bone, and immune cells⁴⁷. OPG binds TRAIL and many ligands, including another member of the TNF family, the receptor activating nuclear factor kB ligand (RANKL)⁴⁸.

Intrinsic pathway: mitochondrial death pathway

Intrinsic apoptosis is activated from within the cell in response to injury or other forms of stress, such as DNA damage, lack of oxygen, UV radiation, nutrient or survival signals, oxidizing agents, drugs, and growth factors⁴⁹ (Fig. 4).

Although mitochondria were considered a passive element in apoptotic cell death, which only reflected damage to critical functions due to cell death⁵⁰, this apoptotic pathway depends on the release

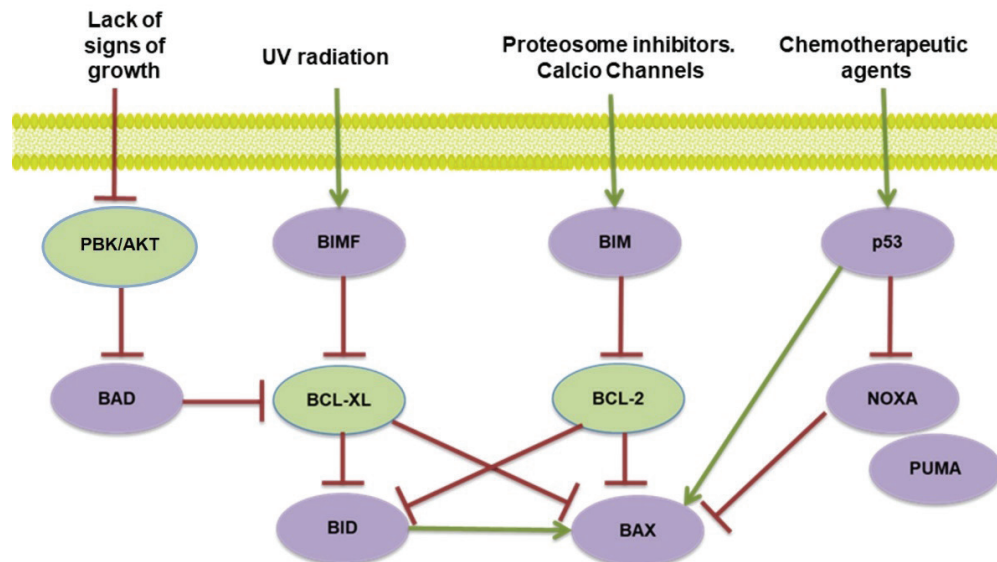


Fig. 4. Potential signals of the activation of the intrinsic apoptotic pathway.

PBK: Protein kinase B; AKT: serine-threonine kinase (also known as protein kinase B (PKB) phosphorylated by PDK1 kinase.; BAD: Bcl-2 agonist of cell death; BIM: B-cell lymphoma 2 interacting mediator of cell death; BIMF: proapoptotic protein BIM family; BID: BH3-interacting domain death agonist; BCL-XL: B-cell lymphoma-extra-large; BCL-2: B-cell lymphoma 2; BAX: bcl-2-like protein 4; NOXA: (Latin for damage) is a proapoptotic member of the Bcl-2 protein family; p53: Tumor protein P53; PUMA: p53 upregulated modulator of apoptosis.

In signaling activation of the mitochondrial pathway of apoptosis, the BH3 domain is essential for apoptotic activity. Proteins that inhibit apoptosis and/or promote cell survival include Bcl-2, and Bcl-XL, located in the outer mitochondrial membrane, and the proteins Bim, Bad, Bid, Bimf, and Bax are found mainly in the cytosol and can be translocated to mitochondria in response to apoptotic stimuli.

into the cytosol of mitochondrial proteins that normally reside in the intermembrane space⁵¹.

Cytochrome-C

Cytochrome C is a protein that participates in the electron transport chain located in the intermembrane space of the mitochondria, and that can be used as a biomarker of the apoptosis process¹. Cytochrome C, performs an entirely different function; after being released into the cytosol, it binds to a procaspase-activating protein called apoptotic protease-activating factor-1 (Apaf1), causing the oligomerization of Apaf-1 into a heptameric wheel-like structure called apoptosome⁵². In the apoptosome, Apaf1 proteins recruit initiator procaspase molecules (procaspase-9); these are activated into Caspase-9 and induce an apoptotic cascade acti-

vating one of the following chain executing procaspases-3, -6, and -7 inducing apoptosis⁵³ (Fig. 5).

Bcl-2 family proteins

Bcl-2 family of proteins controls and regulates the entire process of intrinsic apoptosis. Bcl-2 family proteins actively participate in this pathway, which, through interactions between them, regulates the permeabilization of mitochondria and the release of apoptogenic proteins into the cytosol¹. The Bcl-2 family of proteins contains at least one conserved domain, known as Bcl-2 homology domains (BH [BH1, BH2, BH3 and BH4]). The proteins of the Bcl-2 family are classified based on their function and structure: i) Antiapoptotic proteins, which contain the domains BH1 and BH2; ii) Proapoptotic pro-

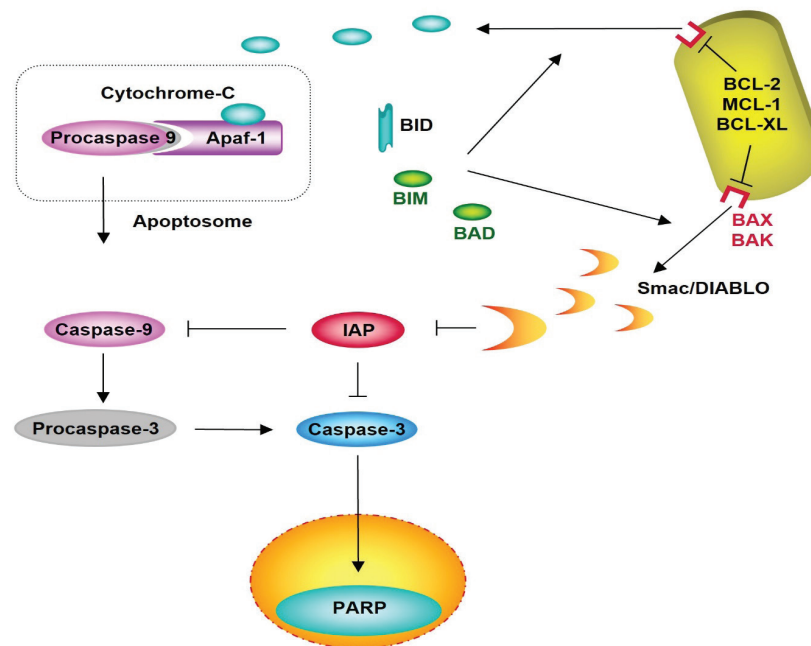


Fig. 5. Intrinsic pathway by Cytochrome C-mediated apoptosis.

Apaf-1: Apoptotic protease-activating factor 1; IAP: Inhibitors of Apoptosis Protein; PARP: Poly (ADP-ribose) polymerase; BID: BH3 Interacting Domain Death Agonist; BIM: B-cell lymphoma 2 interacting mediator of cell death; BAD: Bcl-2 agonist of cell death; BCL-2: B-cell lymphoma 2; MCL-1: Induced myeloid leukemia cell differentiation protein; BCL-XL: B-cell lymphoma-extra-large; BAX: bcl-2-like protein 4; BAK: Bcl-2 homologous antagonist/killer; Smac / DIABLO: Second Mitochondria-derived Activator of Caspase.

Release to the cytosol binds to the Apaf-1 protein and procaspase-9, forming the apoptosome complex, inducing caspase-9 and the caspase activation cascade.

teins containing the BH1, BH2, and BH3 domains; iii) Proapoptotic proteins containing only the BH3 domain⁵⁴. Most of the antiapoptotic members maintain sequence conservation in their four domains, while those with proapoptotic activity have less conservation of the first α -helix BH4 segment. Thus, the proteins of the Bcl-2 family are proapoptotic, and others are antiapoptotic. They can bind to each other in various combinations and form heterodimers in which the two proteins mutually inhibit each other. However, when a more significant proportion of these activities occur, the cell's susceptibility to death or survival is determined^{55,56}.

Antiapoptotic proteins

Antiapoptotic Bcl-2 proteins, such as Bcl-2 itself, Mcl-1, Bcl-w, A1, and Bel-XL, are found on the cytosolic surface of the outer mitochondrial membrane, endoplasmic reticulum, and nuclear envelope, where they help maintain membrane integrity. This group of proteins inhibits apoptosis and/or promotes cell survival⁵⁴. The three antiapoptotic proteins of the Bcl-2 family, Bcl-2, Bcl-XL, and Mcl-1, prevent the activation of the mitochondrial apoptosis pathway, as demonstrated in multiple myeloma (MM)³⁷. In MM, the defect in the cell death pathways is frequently due to an imbalance in the expression of the Bcl-2 family proteins. The Bcl-2 gene has been implicated in resistance to apoptosis induced by dexamethasone but not melphalan in patients with MM. Bcl-XL is expressed in most MM cell lines and cells from patients; increased expression is frequently detected in the relapsed patient and correlates with resistance to chemotherapy. Mcl-1 is expressed in virtually all MM lines and fresh cells from patients. The induction of apoptosis in MM cells has been related to a decrease in the expression of Mcl-1⁵⁷. Also, for acute myeloid leukemia (AML), higher expression of Bcl-2, Bcl-XL, and Mcl-1 and lower expression of Bax increase resistance to apoptosis in CD34+ populations than in CD34- populations, mainly due to AML⁵⁸.

Furthermore, increased expression of Bcl-2 and Bcl-XL blocks doxorubicin-induced apoptosis. Mcl-1 levels are increased in patients with recurrent AML⁵⁹.

Pro-apoptotic Bcl2 proteins

Proapoptotic Bcl-2 proteins comprise two subfamilies: the BH1-4 proteins that share four different homology domains (Bcl-2-associated X protein [Bax] and Bcl-2 homologous antagonist/killer [Bak] and the proteins with restricted homology to BH3. The BH3 domain is essential for apoptotic function⁶⁰. Among the members of the Bcl-2 family that induce apoptosis, with bounded homology to the BH3 domain, the following proteins are grouped: Bcl-2-interacting protein BIM (Bim), Bcl-2 agonist of cell death (Bad), Bid, Bcl-2 adenovirus E1B 19kDa-interacting protein 1 NIP3 (Bnip3), BMF, HRK, Noxa and p53 upregulated modulator of apoptosis (PUMA). These proteins are the largest subclass of the Bcl-2 protein family⁶¹. Bak protein is tightly bound to the outer membrane of the mitochondria even in the absence of an apoptotic signal, whereas Bax is localized primarily in the cytosol and only translocates to the mitochondria if an apoptotic signal is activated. Bax and Bak activation depend on activated "BH3 one" proapoptotic proteins. Bax and Bak act on the endoplasmic reticulum's and nuclear membranes' surface; when activated in response to endoplasmic reticulum stress, they release Ca^{2+} from the endoplasmic reticulum into the cytosol. Bax and Bad are essential gateways for cell death through mitochondria⁶¹. Restricted homology to BH3 proteins provides the crucial link between the apoptotic stimulus and the intrinsic apoptosis pathway; its BH3 domain binds to a long hydrophobic groove of the Bcl-2 antiapoptotic proteins and neutralizes or inhibits their activity. In some cells, the extrinsic apoptotic pathway recruits the intrinsic pathway by amplifying the caspase cascade that kills the cell. In this way, Bid is the link between the

two pathways. Also, Bid, Bim, and PUMA can inhibit all Bcl-2 antiapoptotic proteins^{62,63}. Klee *et al.*⁶⁴ have investigated mitochondrial membrane permeabilization, which depends not only on the canonical mitochondrial Bak and Bax pathway to activate the death program. Therefore, these investigators have also found that the “only-BH3” molecules, Bim and PUMA, can induce the release of cytochrome c and apoptosis with the mere presence of Bak in the endoplasmic reticulum⁶⁴. This pathway for transmitting apoptotic signals from the endoplasmic reticulum to mitochondria involves coordinated communication mediated by the calcium and ER1 α /TRAF2 ER-stress surveillance machinery^{61,63,65}.

Second Mitochondria-derived Activator of Caspase (Smac / Diablo)

Second mitochondria-derived activator of caspase (Smac / Diablo) binds by its N-terminal end to the mitochondria and, in the intermembrane space, proteolyzes, leaving free the domain that allows its union with the IAPs⁶⁶. The loss of mitochondrial potential simultaneously triggers the release of cytochrome-C and Smac/Diablo. Smac/Diablo, in the cytoplasm, is capable of binding to IAPs (XIAP, c-IAP1, c-IAP2, and survivin), inhibiting their function and enhancing caspase activation and triggering the mitochondrial apoptosis pathway⁶⁷. The release of Smac / Diablo is inhibited by Bcl-2 and Bel-xL⁵⁴. In MM cells, Smac plays a functional role in mediating the activation and apoptosis of Caspase-9 induced by dexamethasone treatment³⁷.

Caspase-independent pathways of apoptosis

Mitochondrial caspase - independent pathway

The loss of mitochondrial potential increases the permeability of the mitochondrial membrane, and the result is the release of

these proteins, such as AIF (apoptosis-inducing factor) and Endonuclease G (Endo-G) that activate a caspase-independent apoptosis pathway⁶⁸.

AIF (Apoptosis Inducing Factor)

Apoptosis-inducing factor (AIF) is a highly phylogenetically conserved protein, essential for embryonic development, which is synthesized in the form of an immature precursor; it is translocated to the mitochondria, and in the intermembrane space it is proteolyzed, the mature form has oxidase activity⁶⁹. In response to death signals, AIF leaves the mitochondria and travels through the cytosol to the nucleus, where it binds to DNA, causing chromatin condensation and DNA fragmentation into fragments of approximately 50 kb¹⁶ (Fig. 6). AIF is necessary to induce PARP-dependent death. The processing and activation of PARP occur in response to DNA damage. PARP initiates a signal in the nucleus that induces the release of AIF from the mitochondria. AIF then moves from the mitochondria to the nucleus and induces chromatin condensation and DNA fragmentation^{69,70}.

Endonuclease G (Endo-G)

Endonuclease G (Endo-G) is an essential protein for mitochondrial DNA replication. It was isolated from the mitochondrial fraction treated with the proapoptotic active form of Bid: tBid. Once released to the cytosol, it is transferred to the nucleus, where it fragments DNA, even in the presence of caspase inhibitors (Fig. 6). Endo-G cooperates with exonuclease and DNase, facilitating DNA processing^{71,72}. Apoptotic endonuclease acts cooperatively to fragment DNA and ensure the irreversibility of apoptosis. However, very little is known about the potential regulatory linkages between endonucleases. Therefore, deoxyribonuclease deactivation is caused by cutting. Also, alternative splicing of DNase I pre-mRNA skipping exon 4 occurs in response to overexpression of Endo-G in

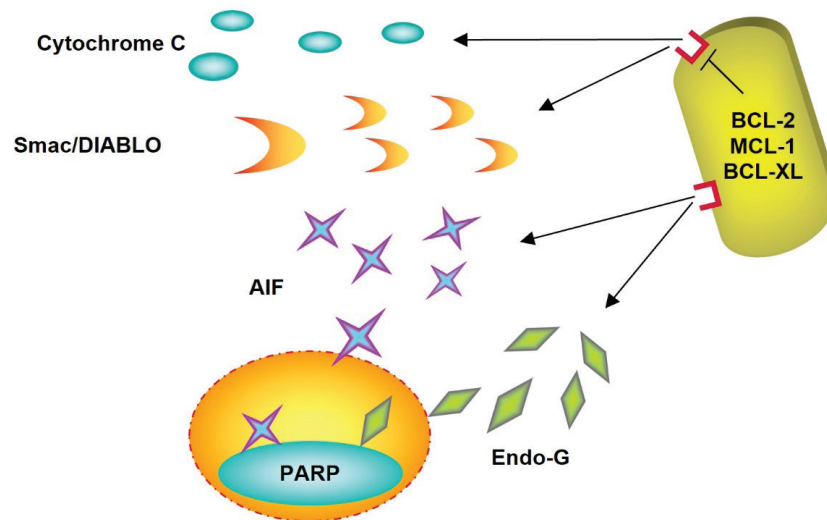


Fig. 6. Proapoptotic factors as Cytochrome-C, Smac/Diablo, Endonuclease, and Apoptosis Inducing Factor are released from the mitochondria.

RIP3: Receptor-interacting serine/threonine-protein kinase 3; RIP1 Receptor-interacting serine/threonine-protein kinase 1; FLIPs: FLICE-inhibitory proteins; FAAD: Fas-associated death domain protein.

In response to death signals, AIF leaves the mitochondria and moves through the cytosol to the nucleus, where it binds to the DNA, causing chromatin condensation and DNA fragmentation.

cells^{16,72}. Likewise, a strong correlation was identified between the expression levels of Endo-G and DNase I splice variants in human lymphocytes. In fact, T cells downregulate the mRNA levels of the active full-length DNase I variant. They also upregulate the levels of the inactive spliced variant, which acts in a dominant-negative fashion^{70,71}.

Necroptosis

Necroptosis is a form of programmed cell death since it is genetically regulated; it is characterized by cell inflammation, mitochondria dysfunction, plasma membrane permeabilization, and the release of cytoplasmic content into the extracellular space, causing inflammatory reactions in the cells of the surrounding tissue. This form of cell death is also associated with mitochondrial reactive oxygen species (ROS) and, unlike apoptosis, does not involve DNA fragmentation⁷³. Necroptosis has been reported to occur in a wide range of human diseases, including retinal ischemia-reperfusion injury, acute pancreatitis, brain trauma, retinal detachment, and Huntington's disease^{73,74}.

In addition, necroptosis has been linked to models of inflammation, including intestinal inflammation and systemic inflammatory response syndrome (SIRS)^{75,76}. Perhaps the detailed knowledge of this cell death pathway can be used to develop drugs that temporarily prevent or block this process to delay the death of some types of cells or, conversely, it could also serve to eliminate selectively, for example, tumor cells⁷⁷.

Activation Pathways of Necroptosis

Necroptosis is triggered as a form of immunity against pathogens, under poor conditions to trigger apoptosis. In necroptosis, as in apoptosis, TNF activates TNFR1, which induces the activation of a serine/threonine kinase interaction protein (RIP1), making integrating a joint inflammatory and necroptotic response possible⁷⁸. RIP3 is activated upon phosphorylation by the serine/threonine kinase RIP1⁷⁹. Necroptosis is RIP3-dependent as RIPK3 protein kinase activity determines whether cells die by apoptosis or necroptosis. Perhaps necroptosis is fundamentally characterized by the

activation of RIP1 or RIPK3, while the caspase cascade is inhibited⁷⁹. Giampietri *et al.*⁸⁰ have proposed a model that differentiates the production of cell death by apoptosis and by necroptosis; the dimerization of Caspase-8 produces apoptosis while in necroptosis it does not occur. The dimerization of C-Flip S and caspase-8 produces a reduction in caspase-8 activity, and it may not produce either apoptosis or necroptosis, finally, the heterodimerization of C-FLIPs and Caspase-8 produces inhibition of Caspase-8 and leads to the production of necroptosis (Fig. 7).

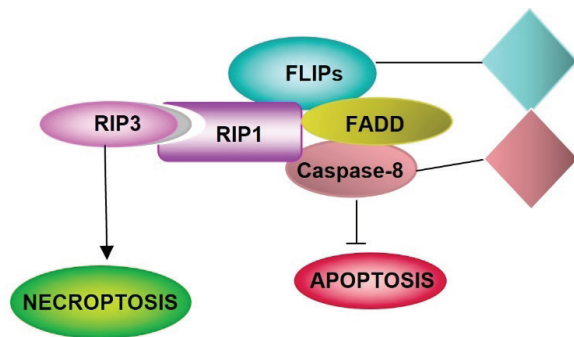


Fig. 7. Pathway of specific activation of necroptosis. RIP3: Receptor-interacting serine/threonine-protein kinase 3; RIP1 Receptor-interacting serine/threonine-protein kinase 1; FLIPs: FLICE-inhibitory proteins; FAAD: Fas-associated death domain protein.

Necroptosis signaling pathways mainly comprise heterodimerization to c-FLIPs that reorganize the catalytic site procaspase-8, producing caspase-8 inhibition, which induces necroptosis.

Regulation Pathways of Necroptosis

Liu *et al.*⁸¹ have shown that the Akt and mTOR pathways regulate necroptosis by inducing RIPK1 activation in neuronal cell death. Just as it has also been verified that necrostatin -1 is an inhibitor of all the biochemical events carried out in this type of cell death. In addition, other investigators⁸² have reported that necroptosis is paired with a mixed lineage kinase domain-like protein (MLKL) gene, an important substrate of RIP3, and the plasma surface pores are constituted by said protein (Fig. 8). These pores cause the absorption of too much wa-

ter, so the cells ultimately burst. The blockade of MLKL activity leads to the inhibition of necroptosis⁸². In this sense, Dondelinger *et al.*⁸² have proposed that a domain of four activated MLKL molecules is required to induce its oligomerization and trigger cell death.

On the other hand, it has been found that phosphatidylinositol (PIP) recruits the MLKL protein to the plasma membrane. Of note, recombinant MLKL lacks positive charges and induces leakage of liposomes containing both PIP and BAX, supporting a model in which MLKL induces necroptosis by directly permeabilizing the plasma membrane. Consequently, inhibition of PIP formation specifically inhibits TNF mediated by necroptosis but not apoptosis⁸².

Autophagy

The term autophagy was introduced in 1996 by De Duve and Wattiaux, who defined the vacuolization process for transporting intracellular material to lysosomes for degradation⁸³. Autophagy is derived from the Greek auto and phagos; it literally means “self-feeding.” Its function mainly regulates intracellular homeostasis since cytoplasmic materials (long-lived proteins and damaged organelles) are degraded in lysosomes and recycled to produce new building blocks and maintain energy metabolism⁸⁴. From a morphological point of view, autophagy has been classified as a form of programmed cell death associated with the massive accumulation of autophagosomes in the cytoplasm, which frequently, but not always, seems to be accompanied by increased blood flow; massive autophagy triggers caspase-independent, necrosis-like death⁸⁵. It has been shown that autophagy participates in natural processes such as growth, embryonic development, or aging. Also, it participates in the death that occurs in mammary cells after lactation and the death of some cancer cells that lack apoptotic modulators, such as Bax and Bak or caspases^{85,86}. Dysfunction of this process has been linked to cardiovascular and respi-

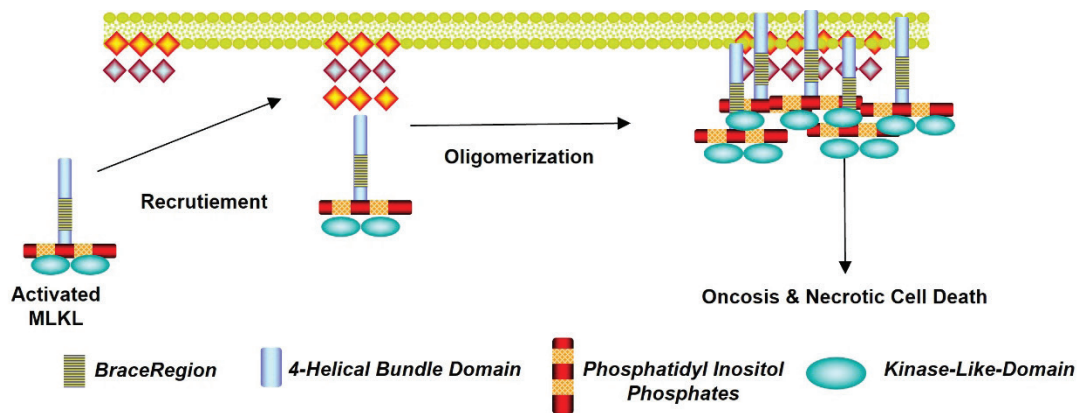


Fig. 8. Recruitment of Mixed Lineage Domain-Like Protein Kinase by Phosphatidylinositol. Pathway to the plasma membrane.

MLKL: Mixed Lineage Domain-Like Protein Kinase

The MLKL protein has become a specific and crucial protein. The 4-Helical Bundle Domain (4HBD) in the N-terminal region of MLKL is required to induce its oligomerization, and trigger cell death.

ratory diseases, neurodegenerative diseases, metabolic diseases, and cancer^{86,87}.

Autophagy is a type of programmed cell death since more than 30 genes have been identified in yeast that regulate autophagy, and it is seen as a survival mechanism to combat environmental stress factors⁸⁸. Autophagy could be induced in response to oxidative or metabolic stress and can also be induced through starvation, which is very commonly used in research⁸⁶. On the other hand, to demonstrate that cell death in an *in vivo* or *in vitro* model is caused by autophagy, it is necessary to demonstrate that said death is inhibited by agents interrupting the autophagic pathway⁸⁸. These agents can be chemical (agents directed against VPS34), genetic (siRNA 3-methyl-adenine), or modulators of autophagy (AMBRA 1, ATG 5, beclin)⁸⁹.

Types of autophagy

Three types of autophagy are identified: i) macroautophagy; ii) microautophagy; iii) chaperone-mediated autophagy⁸⁴. The macroautophagy process, as described by Kwanten *et al.*⁸⁸ begins with the formation of a phagophore, a double membrane structure (also known as an isolation membrane) that sequesters cyto-

plasmic material (long-lived proteins and organelles), which subsequently elongates to create an autophagosome. The autophagosome fuses with a lysosome to form an autolysosome, where its contents will be degraded by lysosomal proteases (e.g., cathepsins) and other hydrolytic enzymes^{90,91}. According to Kwanten *et al.*⁸⁸, phagophore formation is regulated by the ULK1 complex (initiation), which is under the control of the mammalian target of rapamycin (mTOR) complex and the beclin-1/VSP34 interaction complex (nucleation). Two large, conjugated ubiquitin-like complexes are responsible for double membrane elongation: light chain 3 (LC3)-II and ATG5-Atg12-ATG16L1. ATG7 is one of the proteins required to form both elongation complexes. Autophagosomes are generated on or in the vicinity of the endoplasmic reticulum. However, it is not clear whether the ER membrane is used directly for autophagosome formation. Recent studies suggest that additional membranes derived from the Golgi complex, mitochondria, and the plasma membrane also contribute to autophagosome formation^{90,91}. Therefore, autophagosome formation involves multiple and complex processes⁸⁴. Macroautophagy is considered to play the most critical role in autophagy⁹² (Fig. 9).

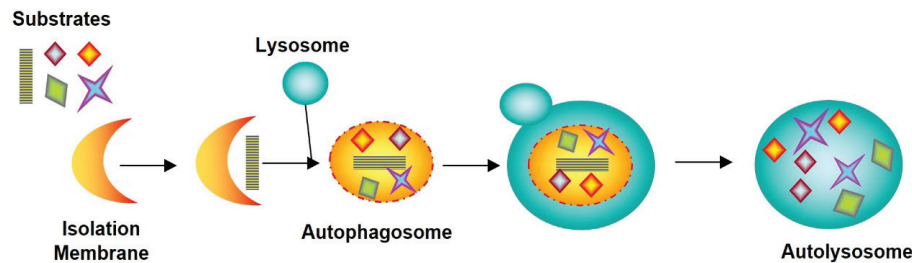


Fig. 9. Macroautophagy process from isolation membrane to autolysosome.

In the autolysosome, the inner membrane and luminal content of the autophagic vesicle are degraded by lysosomal enzymes that act optimally within this acidic compartment.

Microautophagy process is considered when a small portion of the cytoplasm is directly involved by the lysosome / late endosome (Fig. 10). Autolysosome formation is mediated by the accumulation of small membrane structures that envelop portions of the cytoplasm. Phagophores are not formed, and membrane structures invaginate directly into lysosomes, where degradation occurs by direct absorption of cytoplasmic cargo.

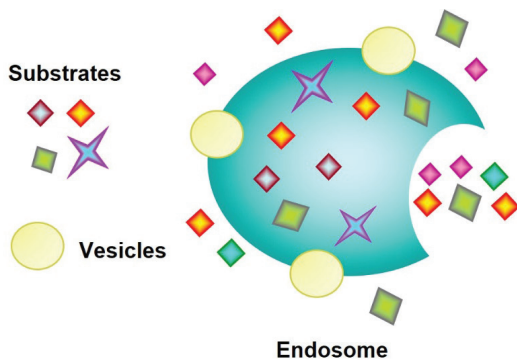


Fig. 10. Endosomes result from the microautophagy process.

Microautophagy is conserved from yeast to mammals and contributes to the degradation of organelles (e.g., peroxisomes, ER, nucleus), protein complexes such as the proteasome, and single proteins.

In Chaperone-Mediated Autophagy (CMA), the proteins to be degraded are delivered selectively to lysosomes; they are recognized by heat shock-like proteins 70 (HSC70) and by co-chaperones; proteins in the degradation phase are internalized through lysosomal membrane-associated protein 2A (LAMP2A)^{91,92} (Fig. 11).

Autophagy: a selective process

Degradation in the autophagy process was believed to be non-selective; however, it has been determined that there are selective pathways to digest specific components, such as “mitophagy” or selective autophagy of mitochondria⁹³, “peroxyphagy” (peroxisomes), “ribophagy” (ribosomes) or “xenophagy” (invading microbes), this phenomenon is called selective autophagy, and in the case of mitochondria, it serves to maintain their homeostasis^{70,84}. Thus, macroautophagy can be non-selective (random uptake of intracellular material) and selective (specific load capture). The morphological and biochemical characteristics of autophagy and apoptosis are different. In this regard, cells undergoing autophagy show an increase in autophagic vesicles (autophagosomes and autophagolysosomes). While chromatin condensation is partial in autophagic cells, DNA fragmentation does not occur. The two processes, autophagy and apoptosis, are not always mutually exclusive and can occur simultaneously in the same type of cells⁹¹.

In summary, homeostasis is maintained between cells produced by mitosis and cell death in the human body. In this sense, this study is a narrative review that reports scientific research in which an attempt has been made to group programmed cell deaths, explaining the molecular mechanisms that involve structural and functional proteomic pathways that intervene by inducing and inhibiting each one of the proteomic pathways. In our study, caspase-dependent pro-

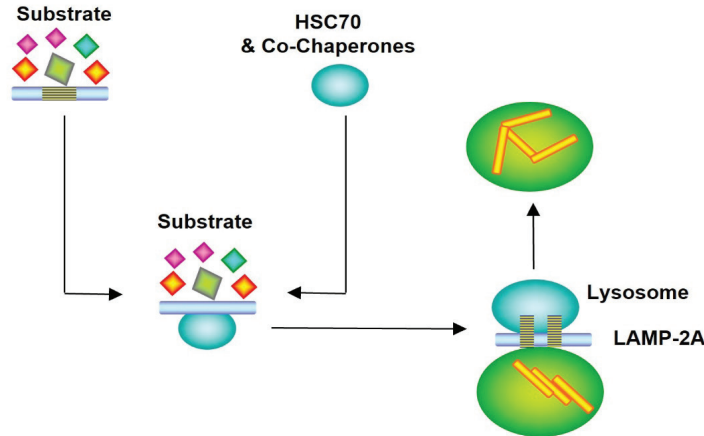


Fig. 11. Lysosome obtained from Chaperone-Mediated Autophagy pathway. HSC70: Heat shock 70 kDa protein cognate; LAMP-2A: Lysosome-associated membrane protein 2A. The proteins to be degraded are delivered selectively to lysosomes, which HSC70 and co-chaperones recognize. Proteins in the degradation phase are internalized through LAMP2A.

grammed cell deaths and caspase-independent programmed cell deaths are described. Although classifying and describing programmed cell death processes is somewhat complex, depending on which aspects are analyzed, their grouping and knowledge of the factors that trigger cell death vary greatly. This study could offer the basis for the design of new pharmacological treatments and discover new potential molecular biomarkers for early diagnosis that serve to cure or modulate the course of some diseases. For this, it is necessary to understand the proteomic signaling mechanisms of programmed cell death since their alteration contributes to a wide variety of diseases, one of which is cancer, which constitutes a global public health problem due to its high mortality.

ACKNOWLEDGMENTS

The authors want to thank the SARCEL-LOMICS® Research Group (Spain), for their collaboration on infrastructure computer support and for presenting their collaboration in advising on the methodological design and interpretation of the results.

Funding

No funding was received.

Competing interests

The authors declare that they have no competing interests.

ORCID numbers of authors

- Diego Fernández-Lázaro (DFL): 0000-0002-6522-8896
- Begoña Sanz (BS): 0000-0002-6354-6401
- Jesús Seco-Calvo (JSC): 0000-0002-7818-9777

Authors' contributions

DFL: searched and selected the literature and wrote the original draft. JSC and BS conceived the study and reviewed and edited the manuscript. DFL designed and created the figures. Data authentication is not applicable. All authors have read and approved the final manuscript.

REFERENCES

1. Danial NN, Korsmeyer SJ. Cell Death: Critical control points. *Cell* 2004;116(2): 205-219. *Doi: 10.1016/s0092-8674(04)00046-7*
2. Fuchs Y, Steller H. Programmed cell death in animal development and disease. *Cell*

- 2011;147(4): 742-758. *Doi: 10.1016/j.cell.2011.10.033*
3. **Božič B, Rozman B.** Apoptosis and autoimmunity. *EJIFCC* 2006;17(3): 69-74. Available from: <https://www.ncbi.nlm.nih.gov/pmc/articles/PMC5938681/pdf/ejifcc-17-069.pdf>
 4. **Marchal JA, Lopez GJ, Peran M, Comino A, Delgado JR, García-García JA, Conde V, Aranda FM, Rivas C, Esteban M, García MA.** The impact of PKR activation: from neurodegeneration to cancer. *FASEB J* 2014;28(5): 1965-1974. *Doi: 10.1096/fj.13-248294*
 5. **Li K, Wu D, Chen X, Zhang T, Zhang L, Yi Y, Miao Z, Jin N, Bi X, Wang H, Xu J, Wang D.** Current and emerging biomarkers of cell death in human disease. *Biomed Res Int* 2014;2014: 690103. *Doi: 10.1155/2014/690103*
 6. **Galluzzi L, Vanden Berghe T, Vanlangenakker N, Buettner S, Eisenberg T, Vandenabeele P, Madeo F, Kroemer G.** Programmed necrosis from molecules to health and disease. *Int Rev Cell Mol Biol* 2011;289: 1-35. *Doi: 10.1016/B978-0-12-386039-2.00001-8*
 7. **Elmore S.** Apoptosis: A review of programmed cell death. *Toxicol Pathol* 2007;35(4): 495-516. *Doi: 10.1080/01926230701320337*
 8. **Kerr JFR, Wyllie AH, Currie AR.** Apoptosis: A basic biological phenomenon with wideranging implications in tissue kinetics. *Br J Cancer* 1972;26(4): 239-257. *Doi: 10.1038/bjc.1972.33*
 9. **Yuan J, Kroemer G.** Alternative cell death mechanisms in development and beyond. *Genes Dev* 2010;24(23): 2592-2602. *Doi: 10.1101/gad.1984410*
 10. **Rowan S, Fisher DE.** Mechanisms of apoptotic cell death. *Leukemia* 1997;11(4): 457-465. *Doi: 10.1038/sj.leu.2400626*
 11. **Zhou JX, Li X [Eds.].** Apoptosis in Polycystic Kidney Disease: From Pathogenesis to Treatment. In: *Polycystic Kidney Disease* [Internet]. Brisbane (AU): Exon Publications; 2015. Chapter 9: 197-230. *Doi: 10.15586/codon.pkd.2015.ch9*
 12. **Strasser A, O'Connor L, Dixit VM.** Apoptosis Signaling. *Annu Rev Biochem* 2000;69: 217-245. *Doi: 10.1146/annurev.biochem.69.1.217*
 13. **Martelli AM, Zweyer M, Ochs RL, Tazzari PL, Tabellini G, Narducci P, Bortul R.** Nuclear apoptotic changes: an overview. *J Cell Biochem* 2001;82(4): 634-646. *Doi: 10.1002/jcb.1186*
 14. **Vitale I, Pietrocola F, Guilbaud E, Aaronson SA, Abrams JM, Adam D, Agostini M, Agostinis P, Alnemri ES, Galluzzi L.** Apoptotic cell death in disease—Current understanding of the NCCD 2023. *Cell Death Differ* 2023;30(5): 1097-1154. *Doi: 10.1038/s41418-023-01153-xw*
 15. **Arandjelovic S, Ravichandran KS.** Phagocytosis of apoptotic cells in homeostasis. *Nat Immunol* 2015;16(9): 907-917. *Doi: 10.1038/ni.3253*
 16. **Abraham MC, Shaham S.** Death without caspases, caspases without death. *Trends Cell Biol* 2004;14(4): 184-193. *Doi: 10.1016/j.tcb.2004.03.002*
 17. **Thornberry NA, Lazebnik Y.** Caspases: enemies within. *Science* 1998;281(5381): 1312-1316. *Doi: 10.1126/science.281.5381.1312*
 18. **Testa U, Riccioni R.** Deregulation of apoptosis in acute myeloid leukemia. *Haematologica* 2007;92(1): 81-89. *Doi: 10.3324/haematol.10279*
 19. **Thornberry NA.** Caspases: A decade of death research. *Cell Death Differ* 1999;6(11): 1023-1027. *Doi: 10.1038/sj.cdd.4400607*
 20. **Ouyang L, Shi Z, Zhao S, Wang FT, Zhou TT, Liu B, Bao JK.** Programmed cell death pathways in cancer: a review of apoptosis, autophagy and programmed necrosis. *Cell Prolif* 2012;45(6): 487-498. *Doi: 10.1111/j.1365-2184.2012.00845.x*
 21. **Schimmer AD, Dalili S, Batey RA, Riedl SJ.** Targeting XIAP for the treatment of malignancy. *Cell Death Differ* 2006;13(2): 179-188. *Doi: 10.1038/sj.cdd.4401826*
 22. **Lens SM, Wolthuis RM, Klompkamp R, Kauw J, Agami R, Brummelkamp T, Kops G, Medema RH.** Survivin is required for a sustained spindle checkpoint arrest

- in response to lack of tension. *EMBO J* 2003;22(12): 2934-2947. *Doi: 10.1093/emboj/cdg307*
23. **Carvalho A, Carmena M, Sambade C, Earnshaw WC, Wheatley SP.** Survivin is required for stable checkpoint activation in taxol-treated HeLa cells. *J Cell Sci* 2003;116(Pt 14): 2987-2998. *Doi: 10.1242/jcs.00612*
 24. **Altieri DC.** New wirings in the survivin networks. *Oncogene* 2008;27(48): 6276-6284. *Doi: 10.1038/onc.2008.303*
 25. **Tamm I, Richter S, Oltersdorf D, Creutzig U, Harbott J, Scholz F, Karawajew L, Ludwig WD, Wuchter C.** High expression levels of X-Linked inhibitor of apoptosis protein and survivin correlate with poor overall survival in childhood *de novo* acute myeloid leukemia. *Clin Cancer Res* 2004;10(11): 3737-3744. *Doi: 10.1158/1078-0432.CCR-03-0642*
 26. **Schimmer AD.** Inhibitor of apoptosis proteins: translating basic knowledge into clinical practice. *Cancer Res* 2004;64(20): 7183-7190. *Doi: 10.1158/0008-5472.CAN-04-1918*
 27. **Chawla-Sarkar M, Bae SI, Reu FJ, Jacobs BS, Lindner DJ, Borden EC.** Downregulation of Bcl-2, FLIP or IAPs (XIAP and survivin) by siRNAs sensitizes resistant melanoma cells to Apo2L/TRAIL-induced apoptosis. *Cell Death Differ* 2004;11(8): 915-923. *Doi: 10.1038/sj.cdd.4401416*
 28. **Huang Y, Lu M, Wu H.** Antagonizing XIAP-mediated caspase-3 inhibition: Achilles' heel of cancers? *Cancer Cell* 2004;5(1): 1-2. *Doi: 10.1016/s1535-6108(03)00340-4*
 29. **Tsuruo T, Naito M, Tomida A, Fujita N, Mashima T, Sakamoto H, Haga N.** Molecular targeting therapy of cancer: drug resistance, apoptosis and survival signal. *Cancer Sci.* 2003;94(1):15-21. *Doi: 10.1111/j.1349-7006.2003.tb01345.x*
 30. **Eimon PM, Kratz E, Varfolomeev E, Hymowitz SG, Stern H, Zha J, Ashkenazi A.** Delineation of the cell-extrinsic apoptosis pathway in the zebrafish. *Cell Death Differ* 2006;13(10): 1619-1630. *Doi: 10.1038/sj.cdd.4402015*
 31. **Diaz Arguello OA, Haisma HJ.** Apoptosis-inducing TNF superfamily ligands for cancer therapy. *Cancers (Basel)* 2021;13(7): 1543. *Doi: 10.3390/cancers13071543*
 32. **Schutters K, Kusters DH, Chatrou ML, Montero-Melendez T, Donners M, Decckers NM, Krysko DV, Vandenabeele P, Perretti M, Schurgers LJ, Reutelingsperger CPM.** Cell surface-expressed phosphatidylserine as therapeutic target to enhance phagocytosis of apoptotic cells. *Cell Death Differ* 2013;20(1): 49-56. *Doi: 10.1038/cdd.2012.107*
 33. **Tran SEF, Meinander A, Eriksson JE.** Instant decisions: transcription-independent control of death-receptor-mediated apoptosis. *Trends Biochem Sci* 2004;29(11): 601-608. *Doi: 10.1016/j.tibs.2004.09.009*
 34. **Fernández-Lázaro D.** Comparative pre-clinical analysis of the efficacy, mechanism of action and resistance mechanisms of two immunomodulatory drugs (IMiDS), lenalidomide and pomalidomide, in multiple myeloma. Doctoral Thesis. University of de Salamanca. 2011. Available from: https://gredos.usal.es/bitstream/handle/10366/110661/DME_Fernandez_Lazaro_D_Analisis_preclinico.pdf?sequence=1&isAllowed=y
 35. **Ashkenazi A, Dixit VM.** Death receptors: signaling and modulation. *Science* 1998;281(5381): 1305-1308. *Doi: 10.1126/science.281.5381.1305*
 36. **Volpe E, Sambucci M, Battistini L, Borsellino G.** Fas-fas ligand: Checkpoint of T cell functions in multiple sclerosis. *Front Immunol* 2016;7: 217466. *Doi: 10.3389/fimmu.2016.00382*
 37. **Fernández-Lázaro D, Fernández-Lázaro CI, Caballero García A, Córdova Martínez A.** Immunomodulatory agents (IMiDs): tools for the treatment of multiple myeloma. *Rev Med Chil* 2018;146(12): 1444-1451. Available from: *Doi: https://www.scielo.cl/scielo.php?script=sci_arttext&pid=S0034-98872018001201444*
 38. **Boatright KM, Deis C, Denault JB, Sutherlin DP, Salvesen GS.** Activation of caspases-8 and -10 by FLIPL. *Biochem J*

- 2004;382(Pt 2): 651-657. *Doi: 10.1042/BJ20040809*
39. **Mahdizadeh SJ, Thomas M, Eriksson LA.** Reconstruction of the Fas-based death-inducing signaling complex (DISC) using a protein-protein docking meta-approach. *J Chem Inf Model* 2021;61(7): 3543-3558. *Doi: 10.1021/acs.jcim.1c00301*
40. **Martínez-Reza I, Díaz L, García-Becerra R.** Preclinical and clinical aspects of TNF- α and its receptors TNFR1 and TNFR2 in breast cancer. *J Biomed Sci* 2017;24(1): 90. *Doi: 10.1186/s12929-017-0398-9*
41. **Harper N, Hughes M, MacFarlane M, Cohen GM.** Fas-associated death domain protein and caspase-8 are not recruited to the tumor necrosis factor receptor 1 signaling complex during tumor necrosis factor-induced apoptosis. *J Biol Chem* 2003;278(28): 25534-25541. *Doi: 10.1074/jbc.M303399200*
42. **Iordanov MS, Kirsch JD, Ryabinina OP, Wong J, Spitz PN, Korcheva VB, Thorburn A, Magun BE.** Recruitment of TRADD, FADD, and caspase 8 to double-stranded RNA-triggered death inducing signaling complexes (dsRNA-DISCs). *Apoptosis* 2005;10(1): 167-176. *Doi: 10.1007/s10495-005-6071-x*
43. **Bodmer JL, Meier P, Tschopp J, Schneider P.** Cysteine 230 is essential for the structure and activity of the cytotoxic ligand TRAIL. *J Biol Chem* 2000;275(27): 20632-20637. *Doi: 10.1074/jbc.M909721199*
44. **Lemke J, Von Karstedt S, Zinngrebe J, Walczak H.** Getting TRAIL back on track for cancer therapy. *Cell Death Differ* 2014;21(9): 1350-1364. *Doi: 10.1038/cdd.2014.81*
45. **Zhang Y, Zhang B.** TRAIL resistance of breast cancer cells is associated with constitutive endocytosis of death receptors 4 and 5. *Mol Cancer Res* 2008(12);6: 1861-1871. *Doi: 10.1158/1541-7786.MCR-08-0313*
46. **Huang Y, Sheikh MS.** TRAIL death receptors and cancer therapeutics. *Toxicol Appl Pharmacol* 2007;224(3): 284-289. *Doi: 10.1016/j.taap.2006.12.007*
47. **Danish L, Stöhr D, Scheurich P, Pollak N.** TRAIL-R3/R4 and Inhibition of TRAIL Signalling in Cancer. [Part of the Resistance to Targeted Anti-Cancer Therapeutics book series (RTACT, vol.12)] Springer, Cham 2017;12: 27-57. Available from: https://link.springer.com/chapter/10.1007/978-3-319-56805-8_2
48. **Boyce BF, Xing L.** Biology of RANK, RANKL, and osteoprotegerin. *Arthritis Res Ther* 2007;9(Suppl 1): S1. *Doi: 10.1186/ar2165*
49. **Van Aken O.** Mitochondria and Cell Death. *Annu Plant Rev* 2018;50: 343-372. *Doi: https://doi.org/10.1002/9781119312994.apr0553*
50. **Ravagnan L, Roumier T, Kroemer G.** Mitochondria, the killer organelles and their weapons. *J Cell Physiol* 2002;192(2): 131-137. *Doi: 10.1002/jcp.10111*
51. **D'Arcy MS.** Cell death: a review of the major forms of apoptosis, necrosis and autophagy. *Cell Biol Int* 2019;43(6): 582-592. *Doi: 10.1002/cbin.11137*
52. **Cai J, Yang J, Jones DP.** Mitochondrial control of apoptosis: the role of cytochrome c. *Biochim Biophys Acta* 1998;1366(1-2): 139-149. *Doi: 10.1016/s0005-2728(98)00109-1*
53. **Jiang X, Wang X.** Cytochrome C-mediated apoptosis. *Annu Rev Biochem* 2004;73: 87-106. *Doi: 10.1146/annurev.biochem.73.011303.073706*
54. **Singh R, Letai A, Sarosiek K.** Regulation of apoptosis in health and disease: the balancing act of BCL-2 family proteins. *Nat Rev Mol Cell Biol* 2019;20(3): 175-193. *Doi: 10.1038/s41580-018-0089-8*
55. **Ramírez-García M, Márquez-González H, Barranco-Lampón G, Enrique López-Aguilar J.** Bel-2: its role in the cell cycle, apoptosis and cancer. *Residente* 2014;9(3): 84-94.
56. **Czabotar PE, Garcia-Saez AJ.** Mechanisms of BCL-2 family proteins in mitochondrial apoptosis. *Nat Rev Mol Cell Biol* 2023;24(10): 732-748. *Doi: 10.1038/s41580-023-00629-4*
57. **Fernández-Lazaro D.** Biological and molecular bases in the development of pathogenesis in multiple myeloma disease. *Invest Clin* 2019;60(3): 247-264. *Doi: https://doi.org/10.22209/IC.v60n3a07*

58. Colado E, Paíno T, Maiso P, Ocio EM, Chen X, Álvarez-Fernández S, Gutiérrez NC, Martín-Sánchez J, Flores-Montero J, San Segundo L, Garayoa M, Fernández-Lázaro D, Vidriales MB, Galmarini CM, Avilés P, Cuevas C, Pandiella A, San-Miguel JF. Zalypsis has in vitro activity in acute myeloid blasts and leukemic progenitor cells through the induction of a DNA damage response. *Haematologica* 2011;96(5): 687-695. *Doi: 10.3324/haematol.2010.036400*
59. Maiso P, Colado E, Ocio EM, Garayoa M, Martín J, Atadja P, Pandiella A, San-Miguel JF. The synergy of panobinostat plus doxorubicin in acute myeloid leukemia suggests a role for HDAC inhibitors in the control of DNA repair. *Leukemia* 2009;23(12): 2265-2274. *Doi: 10.1038/leu.2009.182*
60. Anvekar RA, Ascioia JJ, Missert DJ, Chipuk JE. Born to be alive: a role for the BCL-2 family in melanoma tumor cell survival, apoptosis, and treatment. *Front Oncol* 2011;1(34): 34. *Doi: 10.3389/fonc.2011.00034*
61. Garner TP, Lopez A, Reyna DE, Spitz AZ, Gavathiotis E. Progress in targeting the BCL-2 family of proteins. *Curr Opin Chem Biol* 2017;39: 133-142. *Doi: 10.1016/j.cbpa.2017.06.014*
62. Kastan MB. A BID for the pathway. *Nature* 2005;437(7062):1103. *Doi: 10.1038/4371103a*
63. Omonosova E, Hinnadurai G. BH3-only proteins in apoptosis and beyond: an overview. *Oncogene* 2008;27(Suppl 1): S2-S19. *Doi: 10.1038/onc.2009.39*
64. Klee M, Pallauf K, Alcalá S, Fleischer A, Pimentel-Muños FX. Mitochondrial apoptosis induced by BH3-only molecules in the exclusive presence of endoplasmic reticular Bak. *EMBO J* 2009;28(12): 1757-1568. *Doi: 10.1038/emboj.2009.90*
65. Wei MC, Zong WX, Cheng EHY, Lindsten T, Panoutsakopoulou V, Ross AJ, Roth KA, MacGregor GR, Thompson CB, Korsmeyer SJ. Proapoptotic BAX, and BAK: a requisite gateway to mitochondrial dysfunction and death. *Science* 2001;292(5517): 727-730. *Doi: 10.1126/science.1059108*
66. Wilkinson JC, Wilkinson AS, Scott FL, Csomos RA, Salvesen GS, Duckett CS. Neutralization of Smac/Diablo by inhibitors of apoptosis (IAPs). A caspase-independent mechanism for apoptotic inhibition. *J Biol Chem* 2004;279(49): 51082-51090. *Doi: 10.1074/jbc.M408655200*
67. Sun XM, Bratton SB, Butterworth M, MacFarlane M, Cohen GM. Bcl-2 and Bcl-xL inhibit CD95-mediated apoptosis by preventing mitochondrial release of Smac/DIABLO and subsequent inactivation of X-linked inhibitor-of-apoptosis protein. *J Biol Chem* 2002;277(13): 11345-11351. *Doi: 10.1074/jbc.M109893200*
68. Arnoult D, Gaume B, Karbowski M, Sharpe JC, Cecconi F, Youle RJ. Mitochondrial release of AIF and EndoG requires caspase activation downstream of Bax/Bak-mediated permeabilization. *EMBO J* 2003;22(17): 4385-4399. *Doi: 10.1093/emboj/cdg423*
69. Candé C, Cecconi F, Dessen P, Kroemer G. Apoptosis-inducing factor (AIF): key to the conserved caspase-independent pathways of cell death? *J Cell Sci* 2002;115(Pt 24): 4727-4734. *Doi: 10.1242/jcs.00210*
70. Kroemer G, Martin SJ. Caspase-independent cell death. *Nat Med* 2005;11(7): 725-730. *Doi: 10.1038/nm1263*
71. Li LY, Luo X, Wang X. Endonuclease G is an apoptotic DNase when released from mitochondria. *Nature* 2001;412(6842): 95-99. *Doi: 10.1038/35083620*
72. Van Loo G, Schotte P, Van Gurp M, Demol H, Hoorelbeke B, Gevaert K, Rodríguez I, Ruiz-Carrillo A, Vandekerkhove J, Declercq W, Beyaert R, Vandenabeele P. Endonuclease G: a mitochondrial protein released in apoptosis and involved in caspase-independent DNA degradation. *Cell Death Differ* 2001;8(12): 1136-1142. *Doi: 10.1038/sj.cdd.4400944*
73. Wu W, Liu P, Li J. Necroptosis: an emerging form of programmed cell death. *Crit Rev Oncol Hematol* 2012;82(3): 249-258. *Doi: 10.1016/j.critrevonc.2011.08.004*
74. Galluzzi L, Vanden Berghe T, Vanlangenakker N, Buettner S, Eisenberg T,

- Vandenabeele P, Madeo F, Kroemer G. Programmed necrosis from molecules to health and disease. *Int Rev Cell Mol Biol* 2011;289: 1-35. *Doi: 10.1016/B978-0-12-386039-2.00001-8*
75. Günther C, Martini E, Wittkopf N, Amann K, Weigmann B, Neumann H, Waldner MJ, Hedrick SM, Tenzer S, Neurath MF, Becker C. Caspase-8 regulates TNF- α -induced epithelial necroptosis and terminal ileitis. *Nature* 2011;477(7364): 335-339. *Doi: 10.1038/nature10400*
76. Duprez L, Takahashi N, Van Hauwermeiren F, Vandendriessche B, Goossens V, Vanden Berghe T, Declercq W, Libert C, Cauwels A, Vandenabeele P. RIP kinase-dependent necrosis drives lethal systemic inflammatory response syndrome. *Immunity* 2011;35(6): 908-918. *Doi: 10.1016/j.immuni.2011.09.020*
77. McNamara CR, Ahuja R, Osafo-Addo AD, Barrows D, Kettenbach A, Skidan I, Teng X, Cuny GD, Gerber S, Degterev A. Akt Regulates TNF α synthesis downstream of RIP1 kinase activation during necroptosis. *PLoS One* 2013;8(3): e56576. *Doi: 10.1371/journal.pone.0056576*
78. Wajant H, Siegmund D. TNFR1 and TNFR2 in the control of the life and death balance of macrophages. *Front Cell Dev Biol* 2019;7: 91. *Doi: 10.3389/fcell.2019.00091*
79. Cho YS, Challa S, Moquin D, Genga R, Ray TD, Guildford M, Chan FK. Phosphorylation-driven assembly of the RIP1-RIP3 complex regulates programmed necrosis and virus-induced inflammation. *Cell* 2009;137(6): 1112-1123. *Doi: 10.1016/j.cell.2009.05.037*
80. Giampietri C, Starace D, PetruNGaro S, Filippini A, Ziparo E. Necroptosis: molecular signalling and translational implications. *Int J Cell Biol* 2014;2014: 49027. *Doi: 10.1155/2014/490275*
81. Liu Q, Qiu J, Liang M, Golinski J, Van Leyen K, Jung JE, You Z, Lo EH, Degterev A, Whalen MJ. Akt and mTOR mediate programmed necrosis in neurons. *Cell Death Dis* 2014;5(2): e1084. *Doi: 10.1038/cddis.2014.69*
82. Dondelinger Y, Declercq W, Montessuit S, Roelandt R, Goncalves A, Bruggeman I, Hulpiau P, Weber K, Schon CA, Marquis RW, Bertin J, Gough PJ, Savvides S, Martinou JC, Bertrand MJ, Vandenabeele P. MLKL compromises plasma membrane integrity by binding to phosphatidylinositol phosphates. *Cell Rep* 2014;7(4): 971-981. *Doi: 10.1016/j.celrep.2014.04.026*
83. Uchiyama Y, Shibata M, Koike M, Yoshimura K, Sasaki M. Autophagy-physiology and pathophysiology. *Histochem Cell Biol* 2008;129(4): 407-420. *Doi: 10.1007/s00418-008-0406-y*
84. Mizushima N and Komatsu M. Autophagy: renovation of cells and tissues. *Cell* 2011;147(4): 728-741. *Doi: 10.1016/j.cell.2011.10.026*
85. Lindqvist LM, Heinlein M, Huang DCS, Vaux DL. Prosurvival Bel-2 family members affect autophagy only indirectly, by inhibiting Bax and Bak. *Proc Natl Acad Sci U S A* 2014;111(23): 8512-8517. *Doi: 10.1073/pnas.1406425111*
86. Klionsky DJ, Petroni G, Amaravadi RK, Baehrecke EH, Ballabio A, Boya P, Bravo-San Pedro JM, Cadwell K, Cecconi F, Pietrocola F. Autophagy in major human diseases. *EMBO J* 2021;40(19): e108863. *Doi: 10.15252/embj.2021108863*
87. Choi AMK, Ryter SW, Levine B. Autophagy in human health and disease. *N Engl J Med* 2013;368(7): 651-662. *Doi: 10.1056/NEJMra1205406*
88. Hale AN, Ledbetter DJ, Gawriluk TR, Rucker EB. Autophagy: regulation and role in development. *Autophagy* 2013;9(7): 951-972. *Doi: 10.4161/auto.24273*
89. Cheng Y, Ren X, Hait WN, Yang JM. Therapeutic targeting of autophagy in disease: biology and pharmacology. *Pharmacol Rev* 2013;65(4): 1162-1197. *Doi: 10.1124/pr.112.007120*
90. Johansen T, Lamark T. Selective autophagy mediated by autophagic adapter proteins. *Autophagy* 2011;7(3): 279-296. *Doi: 10.4161/auto.7.3.14487*
91. Ryter SW, Mizumura K, Choi AMK. The impact of autophagy on cell death moda-

- lities. *Int J Cell Biol* 2014;2014: 502676. *Doi: 10.1155/2014/502676*
- 92. Kwanten WJ, Martinet W, Michielsen PP, Francque SM.** Role of autophagy in the pathophysiology of nonalcoholic fatty liver disease: a controversial issue. *World J Gastroenterol* 2014;20(23): 7325-7338. *Doi: 10.3748/wjg.v20.i23.7325*
- 93. Ding WX, Yin XM.** Mitophagy: mechanisms, pathophysiological roles, and analysis. *Biol Chem* 2012;393(7): 547-564. *Doi: 10.1515/hsg-2012-0119*

Valor de la ^{18}F -FDG-PET/CT en la estadificación inicial de pacientes con cáncer de tiroides de moderado/alto riesgo con subtipos histológicos agresivos.

Luis Felipe Colmener^{1,2,3}, Sunil Daryanani⁴, Sergio Zúñiga⁵ y Javier Vilca⁶

¹Universidad del Zulia. Maracaibo. Venezuela.

²Universidad de Sao Paulo, Sao Paulo, Brasil.

³Pontificia Universidad Javeriana de Cali. Cali, Colombia.

⁴Universidad Central de Venezuela. Caracas, Venezuela.

⁵Hospital de la Universidad Nacional de Colombia. Bogotá, Colombia.

⁶Universidad de Montevideo. Montevideo. Uruguay.

Palabras clave: cáncer de tiroides agresivo; ^{131}I ; transportadores de glucosa; tiroglobulina; TgAb.

Resumen. En los últimos años, la tomografía por emisión de positrones / tomografía computarizada (^{18}F -FDG-PET/CT o ^{18}F Fluoro-2-deoxi-D-glucosa-PET/CT) se ha convertido en una herramienta importante para el tratamiento postoperatorio de pacientes con cáncer de tiroides diferenciado (CDT) y es ampliamente utilizado en situaciones clínicas seleccionadas. El papel más valioso que desempeña la ^{18}F -FDG -PET / CT en la práctica clínica es que puede ser utilizada para obtener información pronóstica en pacientes con niveles crecientes de tiroglobulina (Tg), así como un rastreo corporal con yodo radiactivo (^{131}I) negativo y ablación con ^{131}I . La ^{18}F -FDG -PET / CT también puede tener un papel potencial en la estadificación inicial y el seguimiento de los pacientes de intermedio y alto riesgo con subtipos histológicos agresivos, en la identificación de los pacientes con mayor riesgo de mortalidad específica por enfermedad y en el manejo de pacientes con enfermedad refractaria al ^{131}I . Varios artículos apoyan la hipótesis de que la captación de ^{18}F -FDG puede tener valor pronóstico en CDT. Por un lado, la captación de ^{18}F -FDG en el cáncer de tiroides primario está relacionada con la expresión y diferenciación del transportador de glucosa (GLUT) y, por otro lado, se ha encontrado una asociación entre la captación de ^{18}F -FDG y las características histológicas agresivas, el tamaño del tumor y las metástasis a los ganglios linfáticos.

Value of the ^{18}F -FDG-PET/CT in the initial staging of patients with high-risk thyroid cancer with aggressive histological subtypes.

Invest Clin 2024; 65 (2): 253 – 263

Keywords: aggressive thyroid cancer; ^{131}I ; glucose transporters; thyroglobulin; TgAb.

Abstract. In recent years, positron emission tomography / computed tomography (^{18}F -FDG-PET / CT) or 2-(^{18}F) -fluoro-2-deoxy-D-glucose has become an essential tool for the postoperative treatment of patients with differentiated thyroid cancer (CDT), and it is widely used in selected clinical situations. The most valuable role that ^{18}F -FDG -PET / CT plays in clinical practice is that it can be used to obtain prognostic information in patients with increasing levels of thyroglobulin (Tg) and negative radioactive iodine (^{131}I) body scan and ablation with ^{131}I . The ^{18}F -FDG -PET / CT may also have a potential role in the initial staging and monitoring of high-risk patients with aggressive histological subtypes, identifying patients with a higher risk of disease-specific mortality, and managing patients with disease refractory to ^{131}I . Several articles support the hypothesis that the uptake of ^{18}F -FDG may have prognostic value in CDT. On the one hand, the uptake of ^{18}F -FDG in primary thyroid cancer is related to the expression and differentiation of the glucose transporter (GLUT). On the other hand, an association has been found between the uptake of ^{18}F -FDG and the aggressive histological characteristics, tumor size, and lymph node metastases.

Recibido: 05-07-2023

Aceptado: 04-02-2024

INTRODUCCIÓN

El carcinoma diferenciado de tiroides (CDT) es la neoplasia maligna endocrina más común, representa del 80 al 90% de los cánceres de tiroides y muestra un aumento notable en la prevalencia en las últimas décadas. Aunque el CDT generalmente tiene una naturaleza indolente y un pronóstico favorable, un subconjunto de pacientes enfrenta un alto riesgo de recurrencia y mortalidad. Aproximadamente entre el 20% y el 30% de las personas experimentan una recaída y el 7% sucumben dentro de una década del diagnóstico inicial. El seguimiento posoperatorio que incluye tiroidectomía total y ablación con yodo radiactivo es estándar, y la elevación de la tiroglobulina (Tg) sérica

indica enfermedad persistente o recurrente. Sin embargo, surgen desafíos cuando las metástasis no absorben yodo radiactivo, lo que indica una posible resistencia o dediferenciación celular ^{1,2}.

La incapacidad de atrapar yodo radiactivo en el CDT a menudo se asocia con metástasis y disminución de la supervivencia, y estos casos exhiben un comportamiento agresivo. En particular, entre el 10% y el 30% de los pacientes con CDT recurrente presentan yodo radiactivo negativo y niveles elevados de Tg en la gammagrafía, lo cual reduce drásticamente a 3-5 años la mediana de supervivencia después de la detección de metástasis ².

Por otro lado, la presencia de anticuerpos antitiroglobulina (TgAb) en el momento

del diagnóstico, que se encuentran en el 25-30% de los pacientes con CDT, complica la confiabilidad del análisis de Tg sérica. Estos anticuerpos, teóricamente desencadenados por el tejido tiroideo secretor de Tg, podrían reflejar indirectamente la masa tumoral. Después de la cirugía y de la ablación con yodo radiactivo, los niveles de TgAb generalmente disminuyen, pero pueden persistir durante un promedio de tres años. La evidencia emergente sugiere que cuando las pruebas de Tg en suero se ven obstaculizadas por la presencia de TgAb, las tendencias de concentración de anticuerpos podrían servir como un marcador tumoral CDT sustituto ³.

Hallazgos recientes también proponen una correlación entre los títulos de TgAb y la agresividad del CDT; los pacientes positivos para TgAb con frecuencia caen en categorías de mayor riesgo y exhiben diseminación del tumor extratiroideo. Un estudio multicéntrico confirmó además que la positividad de TgAb después del tratamiento primario se correlaciona, significativamente, con la recaída de la enfermedad durante el seguimiento posterior ^{4,5}.

La estratificación del riesgo, según la Asociación Estadounidense de Tiroides, sugiere un riesgo intermedio a alto de enfermedad persistente/recurrente según el estadio y la integridad de la resección quirúrgica, como lo refleja la extensión extratiroidea.

De manera similar, la Asociación Europea de Tiroides clasifica a los pacientes con extensión extratiroidea como de alto riesgo de enfermedad persistente ^{6,7}.

Factores como el tamaño del tumor, la multifocalidad, la invasión extratiroidea, las variantes histológicas (p. ej., células altas, esclerosantes difusas, células tiroideas oncocíticas, anteriormente conocidas como células de Hürthle ⁸ y la resistencia al ¹³¹I son determinantes pronósticos fundamentales en el CDT. La presencia de metástasis linfática o a distancia en el momento del diagnóstico es un factor de pronóstico negativo significativo, que se correlaciona positivamente con los resultados de ¹⁸F-FDG-PET/CT ^{9,10} (Tabla 1).

A pesar de la creciente evidencia científica sobre la utilidad de la ¹⁸F-FDG-PET/CT en el manejo de pacientes con CDT de riesgo alto/intermedio, las guías clínicas a menudo incorporan esta indicación con limitaciones o la omiten por completo. Este artículo proporciona una descripción general de los datos moleculares y clínicos de Pubmed, tesis académicas y directrices estadounidenses y europeas sobre el uso de ¹⁸F-FDG-PET/CT en el tratamiento de pacientes con CDT de riesgo moderado a alto.

¹⁸F-FDG PET/CT y cáncer de tiroides

Como la primera técnica validada de “imágenes metabólicas”, tanto en la ciencia

Tabla 1
Factores de mal pronóstico en el cáncer diferenciado de tiroides.

Factores de mal pronóstico		
Tamaño	Clínicos	>1cm
Multifinalidad	Clínicos	Más de dos lesiones
Invasión vascular	Clínicos	Factor de Crecimiento
Diseminación linfática	Clínicos	Factor de Crecimiento
Metástasis a distancia	Clínicos	Factor de Crecimiento
Variantes histológicas	Histológico	Grado de desdiferenciación y tipos de célula
Citología indeterminada	Citología	RAI negativo
Resistencia al ¹³¹ I	Metabólicos	>de 10ng/dL
Elevación de los TgAb	Metabólicos	
Persistencia o elevación de la Tg		
¹⁸ F-FDG-PET positivo	Metabólicos	>de 10mg/dL

básica como en entornos clínicos, la FDG es el trazador PET más utilizado para la obtención de imágenes de tumores malignos. Una tasa acelerada del metabolismo de la glucosa, mediada por la regulación positiva de enzimas y transportadores glucolíticos (GLUT), es característica de la transformación maligna, un fenómeno reconocido desde hace más de ocho décadas. Sin embargo, en los tumores de tiroides, el aumento de la captación de FDG se limita a neoplasias malignas más agresivas y de alto grado, y los tumores bien diferenciados muestran una captación insignificante del trazador. Se cree que la relación inversa entre la captación de ^{131}I y ^{18}F -FDG en el carcinoma de tiroides, conocida como fenómeno “flip-flop”, se debe a una pérdida de la capacidad de concentración de ^{131}I durante la dediferenciación combinada con una mayor demanda de glucosa por parte de las células tumorales ¹¹ (Fig. 1).

Importancia del tamaño, multimodalidad e invasión vascular tumoral, diseminación linfática y metástasis a distancia

La American Thyroid Association (ATA) incluye la ^{18}F -FDG-PET como una herramienta fundamental en la detección temprana de carcinomas tiroideos de escasa diferenciación y variantes oncocíticas ⁶. Investigaciones han evidenciado que la PET/CT con ^{18}F -FDG, realizada al inicio del seguimiento de pacientes con CDT de riesgo alto o intermedio, puede modificar sustancialmente la estrategia de tratamiento al revelar datos cruciales que no se detectan con métodos convencionales. Se ha demostrado que el tamaño del tumor, la invasión vascular y la diseminación metastásica son factores determinantes en la positividad de la ^{18}F -FDG PET/CT, subrayando su relevancia en la estratificación del riesgo y la toma de decisiones clínicas.

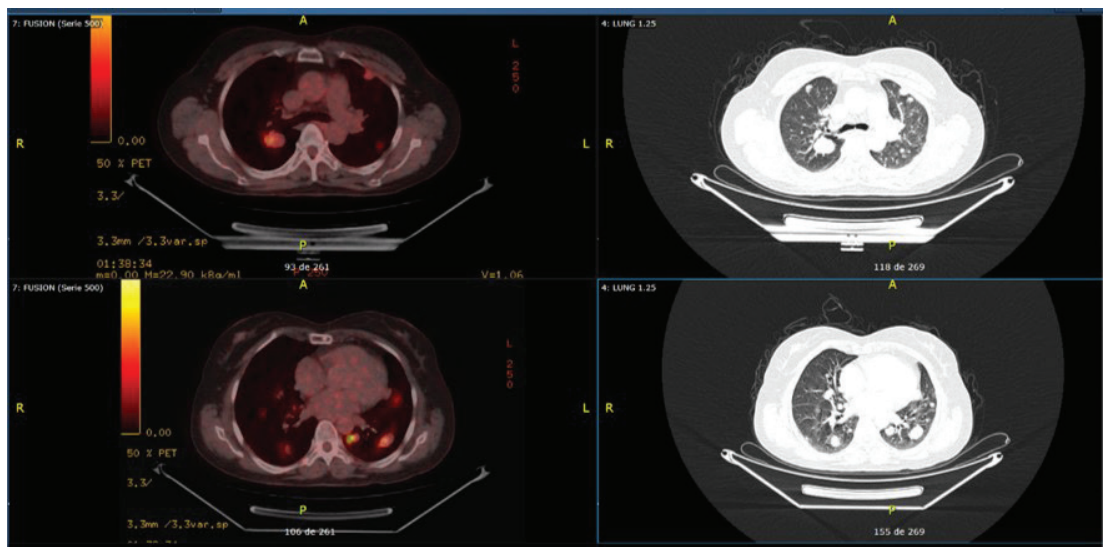


Fig. 1. Ilustra un caso extraído de nuestra práctica clínica habitual, correspondiente a una paciente de 57 años diagnosticada con carcinoma folicular bien diferenciado. En octubre de 2010, se sometió a una tiroidectomía total. El examen histopatológico reveló la presencia de un adenoma folicular con un patrón trabecular y células oncocíticas, sin invasión capsular ni evidencia de invasión vascular. En 2015, una radiografía de tórax reveló un nódulo pulmonar de 3 cm. Para octubre de 2018, los niveles de tiroglobulina se encontraban elevados, y un rastreo con yodo radiactivo (^{131}I) no mostró captación del radioisótopo. Posteriormente, se realizó un estudio con ^{18}F -FDG PET/CT, que demostró la presencia de múltiples nódulos pulmonares hipermetabólicos, con un Valor de Captación Estándar (SUVmax) 8.1, con diámetros de hasta 33 mm y se distribuían en las regiones centrales y periféricas de ambos campos pulmonares. Dichos hallazgos son indicativos de un proceso de dediferenciación y progresión de la enfermedad oncológica.

Rosenbaum-Krumme y col. ¹², en un estudio prospectivo estudiaron el beneficio de la ¹⁸F-FDG PET/CT realizada después de la terapia ablativa con ¹³¹I en 90 pacientes con CDT de alto riesgo, encontrando que el 29% de los pacientes estudiados presentaron un estudio ¹⁸F-FDG PET/CT positivo y cambió la estrategia de tratamiento en el 21% de ellos. Del mismo modo, Iwano y col. ¹³ estudiaron 54 pacientes con CDT a los que le realizaron un estudio ¹⁸F-FDG PET/CT con la estimulación de TSH 3-4 días antes de la ablación con ¹³¹I, y encontraron que el estudio fue positivo en 33% de los pacientes.

La presencia de invasión vascular en el análisis histológico, la afectación ganglionar cervical y la afectación metastásica a distancia en el momento del diagnóstico, son los principales factores asociados con un estudio ¹⁸F-FDG PET/CT positivo ⁹.

TSH, Tiroglobulina y Anti-tiroglobulina

Los niveles de Tiroglobulina (Tg) posquirúrgicos son indicativos del tejido tiroideo residual. Se ha enfatizado la relevancia de Tg y TSH para optimizar la precisión del ¹⁸F-FDG PET/CT. Este último se indica principalmente para el seguimiento de pacientes con CDT bajo el síndrome TENIS (Thyroglobulin Elevated with Negative radioiodine Scintigraphy), acorde a las directrices de la ATA ⁶. Un Tg elevado (> 10 ng/mL) o su duplicación rápida son factores que potencian la detección de la ¹⁸F-FDG-PET/CT, incluso con niveles bajos de Tg. Aproximadamente un tercio de los pacientes con Tg sérica elevada podrían modificar su tratamiento posoperatorio basándose en los resultados de la

¹⁸F-FDG PET/CT, particularmente en etapas avanzadas del CDT ^{2,9}. La PET/CT es también prometedora en la evaluación del CDT con terapia de ablación con yodo negativa y TgAb elevados, reflejando un metabolismo glucémico tumoral activo y posiblemente una mayor agresividad del tumor ¹⁴. Los TgAb pueden actuar como marcadores sustitutos y su disminución post-tratamiento sugiere un menor riesgo de recurrencia o enfermedad persistente.

Diferenciación vs Desdiferenciación

El proceso de desdiferenciación del CDT, se establece con la existencia del metabolismo de la glucosa regulado al alza, (activación de los GLUTs) combinado con el metabolismo del yodo regulado a la baja (inhibición de los NIS) ² (Tabla 2).

En los últimos tiempos, una comprensión cada vez mayor de la oncología molecular ha impulsado el uso de agentes dirigidos y nuevas estrategias de Re-diferenciación para el tratamiento de diferentes tipos de carcinomas de tiroides avanzados. Uno de los cambios oncogénicos más comunes observados en cáncer papilar de tiroides es el reordenamiento RET/ PTC, que resulta en una autofosforilación constitutivamente activa de RET Y1062, y reduce la expresión del gen NIS. Ruan y col. ¹⁵, aclararon parcialmente el mecanismo subyacente del fenómeno de “flip-flop” confirmando que la expresión de los genes de diferenciación tiroidea aumentan significativamente después del tratamiento con sorafenib o cabozantinib, lo que indica que ambos fármacos podrían restaurar efectivamente la expresión de los genes

Tabla 2
Comportamiento metabólico tumoral de la metástasis del CDT.

Comportamiento tumoral	¹⁸ F-FDG PET/ CT	Rastreo con ¹³¹ I	Comportamiento histológico
MT. con Aidez a la Glucosa y Iodos	Positivo	Positivo	Poco diferenciado.
MT. con Aidez a la Glucosa y refractario al Iodo	Positivo	Negativo	Des diferenciado.
MT. con Aidez al yodo y refractario a la glucosa.	Negativo	Positivo	Diferenciado

que manejan yoduro tiroideo y, por lo tanto, la captación de radioyodo en el cáncer de tiroides. En ese estudio, la expresión génica y proteica de GLUT1 y GLUT3 y la captación de ^{18}F -FDG disminuyeron significativamente en las células BHP 2-7 y K1 después del tratamiento con sorafenib o cabozantinib, lo que indica que la respuesta del tratamiento de seguimiento a la terapia TKI utilizando ^{18}F -FDG PET es posible ¹⁵.

Variantes histológicas (células altas, esclerosante difusa, células oncocíticas de la tiroides)

Los carcinomas de tiroides con histología agresiva, incluyendo variantes como el carcinoma mal diferenciado, células altas, células columnares, células oncocíticas, células insulares, escleriosis difusa y carcinoma oncocítico, son propensos a no captar radioyodo, presentando tasas elevadas de enfermedad persistente o recurrente. En el 22%-65% de estas pacientes se presentan enfermedades persistentes o recurrentes después del tratamiento definitivo ¹. Estas variantes, ávidas de FDG, requieren de ^{18}F -FDG PET/CT para evaluar el alcance de la enfermedad y pronosticar su curso. Estudios destacan la alta sensibilidad del PET/CT con FDG en el carcinoma oncocítico de tiroides y sugieren que una intensa captación de FDG indica un pronóstico desfavorable. La PET/CT con FDG se convierte así en una herramienta diagnóstica crucial para estos subtipos, mejorando la estrategia terapéutica y la precisión en la evaluación pronóstica ¹⁶.

El carcinoma de células oncocíticas de la tiroides es un subtipo histológico agresivo de cáncer de tiroides, con un alto riesgo de metástasis y un peor pronóstico en comparación con el CDT. El carcinoma de células oncocíticas de la tiroides parece incapaz de concentrar ^{131}I , pero es un tumor ávido por FDG. La localización precisa de la enfermedad es esencial en el carcinoma de células oncocíticas de la tiroides, ya que la cirugía y la radioterapia de haz externo pueden ser beneficiosas.

Varios estudios han demostrado una alta sensibilidad de la PET con FDG para el carcinoma de células oncocíticas de la tiroides, en relación con otras modalidades de imagen. Un estudio multicéntrico realizado por Rie-man y col. encontraron una sensibilidad del 92% y una especificidad del 95% para la PET/CT con FDG en el carcinoma de tiroides de células de Hürthle, mientras que los valores correspondientes para ^{131}I fueron 65% y 94% y los de ultrasonido fueron 37% y 94% ¹⁷.

Carcinoma de tiroides anaplásico (ATC) vs carcinoma medular

El carcinoma anaplásico de tiroides (ATC) representa el 5% de todos los carcinomas tiroideos, destacándose como uno de los más letales con una supervivencia promedio de apenas 3 meses sin tratamiento efectivo. Generalmente, la mortalidad se asocia con la diseminación metastásica más que con el crecimiento local. Estudios han demostrado que la PET/CT con ^{18}F -FDG supera en precisión a la CT convencional para la detección temprana de metástasis, en especial en ganglios linfáticos mediastínicos y cervicales. Además, la intensidad de captación de FDG y el SUV max resultan ser predictores significativos de la supervivencia, ofreciendo así una herramienta valiosa tanto en la estadificación inicial como en la respuesta al tratamiento ¹⁸.

Bogsrud y col. ¹⁹, investigaron el papel de ^{18}F -FDG PET / CT en el manejo de 16 pacientes con ATC al comparar los datos de PET con otras herramientas de diagnóstico y con el seguimiento clínico. En todos los pacientes, los registros de PET fueron verdaderos positivos para tumores primarios, y en el 50% de los pacientes, los datos de la PET influyeron en el manejo clínico. Estos autores concluyeron que la ^{18}F -FDG PET/CT podría mejorar la estadificación de la enfermedad y, por lo tanto, cambiar potencialmente el manejo clínico de los pacientes con ATC.

El valor de la PET/CT con FDG en el cáncer medular de tiroides (MTC) radica en su utilidad para detectar recurrencias o me-

tástasis del MTC, particularmente en aquellos casos donde las células tumorales han adquirido características metabólicas que les permiten captar la FDG. Aunque otros trazadores como la dihidroxifenilalanina (FDOPA) y los análogos de somatostatina son frecuentemente utilizados, la FDG-PET/CT puede ser especialmente útil en casos de MTC avanzado y en situaciones donde se sospecha una enfermedad más agresiva y menos diferenciada ²⁰.

Refractariedad al ¹³¹I

La refractariedad al ¹³¹I en el contexto del carcinoma diferenciado de tiroides metastásico se refiere a la incapacidad de algunas metástasis para absorber el radioyodo; hasta el 10% de las metástasis se vuelven radioyodo refractario y no pueden beneficiarse de la terapia con ¹³¹I con mayor riesgo de efectos adversos. Por lo tanto, la terapia con ¹³¹I debe limitarse a pacientes con CDT seleccionados con metástasis ávidas con ¹³¹I ². Esta resistencia al ¹³¹I conduce a un pronóstico menos favorable, por lo que es crucial identificar y explorar alternativas terapéuticas para los pacientes afectados. La selección cuidadosa de pacientes para la terapia con ¹³¹I es esencial y dependerá la captación o no del FDG.

La refractariedad al radioyodo (¹³¹I) en el cáncer diferenciado de tiroides (DTC) puede ocurrir debido a la pérdida de características diferenciadas de las células tiroideas, lo que incluye la captación y organificación de yodo. Esto significa que las células cancerosas ya no expresan el transportador de yodo sódico (NIS) adecuadamente o que los mecanismos que permiten la captación y el almacenamiento del yodo dentro de la célula están alterados o ausentes.

Una proporción pequeña pero significativa de cánceres de tiroides diferenciados se vuelven refractarios al tratamiento con radioyodo, ya sea porque pierden la capacidad de captar yodo con el tiempo o porque, a pesar de mantener la capacidad de captación, el efecto del radioyodo se pierde en

términos de reducción de la carga tumoral. Estos pacientes generalmente reciben pocos y transitorios beneficios de otras terapias convencionales y especialmente de la quimioterapia.

En la última década, se han descubierto y probado en ensayos clínicos varios nuevos fármacos, principalmente moléculas inhibitoras de la cinasa proteica, que se deberían proponer a pacientes avanzados y progresivos con cáncer de tiroides refractario a ¹³¹I, inscribiéndolos en ensayos clínicos o mediante el uso “fuera de etiqueta” del fármaco ²¹.

¹⁸F-FDG-PET positivo y SUV (Valor de captación estándar)

Las localizaciones de CDT a menudo se caracterizan por una baja captación de ¹⁸F-FDG, especialmente en pacientes jóvenes afectados por subtipos de cáncer de tiroides bien diferenciados ²². Teóricamente, el nivel de metabolismo de la glucosa puede ser evaluado en forma cualitativa (evaluación visual) o cuantitativamente (medición del SUV) por ¹⁸F-FDG PET / CT.

El volumen de lesiones FDG-ávidas, valor de captación estándar máxima (SUV max) número y la ubicación de las metástasis pueden correlacionarse con el resultado y la supervivencia en los análisis uní variados y multivariados. Stangierski y col.²³ encontraron que el SUVmax se correlacionó significativamente con un alto volumen de enfermedad ávida por FDG, lo que sugiere que los tumores con la mayor actividad metabólica podrían ser los que tienen el potencial de crecimiento más rápido y menor pronóstico.

Otros trabajos han demostrado que la captación de FDG es altamente pronóstica para la supervivencia y que el SUV max y el número de lesiones ávidas de FDG también se relacionaron con la agresividad y pronóstico. Estos datos resaltan la importancia clínica de ¹⁸F-FDG-PET / CT en el tratamiento de pacientes con cáncer de tiroides metastásico ²⁴.

De hecho, las metástasis ávidas por FDG se asocian con un mayor riesgo de mortalidad y las variables absolutas derivadas de

la PET, como SUV mean y SUV max, se han relacionado directamente con el aumento del comportamiento agresivo en varios tipos de tumores, incluido el CDT⁵. Múltiples estudios han tratado de establecer un punto de corte del SUV que defina malignidad vs benignidad en el caso de los nódulos o pronóstico a grado de agresividad en metástasis con avidéz del FDG.

Múltiples estudios han publicado sobre el tema, pero no hay un consenso. Liu²⁵ refiere que con un valor de corte de SUVmax 4.0, si la metástasis fuera mayor que 4.0, se debe sospechar una lesión de CDT metastásico no ávida al ¹³¹I y podría estar indicada una terapia adyuvante para mejorar o restaurar la capacidad de atrapar ¹³¹I.

Evaluación de Nódulos

Un tercio de los hallazgos evaluados son malignos. No se ha identificado un límite adecuado de valor de captación estandarizado (SUV) capaz de distinguir entre lesiones benignas y malignas Kim y col.²⁶ refieren que las imágenes de la ¹⁸F-FDG PET / CT que muestra el aumento captación de FDG en nódulos con volúmenes ≥ 1 cm y un SUVmáx mayor que 6, la probabilidad de malignidad es muy alta.

TSH Recombinante Humano y ¹⁸F-FDG PET/CT

El principal desafío al inducir un estado de hipotiroidismo extremo en pacientes para el tratamiento con yodo radiactivo o estudio con ¹⁸F-FDG PET/CT, es la amplia gama de efectos secundarios que pueden afectar significativamente su calidad de vida. Los pacientes a menudo experimentan síntomas psicológicos y emocionales severos, como depresión, ansiedad y problemas de memoria. Además, pueden presentar alteraciones cognitivas y emocionales que impactan en su vida laboral, extendiendo a veces la baja laboral por un período considerable.

Frente a estos desafíos, el uso de la TSH recombinante humana emerge como una alternativa viable. Esta opción permite evitar

los efectos secundarios del hipotiroidismo, manteniendo la eficacia del tratamiento con yodo radiactivo y minimizando los impactos negativos en la calidad de vida del paciente²⁷. La TSH recombinante humana es una glicoproteína producida mediante tecnología de ADN recombinante y se sintetiza en células de ovario de hámster. Sus propiedades son idénticas a las de la TSH humana natural. Se une a los receptores de TSH de las células tiroideas y ha sido aprobada para fines diagnósticos, como el rastreo de células tiroideas, desde 1998. Desde 2008, la FDA también ha aprobado su uso como parte del tratamiento complementario con yodo radiactivo en pacientes con cáncer de tiroides.

CONCLUSIÓN

La ¹⁸F-FDG PET/CT se está posicionando como una herramienta indispensable en la estrategia de manejo del carcinoma diferenciado de tiroides (CDT), no solo durante la evaluación inicial y postquirúrgica, sino también como un medio efectivo para monitorear la progresión de la enfermedad y la respuesta al tratamiento. Su aplicación es especialmente valiosa en la identificación de recurrencias y en la valoración de tumores con tiroglobulina elevada en ausencia de captación en el rastreo con radioyodo.

Es evidente que la ¹⁸F-FDG PET/CT tiene una función destacada en diferentes etapas de la enfermedad; desde el diagnóstico inicial, especialmente en tipos histológicos agresivos, hasta el seguimiento longitudinal, donde su capacidad para detectar recaídas tempranas influye directamente en las estrategias terapéuticas a seguir. Además, este enfoque de imagen puede guiar la terapia personalizada y adaptativa, tomando en cuenta las características histológicas únicas y la dinámica clínica de cada paciente con CDT. Su integración en la práctica clínica continúa enriqueciendo el espectro diagnóstico y terapéutico, permitiendo intervenciones más precisas y oportunas que mejoran los resultados de los pacientes.

AGRADECIMIENTO

El autor dedica este manuscrito a la Memoria de nuestra siempre colaboradora editorial Lic. Mercedes Berrios. 18/12/1964 – 23/04/2023

Financiamiento

No recibe financiamiento.

Conflicto de interés

No existe ningún conflicto de interés

Números ORCID de los autores

- Luis Felipe Colmener R (LFCR): 0000-0003-4219-9559
- Sergio Zúñiga (SZ): 0000-0002-9903-8548
- Javier Vilar (JV): 0000-0003-0806-8790
- Sunil Daryanani (SD): 0000-0003-9858-1188

Contribución de los autores

LFCR: propuesta, concepto y diseño del trabajo; SZ JV y SD analizaron los artículos y participaron activamente en la revisión del manuscrito enviando sus comentarios y sugerencias.

REFERENCIAS

1. Okuyucu K, Ince S, Alagoz E, Emer O, San H, Balkan E, Ayan A, Meric C, Haymana C, Acikel C, Gunalp B, Karacalioglu AO, Arslan N. Risk factors and stratification for recurrence of patients with differentiated thyroid cancer, elevated thyroglobulin and negative I¹³¹ whole-body scan, by re-staging ¹⁸F-FDG PET/CT. *Hell J Nucl Med* 2016 ;19(3):208-217.
2. Liu M, Cheng L, Jin Y, Ruan M, Sheng S, Chen L. Predicting ¹³¹I-avidity of metastases from differentiated thyroid cancer using ¹⁸F-FDG PET/CT in postoperative patients with elevated thyroglobulin. *Sci Rep* 2018; 8(1): 4352. doi: 10.1038/s41598-018-22656-4.
3. Chiovato L, Latrofa F, Braverman LE, Pacini F, Capezzone M, Masserini L, Grasso L, Pinchera A. Disappearance of humoral thyroid autoimmunity after complete removal of thyroid antigens. *Ann Intern Med* 2003;139(5 Pt 1):346-351.
4. Durante C, Tognini S, Montesano T, Orlandi F, Torlontano M, Puxeddu E, Attard M, Costante G, Tumino S, Meringolo D, Bruno R, Trulli F, Toteda M, Redler A, Ronga G, Filetti S, Monzani F; PTC Study Group. Clinical aggressiveness and long-term outcome in patients with papillary thyroid cancer and circulating anti-thyroglobulin autoantibodies. *Thyroid* 2014;24(7):1139-1145.
5. Morbelli S, Ferrarazzo G, Pomposelli E, Pupo F, Pesce G, Calamia I, Fiz F, Clapason A, Bauckneht M, Minuto M, Sambuceti G, Giusti M, Bagnasco M. Relationship between circulating anti-thyroglobulin antibodies (TgAb) and tumor metabolism in patients with differentiated thyroid cancer (DTC): prognostic implications. *J Endocrinol Invest* 2017;40(4):417-424.
6. Haugen BR, Alexander EK, Bible KC, Doherty GM, Mandel SJ, Nikiforov YE, Pacini F, Randolph GW, Sawka AM, Schlumberger M, Schuff KG, Sherman SI, Sosa JA, Steward DL, Tuttle RM, Wartofsky L. 2015 American Thyroid Association Management Guidelines for Adult Patients with Thyroid Nodules and Differentiated Thyroid Cancer: The American Thyroid Association Guidelines Task Force on Thyroid Nodules and Differentiated Thyroid Cancer. *Thyroid* 2016;26(1):1-133. doi: 10.1089/thy.2015.0020.
7. Pacini F, Fuhrer D, Elisei R, Handkiewicz-Junak D, Leboulleux S, Luster M, Schlumberger M, Smit JW. 2022 ETA Consensus Statement: What are the indications for post-surgical radioiodine therapy in differentiated thyroid cancer? *Eur Thyroid J* 2022; 11 (1): e210046. doi: 10.1530/ETJ-21-0046.

8. **Wong KS, Barletta JA.** The new endocrine WHO classification: What does this mean for thyroid cytology? *Cancer Cytopathol* 2022;130: 658-662. <https://doi.org/10.1002/ency.22634>
9. **Triviño Ibáñez EM.** Utilidad de la ¹⁸F-FDG PET/CT precoz en el manejo terapéutico y estratificación dinámica del riesgo de pacientes con carcinoma diferenciado de tiroides de riesgo alto/intermedio. Facultad de Medicina Departamento de Medicina. Granada, 2015. Tesis Doctoral.
10. **Colmener L, Bastianello M, Estrada E.** Conceptualizando VII: Papel de la glucosa y la ¹⁸F-FDG en tumores malignos, con enfoque en cáncer de tiroides (Parte I). *Alasbimn Journal*, 30 de julio, 2012.
11. **Feine U, Lietzenmayer R, Hanke JP, Wöhrle H, Müller-Schauenburg W.** ¹⁸F-FDG-Ganzkörper-PET bei differenzierten Schilddrüsenkarzinomen. Flipflop im Speichermuster von ¹⁸F-FDG und ¹³¹I [¹⁸F-FDG whole-body PET in differentiated thyroid carcinoma. Flipflop in uptake patterns of ¹⁸F-FDG and I]. *Nuklearmedizin* 1995;34(4):127-134.
12. **Rosenbaum-Krumme SJ, Görge R, Bockisch A, Binse I.** ¹⁸F-FDG PET/CT changes therapy management in high-risk DTC after first radioiodine therapy. *Eur J Nucl Med Mol Imaging* 2012;39(9):1373-1380.
13. **Iwano S, Kato K, Ito S, Tsuchiya K, Naganawa S.** FDG-PET performed concurrently with initial I¹³¹ ablation for differentiated thyroid cancer. *Ann Nucl Med* 2012;26(3):207-213.
14. **Liu Y.** The role of ¹⁸F-FDG PET/CT in the follow-up of well-differentiated thyroid cancer with negative thyroglobulin but positive and/or elevated antithyroglobulin antibody. *Nucl Med Commun* 2016;37(6):577-582.
15. **Ruan M, Liu M, Dong Q, Chen L.** Iodide- and glucose-handling gene expression regulated by sorafenib or cabozantinib in papillary thyroid cancer. *J Clin Endocrinol Metab* 2015;100(5):1771-1779.
16. **Nascimento C, Borget I, Ghuzlan AA, Deandreis D, Hartl D, Lumbroso J, Berdelou A, Lepoutre-Lussey CH, Mirghani H, Baudin E, Schlumberger M, Leboulleux S.** Postoperative fluorine-18-fluorodeoxyglucose positron emission tomography/computed tomography: an important imaging modality in patients with aggressive histology of differentiated thyroid cancer. *Thyroid* 2015; 25 (4):437-444. [doi:10.1089/thy.2014.0320](https://doi.org/10.1089/thy.2014.0320) [10.1089/thy.2014.0320](https://doi.org/10.1089/thy.2014.0320)
17. **Riemann B, Uhrhan K, Dietlein M, Schmidt D, Kuwert T, Dorn R, Sciuk J, Kodalle T, Schober O.** Diagnostic value and therapeutic impact of ¹⁸F-FDG-PET/CT in differentiated thyroid cancer. Results of a German multicentre study. *Nuklearmedizin*. 2013;52(1):1-6.
18. **Pryma DA, Schöder H, Gönen M, Robbins RJ, Larson SM, Yeung HW.** Diagnostic accuracy and prognostic value of ¹⁸F-FDG PET in Hürthle cell thyroid cancer patients. *J Nucl Med* 2006;47(8):1260-1266.
19. **Bogsrud TV, Karantanis D, Nathan MA, Mullan BP, Wiseman GA, Kasperbauer JL, Reading CC, Hay ID, Lowe VJ.** ¹⁸F-FDG PET in the management of patients with anaplastic thyroid carcinoma. *Thyroid* 2008;18(7):713-719.
20. **Giovanella L, Treglia G, Iakovou I, Mihailovic J, Verburg FA, Luster M.** EANM practice guideline for PET/CT imaging in medullary thyroid carcinoma. *Eur J Nucl Med Mol Imaging* 2020;47(1):61-77. [doi: 10.1007/s00259-019-04458-6](https://doi.org/10.1007/s00259-019-04458-6). Epub 2019 Sep 4.
21. **Oh JM, Ahn BC.** Molecular mechanisms of radioactive iodine refractoriness in differentiated thyroid cancer: Impaired sodium iodide symporter (NIS) expression owing to altered signaling pathway activity and intracellular localization of NIS. *Theranostics* 2021;11(13):6251-6277. [doi: 10.7150/thno](https://doi.org/10.7150/thno).
22. **Piccardo A, Puntoni M, Bertagna F, Treglia G, Foppiani L, Arecco F, Giubbini R, Naseri M, Cistaro A, Cabria M, Bardesono F, Ceriani L, Orlandi F, Giovanella L.** ¹⁸F-FDG uptake as a prognostic variable in primary differentiated thyroid cancer incidentally detected by PET/CT: a multicentre study. *Eur J Nucl Med Mol Imaging* 2014;41(8):1482-1491.

23. **Stangierski A, Woliński K, Czepezyński R, Czarnywojtek A, Lodyga M, Wyszo-mirska A, Janicka-Jedyńska M, Bączyk M, Ruchała M.** The usefulness of standardized uptake value in differentiation between benign and malignant thyroid lesions detected incidentally in ¹⁸F-FDG PET/CT examination. *PLoS One* 2014;9(10):e109612. *doi: 10.1371/journal.pone.0109612.*
24. **Deandreis D, Al Ghuzlan A, Auperin A, Vielh P, Caillou B, Chami L, Lombroso J, Travagli JP, Hartl D, Baudin E, Schlumberger M, Leboulleux S.** Is ¹⁸F-fluorodeoxyglucose-PET/CT useful for the presurgical characterization of thyroid nodules with indeterminate fine needle aspiration cytology? *Thyroid* 2012;22(2):165-172. *doi: 10.1089/thy.2011.0255.* *Epub* 2012 Jan 18.
25. **Liu Y.** The role of ¹⁸F-FDG PET/CT in the follow-up of well-differentiated thyroid cancer with negative thyroglobulin but positive and/or elevated antithyroglobulin antibody. *Nucl Med Commun* 2016 ;37(6):577-582.
26. **Kim TH, Ji YB, Song CM, Kim JY, Choi YY, Park JS, Tae K.** SUVmax of ¹⁸F-FDG PET/CT in the differential diagnosis of benign and malignant thyroid nodules according to tumor volume. *World J Surg Oncol* 2015;13:217.
27. **Leboulleux S, Borget I, Schlumberger M.** Postoperative radioactive iodine administration in patients with low-risk thyroid cancer. *Nat Rev Endocrinol* 2022;18(10):585-586. *doi: 10.1038/s41574-022-00709-z.*

Contents

EDITORIAL

Impact of viral infections on autoimmunity

Larreal Y (*E-mail: yrainalareal@gmail.com*), Vargas R. 131
<https://doi.org/10.54817/IC.v65n2a00>

ORIGINAL PAPERS

Surgical complications in children with IgA vasculitis: clinical analysis of 28 cases (English).

Mu J, Hao J (*E-mail: bchhaojing@163.com*), Zhen X, MoX, Sheng Y. 134
<https://doi.org/10.54817/IC.v65n2a01>

Beneficial effects of gentiopiricin inhibiting experimental epilepsy in young rats through the P2X7R/NLRP3/Caspase-1 inflammatory pathway (English).

Li JL, Huang L, Wu X, Ye M, Yu CY (*E-mail: yuchuanrongsub@yeah.net*) 143
<https://doi.org/10.54817/IC.v65n2a02>

Benefits of a modified local precision liver resection using intraoperative laparoscopic ultrasound in the treatment and prognosis of patients with liver cancer (English).

Xu Y (*E-mail: tonggubu9822@163.com*), Shen L. 155
<https://doi.org/10.54817/IC.v65n2a03>

Genetic association study of the rs10774671 variant of the *OAS1* gene with the severity of COVID-19 in an Ecuadorian population (English).

Pilataxi K, Balarezo T, Chávez E, Acosta C, Peña IZ, Narváez K, Álvarez-Nava F
 (*E-mail: fjalvarez@uce.edu.ec*) 169
<https://doi.org/10.54817/IC.v65n2a04>

Insulin-like growth factor-1 promotes the proliferation and odontogenic differentiation of human dental pulp cells *in vitro* and *in vivo* (English).

Wang Y, Du N, Liu C, Li WJ (*E-mail: liwenjing2729@163.com*). 179
<https://doi.org/10.54817/IC.v65n2a05>

Gender-based comparative analysis of knee injury risk during cutting maneuvers in non-professional athletes: a kinetic and kinematic perspective (English).

Feria-Madueño A (*E-mail: aferia1@us.es*), Hewett TE, Sañudo B 192
<https://doi.org/10.54817/IC.v65n2a06>

The effectiveness of personalized medication based on drug-related genes, for schizophrenia patients with resistance to traditional drugs (English).

Zhou S, Zhang G, Wang Z, Wei L, Zhu M, He J (*E-mail: hjqcatdog123@163.com*). 206
<https://doi.org/10.54817/IC.v65n2a07>

Effect of thiamine pyrophosphate on oxidative damage in the brain and heart of rats with experimentally induced occlusion of the common carotid artery (English).

Emir I, Suleyman Z, Suleyman H (*E-mail: halis.suleyman@gmail.com*) 220
<https://doi.org/10.54817/IC.v65n2a08>

REVIEWS

Mechanisms of programmed cell death: structural and functional pathways.

A narrative review (English).

Fernández-Lázaro D (*E-mail: diego.fernandez.lazaro@uva.es*), Sanz B, Seco-Calvo J 230
<https://doi.org/10.54817/IC.v65n2a09>

Value of the ¹⁸F-FDG-PET/CT in the initial staging of patients with high-risk thyroid cancer with aggressive histological subtypes (Spanish).

Colmener LP (*E-mail: luiscolmener@hotmail.com*), Daryanani S, Zúñiga S, Vilar J 253
<https://doi.org/10.54817/IC.v65n2a10>

Contenido

EDITORIAL**Impacto de las infecciones virales en la autoinmunidad**

Larreal Y (*Correo electrónico: yrcamalarreal@gmail.com*), Vargas R. 131
<https://doi.org/10.54817/IC.v65n2a00>

TRABAJOS ORIGINALES**Complicaciones quirúrgicas en niños con vasculitis IgA: análisis clínico de 28 casos (Inglés).**

Mu J, Hao J (*Correo electrónico: bchhaojing@163.com*), Zhen X, MoX, Sheng Y. 134
<https://doi.org/10.54817/IC.v65n2a01>

Efectos inhibitorios de la gentiopirina sobre la epilepsia experimental en ratas jóvenes mediante la vía inflamatoria P2X7R/NLRP3/Caspasa-1 (Inglés).

Li JL, Huang L, Wu X, Ye M, Yu CY (*Correo electrónico: yuchuanrongsub@yeah.net*) 143
<https://doi.org/10.54817/IC.v65n2a02>

Beneficios de la resección hepática de precisión local modificada, utilizando ecografía intraoperatoria laparoscópica en el tratamiento y pronóstico de pacientes con cáncer de hígado (Inglés).

Xu Y (*Correo electrónico: tonggubu9822@163.com*), Shen L 155
<https://doi.org/10.54817/IC.v65n2a03>

Estudio de asociación genética de la variante rs10774671 del gen *OAS1* con la severidad de COVID-19 en una población ecuatoriana (Inglés).

Pilatari K, Balarezo T, Chávez E, Acosta C, Peña IZ, Narváez K, Álvarez-Nava F
(*Correo electrónico: fjalvarez@uce.edu.ec*) 169
<https://doi.org/10.54817/IC.v65n2a04>

El factor de crecimiento similar a la insulina-1 promueve la proliferación y diferenciación odontogénica de células de pulpa dental humana *in vitro* e *in vivo* (Inglés)

Wang Y, Du N, Liu C, Li WJ (*Correo electrónico: liwenjing2729@163.com*) 179
<https://doi.org/10.54817/IC.v65n2a05>

Análisis comparativo, basado en el género, del riesgo de lesión de rodilla durante cambios de dirección en atletas no profesionales: una perspectiva cinética y cinemática (Inglés).

Feria-Madueño A (*Correo electrónico: aferia1@us.es*), Hewett TE, Sañudo B. 192
<https://doi.org/10.54817/IC.v65n2a06>

La eficacia de la medicación personalizada basada en genes relacionados con fármacos, para pacientes con esquizofrenia resistente a los fármacos tradicionales (Inglés).

Zhou S, Zhang G, Wang Z, Wei L, Zhu M, He J (*Correo electrónico: hjqcatdog123@163.com*) 206
<https://doi.org/10.54817/IC.v65n2a07>

Efecto del pirofosfato de tiamina sobre el daño oxidativo en el cerebro y el corazón de ratas con oclusión inducida experimentalmente de la arteria carótida común (Inglés).

Emir I, Suleyman Z, Suleyman H (*Correo electrónico: halis.suleyman@gmail.com*) 220
<https://doi.org/10.54817/IC.v65n2a08>

REVISIONES**Mecanismos de muerte celular programada: vías estructurales y funcionales.****Una revisión narrativa (Inglés).**

Fernández-Lázaro D (*Correo electrónico: diego.fernandez.lazaro@uva.es*), Sanz B,
Seco-Calvo J 230
<https://doi.org/10.54817/IC.v65n2a09>

Valor de la ¹⁸F-FDG-PET/CT en la estadificación inicial de pacientes con cáncer de tiroides de moderado/alto riesgo con subtipos histológicos agresivos (Español).

Colmener LP (*Correo electrónico: luiscolmener@hotmail.com*), Daryanani S, Zúñiga S,
Vilar J 253
<https://doi.org/10.54817/IC.v65n2a10>